Max-Born-Institut
für Nichtlineare Optik
und Kurzzeitspektroskopie
im Forschungsverbund Berlin e.V.

Annual Report 2017

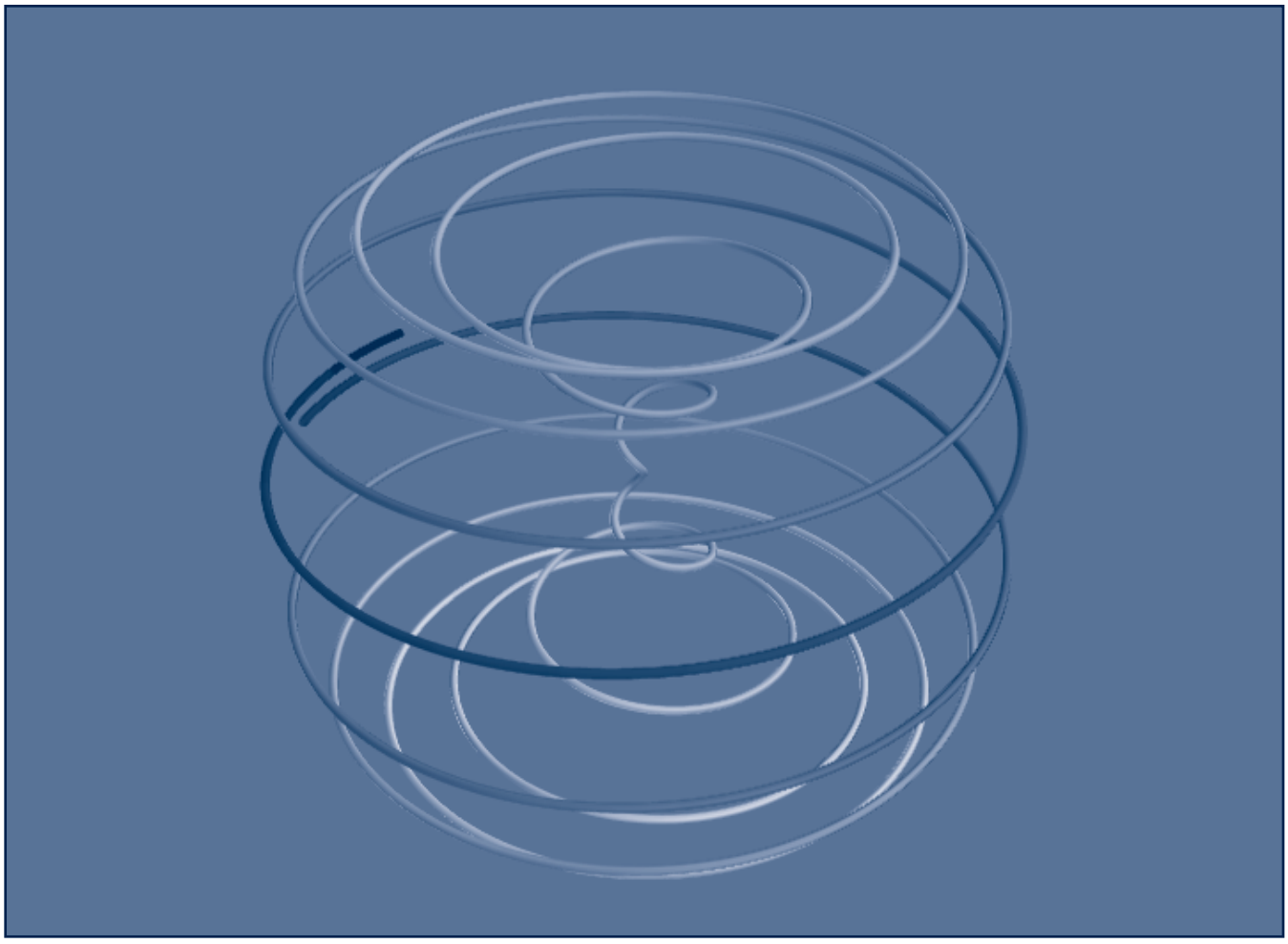

Max-Born-Institut

für Nichtlineare Optik
und Kurzzeitspektroskopie
im Forschungsverbund Berlin e.V.

Annual Report 2017

Annual Report 2017

Max-Born-Institut
für Nichtlineare Optik
und Kurzzeitspektroskopie
im Forschungsverbund Berlin e.V.

Max-Born-Straße 2 A
12489 Berlin
Germany
Phone: (++49 30) 63 92 - 15 05
Fax: (++49 30) 63 92 - 15 19
mbi@mbi-berlin.de
www.mbi-berlin.de

Preface

This Annual Report provides an overview of the research activities and results of the Max-Born-Institut (MBI) in 2017. A presentation of scientific highlights is followed by reports on all projects which are parts of the scientific program of the institute. MBI has stopped the operation of high-field lasers with the end of 2016 and, thus, the related former Project 2.1 as well. A complete record of publications and invited talks is given in the appendix, together with information on academic teaching and training, guest lectures, activities in scientific organizations, and third-party funding. More detailed information is available on the MBI website (http://www.mbi-berlin.de).

In 2017, a number of key results stand out in the strong scientific output of MBI:

- A novel highly sensitive method of optical pump - soft X-ray probe spectroscopy allows for mapping coherent ionic vibrations in small $LiBH_4$ crystals via changes of X-ray absorption. The periodic atomic motions with a tiny amplitude of 3 fm (3×10^{-15} m) modulate the X-ray absorption of the Li^+ ions around 60 eV. The time-resolved X-ray absorption data together with previous X-ray diffraction results allow for an in-depth characterization of the vibrational excitation process and the force field acting on the Li^+ and BH_4^- ions in the crystals.

- Skyrmions in thin magnetic films can be generated deterministically by short current pulses, via the interplay of spin-orbit torques and Dzyaloshinskii–Moriya interaction in suitable magnetic multilayer stacks with lateral nanopatterning. X-ray holography together with micromagnetic simulations, carried out in collaboration with scientists at the Massachusetts Institute of Technology, DESY and Ulm University, allowed to observe, understand and optimize the skyrmion generation mechanism. The ability to deterministically write nanometer-sized magnetic spin textures is a key requirement for novel magnetic data storage concepts.

- Observing the crucial first few femtoseconds of photochemical reactions has become possible using experimental tools provided by attosecond science. Ultrafast nonadiabatic vibronic processes were observed in a prototypical polyatomic molecule - the excited benzene cation. Using few-femtosecond duration extreme ultraviolet and visible/near-infrared laser pulses to prepare and probe excited cationic states, relaxation timescales of 11 +/- 3 fs and 110 +/- 20 fs were observed, and interpreted in terms of population transfer via two sequential conical intersections.

- Distinguishing left- from right-handed chiral molecules is important in physics, chemistry, biology, and medicine. Since the 19th century, molecular chirality is determined using the different absorption of circularly polarized light by the two chiral twins of a molecule. However, this effect is small, because the molecule is too small to see the pitch of the light helix. It is much better to use the helix of the molecule rather than the helix of light. Joint experimental and theoretical work involving the MBI, the INRS in Canada as well as CELIA and the Synchrotron Soleil in France shows how ultrashort pulses of light can be used to trigger and follow helical charge flow inside neutral chiral molecules, which oscillates out-of-phase in left-handed and right-handed molecules, offering a new handle on separating the two chiral twins in space.

- In addition to their use in pump-probe spectroscopy, as illustrated above, XUV/X-ray pulses created by means of high-harmonic generation can be used for coherent diffractive imaging. In recent work, single-shot imaging of isolated helium nanodroplets was demonstrated. Bright wide-angle scattering patterns were obtained, that allow the identification of hitherto unresolved prolate shapes of superfluid helium droplets. These results mark the advent of single-shot gas-phase nanoscopy with lab-based short-wavelength pulses and pave the way to ultrafast coherent diffractive imaging with phase-controlled multicolor fields and attosecond pulses.

- The so-called Zundel cation $H_5O_2^+$, a prototypical geometry of the hydrated proton H^+ in chemistry and biology, was selectively prepared in a polar liquid environment to study ultrafast proton motions by two-dimensional infrared spectroscopy and theoretical QM/MM simulations. The results give the first direct evidence for fluctuating large-amplitude motions of the proton between the two flanking water molecules and the persistence of the Zundel geometry for at least 1 ps. The proton is bound in a low-barrier double minimum potential which is strongly modulated by electric forces the solvent exerts on the Zundel cation. The Zundel geometry represents a major species of protons solvated in water.

- Since the mid-sixties of the 20th century, physical understanding of the interaction of intense infrared light with atoms has been based on two seemingly different pictures. In one, usually associated with moderately strong laser fields, ionization of an atom involves simultaneous absorption of many photons, generalizing the traditional photo-electric effect. In the second, usually associated with higher intensities and larger binding energies, ionization has been viewed as an electron tunneling through the oscillating barrier created by the combination of the laser electric field and the binding core potential. In a study on ultrafast excitation of Argon and Neon atoms in intense short pulse laser fields, MBI scientists could show that these seemingly disparate intuitive pictures of multiphoton vs. tunneling excitation and ionization represent frequency versus time-domain perspectives of the same nonlinear process. Confirming these conclusions with the combination of experimental and theoretical tests, the work resolves the 50-plus years old dilemma.

- Aspirin in form of small crystallites provides new insight into delicate motions of electrons and atomic nuclei. Set into molecular vibration by strong ultrashort far-infrared (terahertz) pulses, the nuclei oscillate much faster than for weak excitation. They gradually return to their intrinsic oscillation frequency, in parallel to the picosecond decay of electronic motions. An analysis of the terahertz waves radiated from the moving particles by in-depth theory reveals the strongly coupled character of electron and nuclear dynamics characteristic for a large class of molecular materials.

- Surface plasmon polaritons play a central role in nano-photonics. Theoretical work predicts a new type of ultrafast nonlinearity of surface plasmon polaritons, which should occur in planar plasmonic structures including a ferromagnetic material layer. Specifically, the surface plasmon polariton with a significant longitudinal component of the electric field creates an effective transverse magnetic field in magnetic thin layers. Its response to the plasmon propagation leads to a strong ultrafast third-order nonlinearity. The new nonlinearity exceeds the optical Kerr effect of typical dielectric materials by five orders of magnitude and that of gold by two orders of magnitude.

More than 200 articles have been published in peer-reviewed journals and books, including a substantial number of papers in a wide range of high-impact journals. The number of invited talks at international conferences has been maintained at a high level.

In 2017, Günther Steinmeyer, department head in Division C, was jointly appointed as a W3-S Professor for Nonlinear Ultrafast Optics with the Humboldt University. Daniela Rupp started her independent junior research group “Ultrafast Dynamics in Nanoplasma” at MBI. In consequence, we now have two independent junior research groups at MBI, one each in the area of experimental and theoretical physics. In September, Stefan Eisebitt took over as managing director of the MBI, succeeding Thomas Elsaesser, who held this position in the previous 3 years. The former High-Field Laser Laboratory has been completely rebuilt and is now available for the EFRE-funded project NanoMovie, with the goal to reliably provide soft X-rays in an application laboratory, based on a novel laser development.

There have been several academic honors and recognitions for MBI scientists and staff members. Lisa Torlina won the Marthe Vogt Award 2017 of the Forschungsverbund Berlin e.V. for her PhD thesis in theoretical strong field physics. Daniel Reiche was awarded the Lise Meitner Prize of the Humboldt University for his MSc thesis on the Casimir-Polder interaction. Esmerando Escoto was awarded with the Young Investigator Award of the Ultrafast Optics Conference for his work on ultrafast pulse characterization. Thomas Fennel from the University of Rostock received a Heisenberg Fellowship of the DFG for a joint project with MBI on imaging and controlling ultrafast electronic motion in nanostructures. Together with three colleagues, Alexandre Mermillod-Blondin received the Thomas Alva Edison Patent Award in the category of Technology Transfer in recognition of his contribution to the development of tunable acoustic gradient index of refraction lenses. Klaus Reimann and Thomas Elsaesser were recognized as outstanding referees by the American Physical Society. Marc Vrakking was appointed as Editor-in-Chief of the Journal of Physics B.

We would like to thank our staff members, guest scientists, and collaboration partners for their enthusiasm and dedicated research work and, last but not least, our funding bodies for the decent support of MBI.

Berlin, March 2018

Stefan Eisebitt Thomas Elsaesser Marc Vrakking

Research Structure of the Max-Born-Institut

1 – Laser Research

1.1 Fundamentals of Extreme Photonics

1.2 Ultrafast Laser Physics and Nonlinear Optics

2 – Ultrafast and Nonlinear Phenomena: Atoms, Molecules, and Plasma

2.2 Strong-field Few-body Physics

2.3 Time-resolved XUV-science

3 – Ultrafast and Nonlinear Phenomena: Condensed Phase

3.1 Dynamics of Condensed Phase Molecular Systems

3.2 Solids and Nanostructures: Electrons, Spins, and Phonons

3.3 Transient Structures and Imaging with X-rays

4 – Laser Infrastructure and Knowledge Transfer

4.1 Implementation of Lasers and Measuring Techniques

4.2 Application Laboratories and Technology Transfer

4.3 Nanoscale Samples and Optics

Organizational Structure of the Max-Born-Institut

Board of Trustees of the Forschungsverbund Berlin e.V.

FVB Managing Director | **Board of Directors** | **Scientific Advisory Board**

Executive Assistant

Division A: Attosecond Physics

A1: Strong-field Processes at Extreme Wavelengths

A2: Ultrafast XUV-Physics

A3: Ultrafast Lasers and Nonlinear Optics

Division B: Transient Electronic Structure and Nanoscience

B1: High Density Laser Plasma

B2: Few Particle Systems in Strong Laser Fields

B3: Laser Development

B4: Electron and Spin Dynamics

Division C: Nonlinear Processes in Condensed Matter

C1: Femtosecond Spectroscopy of Molecular Systems

C2: Solid State Light Sources

C3: Femtosecond Spectroscopy of Solids

Theory Department

Attosecond Theory | Strong-field Theory | Theoretical Optics & Photonics

Junior Group: Ultrafast Dynamics in Nanoplasma

Junior Group: Biomolecular Dynamics

Administration | **IT** | **Maintenance**

Library | **Mechanical Design and Workshop**

Members of the Scientific Advisory Board

Prof. Dr. Giulio Cerullo
Politecnico de Milano, Dipartimento di Fisica, Italy

Prof. Dr. Majed Chergui
École Polytechnique Fédérale de Lausanne (EPFL), Institute of Chemical Sciences and Engineering, Switzerland

Prof. Tony Heinz
Stanford University, Department of Applied Physics, USA

Prof. Dr. Franz X. Kaertner (Chair)
DESY Hamburg, Center for Free-Electron Laser Science (CFEL) & Universität Hamburg, Fachbereich Physik, Germany

Prof. Dr. Jon Marangos
Imperial College London, Department of Physics, UK

Prof. Dr. Didier Normand
IRAMIS, Institut Rayonnement Matière de Saclay, France

Prof. Dr. Christoph Quitmann
Lund University, Max IV Laboratory, Sweden

Prof. Dr. Ursula Roethlisberger
École Polytechnique Fédérale de Lausanne (EPFL), Institute of Chemical Sciences and Engineering, Switzerland

Prof. Dr. Jan Michael Rost
Max-Planck-Institut für Physik komplexer Systeme, Dresden, Germany

Representatives of the Cooperating Universities

Prof. Dr. Oliver Benson
Humboldt-Universtität zu Berlin, Institut für Physik, Germany

Prof. Dr. Ulrike Woggon
Technische Universität Berlin, Institut für Optik und Atomare Physik, Germany

Prof. Dr. Felix von Oppen
Freie Universität Berlin, Fachbereich Physik, Germany

Representatives of the Federal Republic and the State of Berlin

Dr. Frank Wolf
Bundesministerium für Bildung und Forschung, Ref. 711, Bonn, Germany

Dr. Katharina Spiegel
Senatskanzlei, Wirtschaft und Forschung, Ref. VI D, Berlin, Germany

Scientific Highlights

Ultrasmall atom motions recorded with ultrashort X-ray pulses

J. Weisshaupt[1], A. Rouzée[1], M. Woerner[1], M. J. J. Vrakking[1], T. Elsaesser[1], E. L. Shirley[2], and A. Borgschulte[3]
[1] Max-Born-Institut, Berlin, Germany, [2] National Institute of Standards and Technology, Gaithersburg, Maryland, USA,
[3] Swiss Federal Laboratories for Materials Science and Technology, Laboratory for Advanced Analytical Technologies, Dübendorf, Switzerland

X-ray absorption is an important method for mapping equilibrium structures at atomic length scales. The fine structure of X-ray absorption bands reflects distances between neighboring atoms in condensed-phase molecular systems and in crystalline environments. Transient X-ray absorption in the ultrafast time domain thus allows for observing atomic motions and rearrangements in real-time. In the following, we present new results from a femtosecond X-ray absorption study in which periodic motions of atoms over an extremely small length of 10^{-15} m have been recorded using ultrashort X-ray pulses [WRW17a, WRW17b]. This novel experiment is based on a pump-probe scheme with optical excitation and high-harmonics probe pulses.

In the experiment, lattice vibrations or phonons are excited in small crystallites. The spatial elongation of nuclei in a vibration is much smaller than the distance between atoms, the latter being determined by the equilibrium distribution of electrons. Nevertheless, the vibrational motions act back on the electrons, modulate their spatial distribution and change the electric and optical properties of the crystal on a time scale which is shorter than 1 ps (10^{-12} s). To understand these effects and exploit them for novel, e.g., acoustooptical, devices, one needs to image the delicate interplay of nuclear and electronic motions on a time scale much shorter than 1 ps.

In collaborative work of MBI, the Swiss Federal Laboratory for Materials Science and Technology in Dübendorf (Switzerland), and the National Institute of Standards and Technology, Gaithersburg (USA), a novel method of optical pump soft X-ray probe spectroscopy was applied for generating coherent atomic vibrations in small $LiBH_4$ crystals, and reading them out via changes of X-ray absorption. More specifically, an optical pump pulse centered at 800 nm excites a coherent optical phonon with Ag symmetry via impulsive Raman scattering (Fig. 2). The atomic motions change the distances between the Li^+ and $(BH_4)^-$ ions. The change in distance modulates the electron distribution in the crystal and, thus, the X-ray absorption spectrum of the Li^+ ions with the vibrational frequency of 10 THz. In this way, the atomic motions a mapped into a modulation of soft X-ray absorption on the Li K-edge around 60 eV (Figs. 1 and 2, upper panel). Ultrashort X-ray pulses measure the X-ray absorption change at different times. From this series of snapshots the atomic motions are reconstructed.

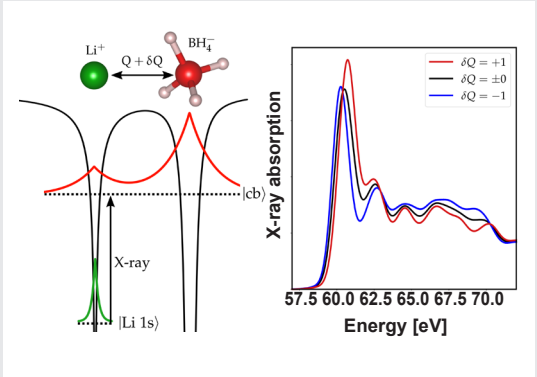

Fig. 1:
In an X-ray absorption experiment light excites a strongly bound core electron into a conduction band state. On the left of the figure such a transition is shown. An electron which is strongly bound to a Lithium nucleus (green) is excited into a conduction band state (red) that interacts with both the lithium nucleus and borohydride group. This conduction band state is therefore sensitive to a modulation of the distance Q between Lithium nucleus and borohydride group and as a result the X-ray absorption process is sensitive to such a modulation (cf. Figs. 2(b) and 3(d) in Ref. [WRW17b]). On the right side of the figure the Lithium K-edge X-ray absorption spectrum for different strongly exaggerated displacements is shown.

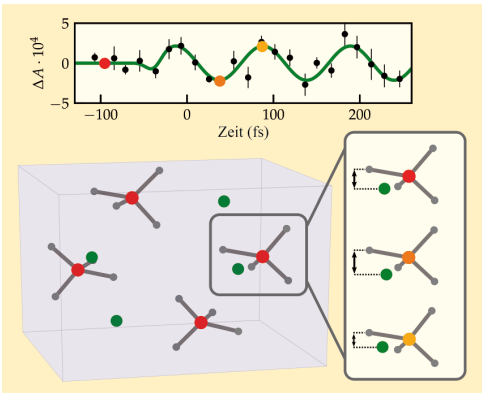

Fig. 2:
What happens in the unit cell of crystalline $LiBH_4$ after impulsive Raman excitation with a femtosecond laser pulse? Upper panel: measured transient absorption change $\Delta A(t)$ (symbols) as we vary the time delay between infrared pump pulses and soft X-ray probe pulses at photon energy of $\hbar\omega$ = 61.5 eV (cf. Fig. 3(a) in Ref. [WRW17b]). The lower box shows the atoms in the unit cell of $LiBH_4$ with red boron atoms, gray hydrogen atoms, and green Li atoms. The moving blue circle in the upper panel is synchronized with the moving atoms in the lower panel. The amplitude of the motion is strongly exaggerated (i.e. times 30000) to visualize the pattern of the motion.

This experimental scheme is highly sensitive and allows for the first time to kick off and detect extremely small amplitudes of atomic vibrations. In our case, the Li^+ ions move over a distance of only 3 femtometers = 3 x 10^{-15} m which is comparable to the diameter of the Li+ nucleus and 100000 times smaller than a distance between the ions in the crystal.

The experimental observations are in excellent agreement with in-depth theoretical calculations of transient X-ray absorption. Moreover, the results together with transient electron density maps from femtosecond X-ray diffraction [SZF12] give detailed insight in the character of the virtual intermediate state in the Raman excitation process. The 800 nm pump pulse induces a shift of electronic charge between neighboring Li^+ and $(BH_4)^-$ entities which results in a Coulomb force on the nuclei. The force field derived from the transient electron density maps displays local components pointing into the same directions as the local elongations of the 10 THz Ag mode, explaining the predominance of this phonon in the transient response.

The new type of optical pump-soft X-ray probe spectroscopy on a femtosecond time scale holds strong potential for measuring and understanding the interplay of nuclear and electronic motions in liquid and solid matter, a major prerequisite for theoretical simulations and applications in technology.

Publications

SZF12: J. Stingl, F. Zamponi, B. Freyer, M. Woerner, T. Elsaesser, and A. Borgschulte; Electron transfer in a virtual quantum state of $LiBH_4$ induced by strong optical fields and mapped by femtosecond X-ray diffraction; Phys. Rev. Lett. **109** (2012) 147402/1-5

WRW17a: J. Weisshaupt, A. Rouzée, and M. Woerner; Atomschwingungen in Superzeitlupe; Physik in unserer Zeit **48** (2017) 113-114

WRW17b: J. Weisshaupt, A. Rouzée, M. Woerner, M. J. J. Vrakking, T. Elsaesser, E. L. Shirley, and A. Borgschulte; Ultrafast modulation of electronic structure by coherent phonon excitations; Phys. Rev. B (R) **95** (2017) 081101/1-5

Deterministic creation of magnetic skyrmions

F. Büttner[1], I. Lemesh[1], M. Schneider[2], B. Pfau[2], C. M. Günther[2,3], P. Hessing[2], J. Geilhufe[2], L. Caretta[1], D. Engel[2], B. Krüger[4], J. Viefhaus[5], S. Eisebitt[2,3], and G. S. D. Beach[1]

[1] Massachusetts Institute of Technology, Cambridge, USA, [2] Max-Born-Institut, Berlin, Germany, [3] Technische Universität Berlin, Germany, [4] Institut für Lasertechnologien in der Medizin und Messtechnik an der Universität Ulm, Germany, [5] Deutsches Elektronen-Synchrotron (DESY), Hamburg, Germany

In magnetic vector fields such as made up by an array of local magnetic moments, skyrmions are localized magnetization textures which are characterized by a topology equivalent to a sphere, i.e., a topological charge of ±1. Isolated skyrmions can be stabilized at room temperature in multilayer films with broken symmetry in the stacking order. The basic unit is a thin magnetic film, such as a CoFeB alloy, sandwiched between a heavy metal (e.g. Platinum) and a non-metal (e.g. MgO). The chiral spin textures are then stabilized by the Dzyaloshinskii-Moriya interaction (DMI) – an asymmetric 3-center exchange interaction mediated via spin-orbit coupling at the interface to the heavy metal. Magnetic skyrmions are particularly interesting due to their application potential as information entities in high-density, non-volatile memory devices. A concept that has been proposed is the so-called skyrmion racetrack memory. This memory consists of a nanoscale stripline with a longitudinal distribution of skyrmions and is operated as a shift register. The digital information is encoded by the presence or absence of a skyrmion. The whole bit pattern of skyrmions has to be moved along the track towards the reading or writing elements, each placed at a fixed position on the track.

It was discovered recently that this movement can be accomplished via a so-called spin-orbit torque. This torque is generated by an electric current through the stripline that leads to spin separation in the heavy-metal layer via the spin Hall effect. When reaching the magnetic layer, the spin-polarized current exerts a torque on the magnetic moments constituting the skyrmion, leading to a transverse motion. While this mechanism allows for very effective movement of the skyrmions, the controlled generation and annihilation of skyrmions (i.e. writing or deleting of a bit in a racetrack) in a device-compatible fashion is a key problem for applications.

As a major step in the ability to write a skyrmion bit, we have recently demonstrated that the same path of spin-orbit torque injection can be used to also create skyrmions. In our experiments, we have patterned a Pt/CoFeB/MgO multilayer into a stripline with sub-micrometer width. After sending single unipolar current pulse through the stripline, we observe the nucleation of skyrmions in the stripline (Fig. 1(b)). The critical current density for this process strongly depends on the pulse length which has been chosen between 0.75 ns and 500 ns in the experiment. Interestingly, a symmetry-breaking external in-plane magnetic field is not required for the process. However, we observed that the nucleation predominantly takes place at particular hotspot positions in the stripline (Fig. 1(c)). Comparing the experiments with micromagnetic simulations, we can show that field-free skyrmion generation via spin-orbit torque is only possible at pinning sites, i.e., defects with reduced perpendicular anisotropy, under the presence of strong DMI.

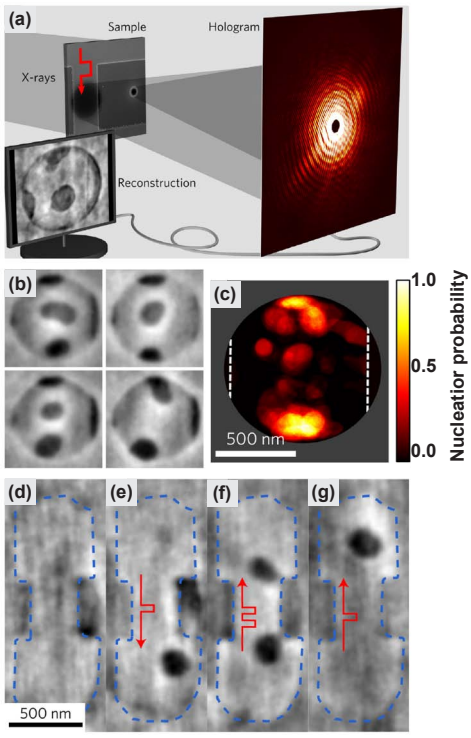

Fig. 1:
(a) Sketch of the holographic soft X-ray setup to image magnetic skyrmions in a stripline. The microscopic field of view is located on the stripline; a pinhole next to the object acts as source for a reference wave. An X-ray sensitive area detector records the interference pattern, i.e., the hologram. The real-space image, showing magnetization contrast only, is retrieved digitally. Prior to recording an image, a current pulse is sent through the magnetically saturated stripline to generate magnetic skyrmions. (b) Four examples of skyrmion configurations created by single current pulses at defects. The stripline is oriented vertically and covers almost the whole field of view with 1 µm diameter. (c) Spatial probability map for the nucleation of skyrmions in the field of view. (d) - (g) Images of skyrmion generation at a constriction. (d) Saturated state before pulse injection, (e) skyrmion generated after single pulse injection, (f) nucleation of another skyrmion at the opposite end of the constriction after applying two pulses with inverted polarity, (g) subsequent movement of the second skyrmion by a single pulse, the first skyrmion was annihilated at the same time.

We have used imaging based on Fourier-transform holography with soft X-rays at 1.6 nm wavelength to make the nanometer-scale skyrmions in the stripline visible. The lensless imaging method is based on the interference of coherent X-rays scattered from the object and an additional reference beam emerging from a tiny pinhole next to the object (Fig. 1(a)). Magnetization contrast is achieved by tuning the wavelength of the radiation to particular electronic excitations of the magnetized element (here Co) and by using circularly polarized X-rays. Due to the very large coherent photon flux delivered by the soft X-ray beamline at the synchrotron radiation facility PETRA III in Hamburg, we are able to image the spin textures with sub-30 nm spatial resolution.

In a second step, we could demonstrate that the position for skyrmion nucleation on the stripline can be perfectly controlled. Towards this end, we lithographically fabricated a constriction into the stripline which now acts as an integrated skyrmion generator due to the combination of increased current density and locally tilted magnetization at the boundary of the structure. We could show that reverse domains nucleate at the downstream corners of the constricted part of the stripline, detaching and forming a skyrmion at one corner only (Fig. 1(e)). This right-left asymmetry reflects the chiral nature of the skyrmion, which experiences a sykrmion Hall effect during the current pulse, in analogy to the Magnus effect on a rotating object. An additional, weaker current pulse can subsequently shift the skyrmion away from the edge (Fig. 1(g)). A change of the current pulse polarity results in a nucleation on the opposite side of the constriction (Fig. 1(f)). The nucleation characteristics observed were again reproduced by micromagnetic simulations, allowing to understand the mechanisms at play.

We could, thus, demonstrate a practical means for deterministic generation of skyrmions in racetrack memories, without having to resort to external magnetic fields, which would be unsuitable in integrated devices. The constriction can be freely positioned in a racetrack and the nucleation times and applied voltages already match today's computer architectures.

Publication

BLS17: F. Büttner, I. Lemesh, M. Schneider, B. Pfau, C. M. Günther, P. Hessing, J. Geilhufe, L. Caretta, D. Engel, B. Krüger, J. Viefhaus, S. Eisebitt, and G. S. D. Beach; Field-free deterministic ultrafast creation of magnetic skyrmions by spin-orbit torques; Nat. Nanotech. **12** (2017) 1040-1044

Few-femtosecond passage of conical intersections in the benzene cation

M. C. E. Galbraith[1], S. Scheit[2], N. V. Golubev[2], G. Reitsma[1], N. Zhavoronkov[1], V. Despré[2], F. Lepiné[3], A. I. Kuleff[2], M. J. J. Vrakking[1], O. Kornilov[1], H. Köppel[2], and J. Mikosch[1]

[1] Max-Born-Institut, Berlin, Germany, [2] Physikalisch-Chemisches Institut, Universität Heidelberg, Germany, [3] Institut Lumière Matière, Université Lyon, Villeurbanne, France

Observing the crucial first few femtoseconds of photochemical reactions requires tools typically not available in the femtochemistry toolkit. Such dynamics are now within reach with the instruments provided by attosecond science. In our work we have characterized one of the fastest internal conversion processes in a molecule studied to date [GSG17b].

When Horst Köppel published his first article on the benzene cation molecule in 1987, Martin Galbraith was just born. Köppel, a professor from Heidelberg, had found the perfect testbed for the ensuing development of a new theoretical methodology, the so-called multi-configurational time-dependent Hartree (MCTDH) method, for which he and his colleagues became famous over the next few decades. The omnipresent benzene molecule turns out to be the perfect compromise between complexity and chemical relevance. That's why the theory specialists from Heidelberg studied it in more and more detail, publishing more than 30 highly cited scientific papers over the years, as they matured the theory into a cutting-edge tool for computational chemistry, which is now being used by researchers all over the word.

One thing was out of reach though until now: The experimental verification of the theoretical results in a time-resolved experiment. The predicted dynamics in the benzene cation was simply too fast – on a timescale of only about 10 femtoseconds. In work performed within the PhD thesis of Martin Galbraith, we have now pushed the experimental limits to the point where measurements of the extremely fast dynamics in the benzene molecule became technically feasible. The development of few-cycle laser pulses and the creation of attosecond pulse trains consisting of only a few bursts allowed us to devise a photochemical experiment with unprecedented time resolution.

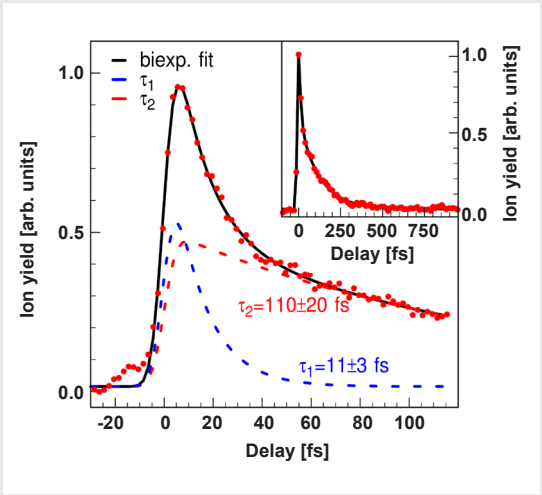

Fig. 1:
Time-resolved experimental data. Shown is the measured $C_4H_3^+$ fragment yield as a function of the pump-probe delay (red dots). The bold black line is a biexponential fit to the data, the dashed lines represent the contributions from two timescales that correspond to crossings of two sequential conical intersections. The inset displays the $C_4H_3^+$ yield over a long – range pump-probe scan.

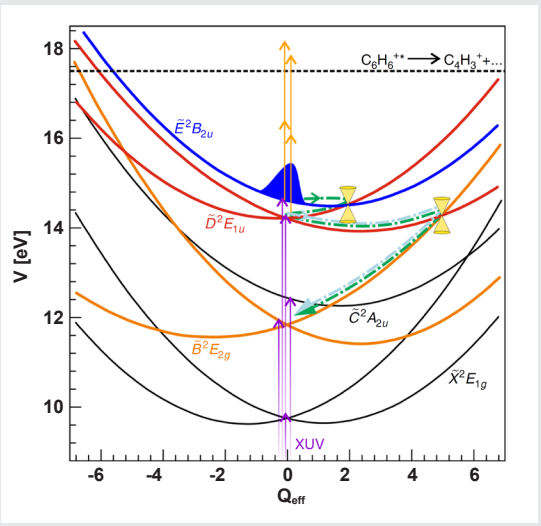

Fig. 2:
Schematic of the studied dynamics. Depicted is an overview of the lowest eight electronic component states of the benzene cation, depicted as potential energy V in eV as a function of a dimensionless effective nuclear coordinate Q_{eff}. The violet arrows represent the ionization by the pump pulse, the orange arrows the excitation by the probe pulse. The dashed black line corresponds to the appearance energy for dissociation producing $C_4H_3^+$. The dashed-dotted green curve is a cartoon drawing of the time-evolution of a cation originally transferred to the $\tilde{E}$ state and then undergoing a series of internal conversion processes to $\tilde{D}$ and subsequently to the $\tilde{B}$ states, via the conical intersections indicated in the figure.

By spectrally filtering high harmonic radiation it became possible to create a defined superposition of electronic states in the benzene cation molecule by ionizing neutral benzene with a few-femtosecond duration vacuum ultraviolet pulse. Time-resolved probing of the excited cationic states by a few-cycle visible/near-infrared pulse, which induces molecular fragmentation, uncovered two relaxation timescales of 11 ± 3 fs and 110 ± 20 fs (see Fig. 1). These are interpreted in terms of population transfer via two sequential conical intersections, from the $\tilde{E}$ to the $\tilde{D}$ and from the $\tilde{D}$ to the $\tilde{E}$ state (see Fig. 2). Conical intersections are often described as molecular

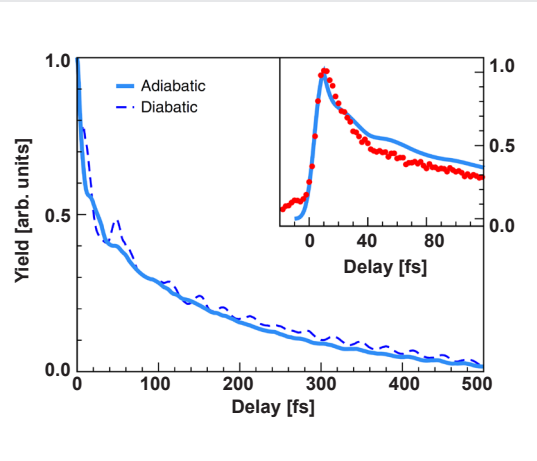

Fig. 3:
Comparison of theory and experiment. Time-dependent 'yields' (blue lines), obtained by summing the populations of the $\tilde{E}$ and $\tilde{D}$ states from an MCTDH calculations. The curves are derived from separate wavepacket calculations for an initial pure excitation in the $\tilde{E}$ and in the $\tilde{D}$ state, respectively. The solid (dashed) line represent the result obtained for adiabatic (diabatic) electronic populations. The inset displays the yield for the adiabatic state calculation, convoluted with the Gaussian instrument response function, for direct comparison to the experiment (red points, cf. Fig. 1).

funnels, where different potential energy surfaces intersect. These are of particular interest since the usually distinct timescales for electronic and nuclear motion become comparable.

While the dynamics in the benzene cation was merely a theoretical benchmark up to now, a detailed comparison of theory and experiment became possible, as described in our study published in Nature Communications [GSG17b]. The work also includes advanced theoretical MCTDH modeling performed within a collaboration of MBI researchers with the theory groups of Prof. Horst Köppel and Priv.-Doz. Alexander Kuleff from the University of Heidelberg. We find an excellent agreement between experiment and computation (see Fig. 3), validating the theoretical approach.

Molecular dynamics near conical intersections play a key role in diverse very active fields of research in modern chemistry, such as in biochemical processes surrounding the stability of DNA with respect to UV light and the first steps of vision in animals and humans. Importantly, the previously inaccessible dynamics within the first few femtoseconds of the photochemical process are often crucial. By characterizing one of the fastest internal conversion processes studied to date, we entered an extreme regime of ultrafast molecular dynamics, paving the way to tracking and controlling purely electronic dynamics in complex molecules on even shorter timescales.

Publication

GSG17b: M. C. E. Galbraith, S. Scheit, N. V. Golubev, G. Reitsma, N. Zhavoronkov, V. Despré, F. Lépine, A. I. Kuleff, M. J. J. Vrakking, O. Kornilov, H. Köppel, and J. Mikosch; Few-femtosecond passage of conical intersections in the benzene cation; Nat. Commun. **8** (2017) 1018/1-7

Exciting and probing chiral charge flow in chiral molecules at ultra-fast time scale

A. F. Ordóñez-Lasso, A. G. Harvey, Z. Mašín, and O. Smirnova

You are standing in front of a mirror, seeing your twin inside. He is your twin, yet he is stubbornly different -- he will raise his right hand if you raise your left. And he will raise his left hand if you raise your right. The tiny mole on your left cheek is on his right. You are right-handed but he is left-handed, and he will write from right to left if you write from left to right. He is your *chiral* twin.

So it is with molecules: many of them are chiral, fundamentally different from their mirror image. Some have chiral twins, while others have lost (or, perhaps, never had) them and exist only in one of the two mirror-image forms. Identifying this form, left- or right-handed, and telling the two chiral twins apart, is important in physics, chemistry, biology, and medicine.

Conventionally, chirality is determined using circularly polarized light, which forms a right-handed or a left-handed helix, with the axis of the helix along the light propagation direction. This light is absorbed slightly differently by the two chiral twins of a molecule. The effect – the absorption circular dichroism – is known since the XIX-th century and is very much in use today. However, this effect is small, because the molecule is too small to see the pitch of the light helix. It would have been so much better to use the helix of the molecule rather than the helix of light, relying on the chiral structure of the molecule itself. After all, it has the molecular size.

This idea has been realized in the joint experimental and theoretical work involving the MBI, the Institut national de la recherche scientifique (INRS) in Canada, the Center for Intense Lasers and Applications (CELIA) at University of Bordeaux, the National Center for Scientific Research (CNRS), the French Alternative Energies and Atomic Energy Commission (CEA), Soleil Synchrotron, the Interactions, Dynamics and Lasers Laboratory (LIDYL). The work by S. Beaulieu *et al.*, published in Nature Physics, reports the discovery of the new chiro-optical effect: the photo-excitation circular dichroism, which is about 10^3 times stronger than the conventional absorption circular dichroism in neutral molecules.

If light absorbed by a chiral molecule comes from an ultra-short laser pulse, several states of the molecule are coherently populated and a wavepacket – a non-stationary quantum state – is created. This non-equilibrium state evolves, inducing the flow of electric charge inside the molecule. The flow of charge can be driven by the electronic degree of freedom only, or by the coupled electronic and nuclear motion. Whatever the exact physical mechanism underlying the charge dynamics, the key point is that now the direction of the charge flow is dictated by the structure of the molecule and not by light. The role of ultrafast light pulse is to excite a ring current in the molecule. Once the molecular helix sets to work, it converts this circular motion into a helical charge motion, with very high efficiency. What is more, the charge flow winds differently in left-handed and right-handed molecules. As a result, in a gas of randomly oriented molecules the dipole moment describing the flow of charge will oscillate out of phase in the two molecular enantiomers. In other words, the two oscillating currents are the two mirror images of each other, with the polarization plane of the exciting laser pulse providing the plane of the mirror.

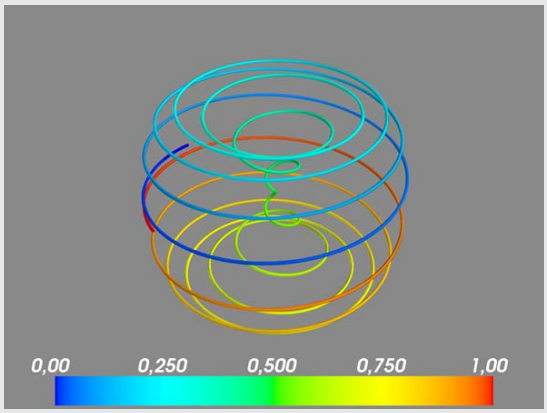

Fig. 1:
A sketch of the charge flow excited inside a chiral molecule by a short laser pulse which coherently populates two electronic chiral states in a molecule. Time in the figure is encoded with color, starting with blue and progressing to red. The picture shows one period of evolution of the excited coherent charge flow, and time is measured in units of this period

A sketch of such helical current is shown in Fig. 1, where different colors encode the time measured in units of one oscillation period. The charge flow starts as blue and, as it progresses towards red, it evolves from circular motion in the polarization plane of the laser pulse (horizontal plane in the figure) into a helix that winds up and down orthogonal to the polarization plane.

Once the charge flow is launched, it can be probed. A short probe pulse, delayed with respect to the pump pulse, will catch the charge flowing out of phase in the two chiral twins, projecting this difference onto the different velocities of photoelectrons generated by probe-induced photoionization. The probe pulse can be linearly polarized, minimizing the effects of the probe on the chiral dynamics induced in the neutral molecule.

Having succeeded in telling the two chiral molecules apart, we can now think about using macroscopic, out-of-phase oscillating dipoles induced in molecular ensembles to separate the two chiral twins in space.

Publication

S. Beaulieu, A. Comby, D. Descamps, B. Fabre, G. A. Garcia, R. Géneaux, A. G. Harvey, F. Légaré, Z. Mašín, L. Nahon, A. F. Ordóñez-Lasso, S. Petit, B. Pons, Y. Mairesse, O. Smirnova, and V. Blanchet; Photoexcitation circular dichroism in chiral molecules; Nat. Phys.; DOI: 10.1038/s41567-017-0038-z

In the Flashlight: Single helium nanodroplets imaged with intense pulses from a high-harmonic source

D. Rupp[1,2], N. Monserud[2], B. Langbehn[1], M. Sauppe[1], J. Zimmermann[1], Y. Ovcharenko[1,3], T. Möller[1], F. Frassetto[4], L. Poletto[4], A. Trabattoni[4,5], F. Calegari[5,6], M. Nisoli[6,7], K. Sander[8], C. Peltz[8], M. J. J. Vrakking[2], T. Fennel[2,8], and A. Rouzée[2]

[1] Technische Universität Berlin, Germany, [2] Max-Born-Institut, Berlin,Germany, [3] European XFEL GmbH, Hamburg, Germany, [4] CNR, Istituto di Fotonica e Nanotecnologie Padova,Italy, [5] Center for Free-Electron Laser Science, DESY, Hamburg, [6] CNR, Istituto di Fotonica e Nanotecnologie Milano, Italy, [7] Politecnico di Milano, Italy, [8] Universität Rostock, Germany

The excitation of nanoparticles, such as clusters and nanodroplets, with intense laser pulses provides a well-defined scenario to study the correlated dynamics of highly excited matter. Via diffractive imaging of single nanoparticles in free flight with XUV and X-ray free-electron lasers (FELs), the light-induced dynamics can be explored with high spatial and temporal resolution. From the measured diffraction patterns, formed by the interference of elastically scattered photons, the nanoparticle's structure can be determined. This technique allows the study of specimen that cannot be deposited on a substrate, such as superfluid helium nanodroplets, and promises routes to observe structural changes like e.g. ultrafast melting.

Even faster electron dynamics also change the scattering response and can therefore, in principle, be mapped by diffractive imaging. However, these dynamics cannot be temporally resolved using FEL pulses with pulse durations in the order of 100 femtoseconds. While sub-femtosecond pulses are currently under development at FELs, isolated attosecond XUV pulses and attosecond pulse trains can already be achieved with laser-based high-harmonic-generation sources, but they are typically orders of magnitude weaker than pulses from FELs.

In a collaborative action, scientists from TU Berlin, the Max-Born-Institut, the national research institutes in Padova and Milano, and the University of Rostock demonstrated diffractive imaging of helium nanodroplets with a high-harmonic generation source [RML17]. In this experiment, single nanoscale particles could be directly imaged in free flight for the first time in a lab-based experiment. Very bright XUV flashes were created with NIR pulses (λ_c = 792 nm, E_p = 12 mJ, t_p =35 fs), which were loosely focused into a xenon-filled gas cell (~2 µJ XUV per pulse generated, 11th to 17th harmonic). The XUV beam was focused to a small spot, reaching high intensities up to 3 x 10^{12} W/cm² in the interaction region, and overlapped with a jet of helium nanodroplets from a cryogenic, pulsed source.

Bright diffraction images (see Fig. 1(a), (b)) with signal detected up to large scattering angles were obtained. The droplet shapes could be determined by matching simulations based on few-parameter model shapes to the wide-angle scattering images (Fig. 1(c)). In particular, crescent-like structures, such as those in Fig. 1(b), could be uniquely assigned to prolate droplet shapes. This finding contributes to the current vivid discussion on the structure of superfluid rotating droplets. The majority of patterns revealed perfectly spherical shapes (e.g. Fig. 1(a)) that in principle allow for the extraction of the particle's refractive indices. This quantity relates directly to the particle's electronic structure and provides a handle to follow light-induced changes. An automatized fitting procedure based on Mie simulations was developed to account for the multi-color contributions of the harmonic wavelengths (see also report for Project 2.3, page 62).

In view of both the advancing capabilities of HHG sources to generate increasingly intense isolated attosecond pulses and pulse trains as well as the fast development of free-electron laser sources towards ever shorter pulse durations, the success of this proof-of-principle experiment has brought in reach the vision of diffractive imaging of attosecond electron dynamics in isolated nanostructures.

Publication

RML17: D. Rupp, N. Monserud, B. Langbehn, M. Sauppe, J. Zimmermann, Y. Ovcharenko, T. Möller, F. Frassetto, L. Poletto, A. Trabattoni, F. Calegari, M. Nisoli, K. Sander, C. Peltz, M. J. J. Vrakking, T. Fennel, and A. Rouzée; Coherent diffractive imaging of single helium nanodroplets with a high harmonic generation source; Nat. Commun. **8** (2017) 493/1-6

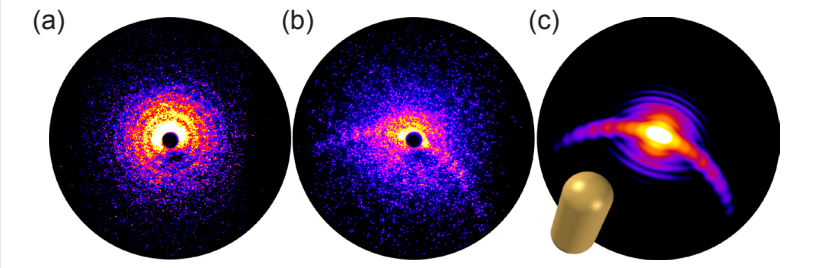

Fig. 1:
Measured HHG-based single-shot diffraction images of (a) spherical and (b) extremely deformed helium nanodroplets. (c) Simulated pattern matching (b), calculated from a prolate shape as visualized in yellow.

Water makes the proton dither – Ultrafast motions and fleeting geometries of hydrated protons

F. Dahms[1], B. P. Fingerhut[1], E. T. J. Nibbering[1], E. Pines[2], and T. Elsaesser[1]
[1] Max-Born-Institut, Berlin, Germany, [2] Ben Gurion University of the Negev, Beer-Sheva, Israel

Basic processes in chemistry and biology involve protons in a water environment. Water structures accommodating protons and their motions have so far remained elusive. Applying ultrafast vibrational spectroscopy, we map fluctuating proton transfer motions and provide direct evidence that protons in liquid water are predominantly shared by two water molecules. Femtosecond proton elongations within a hydration site are 10 to 50 times faster than proton hopping to a new site, the elementary proton transfer step in chemistry.

The proton, the positively charged nucleus H^+ of a hydrogen atom and smallest chemical species, is a key player in chemistry and biology. Acids release protons into a liquid water environment where they are highly mobile and dominate the transport of electric charge. In biology, the gradient of proton concentration across cell membranes is the mechanism driving the respiration and energy storage of cells. Even after decades of research, however, the molecular geometries in which protons are accommodated in water and the elementary steps of proton dynamics have remained highly controversial.

Protons in water are commonly described with the help of two limiting structures (Fig. 1(a)). In the Eigen complex ($H_9O_4^+$) (left), the proton is part of the central H_3O^+ ion surrounded by three water molecules [1]. In the Zundel cation ($H_5O_2^+$) (right), the proton forms strong hydrogen bonds with two flanking water molecules [2]. A description at the molecular level employs the potential energy surface of the proton (Fig. 1(b)) which is markedly different for the two limiting geometries. As shown in Fig. 1(b), one expects an anharmonic single-minimum potential for the Eigen species and a double minimum potential for the Zundel species [3]. In liquid water, such potentials are highly dynamic in nature and undergo ultrafast fluctuations due to thermal motions of surrounding water molecules and the proton.

We have now elucidated the ultrafast motions and structural characteristics of protons in water under ambient conditions [DFN17]. The femtosecond dynamics of proton motions were mapped via vibrational transitions between proton quantum states (red and blue arrows in Fig. 1(b). Two-dimensional vibrational spectroscopy provides the yellow-red and blue contours in Fig. 2(a) which mark the energy range covered by the two transitions. The blue contour occurs at higher detection frequencies than the red, giving the first direct evidence for the double-minimum character of the proton potential in the native aqueous environment. In contrast, the blue contour would appear at smaller detection frequencies than the red one for regular vibrations with anharmonic (Morse-like) potentials.

The orientation of the two contours parallel to the vertical frequency axis demonstrates that the two vibrational transitions explore a huge frequency range within less than 100 fs, a hallmark of ultrafast modulations of the shape of proton potential. In other words, the proton explores all locations between the two water molecules within less than 100 fs and quickly loses the memory of where it has been before. The modulation of the proton potential is caused by the strong electric field imposed by the water molecules in the environment. Their fast thermal motion results in strong field fluctuations and – thus – potential energy modulations on a sub-100 fs time scale. This picture is supported by benchmark experiments with Zundel cations selectively prepared in polar acetonitrile and by detailed theoretical simulations of proton dynamics (Fig. 2(b)). Our experimental and theoretical results identify the Zundel cation as a predominant species in liquid water [DFN17].

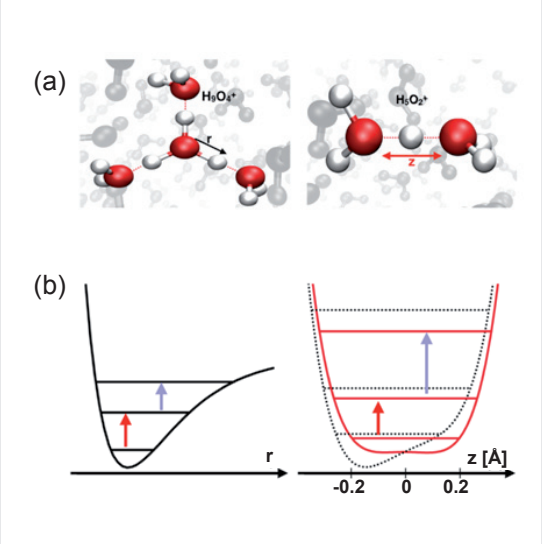

Fig. 1:
Chemical structure of hydrated protons in liquid water. (a) Schematic of the Eigen cation $H_9O_4^+$ (left) and the Zundel cation $H_5O_2^+$ (right). The arrows indicate the O-H bond coordinate r and the (O···H⁺···O) proton transfer coordinate z. In the Eigen cation a covalent O-H bond localizes the proton whereas in the Zundel cation the proton is delocalized between two water molecules. (b) Anharmonic vibrational potential (left) and double minimum potential of the Zundel cation along z (right, red). Distortions by the solvent surrounding impose a modulation of the double minimum potential (right, dotted line). Red and blue arrows indicate transitions between particular quantum states of the proton motion, i.e., the ground-state-to-first-excited-state transition (red) and the first-excited-state-to-second-excited-state transition (blue). The modulation of the potentials leads to spectral shifts of the vibrational transitions which are mapped by two-dimensional infrared spectroscopy.

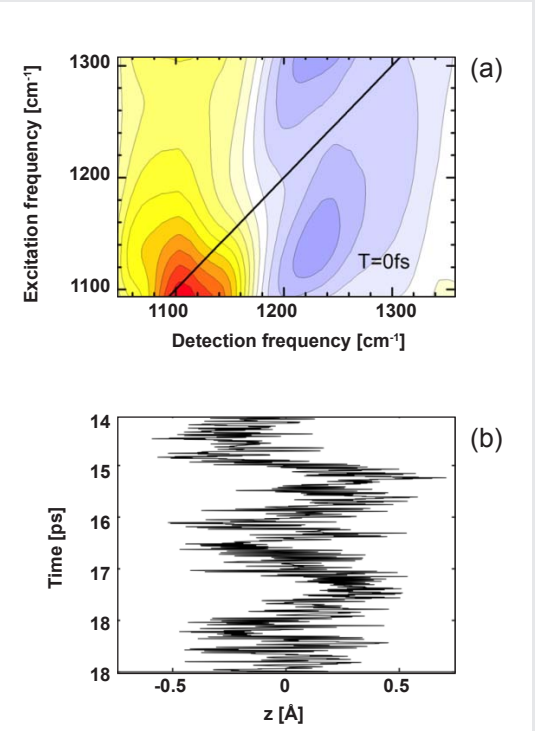

Fig. 2:
Femtosecond dynamics of proton motions. (a) Two-dimensional vibrational spectra with the ground-state-to-first-excited-state transition (red) at lower detection frequency than the first-excited-state-to-second-excited-state transition (blue). The orientation of both contours parallel to the excitation frequency axis is due to ultra-fast frequency fluctuations and the loss of memory in the proton position. (b) Simulated real-time dynamics of the proton motions in the Zundel cation. Within less than 100 fs, the proton displays large amplitude excursions along z, the coordinate linking the two water molecules in the Zundel cation. Due to the ultrafast modulation of the shape of proton potential by surrounding solvent molecules, the proton explores all locations between the two water molecules.

A specific Zundel cation in water transforms into new proton accommodating geometries by the breaking and reformation of hydrogen bonds. Such processes are much slower than the dithering proton motion and occur on a time scale of a few picoseconds. This new picture of proton dynamics is highly relevant for proton transport by the infamous von Grotthuss mechanism [4] and for proton translocation mechanisms in biological systems.

Publication

DFN17: F. Dahms, B. P. Fingerhut, E. T. J. Nibbering, E. Pines, and T. Elsaesser; Large-amplitude transfer motion of hydrated excess protons mapped by ultrafast 2D IR spectroscopy; Science **357** (2017) 491-495

References

[1] E. Wicke, M. Eigen, T. Ackermann; Über den Zustand des Protons in wässriger Lösung; Z. Phys. Chem. **1** (1954) 340-364

[2] G. Zundel and H. Metzger; Energiebänder der tunnelnden Überschuß-Protonen in flüssigen Säuren. Eine IR-spektroskopische Untersuchung der Natur der Gruppierungen $H_5O_2^+$; Z Phys. Chem. Neue Folge **58** (1968) 225-245

[3] R. Janoschek, E. G. Weidemann, H. Pfeiffer, and G. Zundel; Extremely high polarizability of hydrogen bonds; J. Am. Chem. Soc. **94** (1972) 2387-2396

[4] D. Marx, M. E. Tuckerman, J. Hutter, and M. Parrinello; The nature of the hydrated excess proton in water; Nature **397** (1999) 601-604

Unified time and frequency picture of ultrafast atomic excitation in strong fields

H. Zimmermann, S. Patchkovskii, M. Ivanov, and U. Eichmann

The insight that light sometimes needs to be treated as an electromagnetic wave and sometimes as a stream of energy quanta called photons is as old as quantum physics. In the case of interaction of strong laser fields with atoms the dualism finds its analogue in the intuitive pictures used to explain ionization and excitation: The multiphoton picture and the tunneling picture. The Keldysh parameter, introduced in the 1960's by the eponymous Russian physicist, is a measure to clearly distinguish the multiphoton regime and the tunneling regime. However, it has remained an open question, particularly in the field of strong-field excitation, how to reconcile the two seemingly opposing approaches.

In a combined experimental and theoretical study on ultrafast excitation of atoms in intense short pulse laser fields we succeeded to show that the prevailing and seemingly disparate intuitive pictures usually used to describe interaction of atoms with intense laser fields can be ascribed to a single nonlinear process. Moreover, we show how the two pictures can be united. The work appeared in Physical Review Letters and has been chosen as an Editors' suggestion.

In our experiments we measured the excitation yield of Ar and Ne atoms as a function of the laser intensity directly covering both, the multiphoton and tunneling regimes.

In the multiphoton picture typically the photon character shines through as resonant enhancement in the excitation yield, if the energy of n photons matches the excitation energy of an excited (Rydberg) state. The excitation energy, however, shifts upwards with increasing laser intensity, which is for Rydberg states proportional to the quiver energy of a free electron. This results in resonant-like enhancements of the excitation yield close to the n-photon thresholds for ionization (channel closing) when tuning the laser intensity at a fixed laser frequency. These resonances have been observed directly in the excitation for the first time in our experiment, Fig. 1(a). At a laser intensity of 200 TW/cm^2 a strong resonant enhancement of about a factor 100 is visible in the vicinity of a 6-photon channel closing.

In the tunneling picture the laser field is considered as an electromagnetic wave, where only the oscillating electric field is retained. Excitation can be viewed as a process, where initially the bound electron is liberated by a tunneling process, when the laser field reaches a cycle maximum. In many cases the electron does not gain enough drift energy from the laser field to escape the Coulomb potential of the parent ion by the end of the laser pulse, which would lead to ionization of the atom. Instead, it remains bound in an excited Rydberg state. In the tunneling picture there is no room for resonances in the excitation since tunneling proceeds in a quasi-static electric field, where the laser frequency is irrelevant. In fact, using appropriate conditions our experiment shows this behavior, Fig. 1(b).

The numerical solution of the time dependent Schrödinger equation in a strong laser field provided excellent agreement with our experimental data in both regimes. A more detailed analysis revealed that both pictures represent a complementary description in the time and frequency domain of the same nonlinear process. If one considers excitation in the time domain one can assume that electron wave packets are created periodically at the field-cycle maxima. If the successive wave packets are created at the same field strength, as it is the case in the multiphoton regime, their phase difference allows for constructive interference if the

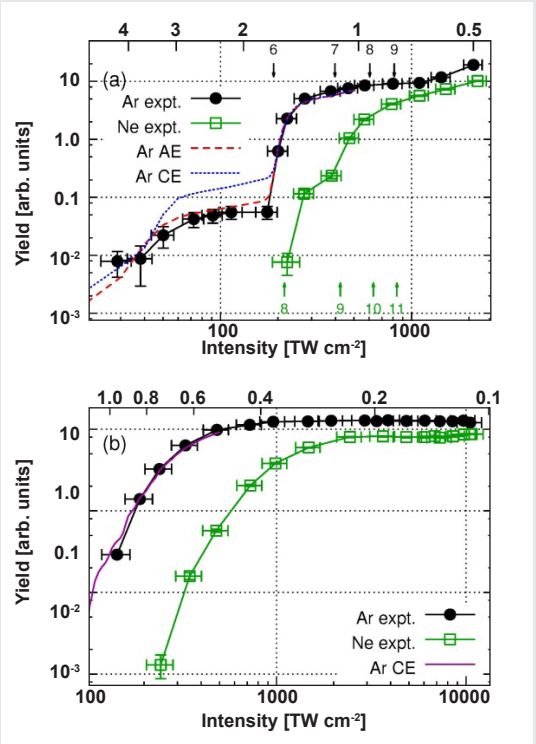

Fig. 1:
Yields of strong-field excited Ar (black disks) and Ne (green squares) atoms as a function of the laser intensity. The Keldysh γ parameter for argon is shown on the upper x axis, where γ <1 indicates the multiphoton regime, γ <1 the tunneling regime. (a) 400 nm laser wavelength. Volume-averaged TDSE results for the all-electron (AE; red dashed line) and core-eliminated (CE; blue dotted line) model potentials are shown. Selected channel-closure intensities are indicated by black (Ar, top) and green (Ne, bottom) vertical arrows. (b) 800 nm laser wavelength.

laser intensity is close to the intensity for a channel closing. With this, regular enhancement in the excitation spectrum occurs effectively only at a separation corresponding to the photon energy. In the tunneling regime wave packets are also created periodically at the field cycle maxima, however, predominantly at the rising edge of the laser pulse. Here, successive wave packets accumulate an additional phase that depends on the intensity change of sucessive laser cycles. This leads to an irregular interference pattern and consequently to irregular variations in the excitation spectrum. These rapid variations are not resolved in the experiment and the detected excitation spectrum is smooth.

We emphasize that the analysis reconciles the multiphoton and tunneling picture by highlighting the smooth transition from a regular to an irregular excitation pattern at the channel closings, where excitation dominates. Beside these fundamental aspects the work opens new pathways to determine laser intensities with high precision and to control coherent Rydberg population by the laser intensity.

Publication

ZPI17: H. Zimmermann, S. Patchkovskii, M. Ivanov, and U. Eichmann; Unified time and frequency picture of ultrafast atomic excitation in strong laser fields; Phys. Rev. Lett. **118** (2017) 013003/1-5

Aspirin tablets help unravel basic physics

G. Folpini[1], K. Reimann[1], M. Woerner[1], T. Elsaesser[1], J. Hoja[2], and A. Tkatchenko[2,3]
[1] Max-Born-Institut, Berlin, Germany, [2] Physics and Materials Science Research Unit, University of Luxembourg, Luxembourg, [3] Fritz-Haber-Institut der Max-Planck-Gesellschaft, Berlin, Germany

Aspirin in form of small crystallites provides new insight into delicate motions of electrons and atomic nuclei. Set into molecular vibration by strong ultrashort far-infrared (terahertz) pulses, the nuclei oscillate much faster than for weak excitation. They gradually return to their intrinsic oscillation frequency, in parallel to the picosecond decay of electronic motions. An analysis of the terahertz waves radiated from the moving particles by in-depth theory reveals the strongly coupled character of electron and nuclear dynamics characteristic for a large class of molecular materials.

Based on its physiological activity, aspirin has found widespread pharmaceutical application in different medical areas. Looking at an individual aspirin molecule from the physics perspective, one can distinguish two types of motions: (i) molecular vibrations, i.e., oscillatory motions of the atomic nuclei in a wide frequency range, among them, e.g., the hindered rotation of the methyl group at a frequency of 6×10^{12} s^{-1} = 6 THz and (ii) oscillatory motions of electrons in the molecule around 1000 THz, as induced, e.g., by ultraviolet light. While the different motions are only weakly coupled in a single aspirin molecule, they develop a very strong electric interaction in a dense polycrystalline packaging such as in the aspirin tablets from the pharmacy. As a result, the character of particular vibrations, the so-called soft modes, changes and their oscillation frequency is substantially reduced. This leads to a blue shift of the vibrational bands as shown schematically in the upper part of Fig. 1. The complex coupling scheme and the resulting molecular dynamics are important for how aspirin and other molecules respond to an external stimulus. So far, this problem has remained unresolved.

The MBI THz team and theoreticians from the University of Luxembourg have combined novel experimental and theoretical methods to unravel the basic properties of soft modes [FRW17]. In the experiments, a sequence of two phase-locked THz pulses interacts with a 700 µm thick tablet of polycrystalline aspirin. The electric field radiated by the moving atoms serves as a probe for mapping the soft-mode oscillations in real time. Two-dimensional scans in which the time delay between the two THz pulses is varied, display a strong nonlinearity of the soft-mode response in aspirin crystals. This nonlinearity is dominated by a pronounced transient shift of the soft mode to higher frequencies as manifested in the pump-probe response of the system (Fig. 1). This response displays a non-instantaneous character with picosecond decay times originating from the generated electric polarization of the crystallites. During the polarization decay, the soft-mode frequency returns gradually to the value it had before excitation.

The theoretical analysis shows that strong electric polarizations in the ensemble of aspirin molecules give the soft mode a hybrid character, combining nuclear and electronic degrees of freedom via dipole-dipole coupling (Fig. 2). In the unexcited aspirin crystallites, there is a strong correlation between electrons and nuclei which determines the equilibrium soft-mode frequency. Strong THz excitation induces a break-up of the electrically mediated correlations, resulting in a transient blue-shift of the soft modes and, via the comparably slow decay

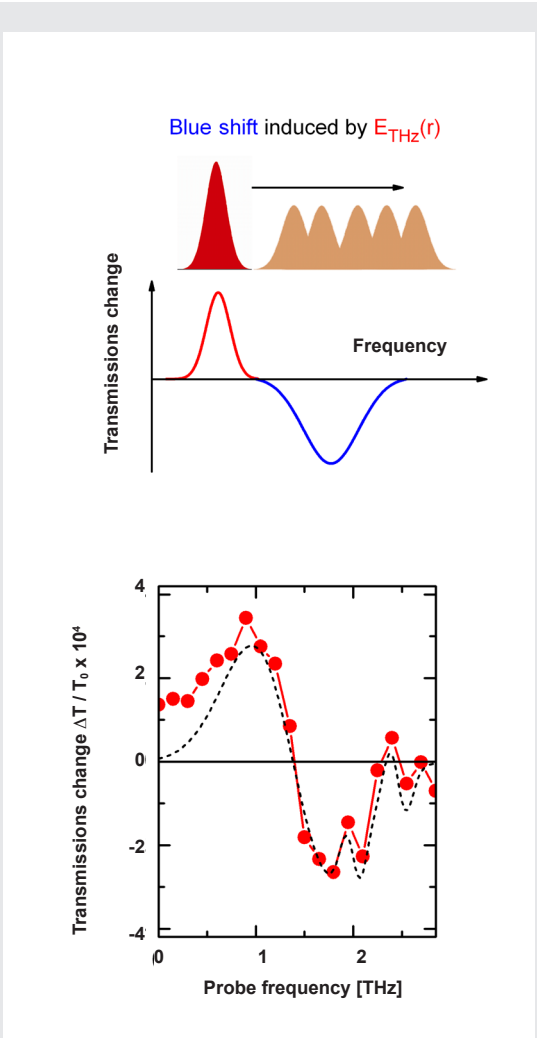

Fig. 1:
Top: Blue shift induced by the THz electric field acting on soft-mode transition dipole in an aspirin crystal. Depending on the electric field strength the soft-mode frequency is shifted from its initial value (red Gaussian, transmission increase) to an instantaneously blue-shifted position (ensemble of orange Gaussians, transmission decrease). Bottom: Symbols: measured transmission change as a function of the probe frequency on a thin film of aspirin crystallites. Dashed line: calculated nonlinear response.

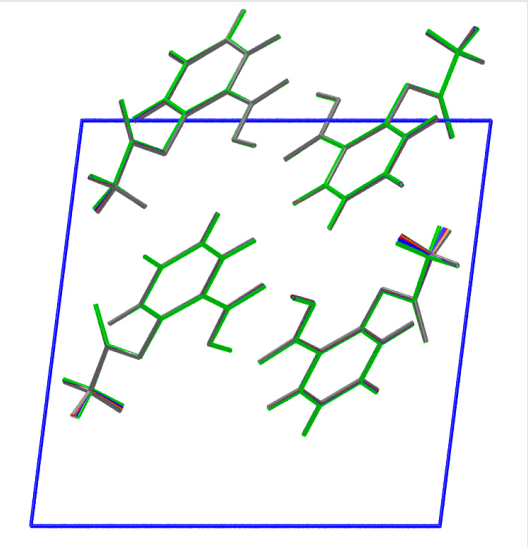

Fig. 2:
Ab-initio calculations of the soft-mode motion of the methyl group in the unit cell of crystalline aspirin. The different phases of the hindered rotation are shown in different colors.

(decoherence) of the polarization, a non-instantaneous response. The scenario discovered here is relevant for a large class of molecular materials, in particular for those with applications in ferroelectrics.

Publication

FRW17: G. Folpini, K. Reimann, M. Woerner, T. Elsaesser, J. Hoja, and A. Tkatchenko; Strong local-field enhancement of the nonlinear soft-mode response in a molecular crystal; Phys. Rev. Lett. **119** (2017) 097404/1-6

A new type of third-order nonlinearity in magneto-plasmonic structures

J. Herrmann

Studies of nonlinear phenomena in magneto-plasmonic waveguides are of great interest, not only due to their fundamental importance but also because of potential applications in integrated nanoplasmonic devices for diverse functionality in chip-scale plasmonic communication systems.

A magnetic material irradiated by circularly polarized light induces a magnetization along the wave vector. This effect is called the inverse Faraday effect (IFE). The light-induced magnetization is proportional to the helicity of the incident light wave and vanishes for linearly polarized waves. Left- and right-handed circular polarization induces magnetization of opposite signs.

While light cannot penetrate into a thin metallic layer, under appropriate conditions surface plasmon-polaritons (SPP) can be excited. These hybrid electron-photon excitations move along the metal surface. Since SPPs exhibit a longitudinal component of the electric field, its chirality does not vanish. Hence, even for a linearly polarized input beam, magnetization can be induced by the plasmons generated by the incident light, even though the plasmons are not circularly polarized in the conventional sense.

In the paper by S.-J. Im *et al.*, a new type of ultrafast nonlinearity of surface-plasmon-polaritons (SPP) in planar magneto-plasmonic structures is predicted. This nonlinearity is based on the inverse Faraday effect. Specifically, the work shows that SPPs with a significant longitudinal component of the electric field can create, via the IFE, an effective transverse magnetic field in magnetic thin layers. Its response to the plasmon propagation leads to a strong ultrafast third-order nonlinearity. The new nonlinearity exceeds the optical Kerr effect of typical dielectric materials by five orders of magnitude and that of gold by two orders of magnitude.

To quantify this new type of IFE-based nonlinear susceptibility in a planar plasmonic structure including a ferromagnetic layer, the group used the Lorentz reciprocity theorem, deriving analytical expressions. The new nonlinearity plays similar role in the plasmonic propagation as the optical Kerr effect, but it originates from a different physical mechanism and differs from the traditional Kerr-related nonlinear susceptibility in magnitude, frequency dependence and the dependence on material parameters.

Magneto-plasmonic structures as building blocks open doors to a new class of plasmonic devices on the nanoscale, such as optical phase modulators, isolators and optical clocks that will satisfy key applications in nanoscale information networks.

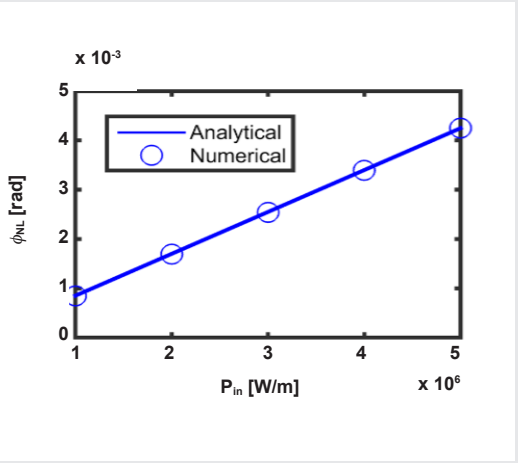

Fig. 1:
Power dependence of the nonlinear phase shift at the carrier wavelength of 1550 nm and for a propagation distance of 1 µm.

Publication

IRH17: S.-J. Im, C.-S. Ri, K.-S. Ho, and J. Herrmann; Third-order nonlinearity by the inverse Faraday effect in planar magnetoplasmonic structures; Phys. Rev. B **96** (2017) 165437/1-6

Short Description of Research Projects

1.1: Fundamental of Extreme Photonics

O. Smirnova, F. Intravaia (project coordinators)
and N. Acharyya, A. A. Andreev , D. Ayuso, I. Babushkin, W. Becker, T. Bredtmann, K. Busch, B. Fingerhut, A. G. Harvey, J. Herrmann, A. Husakou, M. Ivanov, Á. Jiménez Galan, J. Kaushal, Z. Mašín, F. Morales, M. Oelschläger, A. F. Ordóñez-Lasso, M. Osswald, S. Patchkovskii, A. Perez-Leija, E. Pisanty, D. Reiche, H. Reiss, Maria Richter, Martin Richter, R. E. F. Silva, S. Solovyev, F. Trigub, K. Tschernig, P. Varyti

1. Overview

The main objective of the Project 1.1 is the development of analytical and numerical methods for the description of light-matter interactions in extreme conditions. In particular, the number of photons in the electromagnetic field incident on a quantum or semi-classical system can range from zero (vacuum fluctuations), or just a few (quantum electrodynamics and quantum optics regime), to hundreds and thousands of absorbed or emitted photons during the interaction with very intense, mid-infrared (MIR) and terahertz (THz) laser fields. In the case of a low number of photons, the quantum properties of matter and light play a very important role in the description of the interaction and the quantum system. For high intensity fields, the description of light as a classical electromagnetic wave is generally enough, but a precise description of the (often highly nonlinear) quantum response of matter is needed. Non-perturbative theoretical models and methods are developed and applied, focusing on adequate description of system's optical properties and geometrical structure, as well as on many-body effects such as electron-electron correlation, coupled electronic and nuclear dynamics, and the role of quantum coherence in these dynamics. The range of material systems involves atoms, molecules, solids, including nanoscale systems, and photonic structures such as waveguides.

2. Topics and collaborations

The project is currently organized in four general directions:

T1: Theory of attosecond and few-femtosecond electron dynamics

T2: Theory of matter in intense laser fields

T3: Systems with zero or a few photons (Joint HU-MBI Group on Theoretical Optics)

T4: Bio-molecular dynamics in condensed phase.

Emerging direction: Many-body effects and self-organization in strongly correlated systems and their spectroscopy.

Collaboration partners: IC London, UK; HU Berlin, Germany; TU Berlin, Germany; Weizmann Institute, Israel; CEA Saclay, France; CELIA and U Bordeaux, France; U Ottawa, Canada; Ohio State University, USA; RQC Moscow, Russia; UA Madrid, Spain; U Trieste, Italy; Open University; XLIM Limoges, France; U Sherbrook, Canada; ETH Zurich, Switzerland; University of Central Florida, USA; UPMC Paris, France; U Sarajevo, Bosnia and Herzegovina; U Geneva, Switzerland.

In-house collaborations with Projects 1.2, 2.1, 2.2, 2.3, 3.1, and 3.2.

3. Results in 2017

For each of the general directions, representative highlights are given below.

T1: Light amplification during propagation of intense light in gases

The efficient generation of ultra-short laser pulses in the extreme-ultraviolet (XUV) region is central to time-resolved optical sciences. High-order harmonic generation (HHG) is capable of producing such radiation in compact table-top setups with high repetition rates, but with low conversion efficiency. Finding ways to increase this efficiency is important from both fundamental and practical perspective.

Another, seemingly unrelated problem is lasing in open air during the propagation of powerful laser pulses, which leads to laser filamentation. For a range of input powers, filamentation leads to self-guiding of the laser pulse in the medium. The self-guiding can be accompanied by lasing at new frequencies, typically in the visible and near ultraviolet (UV) range, with potentially important applications in remote sensing.

From a purely theoretical perspective, both problems are formulated as amplification of a weak probe signal by atoms or molecules "dressed" by intense laser fields. Previously, we have developed [BCB16, BPI16] rigorous quantum-mechanical theory for studying the possibility of gain in a strongly driven (dressed) quantum system, possibly undergoing rapid ionization. In 2017, we have applied this technique to both problems: amplification of XUV radiation during high harmonic generation in gases [BPI17] and lasing in atomic gases during laser filamentation.

We have identified [BPI17], for the first time, a clear gain mechanism operating in both regimes. The strong IR driving pulse populates Rydberg states via frustrated tunneling [NGS08], creating an effective population inversion between the strongly driven but stable against ionization Rydberg states and the lowest excited states. For sufficiently high IR intensity, even the ground state is deplet-

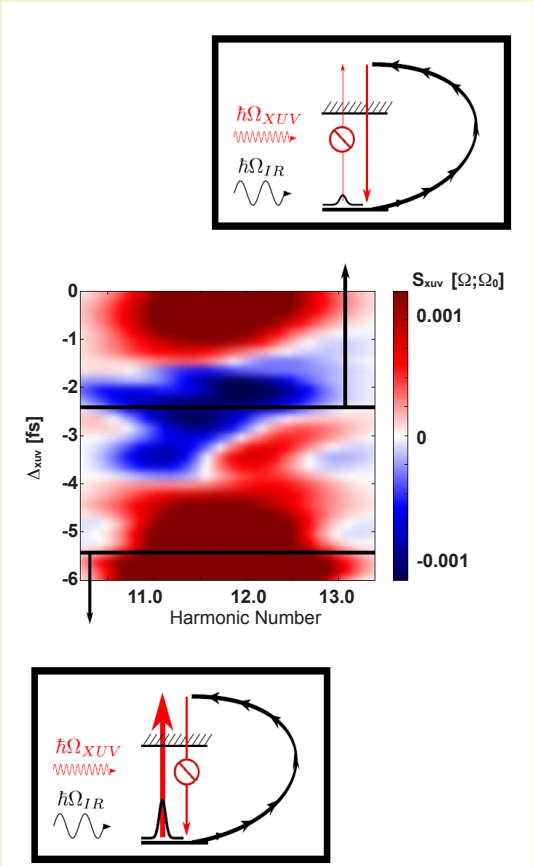

Fig. 1:
Strong-field driven XUV amplification in the hydrogen atom: XUV transient absorption signal, S_{XUV}, as function of the IR–XUV time delay, Δ_{XUV}, and the XUV frequency, Ω_{XUV}. (measured in the harmonic numbers), for the eight-cycle 800 nm IR driving pulse with intensity IR = 6 x 10^{14} W/cm^{-2} and a weak XUV probe pulse with total duration 2.7 fs and central frequency $\Omega_{0,XUV}$ = 18.3 eV.

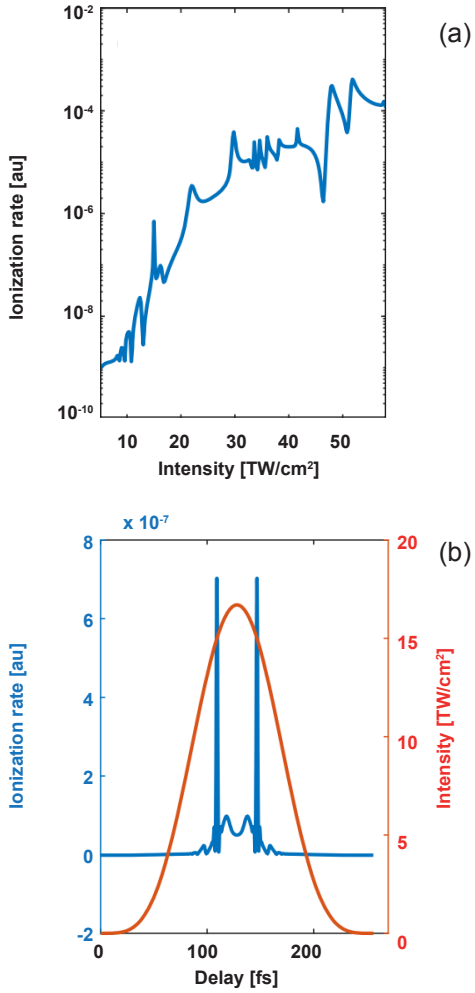

Fig. 2:
The dependence of the ionization rate on the intensity (a) and single-cycle ionization bursts (b) for 240 fs pump pulse in atomic hydrogen.

ed, leading to inversion with respect to the ground state and overcoming the main loss mechanism: XUV absorption from the ground state into the continuum, see Fig. 1.

While promising, the atomic amplification cross sections are nevertheless intrinsically limited by the spreading of the continuum wavepacket. Also, the range of XUV energies where amplification is possible is limited to the vicinity of the ionization threshold. Our calculations on a model molecular system suggest that both restrictions can be relaxed in molecules or clusters.

T1: Symmetry breaking and strong persistent plasma currents via frustrated tunneling

The dynamics of atomic photoionization is central to many recent advances in optics and in physics in general. In 2017, in collaboration with Project 2.2, we have shown theoretically and experimentally [ZPI17] that Freeman resonances, which occur due to the Stark shift of multiphoton-photon resonances, and frustrated tunneling – the recapture of the tunneled electron into the Rydberg states – represent the frequency-domain and the time-domain views of the same process.

Then, in our paper [BHD17], we have shown that this process is able to generate ultra-short spikes of ionization, even on the sub-laser-cycle time-scale. This sub-cycle dynamics breaks the symmetry of the ionization process, leading to the generation of a new comb-like structure in a broad frequency range from THz to visible.

To analyze the ionization process and coherent emission of new frequency components we have utilized both the Floquet eigenfunction formalism and the solution of the time-dependent Schrödinger equation (TDSE). In Fig. 2 the dependence of the ionization rate on intensity and time is shown, exhibiting several sharp Freeman resonances and two pronounced ultrashort ionization bursts. The existence of such isolated bursts leads to unusual spectral signatures of the emitted radiation, in particular, to generation of persistent currents and correspond-ing emission of THz radiation.

In Fig. 3(a), we show the output spectrum for different intensities, indicating efficient generation of broadband radiation including the THz radiation. The sub-cycle nature of the plasma bursts suggests dependence of the dynamics on the carrier-envelope phase (CEP). Indeed, in Fig. 3(b) we predict significant and sensitive dependence of the induced current on the CEP even for very long 240 fs pulses.

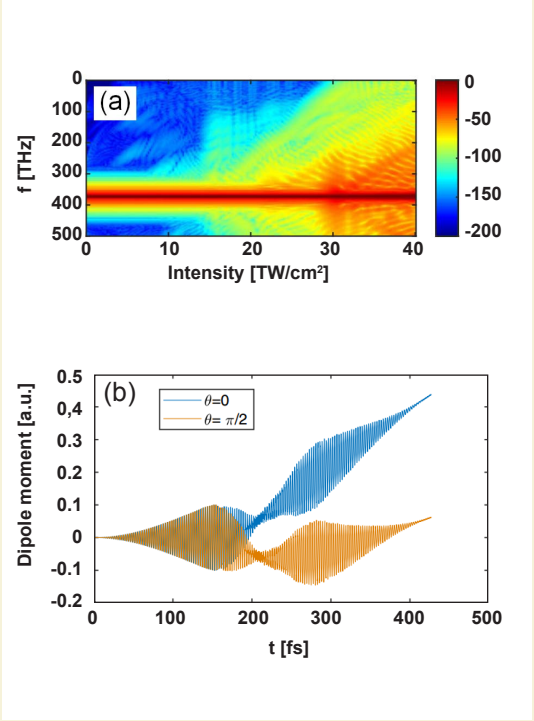

Fig. 3:
The map of emitted spectrum as a function of intensity (a) and CEP dependence of the induced dipole momentum (b) obtained by direct solution of TDSE.

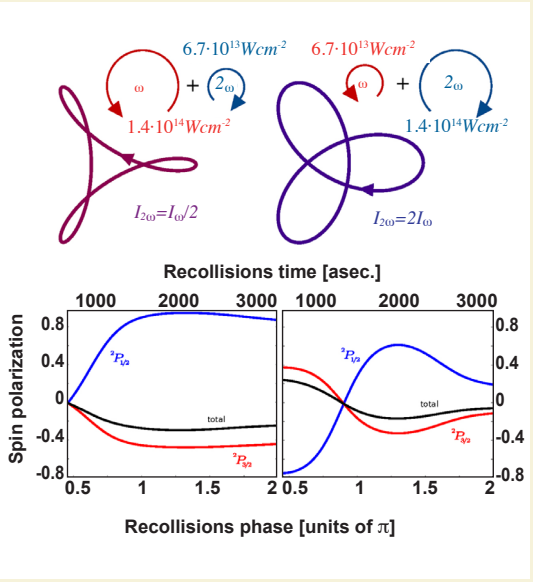

Fig. 4:
Attosecond control of spin polarization. Upper figures: Lissajous curves representing the electric fields resulting from combining a right-circular 800 nm field with the counter-rotating second harmonic, for different relative intensities (marked in the top panel). Middle panels: recollision energy as a function of the recollision time. Lower panels: spin polarization as a function of the recollision time. Results have been calculated by keeping the time of return on the real time axis.

T2: Generation of spin-polarized electrons by strong-field ionization

The possibility of generating spin polarized electrons by using intense laser fields has been pioneered at the MBI [BSm13]. Tunnel ionization of noble gas atoms driven by a strong circularly polarized laser field generates spin-polarized electrons correlated to the spin-polarized ionic core. However, in circularly polarized fields the liberated electrons are spun away by the strong laser field, never returning to the parent ion. Bringing the laser-driven electron back to the parent ion is possible with linearly polarized laser fields, but then the spin-polarization is absent. Fortunately, there are solutions to this problem [HMK16, Mil16]. Our work [HMK16] has shown that strong spin polarization is generated already at modest ellipticities of the driving laser field, without too much loss in the probability of the electron return to the parent ion. When the fundamental laser field is combined with its second harmonic rotating in the opposite direction, spin-polarized electrons can return to the parent ion with high efficiency, enabling the scattering of the spin-polarized electron on the spin-polarized parent ion [Mil16].

In our 2017 work [AJM17] we have shown how one can control the degree of spin polarization as a function of electron energy and recollision time by tuning the laser parameters, such as the relative intensities of the counter-rotating fields. The attosecond precision of the control over the degree of spin polarization opens the door for attosecond control and spectroscopy of spin-resolved dynamics.

The degree of spin polarization in recollision is shown in Fig. 4 as a function of the recollision time, both total and resolved on the two spin-orbit split states of the ionic core, for Xenon. In particular, we analyze the effect of varying the relative intensities of the two counter-rotating fields. Increasing the relative intensity of the fundamental field shrinks the width of the field lobes. Enhancing the relative intensity of the second harmonic has the opposite effect. The corresponding recollision energy and spin polarization, obtained with these fields, are shown as a function of the recollision time, for one optical cycle of the fundamental field. We can see that control of the relative field intensities leads to dramatic changes in the degree of polarization. In particular, it is possible to select the instant at which spin polarization changes it sign: increasing the intensity of the fundamental field shifts the change of sign towards earlier times, whereas increasing the intensity of its second harmonic has the opposite effect.

Each return time is associated with a given recolli-sion energy (Fig. 4, middle panel). Figure 5 shows spin polarization as a function of the recollision energy for short

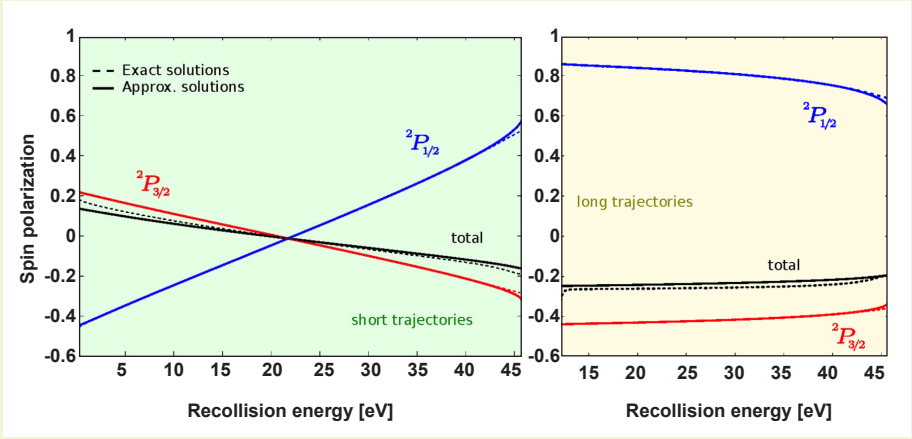

Fig. 5:
Total spin polarization (black lines) and spin polarization resolved on the $P_{3/2}$ (red lines) and $P_{1/2}$ (blue lines) states of the core as a function of the recollision energy for short (left panel) and long (right panel) trajectories, for equal laser intensities of both driving fields, $I = 10^{14}$ W/cm^2.

and long trajectories, for equal intensities of both driving fields. Whereas for the short trajectories spin polarization changes dramatically as a function of the recollision energy, for the long tra-jectories the variation is rather smooth.

Strictly speaking, the correlation between the continuum electron and the hole, i.e. the state of the ion, is beyond classical: the generated wave function describes the entangled electron-hole state. The quantum aspect of electron-ion correlation will manifest in the case of spin-changing and/or inelastic recollisions, which will leave the ion in the same final state after the recollision but will have different intermediate spin-polarized electron-ion states before it. It will also matter for radiative electron-hole recombination – the process responsible for high harmonic generation – which will bring the two parts of the full wave function to the same final state. The quantum nature of electron-ion correlation also manifests in the antisymmetrization of the full wave function, which affects exchange contribution to re-scattering and significantly impacts such processes as recollisiondriven non-sequential double ionization. The possibility of inducing recollision of spin-polarized electrons with the parent ion can open new directions in attosecond spectroscopy.

T3: Systems with zero or a few photons (Joint HUMBI Group on Theoretical Optics)

Quantum mechanics gives rise to numerous fascinating physical effects, especially on submicrometer scales. A prominent class are fluctuation-induced interactions, such as the van der Waals force between two atoms or an atom and a macroscopic object. Recently, there has been a renewed interest in understanding the behavior of interactions in nonequilibrium systems, when one of the objects is in relative motion with respect to the others. A para-digmatic example of phenomena occurring in such case is quantum friction that is a contactless frictional force mediated by the vacuum fluctuations of the electromagnetic field. Many of the articles describing this interaction usually consider an atom (or some other microscopic object) moving in front of a flat surface composed by a material modeled using local optics. At short distances from the surface, where the force is having its largest value, a local description of the material becomes, however, inadequate. Phenomena such as Landau damping connected with nonlocal properties of the material start to be relevant, affecting the behavior of the interaction. Within this scenario we extended the description of quantum friction to nonlocal materials and showed indeed that, for atom-surface separations smaller than electron's mean free path, this quantum drag force is enhanced up to three orders of magnitude with respect to its local counterpart (see Fig. 6). In addition, in a full nonequilibrium description and unlike the treatment based on local optics, spatial dispersion changes not only the strength but also the distance scaling of quantum friction as well as the relevance of nonequilibrium corrections with respect to the commonly used local thermal equilibrium (LTE) approximation.

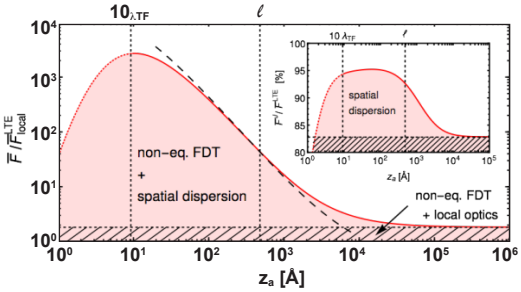

Fig. 6:
Enhancement due to spatial dispersion of the quantum frictional force acting on an atom moving above a surface made by a non-local material. The interaction is characterized by two length scales: The Thomas-Fermi wavelength λ_{TF} and the electron mean-free path ℓ. Adapted from [RDB17].

In a closely related context, we have also shown that photonic lattices can be used to effectively tailor the dynamics of classical and quantum light fields in an advanced-retarded (A-R) fashion. Our strategy here is to exploit the duality between light propagation in space and time evolution, specifically our A-R photonic approach exploits the isomorphism existing between the

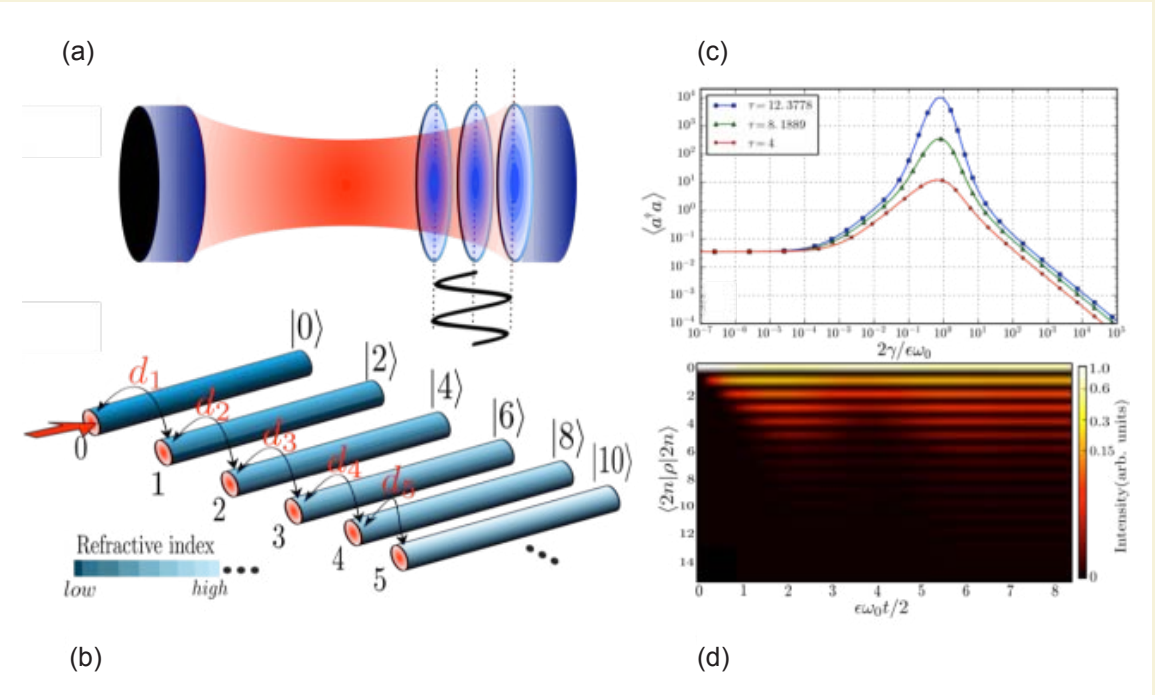

Fig. 7:
(a) Schematic representation of a nonstationary optical cavity, in which the dynamical Casimir effect is manifested.
(b) Proposed semi-infinite squeezed-like waveguide array for the simulation of photon production from vacuum.
(c) Enhancement of photon generation as a function of the scaled dephasing rate at three revival times.
(d) Evolution of the diagonal elements of the system's density matrix. Adapted from [APE17, RRP17, and SPB17].

steady state of judiciously-designed photonic waveguide circuits and solutions of A-R differential equations.

In another project, we have theoretically investigated the dynamical Casimir effect in a single-mode cavity endowed with a driven off-resonant mirror. We have explored the dynamics of photon generation as a function of the ratio between the cavity mode and the mirror's driving frequency (see Fig. 7).

Finally, we have studied the different notions of quantum correlations in multipartite systems of distinguishable and indistinguishable particles. Based on the definition of quantum coherence for a single particle, we have considered two possible extensions of this concept to the many-particle scenarios and determine the influence of the exchange symmetry.

Moreover, we have characterized the relation of multiparticle coherence to the entanglement of the compound quantum system. For different correlated states in the bipartite and multipartite scenarios, we have been able to provide a comprehensive characterization of the various forms and origins of quantum correlations.

T4: Coarse-grained representation of the quasi adiabatic propagator path integral for the treatment of non-Markovian long-time bath memory

The description of dissipative quantum dynamics subject to non-Markovian system-bath memory poses persistent challenges that arise in particular for systems of biological relevance, e.g., composed of multiple exciton states coupled to charge transfer states. Moreover, the 'sluggish' protein environment imposes system-bath memory times of substantial length. We have developed a novel, non-perturbative path-integral approach to study quantum dynamics in the presence of coupling to a thermal bath [RFi17]. The method relies on an intermediate coarse-grained representation of Feynman-Vernon influence coefficients, exploiting physical properties of system decoherence in the form of the initial fast decay of the bath correlation function.

The numerical method speeds up simulations dramatically which brings much larger systems into reach. As a result, this new technique (termed MACGIC-iQUAPI method) has significant potential for time-resolved biophysics and physical-chemistry applications and provides benchmark for novel approximate methods. Numerical performance is demonstrated for a set of benchmark problems that cover bath assisted long range electron transfer (Fig. 8), the transition from coherent to incoherent dynamics in a prototypical molecular dimer and excitation energy transfer in a 24-state model of the Fenna-Matthews-Olson trimer complex where in all cases excellent agreement with numerically exact reference data is obtained.

Crossings of electronic potential energy surfaces in nuclear configuration space, known as conical intersections, determine the rates and outcomes of a large class of photochemical molecular processes. Much theoretical progress has been made in computing strongly coupled electronic and nuclear motions at different levels,

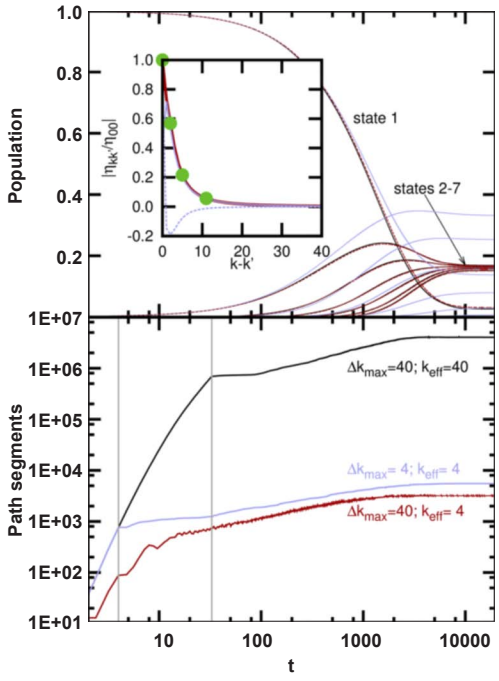

Fig. 8:
Top: Population dynamics of a seven-state model of bath assisted long range electron transfer; red - MACGIC-iQUAPI with ∆kmax = 40 and mask size keff = 4; black - OFPF reference results with ∆kmax = 40; blue - OFPF results with ∆kmax = 4; black arrows denote the canonical equilibrium population of high and low energy states, respectively. The inlay shows the decay of DVR influence functional coefficients ηkk' (red - absolute value, blue solid - real part, blue dotted - imaginary part), green points mark the significant path segments of the mask function M. Bottom: Number of consid-ered path segments, grey vertical lines denote bath memory times 4∆t and 40∆t, respectively.

but how to incorporate them in different spectroscopic signals and the approximations involved are less established. This has been the focus of a recent review [KFD17] in collaboration with the group of Prof. S. Mukamel (University of California, Irvine - UCI). The review surveys a wide range of time-resolved spectroscopic techniques which span from the infrared to the X-ray regimes and can be used for probing the nonadiabatic dy-namics in the vicinity of conical intersections. Transient electronic and vibrational probes and their theoretical signal calculations are classified by their information content. This includes transient vibrational spectroscopic methods (transient infrared and femtosecond off-resonant stimulated Raman), resonant electronic probes (transient absorption and photoelectron spectroscopy), and novel stimulated X-ray Raman techniques. Along with the precise definition of what to calculate for predicting the various signals, a toolbox of protocols for their simulation is outlined.

Own Publications 2017 ff

(for full titles and list of authors see appendix 1)

AAB17: R. M. Arkhipov *et al.*; Quantum Electron. **47** (2017) 589-592

AAP17a: M. V. Arkhipov *et al.*; Opt. Lett. **42** (2017) 2189-2192

AAP17b: R. M. Arkhipov *et al.*; Optics and Spectroscopy **122** (2017) 949–954

AAP17c: R. M. Arkhipov *et al.*; Laser Phys. Lett. **14** (2017) 095402/1-6

AAP17d: R. M. Arkhipov *et al.*; Optics and Spectroscopy **123** (2017) 610-614

ABP17: M. V. Arkhipov *et al.*; Optics and Spectroscopy **122** (2017) 670-674

AJC17: L. Argenti *et al.*; Phys. Rev. A **95** (2017) 043426

AJM17: D. Ayuso *et al.*; New J. Phys. **19** (2017) 073007/1-10

APA17a: R. M. Arkhipov *et al.*; Sci. Rep. **7** (2017) 12467/1-21

APA17b: R. M. Arkhipov *et al.*; JETP Letters **105** (2017) 408-418

APA17c: R. M. Arkhipov *et al.*; Laser Phys. **27** (2017) 053001/1-10

APD17: D. Ayuso *et al.*; Phys. Chem. Chem. Phys. **19** (2017) 19767-19776

APE17: U. Alvarez-Rodriguez *et al.*; Sci. Rep. **7** (2017) 42933/1-6

Bab17: I. Babushkin; Phys. Rev. A **95** (2017) 042101/1-13

BBD17: I. Babushkin *et al.*; J. Mod. Opt. **64** (2017) 1078-1087

BHD17: C. Brée *et al.*; Phys. Rev. Lett. **119** (2017) 243202/1-5

BHH17: D. S. Brambila *et al.*; Phys. Chem. Chem. Phys. **19** (2017) 19673-19682

BHI17: D. S. Brambila *et al.*; Phys. Rev. A **96** (2017) 063825/1-5

BPI17: T. Bredtmann *et al.*; New J. Phys. **19** (2017) 073011/1-11

DMT17: D. Darby-Lewis *et al.*; J. Phys. B **50** (2017) 175201/1-12

HAC17: A. Husakou *et al.*; Nonlin. Phenomena Complex Syst. **20** (2017) 1-11

Hus17: A. Husakou; J. Opt. Soc. Am. B **34** (2017) 137-141

IRH17: S.-J. Im *et al.*; Phys. Rev. B **96** (2017) 165437/1-6

IRP17: S.-J. Im *et al.*; Appl. Phys. Lett. **111** (2017) 071102/1-4

JZS17: Á. Jiménez Galán *et al.*; Opt. Express **25** (2017) 22880-22896

KFD17: M. Kowalewski *et al.*; Chem. Rev. **117** (2017) 12165–12226

KHH17: K.-H. Kim *et al.*; in *Nanoplasmonics: Funda* (IntechOpen, 2017) 96-115

KRH17: G. Kewes *et al.*; Phys. Rev. Lett. **118** (2017) 237402/1-6

KTU17: E. Kukk *et al.*; Phys. Rev. A **95** (2017) 042509/1-12

MBP17: L. Medišauskas *et al.*; J. Phys. B **50** (2017) 144001/1-9

OSM17a: A. F. Ordóñez-Lasso *et al.*; Phys. Rev. A **96** (2017) 052503/1-13

PAB17: A. V. Pakhomov *et al.*; Phys. Rev. A **95** (2017) 013804/1-8

PJi17: E. Pisanty and Á. Jiménez Galán; Phys. Rev. A **96** (2017) 063401/1-18

RAA17: N. N. Rosanov *et al.*; Opt. Spectrosc. **123** (2017) 100-104

RDB17: D. Reiche *et al.*; Phys. Rev. B **95** (2017) 155448/1-10

RFi17: M. Richter and B. P. Fingerhut; J. Chem. Phys. **146** (2017) 214101/1-13

RRP17: R. Román-Ancheyta *et al.*; Phys. Rev. A **96** (2017) 032501/1-6

SPB17: J. Sperling *et al.*; Phys. Rev. A **96** (2017) 032334/1-11

SPP17: D. E. Shipilo *et al.*; Laser Phys. Lett. **14** (2017) 035401/1-6

TSm17: L. Torlina and O. Smirnova; New J. Phys. **19** (2017) 023012/1-13

Other Publications

BCB16: T. Bredtmann *et al.*; Phys. Rev. A **93** (2016) 021402

BPI16: T. Bredtmann *et al.*; Phys. Rev. Lett. **117** (2016) 10940

BSm13: I. Barth and O. Smirnova; Phys. Rev. A **88** (2013) 013401

HMK16: A. Hartung *et al.*; Nature Photonics **10** (2016) 526-528

Mil16: D. B. Milošević; Phys. Rev. A **93** (2016) 051402(R)

NGS08: T. Nubbemeyer *et al.*; Phys. Rev. Lett. **101** (2008) 233001

ZPI17: H. Zimmermann *et al.*; Phys. Rev. Lett. **118** (2017) 013003/1-5

Invited Talks at International Conferences

(for full titles see appendix 2)

K. Busch; 2nd Int. SFB/TRR 142 Workshop on Tailored Nonlinear Photonics (Paderborn, Germany, 2017-02)

K. Busch; SPIE Optics + Optoelectronics (Prague, Czech Republic, 2017-04)

K. Busch; CLEO Europe-EQEC 2017 (Munich, Germany, 2017-06)

K. Busch; PIERS 2017, Keynote Talk in the Focus Session “Electromagnetic Waves in Complex Nanostructures” (Singapore, 2017-11)

B. P. Fingerhut; 5th Molcas Developers’ Workshop (Jerusalem, Israel, 2017-02)

B. P. Fingerhut; FEMTO’13 (Cancun, Mexico, 2017-08)

B. P. Fingerhut, TRSC Vibrational Dynamics 2017 (Telluride, CO, USA, 2017-08)

B. P. Fingerhut; 11th Triennial Congress of the World Association of Theoretical and Computational Chemists, WATOC (Munich, Germany, 2017-08)

F. Intravaia; META 2017 (Seoul, South Korea, 2017-07)

F. Intravaia; Workshop on Dispersion Forces and Dissipation (Leipzig, Germany, 2017-11)

M. Ivanov *together with* T. Bredtmann, F. Morales, and S. Patchkovskii; The Winter Colloquium on the Physics of Quantum Electronics, PQE-2017, (Snowbird, Utah, USA, 2017-01), plenary talk

M. Ivanov; Workshop Advanced Material Science (Dresden, Germany, 2017-09)

M. Ivanov; Int. Workshop of Computational and Theoretical Nanoscience (Madrid, Spain, 2017-11)

F. Morales; The Winter Colloquium on the Physics of Quantum Electronics, PQE-2017 (Snowbird, Utah, USA 2017-01)

S. Patchkovskii; 30th Int. Conference on Photonic Electronic and Atomic Collisions, ICPEAC XXX (Cairns, Australia, 2017-07)

S. Patchkovskii; Intense Field, Short Wavelength Atomic and Molecular Processes, ISWAMP, ICPEAC Satellite Meeting (Brisbane, Australia, 2017-07)

S. Patchkovskii; 6th Int. Conference on Attosecond Physics, ATTO'17 (Xi'an, China, 2017-07)

M. Richter; The Winter Colloquium on the Physics of Quantum Electronics, PQE-2017 (Snowbird, Utah, USA, 2017-01)

R. E. F. Silva; Mid-Infrared Meeting 2017, MURI MIR (Washington, USA, 2017-04)

O. Smirnova; The Winter Colloquium on the Physics of Quantum Electronics, PQE-2017 (Snowbird, Utah, USA, 2017-01), presented by M. Ivanov

O. Smirnova; WPC Theory Workshop (Hamburg, Germany, 2017-06)

O. Smirnova; 30th Int. Conference on Photonic, Electronic and Atomic Collisions, ICPEAC XXX (Cairns, Australia, 2017-07)

O. Smirnova; 14th Int. Conference on Multiphoton Processes, ICOMP (Budapest, Hungary, 2017-09)

O. Smirnova; Workshop on Chiral and Topological Matter (Vancouver, Canada, 2017-12)

1.2: Ultrafast Laser Physics and Nonlinear Optics

G. Steinmeyer, U. Griebner, V. Petrov (project coordinators)
and M. Bock, W. Chen, E. Escoto, T. Feng, L. v. Grafenstein, R. Grunwald, J. Hyyti, M. Kalashnikov, N. Khodakovskiy, R. Liao, M. Mero, X. Mateos, Z. Pan, N. Raabe, A. Treffer, J. Tümmler, Y. Wang, I. Will, Y. Zhao

1. Overview

The main objective of this project is to develop advanced sources of ultrashort pulses in the near- and mid-infrared (IR) wavelength range. To this aim, new laser geometries and pump sources, special operational modes and pulse-shaping techniques are investigated. A major part of the results generated in this project is directly applied for implementing new laser systems for other research projects.

In part this project is dedicated to fundamental research on ultrafast nonlinear optics, carrier-envelope phase effects, pulse characterization, and beam shaping techniques. There currently is a strong trend towards the development of CEP-stable mid-infrared sources at wavelengths >1.5 µm. Such wavelengths are desirable for shorter cut-off wavelengths in high-harmonic generation but also for driving hard X-ray plasma sources, where presently no CEP control is required. A great deal of the activities is devoted to exploring components for such systems which includes characterization and testing of various laser and nonlinear materials in diverse operational regimes. A first complete OPA system for use in other MBI projects, a novel 100 kHz few-cycle OPCPA source, is pumped at ~1 µm and seeded near 1.5 µm, with the option for generation of broadband femtosecond pulses also at ~3 µm. The first two OPA stages of this system were completed in 2016, providing output energies already at the desired level. For reliability reasons the OPA system was redesigned and rebuilt in 2017. The work on a second large scale OPCPA system targeting the 5 µm wavelength range in the mid-IR and aiming at sub-100 fs, 1 kHz pulses, has continued in 2017 with the completion of the femtosecond mid-IR parametric amplifiers delivering unprecedented output parameters.

A separate topic of the project encompasses the development of picosecond thin-disk amplifiers for high output energy at 1 µm. The Yb:YAG thin-disk laser systems pumped with diodes from the Ferdinand-Braun-Institut have been continuously improved and are now applied as drivers for OPCPA with terawatt peak power (Project 4.1).

Activities on ultrahigh intensity lasers are part of the project and were primarily focused on development of methods for improvement of the pulse parameters. This concerns broadening the amplification bandwidth of the gain medium and implementing novel Ti:sapphire thin-disk booster amplifiers.

Moreover, we continued our work on spatio-temporal shaping and characterization of ultrashort wavepackets, employing adaptive optical components. This fundamental research on ultrafast singular optics consists in high-resolution measurements, in particular on array-specific effects and self-reconstruction in the time domain.

2. Topics and collaborations

At present the project is organized in three topics:

T1: Ultrafast nonlinear optics

Partly supported by DFG (STE 762/11-1, GR 1782/14-1 and GR 11782/14-2) and CSC/DAAD

- Carrier-envelope phase noise and stabilization
- Novel nonlinear optical effects
- Adaptive shaping and propagation of structured non-diffracting few-cycle wavepackets
- Advanced pulse characterization methods
- Ultrafast singular optics in the spectral and the temporal domain with high resolution and high sensitivity.

T2: Thin-disk and ultrahigh intensity lasers

Partly supported by EU Laserlab JRA EUROLITE and EU Marie Skłodowska-Curie Foundation (JMAP)

- Application of the developed thin-disk laser systems at 1 µm as driver for an OPCPA amplifier and a soft X-ray plasma source
- Enhancements of the laser systems to the benefit of applications
- Development of methods for broadening the amplification bandwidth in high-energy lasers
- Implementation of thin-disk Ti:sapphire boosters in the high-energy amplifier chains.

T3: Power scaling of diode-pumped femtosecond laser systems beyond Ti:sapphire

Partly supported by EU Marie Skłodowska-Curie Foundation and EU Laserlab JRA ILAT grants

- Ultrafast lasers/amplifiers based on different dopant-host combinations for the 1 to 2 µm spectral range
- Second-order nonlinear frequency conversion for ultrafast systems, especially OPA and OPCPA for down-conversion to longer wavelengths in the near- and mid-IR.

Collaboration partners: M. Guina (ORC, Tampere, Finland), G. Genty (TUT, Tampere, Finland), A. Demircan, U. Morgner (Leibniz-Universität Hannover, Germany), C. Brée (Weierstraß-Institut, Berlin, Germany), R.

Trebino (Georgiatech, Atlanta, GA, USA), A. Fry (SLAC, USA), B. Hofmann (TU Chemnitz, Germany), Y. Song (Tianjin University, China), A. Zach and W. Kaenders (Toptica Photonics, Germany), W. Hänsel and R. Holzwarth (Menlo Systems, Germany), U. Wallrabe (IMTEK, University Freiburg, Germany), metrolux GmbH (Göttingen, Germany), J. Jahns (FernUniversity, Hagen, Germany), W. Seeber (Otto Schott Institute, FSU Jena, Germany), E. McGlynn (School of Physics, Dublin City University, Ireland), F. Güell (University Barcelona, Spain), HoloEye Photonics AG (Berlin, Germany), F. Diaz (University Tarragona, Spain), P. Fuhrberg (LISA laser OHG, Germany), H. Zhang (Shandong University, P. R. China), F. Rotermund (Ajou University, Korea), A. Agnesi (Pavia University, Italy), J. Liu (Qindao University, China), A. Kovacs, K. Osvay (University Szeged, Hungary), M. Romanovsky (General Physics Institute, Russia), A. Savelev (Moscow State University, Russia), B. Kanngießer (TU Berlin, Germany), L. Isaenko (DTIM Novosibirsk, Russia), V. Pasiskevicius, (KTH, Stockholm, Sweden), P. Schunemann (BAE Systems, Nashua, USA), V. Badikov (HTL, Krasnodar, Russia), K. Kato (Chitose, Japan), I. Buchvarov (Sofia University, Bulgaria), M. Ebrahim-Zadeh (ICFO, Barcelona, Spain), M. Eichhorn (ISL, France), V. Panyutin (Kuban State University, Russia), and G. Arisholm (FFI, Norway).

3. Results in 2017

T1: Ultrafast nonlinear optics

Intrapulse coherence

Coherence is the central concept to distinguish between laser sources and conventional light sources. A single-frequency laser can easily display a coherence length of many kilometers whereas, e.g., the coherence length of an incandescent light source is on the order of the wavelength. While this is known for a long time now, it is not straightforward to unambiguously transfer the concept of coherence length to short-pulse lasers. If one simply measures the first-order correlation function of a few-cycle laser pulse train, e.g., in a Fourier-transform infrared spectrometer (FTIR), one would come to the conclusion that this very laser displays a coherence length that is comparable to an incandescent light source. On the other hand, however, one typically also observes coherence between successive pulses in a mode-locked pulse train, and resulting coherence lengths are similar to those observed in continuous operation of the same laser. This ambiguity leads to two different definitions, namely the interpulse coherence and the intrapulse coherence. The former is often lost when a coherent pulse train is launched into a photonic crystal fiber. Depending on the nonlinearity and the length of the nonlinear propagation, input noise on the level of quantum fluctuation often suffices to induce substantial variations in the output spectra, both in amplitude and phase. Consequently, such broadened spectra are not compressible anymore. Given the rather high repetition rate of a mode-locked laser, it seems virtually impossible to adapt dispersion compensation schemes sufficiently rapid enough to warrant compression anywhere close to the bandwidth limit. In fact, such a white-light source has coherence properties that are nowhere better than a light bulb.

Quite surprisingly, however, supercontinuum generation in photonic crystal fibers has found ample application in precision frequency metrology. For the latter method, one typically requires a phase comparison between a fundamental frequency and its second harmonic within a white-light supercontinuum, i.e., a method that is known as *f-2f* interferometry. Here the interpulse coherence discussed above does not play any role; as long as

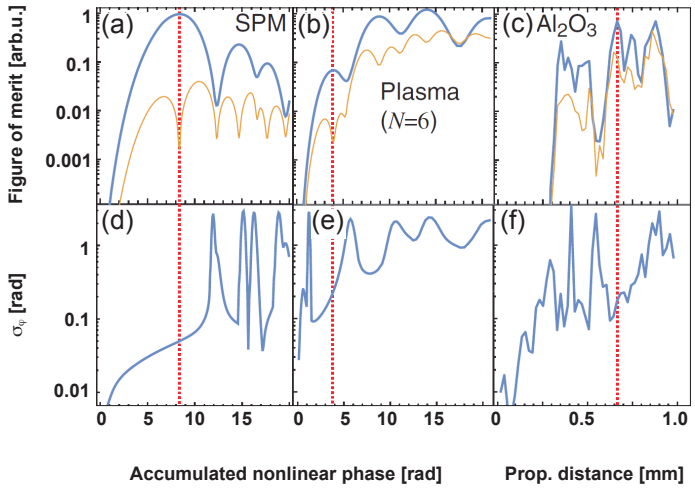

Fig. 1:
Numerical simulations of the intrapulse coherence of supercontinuum pulses according to Eq. (1). Simulations are based on an ensemble of 1000 input pulses with 10 fs duration and 1% energy standard deviation. (a) - (c) Mean value (thick blue line) and standard deviation (thin orange line) of the figure of merit (FOM). The first maximum of the FOM has been marked by a dashed red line.
(d) - (f) Standard deviation of resulting phase fluctuation $\Delta\varphi$. (a), (d) Symmetric spectral broadening due to self-phase modulation. (b), (e) Asymmetric spectral broadening due to plasma generation driven by a multiphoton process of the order of 6. (c), (f) Full simulation of nonlinear propagation in sapphire. Adapted from [RFW17].

pulse energy fluctuations cause common mode phase fluctuations of the f and the 2f spectral component, the resulting phase jitters cancel out and do not corrupt the frequency measurement. To this end, we proposed a new definition of intrapulse coherence [RFW17]

$$\Gamma^{(\mathrm{CEP})} = \frac{|\langle \tilde{E}_i^2(2\lambda)\tilde{E}_i^*(\lambda)\rangle|}{\langle|\tilde{E}_i^2(2\lambda)\tilde{E}_i^*(\lambda)|\rangle} \qquad (1)$$

where $E_i(\lambda)$ is the electric field component of the i-th pulse in a pulse train at wavelength λ. Using this definition, we find very different behavior for different types of spectral broadening: in a self-phase modulation dominated scenario (Figs. 1(a), 1(d)), e.g., as is typically observed in photonic crystal fibers, intrapulse coherence proves to be rather robust. At the "sweet spot" of maximum efficiency within an *f-2f* interferometer, resulting phase noise is rather negligible and stays well below 100 mrad. However, if the spectral broadening scenario becomes asymmetric, as, e.g., in plasma-dominated filament broadening, then the resulting phase fluctuations quickly reach many radians, which turns such spectral broadening useless for frequency metrology or carrier-envelope phase stabilization.

Our analysis clearly shows that intrapulse and interpulse coherence are two completely uncorrelated aspects: regimes exist where one is perfectly maintained but the other is lost. For example, filament compression provides perfectly compressible pulse whereas such supercontinua appear utterly unsuitable for CEP-stabilization. In contrast, fiber-based supercontinua often prove to be incompressible while they show remarkable resistance against a loss of intrapulse coherence.

Temporal self-imaging of arrays of nondiffracting few-cycle wavepackets

Adaptive shaping of structured ultrashort wavepackets was performed with spatial light modulators and different types of electrically and thermally driven low-dispersion MEMS axicons. The spatio-temporal propagation characteristics were analyzed by spatially resolved nonlinear autocorrelation. Temporal self-imaging of arrays of needle beams (i.e., the central lobes of ultrashort-pulsed ultrabroadband Bessel beams) was theoretically described and experimentally demonstrated [BTG17, TBW17]. Similar to the well-known diffractive Talbot effect, where a periodic phase or amplitude structure reappears periodically at discrete distances, a periodic revival of zones of undistorted temporal pulse properties is obtained by the geometrical superposition of conical non-diffracting beams in free space. The arrangement is drawn schematically in Fig. 2. A uniform array of microaxicons (diameter *d*, period *a*) generates an array of conical beams propagating with a half conical beam angle θ against the optical axis. Directly behind the axicons, a first array of needle beams appears with a half axial extension of L_0.

Under idealized conditions (narrow angular spectrum, low divergence), non-diffractive self-imaging is expected for distances $[N(a/\tan\theta)+L_0]$, where N is an integer number. Experiments were performed with Ti:sapphire oscillator pulses at an initial pulse duration of about 7 fs. Arrays of needle beams were shaped by a reflective, liquid-crystal-on-silicon spatial light modulator. Two-dimensional second order autocorrelations were detected by an EMCCD camera. For reference measurements, we employed spectral phase interfer-

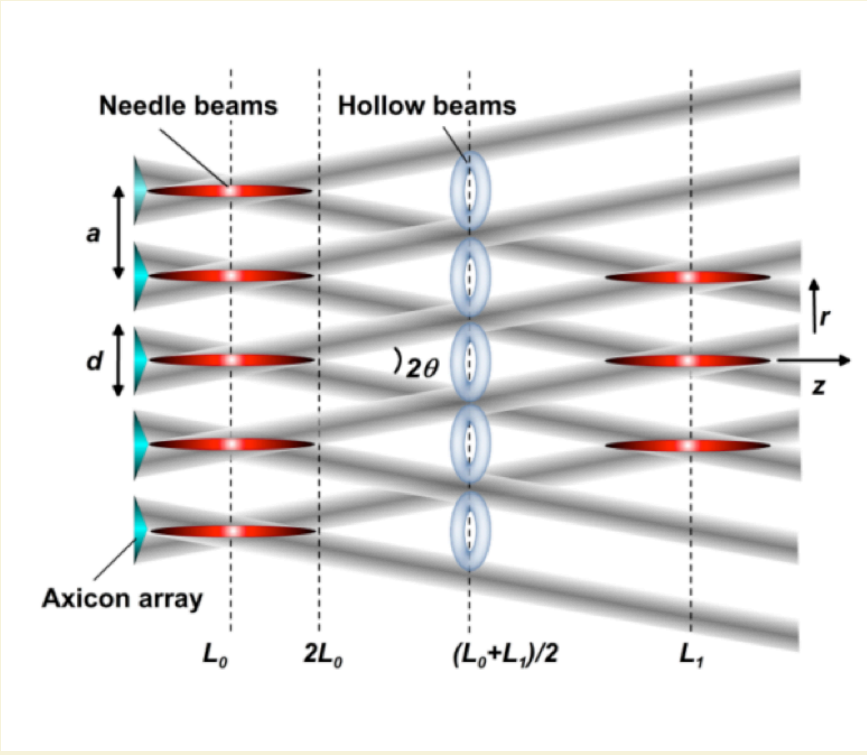

Fig. 2:
Non-diffractive Talbot effect as a periodical constructive interference behind a finite uniform array of axicons of period a and element diameter d (schematically). θ is the half-conical beam angle. Needle beams and ring-shaped hollow beams appear alternatingly (L_0: intensity maxima of first focal zones, L_1: first nondiffractive Talbot distance; $(L_0+L_1)/2$: hollow beams with dark central regions [BTG17].

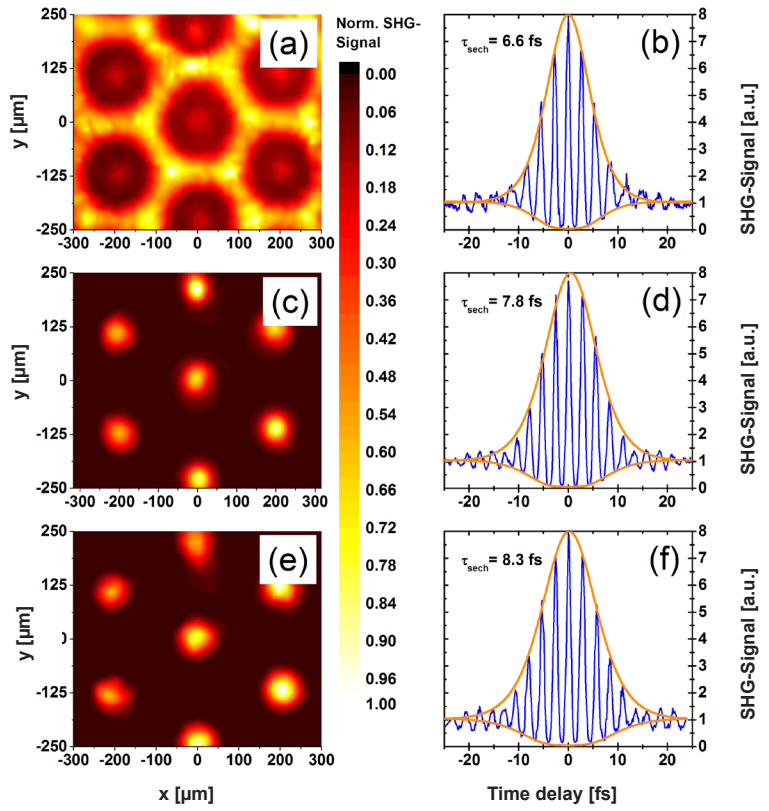

Fig. 3:
Temporal self-imaging of few-cycle pulses demonstrated by spatially resolved second order autocorrelation of several non-diffractive Talbot planes behind a hexagonal array of microaxicons (d = 230 µm, a = 445 µm). Transversal intensity profiles (left) and second order autocorrelation (right) are shown for the axial distances of dark rings $(L_0+L_1)/2$ = 60 mm (a, b), first non-diffractive Talbot distance L_1 = 105 mm (c, d), and second non-diffractive Talbot plane L_2 = 195 mm (e, f). Adapted from [BTG17].

ometry for direct electric-field reconstruction. The illumination was performed at large angles (up to 50°) with ellipticity correction. Measurements of the nonlinear autocorrelation at three different distances show only a slight increase of the pulse duration (Fig. 3). After a propagation distance of 195 mm, the self-image of the needle pulse array in the second non-diffractive Talbot plane has a pulse duration of 8.3 fs, which still qualifies as a 3-cycle pulse.

The results show that (i) nondiffracting or geometrical self-imaging enables to generate distant focused undistorted ultrashort pulses well beyond the Rayleigh ranges of single focused pulses, and (ii) diffractionless geometrical propagation of conical beams can be used to refocus the pulses periodically. In contrast to classical space-time focusing schemes on the basis of diffractive or dispersive stretcher-compressor arrangements, the pulse duration remains largely conserved whereas the intensity is found to be periodically modulated. Non-diffractive self-images of amplitude-modulated wavepackets are generated with angular-dependent time delay between the Talbot planes. Thus, axial positions of self-images and the time scale of subsequent focusing can be tuned with adaptive axicon arrays.

T2: Thin-disk and ultrahigh intensity lasers

High average power thin-disk lasers at 1 µm

The efforts in 2016 allowed us to set-up and operate two home-built high-average power Yb:YAG thin-disk lasers systems at the MBI on a routine basis:

- The first Yb:YAG thin-disk laser is applied as driver for plasma X-ray generation (see Project 3.3).
- The second one has been moved to the former High-Field Laboratory, where it is used as the driver for the TW-OPCPA system being developed in Project 4.1. This work is described in detail in the report on Project 4.1.

The research related tasks of the Yb:YAG thin-disk laser systems within Project 1.2 were finished at the beginning of 2017, and further development of the underlying technology of these lasers is not pursued at the MBI at present.

Nonlinear rotation of the polarization ellipse in a hollow-core fiber

A high temporal contrast of high peak power lasers is achieved by cutting ASE and pre-pulses in a nonlinear medium. Most commonly cross-polarized wave (XPW) generation is used for this purpose. However this method has several issues. It is typically driven at a peak power above the critical power for self-focusing. At these conditions nonlinear spatial effects may degrade the beam profile, reduce the overall efficiency and lead to instabilities in the output spatial profile. Typically the BaF_2 crystals that are used as a nonlinear medium for XPW degrade with time.

In contrast, nonlinear rotation of the polarization ellipse (NER) in gases is not connected with degradation of the gas medium. Applying a hollow-core fiber (HCF)

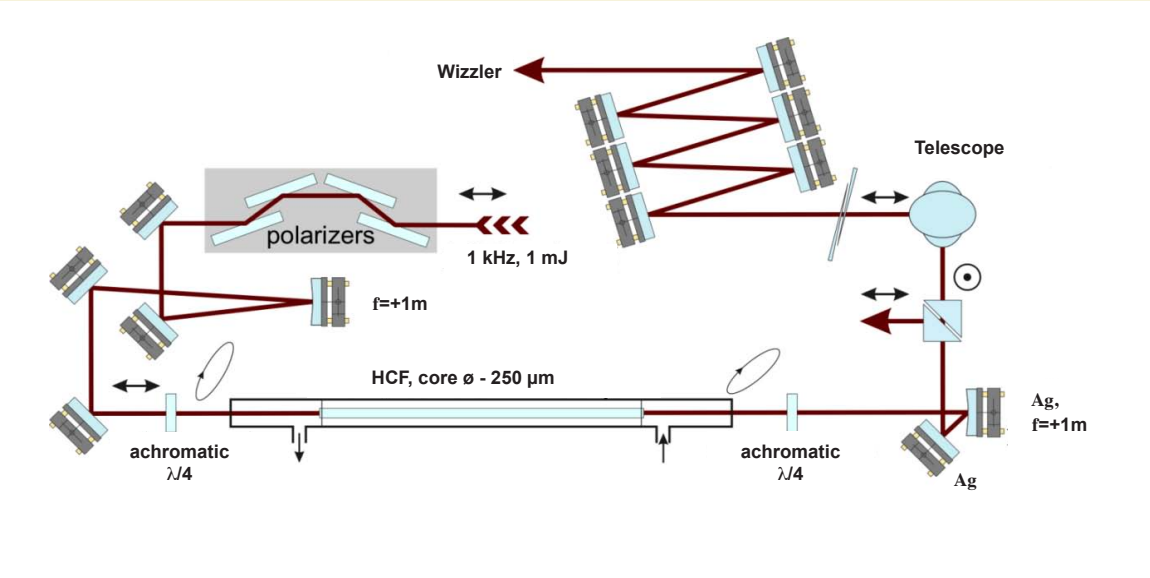

Fig. 4:
Experimental setup for investigation of spectral broadening and recompression of ultrashort pulses at 800 nm via nonlinear rotation of the polarization ellipse in gases (HCF: hollow-core fiber. Ag: silver mirrors).

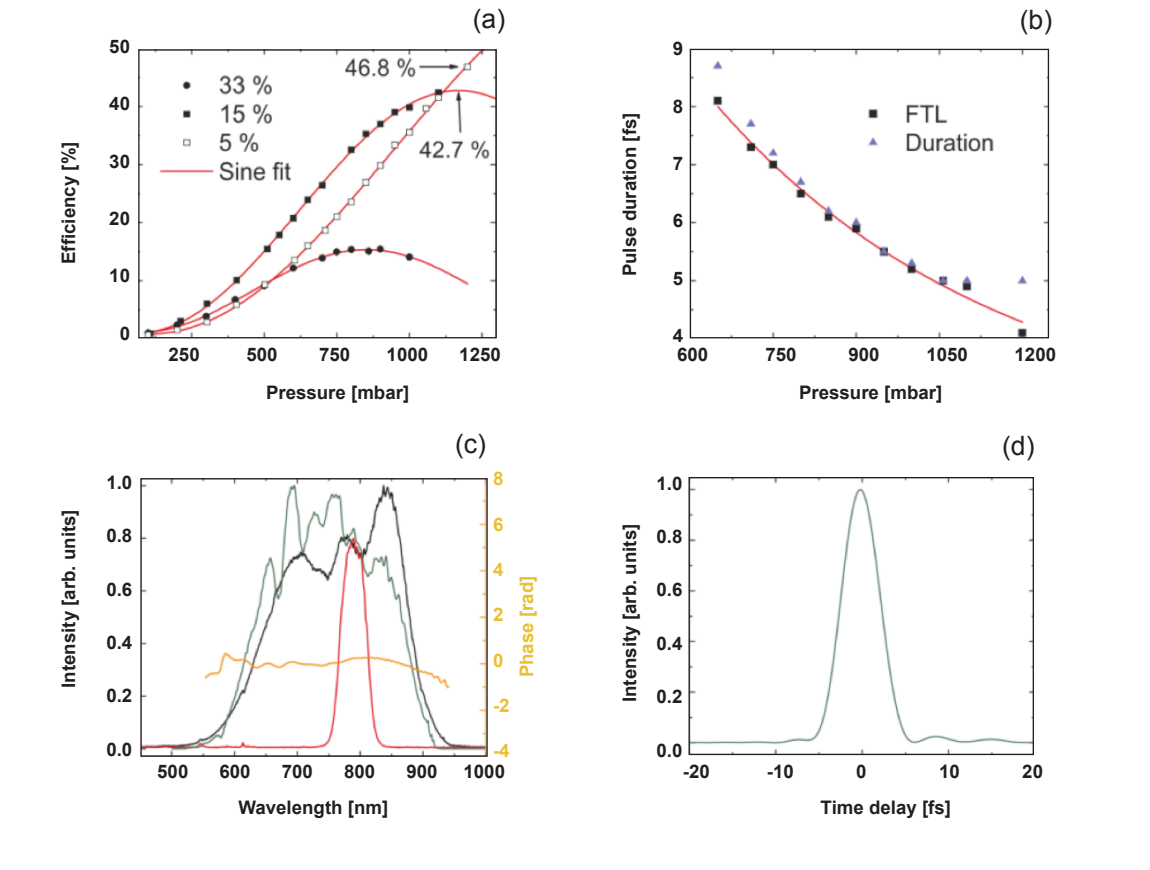

Fig. 5:
Nonlinear rotation of the polarization ellipse (NER) of ultrashort pulses in gases.
(a) NER efficiency as a function of Ar pressure and ellipticity; (b) Duration of the recompressed pulses and spectral FTL measured as a function of Ar pressure for 5% ellipticity, Red: Gaussian fit; (c) Evolution of the laser spectrum. Red: initial laser spectrum, black: spectrum after NER for 5% ellipticity, green: retrieved spectrum, orange: retrieved spectral phase; (d) Retrieved temporal pulse profile at optimal Ar pressure (1.1 bar) for 5% ellipticity.

allows to broaden the pulse spectrum simultaneously during propagation. The guiding nature of the fiber provides extended nonlinear propagation below the critical power for self-focusing with the possibility of adjusting the nonlinear strength by changing the gas pressure. In addition, NER combined with spectral broadening via self-phase modulation (SPM) can be used to shorten the pulse duration.

Preliminary NER experiments were done at MBI using 1 mJ, 800 nm laser pulses at a repetition rate of 10 Hz. Joint experiments followed at LOA in the frame of Laserlab-Europe (project LOA002361).

The experimental scheme is presented in Fig. 4. A CEP stabilized front-end laser system (1.3 mJ, 1 kHz, 30 fs) provided the input pulses. An achromatic λ/4 wave plate set the input ellipticity. 270 μJ pulses are coupled into a flexible 46 cm long, 250 μm core diameter HCF exhibiting a transmission of 68%. Ar gas was fed into the exit of the fiber to achieve a stable pressure gradient. A second achromatic λ/4 wave plate compensates the input ellipticity when the fiber was fully evacuated and no nonlinear rotation occurs. A broadband polarizer, crossed with the first polarizer, was applied to transmit the rotated component of the pulses only, when the gas was fed through the fiber. Subsequently the filtered pulses were re-compressed by a chirped mirror compressor and a wedge pair. A Wizzler USP-4 device was used to measure the compressed pulse duration.

Figure 5(a) shows the measured overall NER efficiency for different input ellipticity as a function of Ar pressure. Maximum efficiency was not reached for the highest ellipticity (5%) due to the onset of self-focusing and ionization at the fiber entrance that was manifested by a drop in transmission. Nevertheless, a very high NER efficiency of 47% was achieved. Figure 5(b) compares the pulse duration retrieved by the Wizzler together with the Fourier-transform limit (FTL) of the broadened NER spectra as a function of Ar pressure for highest ellipticity (5%). The spectral smoothing effect induced by simultaneous NER and SPM is clearly visible as the measured pulse FWHM is close to the FTL. The data starts to diverge around the 5 fs mark, where the pressure inside the fiber starts to degrade the pulse quality. Note that this duration is also quite close to the resolution limit of the Wizzler. Figures 5(c) and 5(d) show the Wizzler measurement results for the highest ellipticity (5%) and the optimal Ar pressure of 1.1 bar. The initial 42 nm input Gaussian spectrum (FWHM) is smoothly broadened up to a remarkably FWHM of 240 nm. The retrieved spectral phase, almost devoid of any modulations (apart from those stemming from the chirped mirrors), warrants re-compression to a near-FTL Gaussian pulse shape with a FWHM of 4.9 fs.

NER in a gas-filled HCF operated in the pressure gradient mode significantly reduces the strong spectral amplitude and phase distortions typically induced by SPM broadening. This method allows to generate routinely high-quality sub-5 fs pulses with the high efficiency for NER (>46%). The temporal contrast enhancement is limited by the extinction ratio of the crossed polarizers (four orders of magnitude) used to discriminate the NER signal.

T3: Power scaling of diode-pumped femtosecond laser systems beyond Ti:sapphire

Sub-100 fs bulk solid-state lasers in the 2 μm spectral range

Exploring novel Tm-doped laser crystals in connection with an advanced dispersion management, the first sub-100 fs bulk solid-state laser in the 2 μm spectral range was demonstrated. Employing graphene with extended wavelength coverage in the IR compared to SWCNTs as a saturable absorber (SA) and chirped mirrors for dispersion management 86 fs pulses were achieved with the monoclinic divalent metal mono-tungstate crystal Tm:$MgWO_4$ (Tm:MgW) [WCM17].

Tm:MgW exhibits very broad and smooth gain characteristics with the gain maximum at 2017 nm. The latter intrinsically avoids the strong water vapor absorption below 1960 nm. The thermal conductivity of the MgW host measured for an arbitrary orientation is ~8.7 W/mK, i.e. almost 3 times higher compared to the previously studied monoclinic double tungstates, such as Tm:$KLu(WO_4)_2$ (~3 W/mK) [ZLZ17].

The employed X-shaped laser cavity with the 0.89 at.% Tm-doped MgW crystal and the graphene-SA (GSA) is shown in Fig. 6. The intracavity group delay dispersion (GDD) was varied by the number of bounces (2, 4, and 6 in single pass) on the plane chirped mirrors CM_2 - CM_5. All CMs exhibited GDD = −125 fs^2 per bounce. As pump source we used a cw Ti:sapphire laser at ~796 nm with up to 2.7 W. Using a bi-layer GSA on 2-mm thick CaF_2 substrate, mode-locking was self-starting and stable from ~0.5 W of absorbed pump power, for all output couplers (OCs) studied (0.2%, 0.5% and1.5%), and up to 13 bounces on the chirped mirrors per cavity round trip.

The highest average powers were achieved with a 1.5% OC. When decreasing the negative GDD, the output power increased from 62 mW (6 bounces) to 91 mW (4 bounces), and to 96 mW (2 bounces) due to the decreasing cavity losses (~0.02% per bounce).

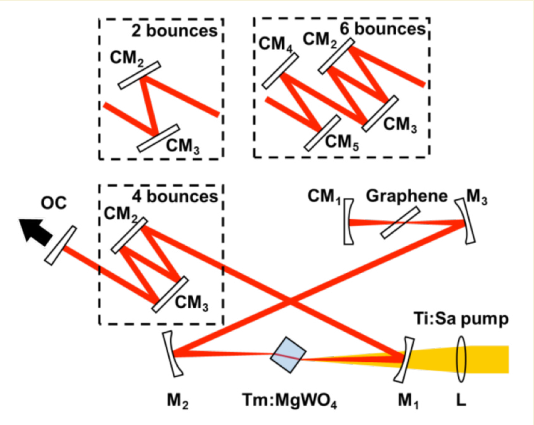

Fig. 6:
Scheme of the mode-locked Tm:$MgWO_4$ laser (L: lens; M_1-M_3: dichroic folding mirrors; CM_1-CM_5: chirped mirrors; OC: output coupler).

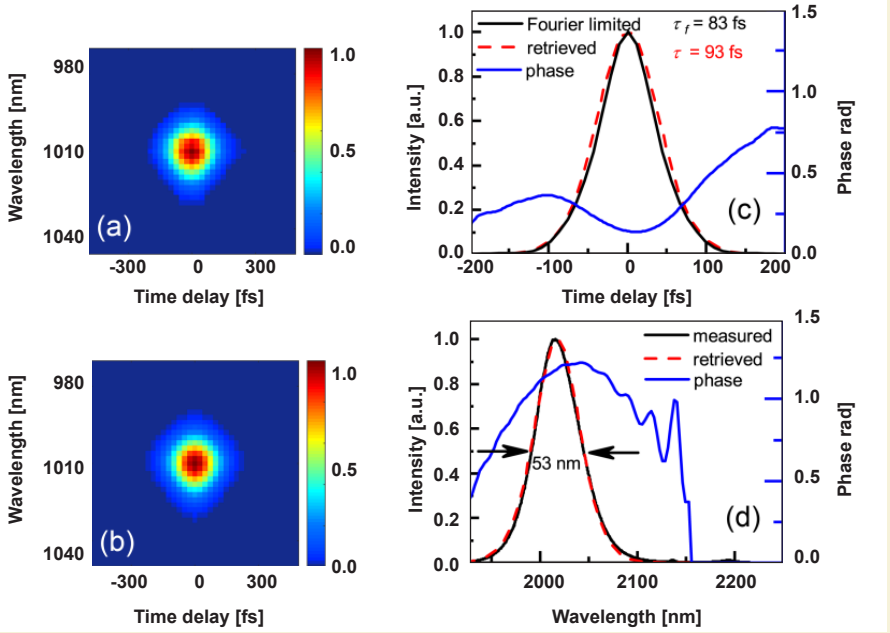

Fig. 7:
SHG-FROG measurement for the shortest pulse: measured (a) and retrieved (b) SHG FROG traces, derived temporal (c) and spectral (d) intensity and phase (black curve: directly measured spectrum by an InGaAs spectrometer).

The pulses reached a pulse duration of 96 fs (FWHM for a sech^2-pulse shape) for 2 bounces or additional round trip GDD of -735 fs^2, at a single pulse energy of 1.1 nJ at 87 MHz.

Reducing the OC transmission, the laser had a trend towards double pulse operation when the intracavity energy was highest and the negative GDD was decreasing. Thus, single pulses as short as 86 fs with ultimate stability were achieved using a 0.5% OC, at an average output power of 39 mW. The resulting time-bandwidth product is 0.335, very close to the Fourier-limit for sech^2-shaped pulses. We characterized the shortest pulses by the SHG-FROG technique, see Figs. 7(a) - 7(d). From the FROG-retrieval, a pulse duration of 93 fs was obtained with an almost symmetric pulse shape, in excellent agreement with the simultaneously measured autocorrelation trace. The spectral bandwidth resulting from the FROG-retrieval was 53 nm with the one estimated from the directly measured spectrum, cf. Fig. 7(d). The residual linear chirp parameter (-640 fs^2) was derived from a parabolic fit to the spectral phase. It indicates operation in the negative GDD regime as desirable for maximum stability. To verify the stability and the absence of Q-switching, radio frequency (RF) spectra were recorded in different span ranges. The fundamental beat note at 75.95 MHz displays an extinction ratio of 80 dBc above carrier and the harmonic beat notes show almost a constant extinction ratio.

100 kHz OPCPA at 1.55 µm/3.1 µm

The Leibniz SAW project launched in 2012 has been devoted to the development of a high average power OPCPA system pumped with 1.03 µm pulses at a repetition rate of 100 kHz with a dual output of 1.55 µm, carrier-envelope phase (CEP)-stable and 3.1 µm, non-CEP stable beams. The two-stage OPCPA system completed and used for application experiments in 2016 revealed further issues with respect to the commercial 1.56 µm Er:fiber seed laser. In addition to its CEP noise characteristics preventing active CEP stabilization, (i) the seed laser also led to a strongly structured amplified spectrum resulting in uncompressible, several-100-fs-long pedestals in both the 1.55 and the 3.1 µm output beams severely limiting

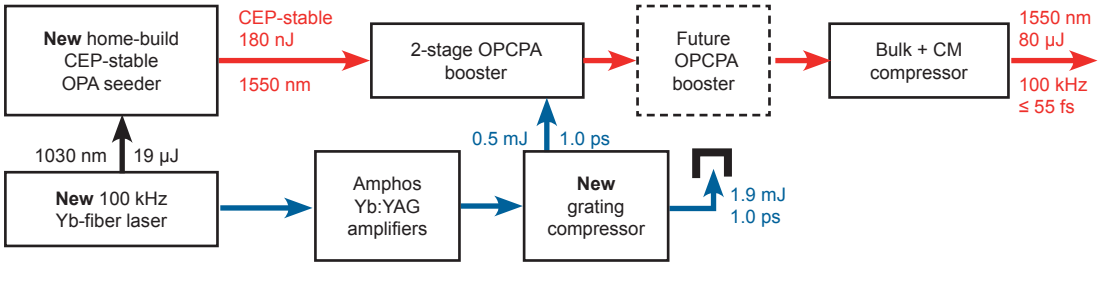

Fig. 8:
Present status of the 100 kHz, 1.55 µm/3.1 µm OPCPA system.

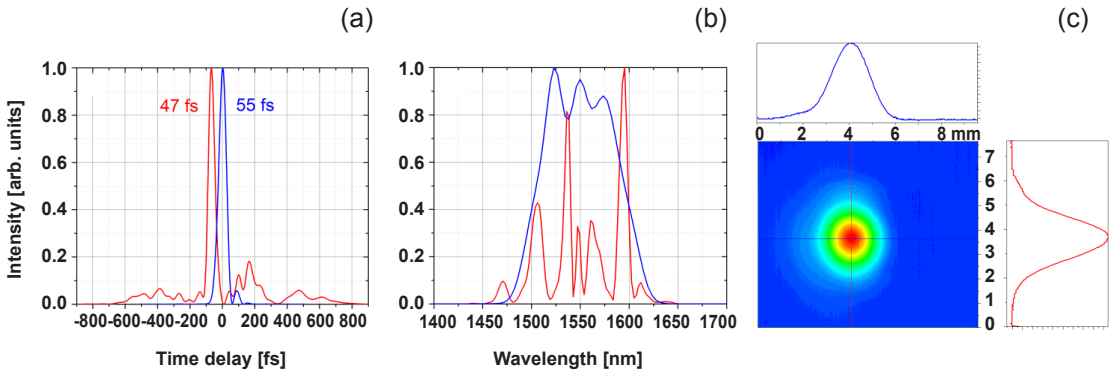

Fig. 9:
Recompressed temporal profiles (a) and spectra (b) of the old versus the new OPCPA system based on the Er-fiber laser seeder (red) and the new home-built seeder (blue). (c) Near-field profile of the 1.55 µm beam at the 9 W output level.

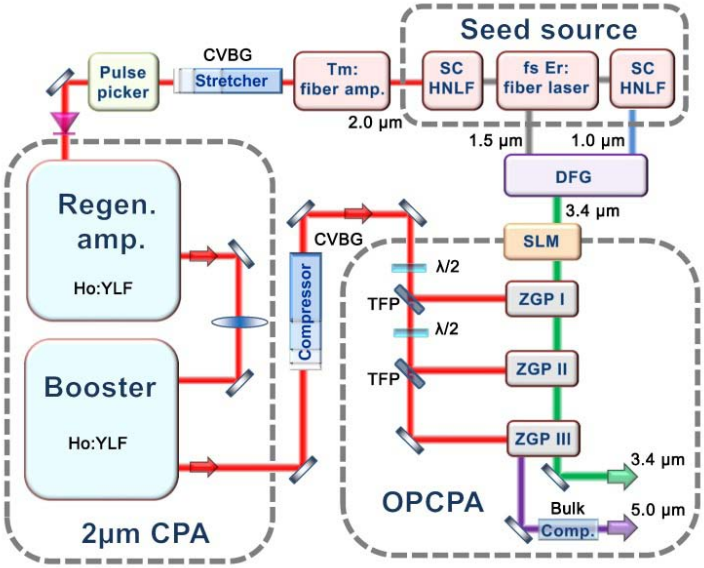

Fig. 10:
Setup of the mid-IR OPCPA source pumped at 2 µm. The main parts are the seed source, the 2 µm Ho:YLF CPA amplifiers, the difference frequency generation (DFG), the spatial light modulator (SLM) and the three OPA stages based on ZGP crystals. (Regen. amp., regenerative amplifier; Booster, power amplifier; CVBG, chirped volume Bragg grating; SC, supercontinuum gen.; HNLF, highly nonlinear fiber; TFP, thin-film polarizer).

the peak intensity and (ii) the stability of the supercontinuum branch of the seeder caused damage in the main Yb:YAG pump amplifier.

In 2017 the Er-fiber laser seeder was replaced by a combination of an Yb-fiber pump laser and a home-built, white-light-seeded, difference frequency generation (DFG) stage (cf. Fig. 8). The two-branch Yb-laser features a fiber-coupled arm seeding the main Yb:YAG amplifiers and a free-space arm serving as the pump laser for the DFG-based front-end. As now the Yb:YAG amplifiers are seeded directly from a stable Yb-fiber laser oscillator equipped with a sophisticated interlock, laser damage due to missing pulses is avoided. Furthermore, as the DFG stage is seeded by white light continuum pulses obtained from 515 nm, frequency-doubled pulses and pumped by the same green pulses, it provides passively CEP-stable, 1.55 µm pulses. Finally, the spectrum of the white light continuum pulses is smooth leading to clean, compressible pulses even after the PPLN OPCPA stage with strong parasitic frequency mixing processes. The temporal, spectral, and spatial intensity characteristics of the amplified 1.55 µm pulses are shown in Fig. 9. The power stability exhibits an rms value of 0.6% over a time duration of 2 hours.

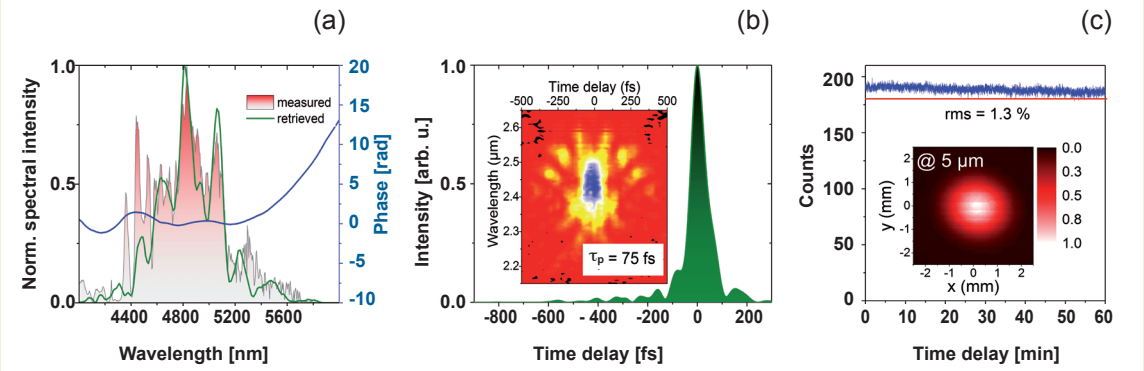

Fig. 11:
(a), (b) SHG-FROG characterization of the idler pulses after the third OPA stage. (a) Optical spectrum, measured and retrieved; b) retrieved temporal pulse shape (green) and retrieved SHG-FROG trace (inset); (c) long time pulse stability, inset: Far-field intensity distribution.

A further development in 2017 was the replacement of the transmission-grating-based pump compressor by one with high-efficiency reflection gratings (cf. Fig. 8). The new compressor features 83% throughput; much higher than the 65% throughput of the old compressor. In addition, adjustment of the grating distance is now possible, which helps to compensate the regular drifts in pulse duration during day-to-day operation.

1 kHz OPCPA at 5 µm

The second SAW project launched in 2014 aims at the development of a high energy (>1 mJ) OPCPA system at a repetition rate of 1 kHz with sub-100 fs pulses at 5 µm. In 2017, the main activities were devoted to achieve the target parameters of the mid-IR optical parametric amplifier (OPA) chain.

The layout of the 5 µm OPCPA source is presented in Fig. 10. A femtosecond Er:fiber laser operating at 40 MHz serves as master, feeding two supercontinuum (SC) sources. This three-color front-end seeds both the OPA and the 2 µm pump channel emitting synchronized femtosecond pulses at 1.0 µm, 1.5 µm and 2.0 µm. The long wavelength part of the 2 µm SC spectrum is injected into a single-stage Tm:fiber pre-amplifier. After pre-amplification, a pulse picker reduces the 40 MHz repetition rate to 1 kHz. Subsequently, the pulses are stretched to ~1 ns in a chirped volume Bragg grating (CVBG) and fed into the Ho:YLF regenerative amplifier (RA). For power scaling two Ho:YLF booster amplifiers are added in a single-pass geometry, yielding up to 55 mJ pulse energy when seeding with 10 mJ pulses emitted by the RA. This CPA system displays an excellent stability with a pulse-to-pulse rms as low as 0.3%. To prevent nonlinear effects and thermal problems in the available CVBGs we limited the pulse energy for compression to 25 mJ. Using two CVBGs with adapted dispersion provides nearly transformed limited pulses with a duration of 4.3 ps.

The signal pulses for the OPA are generated at 3.4 µm via difference-frequency generation (DFG) between the 1.0 and 1.5 µm pulses of the front-end. The spectrum of the signal pulses covers >700 nm bandwidth (FWHM) and the pulses are stretched to ~3 ps duration. For spectral shaping of the signal beam, a mid-IR spatial light modulator (SLM) is introduced after the DFG. The SLM is implemented in a 4-*f* configuration using a sapphire prism as dispersive element which provides a throughput of 30%, much higher than the competing solution based on the so-called acousto-optic programmable dispersive filter (i.e. <10%). The SLM ensures more straightforward chirp compensation for the signal pulses that can also indirectly be applied to recompress the 5 µm idler pulses thanks to the chirp transfer during parametric amplification

The OPA chain is composed of three stages, designed for different gain levels (Fig. 10). We chose ZGP crystals, the most promising nonlinear material for 2 µm pumped OPCPA, which features an extremely high nonlinearity. In the first two OPA stages a non-collinear geometry is applied ensuring broadband phase-matching. In the final stage a large aperture ZGP crystal (10 x 10 mm^2) is employed and a collinear OPA design is chosen to prevent an angular dispersed idler. To avoid damage of the ZGP crystals only 10 mJ of the available 2 µm pulse energy is applied in the final OPA stage. Seeding with 160 µJ of the stretched signal pulses resulted in 0.65 mJ per pulse in the idler, the highest energy so far in the mid-IR.

The recorded broadband idler spectrum, shown in Fig. 11(a), extends from 4350 to 5400 nm at $1/e^2$ and supports a Fourier-transform limited pulse duration of 64 fs. Stretching and compression in the OPCPA is performed with bulk materials for managing the group-delay dispersion (GDD). The residual third- and fourth-order dispersion is mostly compensated by the SLM. The SHG-FROG characterization of the compressed pulses is shown in Fig. 11. The flat spectral phase confirms the excellent pulse quality (Fig. 11(a)). The retrieved pulse shape yields a pulse duration of 75 fs with an estimated energy content of 88% (Fig. 11(b)). The nearly diffraction-limited Gaussian far-field intensity distribution and the excellent stability of the recompressed

pulses at the 1 kHz repetition rate with an rms of 1.3% are presented in Fig. 11(c) [GBU17].

The 75 fs pulse duration represents a record value for high energy mid-IR OPCPA and corresponds to only sub-five optical cycles. Taking into account the idler pulse energy of 0.65 mJ in this configuration, it translates into the highest peak power of 7.7 GW achieved for mid-IR OPCPAs beyond 4 µm so far.

In 2018 further pulse energy scaling by utilizing of the available 2 µm pump energy of 50 mJ will be performed. Furthermore, first applications of the system are planned, like generating of broadband pulses from the mid- to the far-infrared.

Own Publications 2017 ff

(for full titles and list of authors see appendix 1)

BKB17: A. A. Boyko *et al.;* Appl. Opt. **56** (2017) 2783-2786

BMC17: F. Bach *et al.;* Opt. Mater. Express **7** (2017) 240-252

BMP17: F. Bach *et al.;* Opt. Mater. Express **7** (2017) 744-750

BTG17: M. Bock et al.; Opt. Lett. **42** (2017) 2374-2377

BTS17: I. Babushkin *et al.;* Light: Sci. Appl. **6** (2017) e162218/1-8

FFP17: L. Fregnani *et al.;* Appl. Opt. **56** (2017) 662-665

FWG17: F. J. Furch *et al.;* Opt. Lett. **42** (2017) 2495-2498

GBU17: L. v. Grafenstein *et al.;* Opt. Lett. **42** (2017) 3796-3799

GKY17: K. Gorbachenya *et al.;* Appl. Opt. **56** (2017) 4745-4749

GMA17: A. Giree *et al.;* Opt. Express **25** (2017) 3104-3121

HES17a: J. Hyyti *et al.;* Rev. Sci. Instrum. **88** (2017) 103102/1-14

HES17b: J. Hyyti *et al.;* J. Opt. Soc. Am. B **34** (2017) 2367-2375

HES17c: J. Hyyti *et al.;* Opt. Lett. **42** (2017) 2185-2188

HPM17: Z. Heiner *et al.;* APL Photonics **2** (2017) 066102/1-7

JPS17: W. Jing et al., Opt. Mater. Express **7** (2017) 4192-4202

KLM17: E. Kifle *et al.;* Opt. Mater. Express **7** (2017) 4258-4268

KMI17: K. Kato *et al.;* Opt. Lett. **42** (2017) 4363-4366

KML17: E. Kifle *et al.;* Laser Phys. **27** (2017) 045801/1-6

KMP17: K. Kato *et al.;* Appl. Opt. **56** (2017) 2978-2981

KMV17: E. Kifle *et al.;* Opt. Lett. **42** (2017) 1169-1172

KUP17: K. Kato *et al.;* Opt. Commun. **386** (2017) 49-52

LBB17: P. Loiko *et al.;* Opt. Lett. **42** (2017) 2275-2278

LLZ17: J. Lu *et al.;* Laser Phys. Lett. **14** (2017) 085807/1-6

LMC17: P. Loiko *et al.;* SPIE Proc. **10082** (2017) 1008228/1-6

LMW17: R. Lan *et al.;* Opt. Express **25** (2017) 4579-4584

LSM17a: P. Loiko *et al.;* Opt. Lett. **42** (2017) 1177-1180

LSM17b: P. Loiko *et al.;* Opt. Mater. Express **7** (2017) 844-854

LSM17c: P. Loiko *et al.;* Opt. Lett. **42** (2017) 2431-2434

LSM17d: P. Loiko *et al.;* SPIE Proc. **10082** (2017) 1008215/1-7

LSM17e: P. Loiko *et al.;* in: *Nano-Optics: Principles Enabling Basic Research and Applications* Springer, Dordrecht (2017) 533-535

LTB17: M. Liebmann *et al.,* Opt. Express **25** (2017) 26076-26088

LZW17: R. Lan *et al.*; Opt. Eng. **56** (2017) 096112/1-5

LZZ17a: H. Lin *et al.;* Opt. Express **25** (2017) 11827-11832

LZZ17b: H. Lin *et al.;* Opt. Mater. Express **7** (2017) 3791-3795

MAK17: S. K. Mishra *et al.;* Opt. Express **25** (2017) 11637-11651

MLC17: X. Mateos *et al.;* Laser Phys. Lett. **14** (2017) 095801/1-7

MLS17a: X. Mateos *et al.;* Opt. Lett. **42** (2017) 3490-3493

MLS17b: X. Mateos *et al.;* IEEE J. Quantum Electron. **53** (2017) 1700110/1-10

MPe17: M. Mero and V. Petrov; IEEE Photonics J. **9** (2017) 3200408/1-8

MPK17: K. Miyata *et al.;* Appl. Opt. **56** (2017) 6162-6129

MSL17: X. Mateos *et al.;* SPIE Proc. **10082** (2017) 1008214/1-6

NCP17: R. S. Nagymihaly *et al.;* Opt. Express **25** (2017) 6664-6677

NJD17: P. Navratil *et al.;* Opt. Express **25** (2017) 25886-25893

PBK17: V. Petrov *et al.;* SPIE Proc. **10088** (2017) 1008810/1-11

Pet17: V. Petrov; phys. status solidi c **14** (2017) 1600161/1-9

RFM17a: N. Raabe *et al.;* SPIE Proc. **10089** (2017) 1008907/1-7

RFM17b: N. Raabe *et al.;* Opt. Lett. **42** (2017) 1068-1071

RFW17: N. Raabe *et al.;* Phys. Rev. Lett. **119** (2017) 123901/1-5

SIN17: L. Shi *et al.;* Optica **4** (2017) 1038-1043

SLM17: J. M. Serres *et al.;* SPIE Proc. **10082** (2017) 100820T/1-6

SML17: J. M. Serres *et al.;* J. Luminies. **183** (2017) 391-400

TBW17: A. Treffer *et al.;* SPIE Proc. **10120** (2017) 01200S/1-8

WCM17: Y. Wang *et al.;* Opt. Lett. **42** (2017) 3076-3079

WLM17: Y. Wang *et al.;* Opt. Express **25** (2017) 7084-7091

YLG17: A. S. Yasukevich *et al.;* Opt. Commun. **389** (2017) 15-22

ZLM17: X. Zhang *et al.;* Opt. Mater. Express **7** (2017) 3626-3633

ZLW17: Z. Zhang *et al.;* Opt. Mater. Express **7** (2017) 484-493

ZLZ17: L. Zhang *et al.;* Opt. Express **25** (2017) 3682-3693

Invited Talks at International Conferences

(for full titles see appendix 2)

U. Griebner *together with* L. v. Grafenstein, M. Bock, and T. Elsaesser; OSA Laser Congress 2017 (Nagoya, Aichi, Japan, 2017-10)

J. W. Kim *together with* S. Y. Choi, J. Bae, X. Mateos, F. Díaz, U. Griebner, V. Petrov, G.-H. Kim, and F. Rotermund; 25th Int. Conference on Advanced Laser Technologies, ALT'17 (Busan, Korea, 2017-09)

X. Mateos *together with* P. Loiko, S. Lamrini, K. Scholle, P. Fuhrberg, S. Vatnik, I. Vedin, M. Aguiló, F. Díaz, U. Griebner, and V. Petrov; 25th Int. Conference on Advanced Laser Technologies, ALT'17 (Busan, Korea, 2017-09)

M. Mero; Photonic Net Workshop "Simulationen in der Photonik" (Hannover, Germany, 2017-04)

V. Petrov; Photonics West'17: Lasers and Applications in Science and Engineering, SPIE Conference 10088: Nonlinear Frequency Generation and Conversion: Materials, Devices, and Applications XVI (San Francisco, CA, USA, 2017-01)

V. Petrov *together with* V. V. Badikov, D. V. Badikov, V. B. Laptev, K. V. Mitin, G. S. Shevyrdyaeva, A. Kwasniewski, E. Boursier, N. I. Shchebetova, A. Tyazhev, G. Marchev, V. Panyutin, P. Segonds, and B. Boulanger; The 6th Advanced Lasers and Photon Sources, ALPS'17 (Yokohama, Japan, 2017-04)

V. Petrov *together with* V. Badikov, D. Badikov, V. Laptev, K. Mitin, G. Shevyrdyaeva, N. Kostyukova, A. Boyko, E. Boursier, V. Panyutin, N. Shchebetova, A. Tyazhev, G. Marchev, A. Kwasniewski, D. Kolker, P. Segonds, and B. Boulanger; 25th Int. Conference on Advanced Laser Technologies, ALT'17 (Busan, Korea, 2017-09)

V. Petrov *together with* V. Badikov, D. Badikov, V. Laptev, K. Mitin, G. Shevyrdyaeva, N. Kostyukova, A. Boyko, E. Boursier, V. Panyutin, N. Shchebetova, A. Tyazhev, G. Marchev, A. Kwasniewski, D. Kolker, P. Segonds, and B. Boulanger; The 7th Asian Conference on Crystal Growth and Crystal Technology, CGCT-7 (Changchun, China, 2017-10), plenary talk

V. Petrov, Sino-German Ultrafast Optics and Photonics Symposium (Tianjin, China, 2017-11)

G. Steinmeyer *together with* N. Raabe, T. Feng, M. Merö, H. Tian, Y. Song, W. Hänsel, R. Holzwarth, A. Sell, and A. Zach; SPIE Photonics West 2017 (San Francisco, CA, USA, 2017-01)

G. Steinmeyer; Nonlinear phenomena in strong fields (Hannover, Germany, 2017-01)

G. Steinmeyer; Nonlinear Waves and Turbulences in Optics and Hydrodynamics (Berlin, Germany, 2017-03)

G. Steinmeyer; PIERS 2017 (St. Petersburg, Russia, 2017-05)

G. Steinmeyer; CLEO/Europe-EQEC 2017 (Munich, Germany, 2017-06)

G. Steinmeyer; 9th Int. Summer School New Frontiers in Optical Technologies (Tampere, Finland, 2017-08)

G. Steinmeyer; SPIE Laser Damage (Boulder, CO, USA, 2017-09), plenary talk

G. Steinmeyer; Sino-German Ultrafast Optics and Photonics Symposium (Tianjin, China, 2017-11)

G. Thomas; CLEO/Europe-EQEC 2017 (Munich, Germany, 2017-06)

2.2: Strong-field Few-body Physics

F. Morales Moreno, H. Rottke (project coordinators)
and D. Ayuso, W. Becker, F. Branchi, F. Braußе, T. Bredtmann, U. Eichmann, A. Husakou, M. Yu. Ivanov, Á. Jiménez Galán, J. Kaushal, S. Meise, J. Mikosch, D. B. Milošević, S. Patchkovskii, K. Reininger, H. R. Reiss, M. Richter, A. Rouzée, F. Schell, C. P. Schulz, B. Schütte, O. Smirnova, P. M. Stammer, S. Yarlagadda

1. Overview

On a sub-femtosecond temporal and Ångström spatial scale the project aims at

- Understanding the strong-field induced dynamics in atoms and molecules
- Employing strong-field processes as a tool for imaging and understanding atomic and molecular electron dynamics and molecular structural changes.

We put specific focus on the fundamental aspects of strong-field induced multi-electron dynamics, on the excitation of neutrals, on the forces exerted on these neutrals, and on the role played by molecular structure and dynamics. The strong-field regime of interaction of light with matter is typically entered at light intensities beyond 10^{13} Watt/cm^2 in the infrared spectral range. There the electric field of the light wave starts to become comparable with the inner-atomic/inner-molecular field experienced by the valence electrons. Based on the knowledge of the fundamental strong-field interaction mechanisms gained we employ these phenomena to track and image molecular dynamics, of both the electronic and the nuclear degrees of freedom and of their coupling, in real-time, through strong-field ionization mapping.

2. Topics and collaborations

We tackle the objectives from the experimental side and closely linked therewith by a focused theory presently on three topical research fields:

T1: Single- and multi-electron strong-field phenomena and their time resolution

T2: Dynamics of strong-field ionization of ordered structures and clusters

T3: Probing molecular dynamics by strong-field ionization.

Collaboration partners: G. G. Paulus (Friedrich Schiller Universität, Jena, Germany), C. Faria (City College London, UK), S. P. Goreslavski, S. V. Popruzhenko (National Research Nuclear University (MEPhi), Moscow, Russia), A. Saenz (HU Berlin, Germany), Y. Mairesse (CELIA, Université Bordeaux, France), N. Dudovich (Weizmann Institute, Rehovot, Israel), J. Marangos (Imperial College, London, UK), X. J. Liu (Wuhan, Chinese Academy of Sciences, China), J. Chen (Peking University, Beijing, China), T. Marchenko (Université Pierre et Marie Curie, Paris, France), J. M. Bakker, G. Berden, B. Redlich (FOM-Institute for Plasma Physics Rijnhuizen, The Netherlands), A. Stolow, A. E. Boguslavskiy (Steacie Institute for Molecular Sciences, National Research Council of Canada), F. Martín (Universidad Autónoma de Madrid, Spain), H. Stapelfeldt (Aarhus University, Denmark), J. Küpper, A. Rubio (Center for Free Electron Laser, Universität Hamburg, Germany), T. Fennel (Universität Rostock, Germany), A. I. Kuleff (Universität Heidelberg, Germany), M. Krikunova (TU Berlin, Germany), V. R. Bhardwaj (University of Ottawa, Canada), R. Cireasa (Institut des Sciences Moléculaires d'Orsay, France), F. Legare (ALLS Montreal, Canada), H. Köppel, A. Kuleff (Universität Heidelberg, Germany), V. S. Makhija (University of Ottawa, Canada), J. P. Wolf (University of Geneva, Switzerland).

In-house collaborations with Projects 2.3, 4.1, and 4.2 (FAL, G. Steinmeyer).

3. Results in 2017

T1: Single- and multi-electron strong-field phenomena and their time resolution

Limit on excitation and stabilization of atoms in intense optical laser fields

We explore the limits of atomic excitation and stabilization in strong near-infrared (NIR) laser fields imposed by the spatial field envelope and the field propagation [ZMK]. It is known from experiments and theoretical investigations both classically and quantum mechanically that excitation of atoms is possible even for laser intensities reaching beyond the saturation intensity [ZPI17]. However, it is expected that field gradients as present in a focused laser beam and the relativistic vxB drift become important for low frequency laser fields and essentially hinder the occurrence of bound states.

We use an experimental setup which allows for the direct detection of excited atoms after strong-field excitation and simultaneously monitor the atomic center of mass (CM) deflection in the strong laser field as a sensitive probe to gradient fields inside the laser focus [ENR09]. Using He with its high ionization potentials for the two electrons as a target atom the application of high laser intensities up to 10 PW cm^{-2} to study neutral excitation is possible before substantial suppression of excited-state formation sets in due to ionization of the otherwise uninvolved second electron. We apply semi-classical models [NGS08, ENR09] to identify physical mechanisms responsible for strongly reduced excitation and to finally reach a quantitative understanding. Quantum mechanical single-active-electron time-dependent Schrödinger equation (TDSE) calculations are shown to confirm the classical results.

The experimental data displayed in Fig. 1 show the deflection of atoms which were initially located in the focal plane (z = 0 ±100 µm). We can clearly follow the increasing deflection of atoms with increasing laser peak intensity up to I_0 = 10 PW cm^{-2}, Figs. 1(a) - (c). Further increase of the laser intensity substantially diminishes the number of surviving atoms that experience the enhanced deflection, Figs.1(d) and (e). In order to describe the experimental results theoretically we exploit the semi-classical model of frustrated tunneling ionization (FTI) [NGS08, ENR09, ZEi16] to perform classical-trajectory Monte Carlo calculations. We solve the coupled classical Newton equations for a He^+ ion and the electron subjected to the Lorentz force and the Coulomb force.

The classical full field calculations very well describe the experimental observations. Analyzing the results we find that a substantial decrease of the yield of bound states occur around half the beam waist $w_0/2$, i.e., around the maximum gradient. Thus the decrease can be attributed to the gradient (ponderomotive) force acting on the system. This force is much stronger than the magnetic component of the Lorentz force at the intensities indicated in Fig. 1. The magnetic component of the Lorentz force becomes only appreciable at even higher intensities. It is important to note that the decrease in the yield due to the gradient force clearly occurs before double ionization sets in at higher intensity.

The calculations also allow for the insight what n states are mostly affected. In Fig. 2 we show the n distributions from the classical and the quantum mechanical calculations. Both results basically agree underpinning the importance of the spatial envelope effect of the intensity on excitation and possible stabilization of atoms in strong laser fields. The calculations reveal that the depletion takes place around n = 10, which corresponds to the maximum of excited states in the dipole approximation. High n states are rather unaffected by the gradient field.

Molecular Orbital Imprint in Laser-Driven Electron Recollision

The essence of attosecond strong-field spectroscopies and attosecond pulse generation is captured by the well-known and widely-used three-step model. The

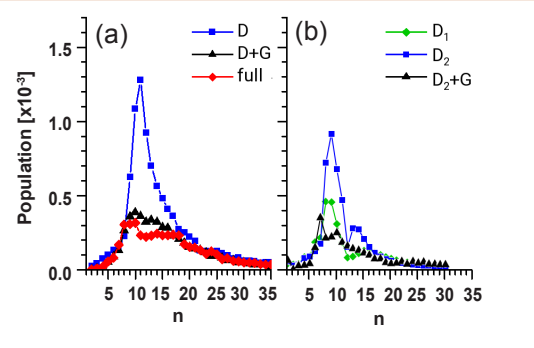

Fig. 2:
The n-distributions (b) at a peak intensity I_0 = 8.8 PW cm^{-2} for pure dipole approximation (D) and additionally including the field envelope at $w_0/2$ (D+G) and full field (full). (a) TDSE calculations for 40 fs laser pulse (cos^2 envelope), in dipole approximation at peak intensity I_0 = 10 PW cm^{-2} (D_1); at an effective intensity I = 6 PW cm^{-2} (corresponds $w_0/2$) (D_2); as (D_2), but additionally with field gradient (D_2+G).

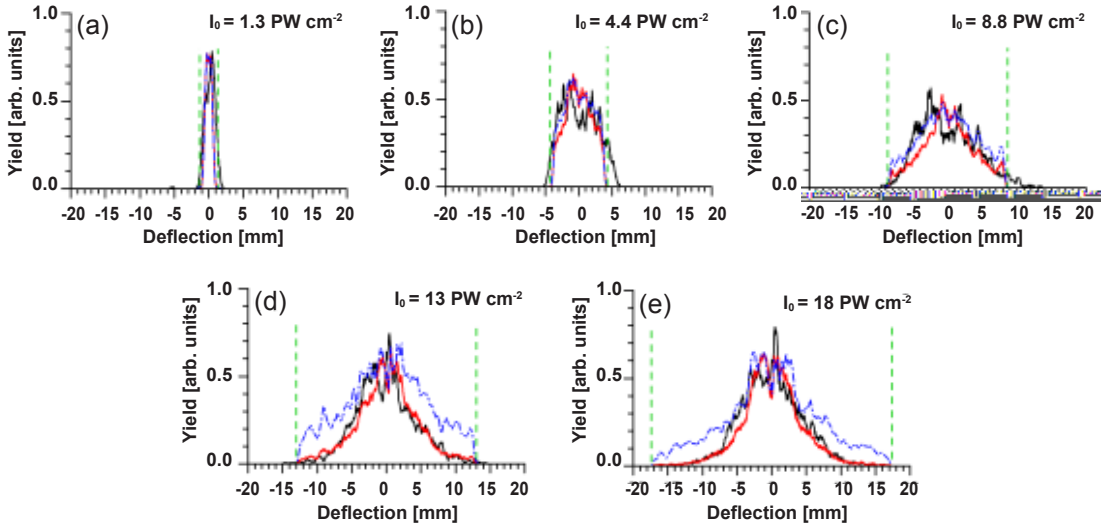

Fig. 1:
Measured and calculated deflection of the CM of excited atoms after exposing ground state He atoms to laser pulses with the indicated peak intensities I_0. Experimental data (black curves); calculated distribution for bound trajectories (red curves); CM deflections for unbound trajectories (dashed blue curves). Vertical dashed green lines indicate limits of deflection in a ponderomotive model [ENR09].

three steps consist of laser-driven tunnel ionization, propagation of the electron in the continuum and interaction with the ion core upon recollision, all of which occur consecutively within a fraction of a laser cycle. While the first two steps are common to all recollision processes, the interaction step can take the form of radiative recombination in High Harmonic Generation (HHG), or of inelastic or elastic scattering, as is the case in non-sequential double ionization and Laser-Induced Electron Diffraction (LIED). While many experimental observations to date were attributed to the molecular-frame angle dependence of the Strong-Field Ionization (SFI) and the electron-ion interaction steps, it is one of the central assumptions underlying attosecond strong-field spectroscopies that the propagation step is largely system-independent. The propagation is usually assumed to 'wash out' the phase structure of the initial state, so that the electron returns to its core as a plane wave.

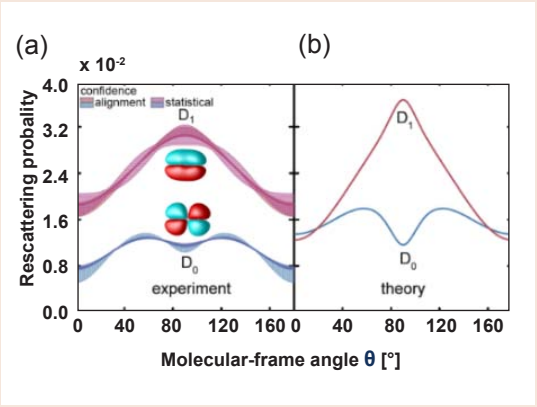

Fig. 3:
(a) Experimental channel-resolved molecular-frame rescattering probability R(θ) x Q(θ) in 1,3-butadiene. To obtain this quantity, the channel-resolved electron yield of direct electrons and electrons in the rescattering plateau was determined for non-adiabatically aligned molecules in dependence of the angle between the polarizations of the alignment and the SFI pulses. This lab-frame measurement was then transformed into the molecular frame using the independently determined alignment distribution of the molecular ensemble. Also shown are the Dyson orbitals corresponding to D_0 and D_1 ionization.
(b) The same quantity as in A obtained from TD-RIS calculations.

We examined this central proposition both experimentally, using laser-aligned 1,3-butadiene molecules, and theoretically [SBSa, SBSb]. We performed measurements of the θ-dependence of the laser-driven rescattering yield associated with two different SFI continuum channels, where θ is the angle between the major axis of the 1,3-butadiene molecules and the driving laser polarization axis. The two channels correspond to different states (D_0, D_1) of the cation formed by SFI and are separated by means of a coincidence measurement using a reaction microscope. The molecular-frame rescattering yield is given by the product of the molecular-frame ionization probability S(θ) and the rescattering probability RQ(θ),which is almost generally assumed to factorize into the return probability R(θ) and the high-angle scattering probability Q(θ), following the three-step model. Moreover, in the analysis of strong-field spectroscopy experiments, a common approach is to regard R(θ) as a constant that does hence not depend on θ. Q(θ) then contains the structural information on the molecule. It captures the molecular-frame dependence of the rescattering Differential Cross Section (DCS), which is extracted in LIED experiments. Since the electronic structure of the cation differs by the contribution of only one valence electron, Q(θ) is expected to be nearly the same for the two channels in our study. We confirmed this expectation by a calculation.

The angular dependence of the yield of direct (S(θ)) and rescattered (S(θ) x R(θ) x Q(θ)) electrons thus provides experimental access to the channel-resolved rescattering probability R(θ) x Q(θ). Figure 3(a) shows unambiguously that the experimental channel-specific R(θ) x Q(θ) differs significantly between D_0 and D_1, both in shape as well as in amplitude. To independently corroborate our experimental results, we performed numerical calculations using the Time-Dependent Resolution-in-Ionic-States (TD-RIS) theory method, which reproduce all key features found in the experiment (see Fig. 3(b)).

Given the identical high-angle scattering probability distributions Q for both channels, the channel dependence of the molecular-frame rescattering probability R(θ) x Q(θ) implies that the molecular-frame return probability distribution R(θ) depends on the ionization channel. In other words, contrary to common expectations, R(θ) is a distribution that is strongly system-dependent. The molecular-frame and channel dependence of R can be understood in terms of the Dyson orbitals associated with the two continuum channels (see Fig. 3(a)): In order to strong-field ionize a molecule with a field directed along the nodal plane of a Dyson orbital, the outgoing photoelectron must acquire non-zero transverse momentum. This transverse spread of the wavepacket strongly decreases the probability of recollision.

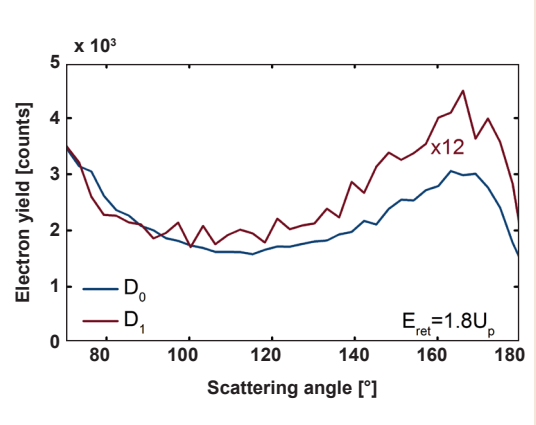

Fig. 4:
Channel-resolved Differential Cross Section (DCS) extracted from the measured three-dimensional electron momentum distributions for randomly aligned 1,3-butadiene molecules. Given a good enough signal-to-noise ratio, molecular structure can be obtained from the DCS.

1,3-butadiene can be regarded as a model system representative for molecules featuring nodal planes. We hence anticipate that our findings of molecular orbital imprint in laser-driven electron recollision are of general nature. Our results caution that the relative contribution of different SFI channels to HHG and LIED probes of molecular dynamics is not simply reflected by the SFI yield and by the interaction cross sections associated with these channels. As a next step, LIED measurements extracting molecular structure from the DCS for each of the two channels should help to quantify the relevance of the θ-dependence of R in the analysis of strong-field spectroscopies. A first attempt is shown in Fig. 4. A difference in the DCS can be observed between the D_0 and the D_1 channel, which can be attributed to the θ-dependence of S and R when averaging over the molecular ensemble.

Sequential and direct ionic excitation in the strong-field ionization of 1-butene molecules

As attosecond science moves into the realm of polyatomic molecules, the many-electron and non-adiabatic nature of strong-field spectroscopies becomes important. An example is SFI directly to different electronic states of the cation, which is interpreted as simultaneous ionization from the highest occupied molecular orbital (HOMO) as well as from lower-lying orbitals (HOMO-1, HOMO-2, etc.).

Direct observation of SFI populating excited cation states is achieved via Channel-Resolved Above Threshold Ionization (CRATI), which relies on the fact that, in many polyatomic molecules, only the ground (D_0) state of the cation is stable with respect to spontaneous unimolecular fragmentation. The excitation of higher-lying electronic states of the cation inevitably leads to dissociation. However, while the appearance of ionic fragments in the mass spectrum is a sign of the population of excited cation states, direct SFI to excited cation states needs to be distinguished from sequential pathways such as SFI to the ground cationic state followed by post-ionization excitation. The CRATI method disentangles direct from sequential channels by measuring Photoelectron kinetic Energy Spectra (PES) correlated to different ions in the mass spectrum (parent or fragment ions) using coincidence or covariance techniques. The PES from SFI is comprised of an ATI comb, i.e. a series of equidistant peaks separated by the photon energy and related to the above threshold absorption of integer numbers n of photons of energy hv:

$$E_{kin} = n \times h\nu - IP - U_p \qquad (1).$$

The ATI comb is phase-shifted in photoelectron energy by the channel-specific ionization potential (IP) and by the ponderomotive potential U_p.

In a recent study [ZSR14], where direct and sequential population pathways to dissociative cation states were discerned for a range of molecular systems at a fixed SFI wavelength of 800 nm, it was found that direct SFI to electronically excited dissociative states strongly decreases as the gap energy (defined as the energy difference between the energetically lowest-lying dissociative cation electronic state and the energetically highest-lying stable cation electronic state) increases. Variation of the target molecule, however, introduces many critical changes in molecular properties, which may affect the SFI rates and channel-resolved yields. For this reason, we performed an SFI study of a single molecule, the hydrocarbon 1-butene (C_4H_8), systematically tuning the photon energy, in three steps (wavelengths λ = 795, 634, 401 nm), from below to above the gap energy of 2.0 eV [SBSc]. The measurements were partly performed in a PEPICO machine at NRC, Ottawa, (λ = 795 and 634 nm) and partly at MBI (λ = 401 nm) using a reaction microscope for the coincident detection of ion and electron momentum distributions.

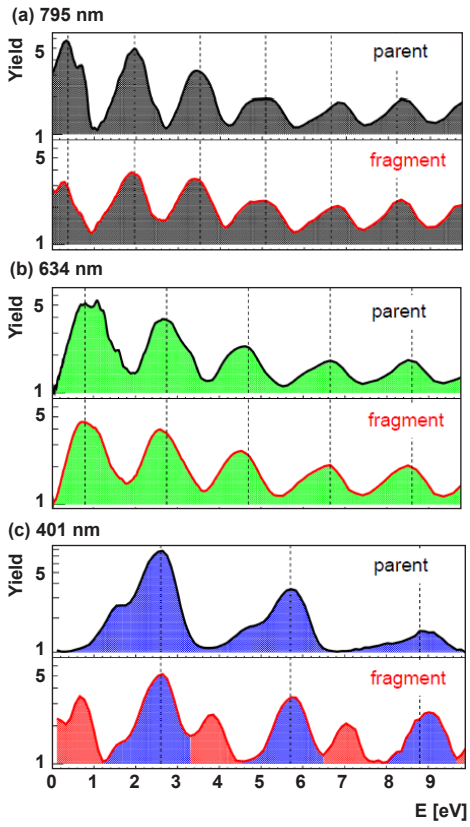

Fig. 5:
Exponentially corrected PES correlated to the parent ion (upper panels) and the dominant $C_3H_5^+$/ $C_3H_n^+$ fragment ion (lower panels), for the three employed SFI wavelengths. The vertical dashed lines are spaced by the photon energy.

Figure 5 shows SFI spectra correlated to the parent ion and one fragment (representative for all fragments, as they display very similar PES) for the three employed wavelengths. For better visibility the exponential decrease of the ATI signal towards higher energies has been removed. Each spectrum features a comb of peaks spaced by the photon energy, as expected for ATI. For all wavelengths, we observe that the ATI progression of the respective parent ion is also reproduced in all fragment spectra. Importantly, however, only for

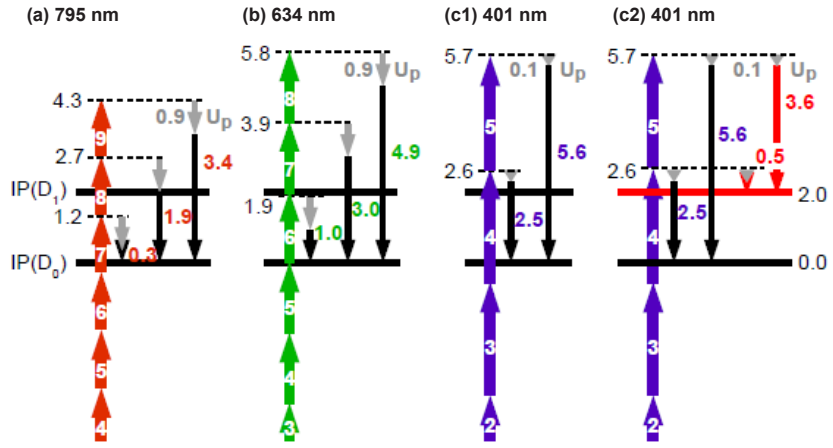

Fig. 6:
Wavelength-dependent SFI schemes for ATI of 1-butene molecules. In this analysis, we include the known experimental value of $IP_0(D_0)$ = 9.77 eV, the experimentally known 2.0 eV energy difference between the vertical D_0 and D_1 ionization energies, the respective photon energies (lengths of colored arrows) and the independently determined ponderomotive potential U_p shift (grey arrows). The expected ATI peak positions for direct D_0/D_1 SFI (length of black/red arrows) are denoted in units of eV.

λ = 401 nm, a second ATI progression is clearly visible in the fragment-correlated PES (marked in red in the lower panel of Fig. 5(c)), which is absent in the parent-correlated PES.

Since in 1-butene only the electronic ground state of the cation is non-dissociative, the PES correlated with the parent ion stems from ionization to the D_0 state without further excitation of the cation. Indeed, the peak positions calculated from equation (1) for direct D_0 ionization (schematically depicted in Figs. 6(a), (b), (c1)) agree well with the peaks in the parent ion correlated PES. Furthermore, the observation that the parent ion ATI comb is reproduced in the fragment-associated progressions shows that the dominant pathway for fragment ion formation under the conditions of this study is associated with direct D_0 SFI followed by a sequential excitation processes in the 1-butene cation: SFI to the ionic ground state produces the D_0 ATI comb. The ground-state ion, produced in a given field cycle, is further excited in subsequent laser cycles.

For SFI at λ = 401 nm, the very prominent second ATI progression appearing in the fragment-associated PES is shifted with respect to the D_0 ATI progression to lower photoelectron energies by about 1.85 eV. A shift of this magnitude is close to the field-free gap energy of 2.0 eV. Given that small differential Stark shifts are expected and not accounted for, we assign the second ATI progression to D_1 SFI, i.e. SFI producing directly the first excited cation state (see Fig. 6(c2)). The strong contribution of direct ionization to excited cation states represents a marked difference for λ = 401 nm (photon energy above the gap energy) as compared to the two longer wavelengths (photon energies below the gap energy). Our wavelength-dependent study therefore confirms the previously suggested relevance of the gap energy for the occurrence of direct ionization to excited states of the cation. Further work is needed to clarify the physical mechanisms behind this observation.

Auger decay following strong-field ionization of CH_4 clusters

An inner-shell vacancy in an atom or molecule can decay very efficiently via the emission of an Auger electron. Thus far, Auger decay has been observed in atoms, molecules and clusters following the ionization or excitation by radiation with high photon energies in the extreme-ultraviolet (XUV) and X-ray regime. The interaction of strong laser fields with nanometer-sized clusters leads to very efficient ionization processes via avalanching and may as well result in the formation of inner-shell vacancies. This was e.g. demonstrated by measuring XUV and X-ray emission from strong-field ionized clusters.

We have recently observed Auger decay following NIR strong-field ionization of molecular CH_4 clusters [SVR17]. Fig. 7(a) shows an electron kinetic energy spectrum that was recorded after the ionization of CH_4 clusters with an average size of <N> = 15000 molecules by NIR pulses with a duration of 400 fs and an intensity of 1×10^{14} W/cm^2. In the logarithmic plot, an exponential contribution indicated by the straight line is attributed to thermal electron emission. In addition, a peak is observed at 7 eV that we attribute to electron emission via Auger decay in carbon ions. We explain Auger electron emission from expanding clusters by a three-step process. In a first step, extremely efficient ionization avalanching leads to the depopulation of outer- and inner-valence states of carbon as well as to the generation of protons by removing electrons from the hydrogen atoms. Only a small fraction of the generated electrons can overcome the Coulomb potential of the cluster, whereas the largest fraction of electrons remains trapped and forms a nanoplasma with

the ions. At the same time, ionization leads to fragmentation of both the molecules and the entire cluster, which in the following starts to expand. In a second step, electrons in the nanoplasma recombine with ions and populate Rydberg states as well as outer-valence states. In the left panel of Fig. 7(b), the example of a carbon ion is shown, which has two inner-valence and two outer-valence vacancies after the end of the laser pulse. In this example, two electron-ion recombination processes lead to the population of a Rydberg state as well as a 2p excited state. In a third step, this doubly-excited ion may decay via Auger decay, see the right panel of Fig. 7(b). One electron relaxes to the ground state and transfers the excess energy to a second electron that is emitted from the cluster.

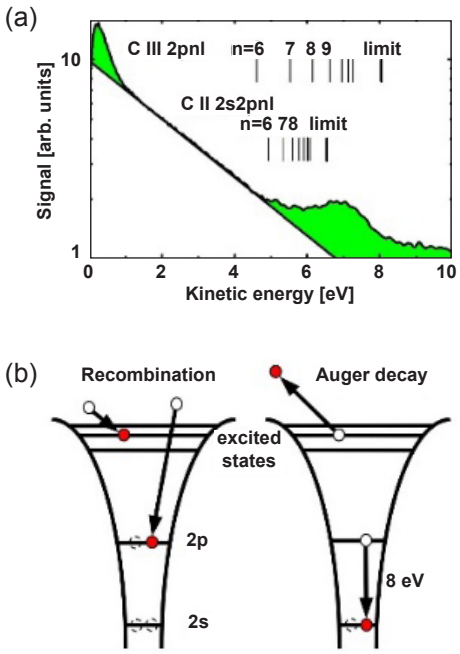

Fig. 7:
(a) Electron spectrum from CH_4 clusters ionized by 400 fs NIR pulses ($I = 1 \times 10^{14}$ W/cm^2). In addition to an exponential contribution, which is indicated by the straight line in the logarithmic plot, a clear peak is observed at 7 eV. The latter is attributed to series of autoionizing states are indicated. The observed feature at 7 eV is attributed to a combination of Auger processes involving different initial states.
(b) Schematic of the observed Auger decay, where the population of Rydberg states and the repopulation of outer-valence states via electron-ion recombination processes in expanding clusters is shown. The doubly-excited ion can relax via the emission of an Auger electron. In the right panel an example is shown where the recombination results in the formation of C III 2pnl. After recombination, the ion can relax to the ground state, releasing the second excited electron into the continuum.

In addition to the peak observed at 7 eV in Fig. 7(a), electron signal exceeding the exponential curve is also visible at kinetic energies <1 eV. This signal can be explained, on the one hand, by the influence of the static electric field that is used for the detection of the electrons. This detector field reionizes electrons that become trapped in high Rydberg states during the expansion of the cluster. On the other hand, autoionization processes, in which two or more electrons populate Rydberg states of the same ion, may contribute to the observation of the low-energy electron signal.

In the future, sophisticated experimental and theoretical investigations are required to shed more light on the complex electron dynamics evolving during the expansion of clusters following their interaction with intense laser pulses. Furthermore, the observed population inversion in the carbon ions may be exploited for the development of an XUV or X-ray laser.

Atomic processes in bicircular fields

The superposition of two circularly polarized fields with different frequencies $r\omega$ and $s\omega$ that rotate in the same plane with equal or opposite helicities is called a bicircular field. Counterrotating fields normally produce more interesting phenomena than corotating fields. Bicircular fields, in contrast to a single circularly polarized field, generate bright high-order harmonics with frequencies $[q(r+s) \pm r]\ \omega$ with integer q and, for an atom, circular polarization the helicity of which alters from one harmonic to the next. More possibilities exist for a molecular target.

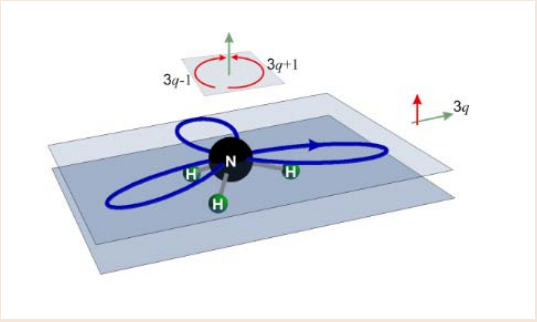

Fig. 8:
Harmonics emitted by the molecule NH_3 driven by a bicircular field with r = 1 and s = 2 (depicted in blue) polarized in the molecular plane. The propagation direction of the emitted harmonics is indicated by the green arrows.

Here we present the example of the nonplanar molecule NH_3 for r = 1 and s = 2. The situation is depicted in Fig. 8 [HOB17]. The afore-mentioned harmonics have the frequencies $3q\omega \pm 1$. They are polarized in the plane of the three H atoms and propagate in the direction of the molecular axis. In addition, there are linearly polarized harmonics with frequencies $3q\omega$ that propagate perpendicularly to the molecular axis. Figure 9 presents harmonic spectra, for the case where the field is polarized in the molecular plane and for a small misalignment. In the latter case, the selection rules mentioned above are no longer strictly observed. In general, the polarization changes from predominantly linear to predominantly circular for increasing order.

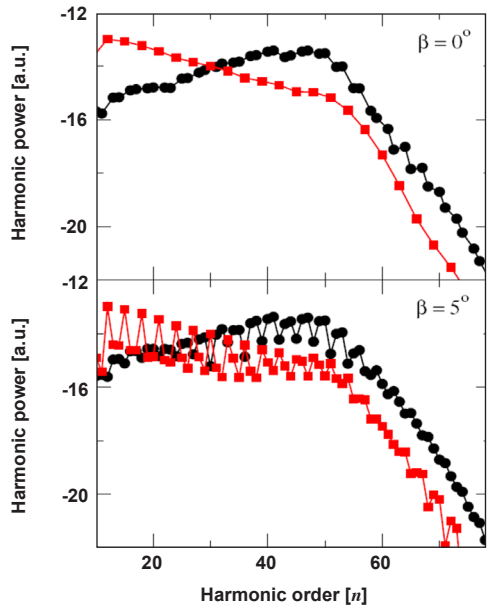

Fig. 9:
Harmonic spectra for NH_3 irradiated by a ω-2ω bicircular field with ω = 1.5 eV and intensities of 10^{14} W/cm^2 for both fields, calculated via the molecular strong-field approximation. For the upper panel, the field is polarized in the molecular plane, for the lower panel there is a misalignment of 5°. Black dots (red squares) denote the circularly (linearly) polarized harmonics.

The presence of well separated linearly and circularly polarized harmonics in the same system is unique to nonplanar molecules. Different frequency and intensity ratios of the driving fields allow for a large parameter space allowing for unprecedented control of harmonic generation and, also, above-threshold ionization [BMI17, HBM17, HOB17, OHB17].

T2: Dynamics of strong-field ionization of ordered structures and clusters

The effect of two-equivalent-centers interference and of driving ionic transitions on strong-field ionization of xenon dimers

The effect of two-equivalent emission centers on strong-field ionization (SFI) of molecules has attracted attention since first hints of its possible influence have been detected in the total ionization rate of homonuclear diatomic molecules and in the momentum distribution of directly emitted photoelectrons, which have not rescattered on the ion core. In the momentum distribution the two emission centers can give rise to interference phenomena. Ideal candidates to investigate interference are molecules with a large internuclear separation of the constituting atoms as there is for example the Xe_2 dimer with an internuclear separation of R = 8.35 au. At this separation the momentum distribution of directly emitted photoelectrons is wide enough to cover a momentum range up to π/2R and more, necessary to observe more than one half of the period of an interference structure before saturation of ionization of the molecule is reached in high intensity laser pulses. The width of the momentum distribution of directly emitted photoelectrons is limited to $2U_p^{1/2}$, with U_p being the intensity dependent ponderomotive potential of a free electron in the laser pulse.

A second phenomenon in molecules which is known to influence high order harmonic generation (HHG) is the open shell structure of the singly charged molecular ion. It gives rise to partly closely spaced electronic states near the ionic electronic ground state with energy level separations of the order of the photon energy usually used for SFI and HHG. Partly large transition dipole moments couple these states. This may bring about strong transitions between ionic states during SFI and non-standard AC-Stark shifts of the ionization potentials of the neutral molecule which are associated with every ionic electronic state. Non-standard Stark shifts meaning potentially strong deviations from a close to ponderomotive shift of the thresholds. Besides influencing HHG these phenomena are also expected to influence SFI and thus photoelectron momentum distributions (see [ZFR] and references cited there).

We investigated the two phenomena introduced above by SFI of Xe_2 dimers [ZFR]. The Xe_2^+ ion has altogether five further electronic states located close to the electronic ground state. They form pairs of charge resonance states which are coupled by large transition dipole moments of the order of R/2. They are separated by energy differences of the order of the photon energy of the Ti:sapphire laser pulses ($h\nu$ = 1.55 eV) we used for the experimental investigation.

Representative photoelectron momentum distributions for SFI of Xe atoms Xe_2 and ArXe dimers are shown in Fig. 10. They were taken with linearly polarized light at an intensity of 8.0 x 10^{13} W/cm^2. The ionization potentials of the atom and of the dimers are practically the same. Differences in the photoelectron momentum distributions are thus related to the structure of the particles. SFI of Xe and ArXe result in practically the same momentum distributions (Fig. 10, upper and lower spectra). A significant difference is only found for SFI of Xe_2 (middle spectrum). For ArXe SFI at the light intensity used means SFI of the Xe site of the dimer since the ionization potential of Ar is significantly higher. Thus one already expects similar momentum distributions for directly emitted electrons, which predominate in the spectra shown in Fig. 10. The distributions mainly depend on the ionization potential only.

SFI of the Xe_2 dimer gives rise to a momentum distribution which differs significantly from that of Xe and ArXe. We attribute the main difference to two-emission-centers interference present in SFI of Xe_2. The difference of the Xe and Xe_2 momentum distributions is most obvious in the experimental electron yield ratio spectra shown in Fig. 11 for electrons emitted into a small cone along the laser beam polarization direction. The ratios are plotted for several light intensities. All show a pronounced minimum in an energy (momentum) range where directly

emitted electrons are detected. The width of the valley increases with the light intensity and the position of the minimum shifts slightly to higher kinetic energies.

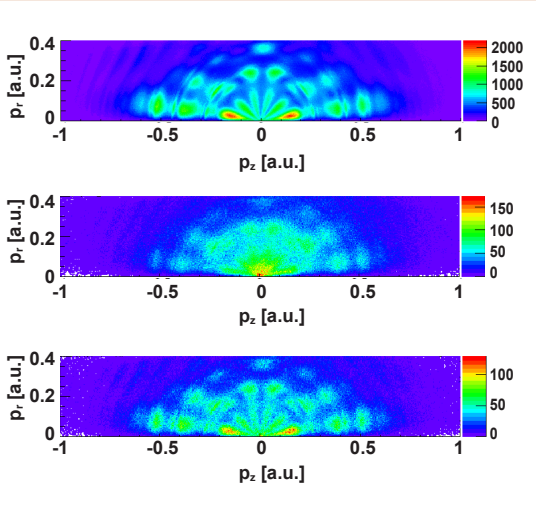

Fig. 10:
From top to bottom: momentum distributions of photoelectrons detected together with Xe^+, Xe_2^+ and $ArXe^+$ ions at a light intensity of 8.0 x 10^{13} W/cm². The polarization of the laser pulses was linear and directed along the z-axis. The numbers on the color scale represent electron counts per momentum bin.

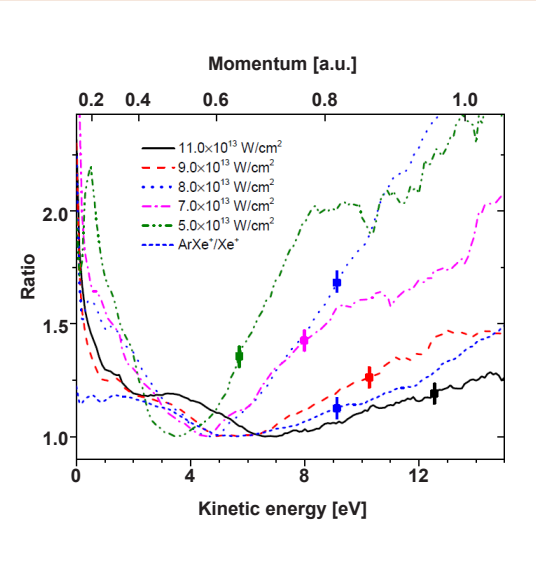

Fig. 11:
The ratios $Y_{dimer}(E_{kin})/Y_{Xe}(E_{kin})$ of the dimer to monomer (Xe) photoelectron yields at laser pulse intensities in the range between 5.0 x 10^{13} W/cm² and 1.1 x 10^{14} W/cm². The ratio for the ArXe dimer is only shown at an intensity of 8.0 x 10^{13} W/cm². At each light intensity the ratios are normalized to 1 at the respective ratio minimum. The squares with the vertical bar on each curve indicate the point where the kinetic energy of the photoelectrons reaches $2U_p$, i.e. the upper limit for directly emitted photoelectrons.

The overall features observed in the photoelectron yield ratios have been reproduced in a model calculation based on the strong-field approximation (SFA). It shows that the minimum we observe experimentally in the photoelectron yield ratio for SFI of Xe_2 may actually be attributed to two-equivalent-center-interference [ZFR]. The model calculation took the presence of a charge resonance pair of electronic states in the dimer ion into account. The energetic separation of this pair was chosen to be equal to that of the actual Xe_2^+ pair $I(1/2)_u$ (ion ground state) and $I(1/2)_g$ at the equilibrium internuclear separation of Xe_2 [Wad78]. The transition dipole moment coupling these electronic states was chosen to be R/2 which is close to the actual value [Wad80]. The calculation indicates that the electrons we detected in the experiment in coincidence with Xe_2^+ ions have the ion left predominantly in an ungerade electronic state after the laser pulse. This state is presumably the electronic ground state $I(1/2)_u$. A dependence of the results of the model calculation on the light intensity also indicates that the interference phenomenon observed is influenced by driving ionic transitions and by Stark shifting the ionic electronic states during SFI [ZFR].

T3: Probing molecular dynamics by strong-field ionization

First molecular dynamics studied with the Timepix detector: O_2N-NO_2 vibration in $(NO_2)_2$

The standard approach for recording the three-dimensional momentum in ion/electron imaging or COLTRIMS experiments is to use an analogue detector, such as the widely spread delay-line anode. Recently, alternative digital detector technologies capable of recording the particle impact position and time, under coincidence conditions, are being increasingly explored. MBI is at the forefront of this evolution, contributing to the development of the Timepix technology into a three-dimensional coincidence imaging detector [LFD17].

Timepix is a solid-state, in-vacuum coincidence pixel detector, developed by the Medipix collaboration at CERN [MED]. In the setup constructed at MBI (see Fig. 12), it is used to digitize the signals from a micro-channel plate (MCP) amplifier coupled to a velocity map imaging (VMI) spectrometer. Here we combined the Timepix VMI setup with an in-house built, high repetition rate OPCPA system [FGM16] to perform a first pump-probe experiment studying molecular dynamics. The laser system delivers 7 fs duration pulses at 800 nm central wavelength and a repetition rate of 400 kHz.

In the work presented here, we determine the amplitude of the intermolecular vibration in the dimer of NO_2. In the experiment, we recorded the fragment ions resulting from a strong-field pump – strong-field probe interaction, measuring their kinetic energy. In the delay-dependent kinetic energy release spectrum of NO_2^+ fragments we distinguish two separable features: (i) We find a band with a kinetic energy which exponentially decreases with time-delay. It is attributed to strong-field ionization (SFI) by the pump pulse, producing excited $(NO_2)_2^+$. The ensuing two-body breakup is probed by SFI with the

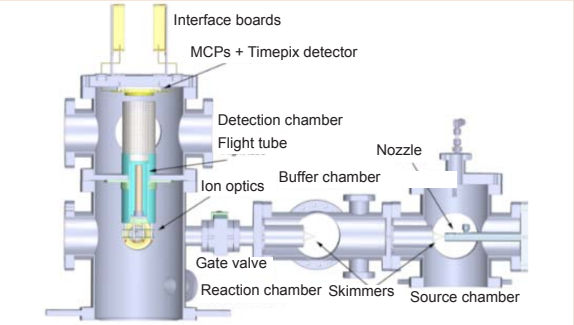

Fig. 12:
Schematic of the Timepix VMI experimental setup [1]. A neutral gas jet is expanded through the nozzle in the source chamber. After passing two skimmers it reaches the reaction chamber where it is overlapped with the laser beam inside a VMI spectrometer. The three-dimensional momenta of the resulting ions are recorded in coincidence with a solid-state Timepix detector coupled to an MCP amplifier.

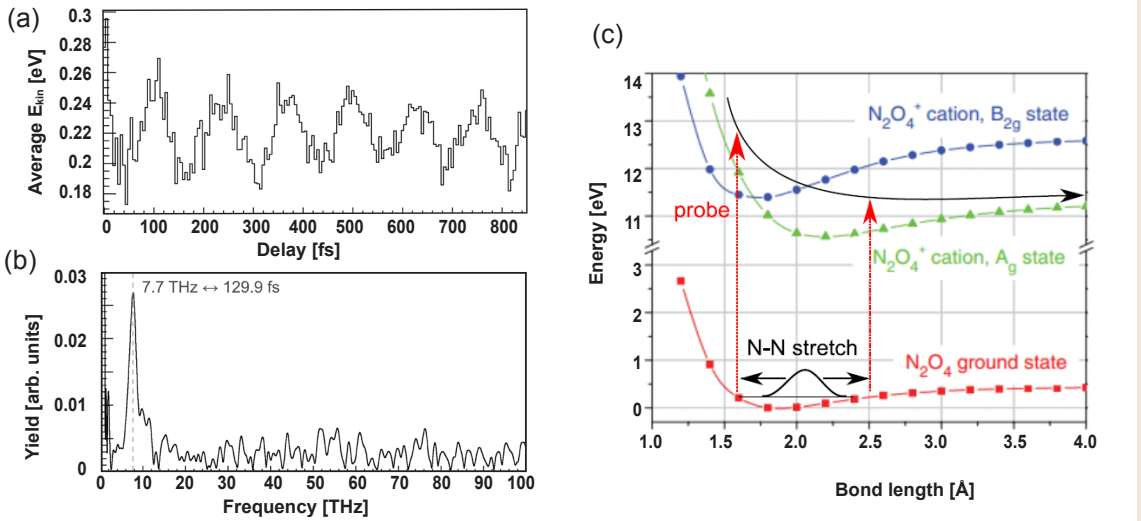

Fig. 13:
(a) Delay-dependent mean kinetic energy in the low-kinetic energy band of NO_2^+ fragments resulting from SFI of vibrationally excited NO_2 dimers. (b) Fourier transformation showing a vibrational period of about 130 fs, in accordance with the intermolecular vibration. (c) From the published excited state potential curves the inner turning point of the vibration and the vibrational amplitude are inferred from the measurement in panel (a) as 1.6 Å and 0.15 Å, respectively.

probe pulse, resulting in a time-dependent Coulomb repulsion. (ii) At low kinetic energies, we observe an oscillatory structure. This band is assigned to an excitation of the intermolecular ground-state O_2N-NO_2 vibration with impulsive stimulated Raman scattering and subsequent SFI probing.

The time-dependent mean kinetic energy in the low-kinetic energy band is depicted in Fig. 13(a). The oscillation period is determined to be 130 fs (see Fig. 13(b)), in accordance with the literature. From the published excited state potential curves [LZL08], the inner turning point of the vibration and the vibrational amplitude are inferred as 1.6 Å and 0.15 Å, respectively (see Fig. 13(c)).

Own Publications in 2017 ff

(for full titles and list of authors see appendix 1)

BMi17: W. Becker and D. B. Milošević; J. Phys. Conf. Ser. **826** (2017) 012008/1-8

HBM17: E. Hasović *et al.*; J. Phys. Conf. Ser. **826** (2017) 012009/1-7

HOB17: E. Hasović *et al.*; Molec. Phys. **115** (2017) 1750-1757

KBG17: S. Kelvich *et al.*; Phys. Rev. A **96** (2017) 023427/1-5

LFD17: J. Long *et al.*; J. Chem. Phys. **147** (2017) 013919/1-10

Mil17a: D. B. Milošević *et al.*; J. Phys. B. **50** (2017) 164003/1-10

Mil17b: D. B. Milošević; Phys. Rev. A **96** (2017) 023413/1-17

OHB17: S. Odžak *et al.*; J. Mod. Opt. **64** (2017) 971-980

QHH17: W. Quan *et al.*; Phys. Rev. Lett. **119** (2017) 243203/1-6

QHW17: W. Quan *et al.*; Phys. Rev. A **96** (2017) 032511/1-9

Rei17: H. R. Reiss; J. Phys. B **50** (2017) 075003/1-8

SVR17: B. Schütte *et al.*; Phys. Rev. A **95** (2017) 063417/1-5

SWV17: K. J. Schafer *et al.*; Editorial: Special issue celebrating 25 years of re-collision physics, J. Phys. B **50** (2017) 170201/1-2

WXC17: Y. L. Wang *et al.*; Phys. Rev. A **95** (2017) 063415/1-7

ZPI17: H. Zimmermann *et al.*; Phys. Rev. Lett. **118** (2017) 013003/1-5

ZSM17: D. Zille *et al.*; Phys. Rev. A **95** (2017) 063408/1-6

in press

JZA: Á. Jiménez Galán *et al.*; Phys. Rev. A

SBSa: F. Schell *et al.*; Proceedings of ATTO06 Conference; Springer Proceedings in Physics Series

SBSb: F. Schell *et al.*; Sci. Adv.

ZFR: C. Zhang *et al.*; Phys. Rev. A

ZMK: H. Zimmermann *et al.*; Phys. Rev. Lett.

submitted

SBSc: F. Schell *et al.*; Phys. Chem. Chem. Phys.

Other Publications

ENR09: U. Eichmann *et al.*; Nature **461** (2009) 1261

FGM16: F. Furch *et al.;* Opt. Express **24** (2016) 19293

LZL08 : W. Li *et al.*; Science **322** (2008) 1207

MED: Medipix Collaboration CERN; URL: http://medipix.web.cern.ch/

NGS08: T. Nubbemeyer *at al.*; Phys. Rev. Lett. **101** (2008) 233001

Wad78: W. R. Wadt; J. Chem. Phys. **68** (1978) 402

Wad80: W. R. Wadt; J. Chem. Phys. **73** (1980) 3915

ZEi16: H. Zimmermann and U. Eichmann; Phys. Scr. **91** (2016) 104002

ZSR14: A. Zhao, P. Sandor, T. Rozgonyi, and T. C. Weinacht; J. Phys. B **47** (2014) 204023

Invited Talks at International Conferences

(for full titles see appendix 2)

W. Becker *together with* S. Kelvich, and S. P. Goreslavski; 26th Annual Int. Laser Physics Workshop, LPHYS'17 (Kazan, Russia, 2017-07)

U. Eichmann; Intense Field, Short Wavelength Atomic and Molecular Processes（ISWAMP), ICPEAC Satellite Meeting (Brisbane, Australia, 2017-07)

H. Reiss; 26th Annual Int. Laser Physics Workshop, LPHYS'17 (Kazan, Russia, 2017-07)

B. Schütte; Extreme Atomic Systems 2017 (Riezlern, Österreich, 2017-01)

2.3: Time-resolved XUV-science

A. Rouzée, S. Patchkovskii (project coordinators)
and U. Bengs, F. Braußе, T. Bredtmann, L. Drescher, T. Fennel, F. Furch, G. Goldsztejn, A. Harvey, J. Hummert, M. Ivanov, Á. Jiménez Galán, I. Katechis, K. Kolatzki, O. Kornilov, L. Loechner, J. Long, C. Luan, Z. Mašín, N. Mayer, J. Mikosch, N. Monserud, F. Morales Moreno, T. Nagy, S. Raabe, G. Reitsma, M. Richter, H.-H. Ritze, D. Rupp, M. Sauppe, F. Schell, C. P. Schulz, B. Schütte, B. Senfftlenben, V. Shokeen, O. Smirnova, M. J. J. Vrakking, T. Witting, N. Zhavoronkov, J. Zimmerman

1. Overview

The main goal of Project 2.3 is to study real-time electronic and nuclear dynamics in simple and complex photochemical and photobiological processes. The project has both experimental and theoretical components. Experimentally, we are developing a framework of closely interconnected time-resolved methods, unified by the application of novel XUV/X-ray light sources, both table-top, such as obtained by high harmonic generation (HHG), or at free electron laser facilities. Using photoionization as a probe step in a pump-probe configuration, we investigate attosecond electron motion in atoms, molecules and nanoparticles and its coupling with the nuclear motion. This is done by combining the extreme temporal resolution (attosecond) with atomic–scale spatial resolution provided by these new light sources. Our experimental framework is complemented by an advanced theory program aiming at (i) tracking down and resolving correlated multi-electron dynamics on the attosecond time scale, and (ii) understanding the impact of coherently excited attosecond multi-electron dynamics on the longer, femtosecond-scale nuclear motion. Our common goal is to push atomic and molecular science beyond the present state-of-the-art by looking at the new time scale in chemical and physical processes.

2. Topics and collaborations

Presently, the project is organized in four topics:

T1: Attosecond electron and nuclear dynamics and control in atoms and molecules

T2: Atoms, molecules and clusters in intense XUV pulses

T3: Time-resolved X-ray spectroscopy of ultrafast molecular processes

T4: Theory of attosecond electron dynamics and its coupling to nuclear motion.

Collaboration partners: P. Johnsson (Lund University, Sweden); A. Rudenko, D. Rolles (Kansas State University, Manhattan, USA); J. Küpper (Center For Free-Electron Laser, Hamburg, Germany); H. Stapelfeldt (Aarhus University, Denmark); K. Ueda (Tohoku University, Japan); F. Calegari (DESY Hamburg, Germany); F. Lépine (Institut Lumière et Matière, Lyon, France); D. Holland (Science and technology facility council); Th. Pfeiffer (Max Planck Institute for nuclear physics, Germany), K. Varju (University of Szeged, Hungary), L. Bañares (Universidad Complutense de Madrid, Spain), H. Köppel, A. Kuleff (University of Heidelberg, Germany), K. H. Meiwes-Broer, I. Barke (Universität Rostock, Germany), B. v. Issendorff (Universität Freiburg, Germany), P. Piseri (Università di Milano, Italy), A. Orr-Ewing and M. Ashfold (University of Bristol, UK).

In-house collaborations with Projects 1.1, 2.2, 3.1 and 4.1.

3. Results in 2017

XUV optics

Refractive lenses and prisms are indispensable tools used to control the properties of light beams at visible, infrared and ultraviolet wavelengths. The strong absorption of XUV radiation in matter has so far hindered the development of refractive optical elements for the XUV region of the spectrum. In order to overcome this limitation, it was suggested to use extremely thin lenses. The sophisticated design of such lenses, however, makes the fabrication and handling of these lenses very challenging.

Recently, we have designed refractive optical elements for the XUV region following an alternative approach. We have shown that the refraction of XUV pulses can be controlled using an inhomogeneous gas jet, for which the absorption of XUV radiation is much lower compared to a solid target. Two sets of experiments were performed, in which a gas-phase refractive prism as well as a gas-phase refractive lens were demonstrated.

In the first set of experiments, broadband attosecond pulse trains were produced via HHG. The spectral region around the 13th harmonic is depicted in Fig. 1(a), showing the spectral dependence along the horizontal axis and the XUV beam divergence along the vertical axis. When switching on a He gas jet with a density gradient across the XUV beam profile, the angle-resolved XUV spectrum was severely modified, see Fig. 1(b). Spectral components of the XUV beam with photon energies below the 1s2p resonance of He at 21.22 eV were deflected upwards, whereas spectral components with higher photon energies were deflected downwards.

This behavior is explained by the refractive index dependence in the vicinity of an atomic resonance. When approaching the resonance from lower frequencies, the refractive index increases. Close to the resonant energy, the refractive index shows a steep decrease, changing from values above unity to values below unity. This behavior is also known as anomalous dispersion. Towards higher frequencies, the refractive index increases again.

The gas jet that deflects the XUV beam as observed in Fig. 1(b), thus acts as an XUV refractive prism, in analogy to an optical prism used to refract visible light. The deflection angle at a given photon energy was controlled by varying the gas pressure, the gas jet position and the gas type.

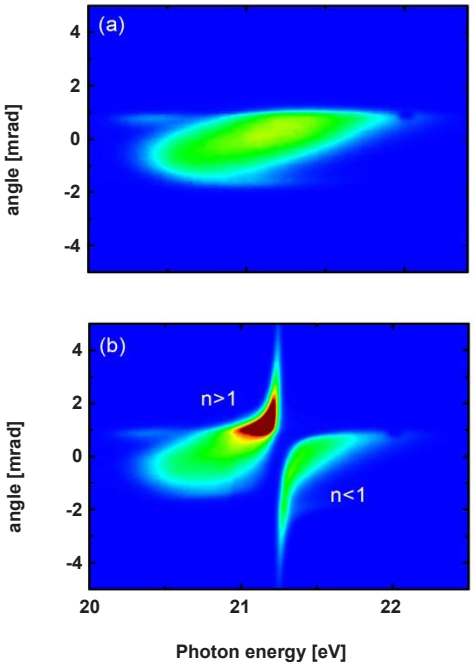

Fig. 1:
(a) Angle-resolved XUV spectrum in the region of the 13th harmonic that was generated in Xe. The horizontal axis represents the spectral coordinate, while the vertical axis shows the divergence of the XUV beam. (b) Following propagation of the same XUV pulse at a distance of 0.5 mm below the center of a dense He gas jet, the XUV spectrum is severely modified. Spectral components with photon energies below the 1s2p resonance of He (at 1.22 eV) are deflected upwards, whereas spectral components with higher photon energies are deflected downwards.

In the second set of experiments, we have exploited the observed deflection of XUV radiation in the vicinity of atomic resonances to demonstrate an XUV refractive lens. In a proof-of-principle experiment using narrowband HHG pulses, the divergence of an unfocused XUV beam was altered by a He gas jet. The vertical beam size of the 13th harmonic at a photon energy of 20.2 eV was reduced from 2.7 mm to 0.4 mm when switching on an He gas. At the same time, the absorption of the 13th harmonic by the gas jet was negligible. The vertical beam size of the 9th harmonic was reduced from 1.8 mm to 0.27 mm when switching on an Ar gas jet at a backing pressure of 2.5 bar. While the achievable focus size is currently limited by geometrical and chromatic aberrations, the design of optimized gas jets as well as achromatic lenses may enable tighter focusing of the XUV pulses in the future.

Our results show that it is possible to design refractive elements for the XUV region, thereby opening the route towards a transfer of techniques based on refraction that are widely used in other spectral regions. Examples are the compression of ultrashort laser pulses using refractive prisms, as well as nano-focusing and microscopy applications using refractive lenses.

State-resolved probing of attosecond timescale molecular dipoles

The interaction of bound electrons with the oscillating electric field of a laser can lead to an induced, time-dependent dipole. This effect underlies diverse physical phenomena ranging from spatial molecular laser alignment to HHG. Attosecond science allows to investigate the instantaneous driven-dipole response on a sub-cycle timescale.

In pioneering previous work by Neidel *et al.* [NKY13] it was shown that the probability of photoionization of small molecules by an extreme ultraviolet (XUV) attosecond pulse train (APT) depends on its relative phase with respect to a co-propagating near infrared (NIR) field. It was argued that this effect arises since the dipole moment induced by the NIR field leads to a screening of the XUV radiation.

Importantly however, the amplitude of the NIR-induced dipole is anticipated to be electronic state dependent, via the state-specific polarizability. As merely the overall ionization yield was recorded in the previous work, no information about the state-specific response was obtained.

To shed light on the state-resolved driven-dipole response of a molecule in an NIR field, attosecond transient absorption spectroscopy (ATAS) was employed in our present work. Our study of iodomethane molecules (CH_3I) extends recent work on the modification of the free induction decay (FID) in rare gas atoms and homonuclear diatomic molecules to a molecular regime where core-to-valence and core-to-Rydberg transitions, whose response to the NIR field are significantly different coexist. Our work illustrates the potential for applying NIR phase-locked ATAS to polyatomic molecules, where the core-level transitions driven by the XUV/soft X-ray pulses serve as a local probe within the molecule, due to the high localization of the initial core-level state.

In the experiment, a spectrally broad XUV APT obtained from HHG and a moderately strong NIR laser field co-propagated through a CH_3I sample with a controlled relative delay. The APT excited the 4d core-electrons into previously unoccupied valence and Rydberg states.

The effect of the NIR field on the populated states was inferred from the observed spectrally resolved modification of absorption due to the modified FID in the region of transitions from the 4d semi-core of iodine to the molecular valence and Rydberg states of CH_3I (49 eV to 61 eV). The experimental observations (Fig. 2(a)) were corroborated by numerical simulation of the transient absorption signal (Fig. 2(b)) using state energies and transition dipole moments obtained by *ab-initio* calculation.

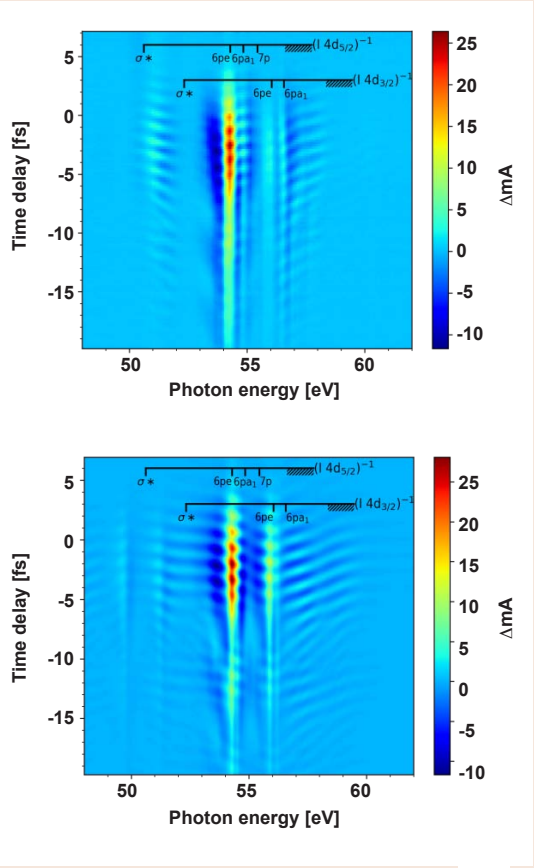

Fig. 2:
Transient change of absorbance of CH3I in the 4d-to-valence and 4d-to-Rydberg spectral region. Shown is a 28 fs range of XUV-NIR time-delays near overlap. At positive time-delays the NIR pulse arrives at the sample before the XUV pulse. (a) Experimental measurement that was obtained by quickly alternating data acquisition with and without the NIR beam. (b) Numerical simulation obtained from solving the Liouville-von-Neumann equation. A strong transient absorbance is associated with the 4d-to-Rydberg transitions, while the response of the 4d-to-valence transitions remains weak. Slanted bands of oscillating transient absorbance are associated with two-pathway-interferences for populating core-excited Rydberg states. The two weaker replicas of the observed features at negative time-delays can be associated with independently characterized pre-pulses of the NIR laser.

Importantly, while the core-to-valence transitions dominate the XUV excitation in the investigated photon energy range, we observe that the core-to-Rydberg transitions dominantly respond to the NIR field. This can be seen from the strong transient changes of absorbance observed for the transitions into the 6p and 7p Rydberg series (photon energies 53 eV to 57 eV). In the region corresponding to strong core-to-valence transitions (e.g. at 50.6 eV and 52.3 eV) only weak change of absorbance is observed.

The transient change of absorbance results as the absorption line shapes transform from a symmetric (Lorentzian) shape to a dispersive (Fano-like) shape. This effect can be attributed to the light induced phase (LIP) accumulated during the FID through state-specific shifts of the core-excited states [OKR13]. These shifts arise from the AC Stark effects, originating from the NIR-induced couplings to the nearby state manifold. Since the XUV excitation is constrained to the short duration of the APT and the FID is on the order of only a few NIR optical cycles, the LIP depends on the time-delay between NIR and XUV pulses with sub-cycle precision (see observation in Fig. 2).

The result of an *ab-initio* calculation of the state-to-state transition dipole moments is shown in Fig. 3. As can be seen, the couplings within the Rydberg state manifold are much stronger than the couplings of the relatively isolated valence states. The NIR field hence induces large dipole moments in the polarizable Rydberg orbitals, while the relatively localized valence orbitals that are dominantly populated by the XUV respond only weakly to the NIR field.

Our study illustrates that attosecond transient absorption spectroscopy of core-excited states in molecules is well suited to study the role of light-induced couplings in a state-resolved manner. As the observed changes of absorbance are sensitive to small shifts in coupling and energy during the fast decay of core-excited states, the described technique is well suited to observe ultrafast changes in the intra-molecular structure. With the advent of attosecond light sources in the soft X-ray regime, where transitions from core-orbitals in nitrogen, carbon and oxygen atoms are located, we anticipate that attosecond transient absorption spectroscopy of light-induced couplings in molecules will become a tool to study ultrafast phenomena in organic molecules not

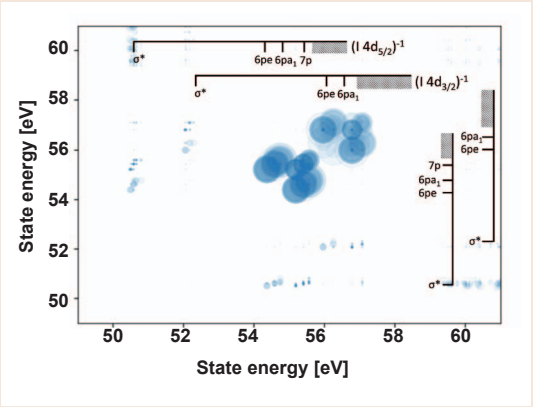

Fig. 3:
Absolute square of the transition dipole moments of 4d core-excited states (energy range 49-61eV) of CH_3I obtained from ab-initio calculation. Computed three-dimensional transition dipole moments were averaged over the random orientation of the molecule and projected onto the laboratory frame. The derived values are plotted as the radius of blue circles at the energetic position of the coupled states with an opacity of 5% to visualize overlapping contributions. Transition dipole moments between different core-excited Rydberg states are dominant, while the coupling of the core-excited valence states is weak.

only with excellent time and energy resolution, but also from the local perspective of an intramolecular reporter atom.

Diffractive imaging of ultrafast nanoscale dynamics with multicolor pulses

In the context of the SAW project 2017, we use the excitation of nanoparticles, such as clusters and nanodroplets, with intense laser pulses as a well-defined scenario for the experimental investigation and theoretical modeling of collective and correlated dynamics of highly excited matter [RFM17]. With the intense and short XUV pulses from free-electron lasers (FELs) and high harmonic generation sources, we study the structure and dynamics of single nanoparticles in free flight with both high spatial and temporal resolution by measuring coherent diffraction images. From the interference patterns of the elastically scattered photons, the nanoparticles' structure can be determined. Even three-dimensional structural information is contained in wide-angle diffraction images obtained in the XUV regime and can be retrieved with forward-fitting procedures. In our current project, we aim at observing ultrafast electron dynamics in the photoexcited nanoparticles via the diffraction images. In 2017, we have developed and employed novel experimental and analysis approaches based on multicolor-XUV pulses that represent an important milestone of the project.

Extracting refractive indices from multicolor diffraction images of helium nanodroplets

Up to recently, single-particle diffraction experiments were only possible using FELs. With their pulse duration in the 100 fs regime, faster dynamics such as electronic excitation, ionization and plasma formation cannot be temporally resolved. Attosecond pulses and pulse trains can on the other hand be generated with HHG sources, but achievable pulse energies are typically orders of magnitude weaker than those provided by FELs. Our recent demonstration of single-particle single-shot diffractive imaging of individual helium nanodroplets with the high-intensity XUV pulses from an HHG source, published in 2017 [RML17] (see also Scientific Highlights, page 19), has opened routes to map excitation and charge separation processes in nanoscale matter on their natural time scale.

Most of the helium diffraction images revealed perfectly spherical droplet shapes (cf. Fig. 4a) that can be described via Mie simulations. These patterns are therefore ideally suited for extracting the droplets' refractive indices, which reflect the electronic structure. However, due to the multicolor contributions of four harmonic wavelengths (11th-17th HH), this has proven to be a difficult task. In our first analysis the automatized Mie-fitting procedure has led to two solutions (see examples in Fig. 4b, c).

To resolve the remaining ambiguity, we extended the analysis to a large dataset of single-droplet images with simultaneously measured single-shot XUV spectra (see sketch of the setup in Fig. 5). Within the ongoing analysis, we aim to develop a robust multicolor extraction tool of the droplets' refractive indices that builds the basis for our time-resolved studies, which are currently under way.

Two-color diffractive imaging of resonantly excited helium nanodroplets at FERMI

In a complementary approach we exploited the possibilities of the FERMI FEL (Trieste, Italy) to create two-color XUV pulses from the same electron packet. Presently, key aspects of the plasma generation and decay in na-

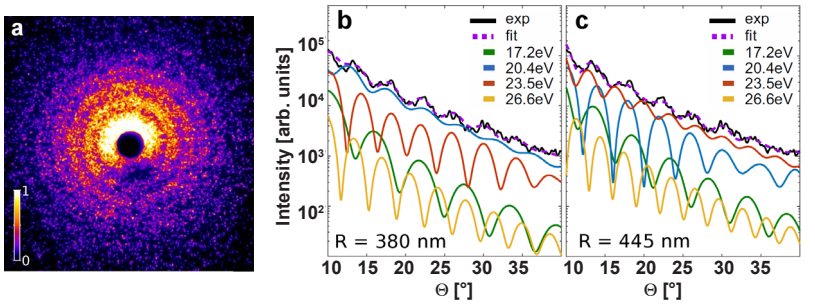

Fig. 4:
a) Typical scattering image of a spherical droplet. b) and c) Multicolour Mie-fits reproduce the measured profiles but two solutions with small residual errors are found. Adapted from [RML17].

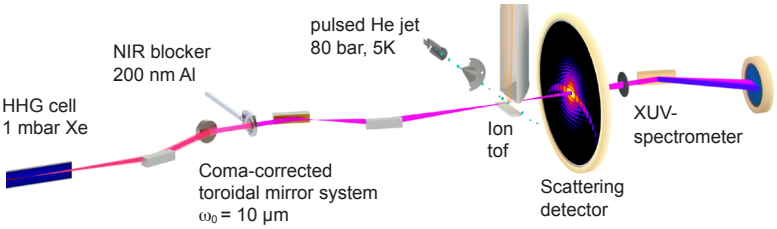

Fig. 5:
Sketch of the experimental setup for single-shot diffraction imaging of single helium nanodroplets. The setup from [RML17] was complemented by a single-shot XUV spectrometer.

noscale matter after excitation with a strong short-wavelength light pulse are unclear or discussed controversially. The case of resonant excitation, when numerous atoms are excited simultaneously, is especially interesting. Efficient and extremely fast interatomic Coulombic decay and collective autoionization can drastically change the nanoplasma formation and dynamics.

Helium nanodroplets were used as model systems because of their interesting structural properties (e.g. superfluidity) and their simple electronic structure with the first excitation transition in the accessible wavelength regime of FERMI ($1s^2$->1s2p at 21.4 eV). As their size and shape differs from droplet to droplet, imaging of initial and final states is essential, which can be achieved in an elegant way by two-color scattering. The interaction with the pump pulse (~20 eV) was utilized for both an energetically tunable excitation and initial state characterization via the resulting diffraction image.

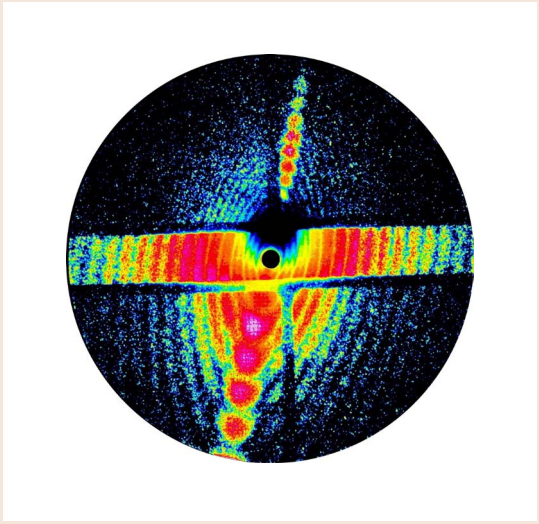

Fig. 6:
Two-color diffraction image of a prolate droplet measured with 21.5 eV and 43 eV photon energies. Filter foils in front of the detector separate the superimposed scattering patterns.

The scattering pattern from the higher energy probe pulse should then provide an image of the same nanodroplet after an adjustable delay to monitor the plasma evolution and cluster decay. In our beamtime in June 2017, our team around D. Rupp, T. Fennel, and T. Möller (TU Berlin, further collaborations with P. Piseri, Universitá di Milano, and C. Callegari and team at FERMI) successfully recorded two-color scattering patterns using large-area filter foils in front of the detector to separate the superimposed scattering patterns (see Fig. 6). Due to an actuator failure in the split-and-delay unit at FERMI, we could only measure at zero time delay, therefore we have applied for an extension beamtime in 2018. The already obtained data contain valuable information, which we are presently analyzing. The results will determine the most suitable excitation energies, complex index of refraction and critical power densities, thus providing the best conditions for the time-resolved study planned for the next round of experiments.

High repetition rate XUV-IR pump-probe setup

In 2017, the high repetition rate 800 nm NOPA became operational. The system produces 2.5 cycle pulses (7 fs FWHM) with 190 µJ pulse energy at 100 kHz repetition rate. Pulse compression to 1.5 cycles has been demonstrated and single shot CEP measurement at full repetition rate has been performed with a phasemeter. For a more detailed description see Project 4.2.

The system has been designed with the aim to enable pump-probe experiments with isolated attosecond XUV and few cycle IR pulses in a reaction microscope. As a first step towards this goal, high harmonic generation (HHG) has been tested. The high available pulse energy of more than 100 µJ allows using a loose focusing geometry as it is common in low repetition rate systems. Thus, the high repetition rate laser beam has been focused by an f = 50 cm mirror into a gas jet created by expanding Argon gas through a 400 µm nozzle. To remove the remaining power (>10 W) of the driving laser, the high harmonics generated are reflected off a silicon plate, which absorbs most of the 800 nm beam. The high harmonics then pass a thin Al foil filtering the residual NIR and enter a home-built XUV spectrometer with an aberration corrected grating to disperse the beam spectrally. An MCP-phosphor screen assembly detects the XUV radiation. Figure 7 shows a typical high harmonics spectrum with a cut-off around 50 eV. Presently, ranges of different parameters, like pressure, nozzle diameter, focusing etc., are explored to optimize the high harmonic flux. In addition, also the 'classical' HHG cell geometries, which so far have only been used in low repetition rate systems, will be investigated.

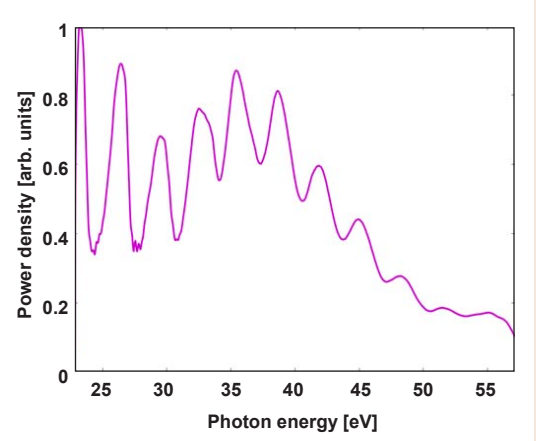

Fig. 7:
HHG spectrum obtained from 150 µJ energy, 7 fs duration laser pulses, focused (f = 50 cm) onto an Argon gas jet, 400 µm nozzle, 800 mbar pressure.

Own Publications 2017 ff

(for full titles and list of authors see appendix 1)

ABL17: K. Amini *et al.*; J. Chem. Phys. **147** (2017) 013933/1-8

BBL17: M. Burt *et al.*; Phys. Rev. A **96** (2017) 043415/1-8

BPB17: G. Bart *et al.*; Comp. Phys. Commun. **219** (2017) 269-285

CPL17: M. F. Ciappina *et al.*; Rep. Prog. Phys. **80** (2017) 054401/1-50

CTF17: C. Callegari *et al.*; Appl. Sci. **7** (2017) 621/1-9

FDS17: M. Floegel *et al.*; Phys. Rev. A **95** (2017) 021401R/1-5

FEC17: R. Feifel *et al.*; Scient. Rep. **7** (2017) 133171-11

GPJ17: G. Goldsztejn *et al.*; Phys. Rev. A **96** (2017) 012513/1-9

GSG17b: M. Galbraith *et al.*; Nat. Commun. **8** (2017) 1018/1-7

GSR17: M. Galbraith *et al.*; Phys. Chem. Chem. Phys. **19** (2017) 19822-19828

MGJ17 : T. Marchenko *et al.*; Phys. Rev. Lett. **119** (2017) 133001/1-6

OSM17b: T. Oelze *et al.*; Scient. Rep. **7** (2017) 40736/1-8

PJK17: R. Puettner *et al.*; Phys. Rev. A **96** (2017) 022501/1-13

PZI17: J. Passig *et al.*; Nat. Commun. **8** (2017) 1181/-7

RFM17c: D. Rupp *et al.*; Physik Journal **11** (2017) 33-39

RML17: D. Rupp *et al.*; Nat. Commun. **8** (2017) 493/1-6

RSL17: P. Rupp *et al.*; J. Mod. Opt. **64** (2017) 995-1003

Sch17: B. Schütte; in *Progress in Ultrafast Intense Laser Science XIII* (Springer, Cham, 2017) 85-110

SBB17: E. Savelyev *et al.*; New J. Phys. **19** (2017) 043009/1-13

SFC17: L. Seiffert *et al.*; Physik in unserer Zeit **48** (2017) 217-218

SHR17: L. Seiffert *et al.*; J. Mod. Opt. **64** (2017) 1096-1103

SKP17: L. Seiffert *et al.*; J. Phys. B **50** (2017) 224001/1-8

SLR17: A. Stodolna *et al.*; J. Phys. B **50** (2017) 164001/1-7

SLZ17 : L. Seiffert *et al.*; Nat. Phys. **13** (2017) 766-770

TCG17: T. Takanashi *et al.*; Phys. Rev. Lett. **118** (2017) 033202/1-6

VHV17: D. Villeneuve *et al.*; Science **365** (2017) 1150-1153

ZIv17: N. Zhavoronkov and M. Ivanov; Opt. Lett. **42** (2017) 4720-4723

Other Publications

NKY13: Ch. Neidel *et al.*; Phys. Rev. Lett. **111** (2013) 033001/1-5

OKR13: C. Ott *et al.*; Science **340** (2013) 716

Invited Talks at International Conferences

(for full titles see appendix 2)

T. Fennel; QUTIF Annual Meeting (Dresden, Germany, 2017-02)

T. Fennel; DPG Spring Meeting (Dresden, Germany, 2017-03)

O. Kornilov; Intense Field, Short Wavelength Atomic and Molecular Processes, ISWAMP, ICPEAC Satellite Meeting (Brisbane, Australia, 2017-07)

J. Mikosch; Int. Conference on Molecular Energy Transfer in Complex Systems, ICOMET 2017 (Innsbruck, Austria, 2017-01)

A. Rouzée; DPG Spring Meeting 2017 (Mainz, Germany, 2017-03)

D. Rupp; Int. DESY Photon Science Workshop: Future of Science at FLASH (Hamburg, Germany, 2017-09)

D. Rupp; Int. Conference on Extreme Light, ICEL 2017 (Szeged, Hungary, 2017-11)

B. Schütte; Extreme Atomic Systems 2017 (Riezlern, Austria, 2017-01)

M. J. J. Vrakking; European Conference on Nonlinear Optical Spectroscopy, ECONOS 2017 (Jena, Germany, 2017-04)

M. J. J. Vrakking; Int. Symposium on Molecular Beams 2017, ISMB 2017 (Nijmegen, The Netherlands, 2017-06)

M. J. J. Vrakking; ATTO 2017 (Xi'an, China, 2017-07)

M. J. J. Vrakking; Artemis and Research Complex User Meeting 2017 (Oxford, UK, 2017-09)

M. J. J. Vrakking; QUTIF Int. Conference 2017 (Bad Honnef, Germany, 2017-09)

3.1: Dynamics of Condensed Phase Molecular Systems

E. T. J. Nibbering, O. Kornilov (project coordinators)
and E.-M. Brüning, F. Dahms, M. Ekimova, B. P. Fingerhut, J. Hummert, A. Kundu, N. Mayer, M. Oßwald, G. Reitsma, M. Richter, H.-H. Ritze, Y. Liu

1. Overview

This project aims at a real-time observation of ultrafast molecular processes in the condensed phase, addressing the dynamics of elementary excitations, photoinduced chemical reactions and ultrafast changes of the electronic and/or chemical structure of molecular systems. The project makes use of a broad range of experimental techniques including all-optical pump-probe spectroscopy in a range from the ultraviolet to mid-infrared, infrared photon-echo and multidimensional vibrational spectroscopies, and photoelectron spectroscopy using ultrashort VUV, XUV, and soft-X-ray pulses.

2. Topics and collaborations

Research in this project has been structured into four major topical directions:

T1: Hydrogen bond dynamics in hydrated biomimetic and biomolecular systems

Collaboration partners: J. T. Hynes (University of Colorado, Boulder, USA), D. Laage (École Normale Supérieure, Paris, France), S. Mukamel (University of California at Irvine, USA), E. Pines (Ben Gurion University of the Negev, Beer-Sheva, Israel).

T2: Transient structure determination of hydrogen bonded acid-base pairs

Collaboration partners: M. Odelius (Stockholm University, Sweden), Ph. Wernet (Helmholtz Zentrum Berlin, Germany), P. M. Tolstoy (St. Petersburg State University, Russia).

T3: Charge transport in biomimetic and biological systems

Collaboration partners: V. S. Batista (Yale University, New Haven, CT, USA), D. Sebastiani (Martin Luther University, Halle-Wittenberg, Germany).

T4: Electronic excited state dynamics in molecular model systems

Collaboration partners: O. Rader (Helmholtz Zentrum Berlin, Germany), D. Arbi (University of Buenos Ayres), L. Bañares (Compulensa University, Madrid, Spain).

Internal collaboration with Projects 2.3 and 3.3 has been established.

3. Results in 2017

T1: Hydrogen bond dynamics in hydrated biomimetic and biomolecular systems

Biomimetic and biomolecular systems and their interactions with water are studied in a wide range of hydration levels to unravel the couplings between the molecular systems and the fluctuating water shells in the electronic ground state [LEH17a, LEH17b]. Hydration dynamics of artificial short DNA RNA oligomers and native salmon DNA in thin films and solution [LGS17, BSS], in hydrated phospholipid reverse micelles, as well as of phosphate ions are the main topics in recent years. A second research line is the investigation of the vibrational dynamics of the hydrated proton. Results on the Zundel cation, $H_5O_2^+$ [DFN17] are described in the Scientific Highlights, page 20. The experiments are based on ultrafast two-color infrared (IR) pump-probe and multi-dimensional photon echo spectroscopies, complemented by computational methods such as density functional theory and ab initio molecular dynamics to simulate linear and multidimensional spectra.

The structure and dynamics of the DNA double helix are influenced in a decisive way by the surrounding water shell due to the interaction with their water environment. In previous years we have explored the ultrafast vibrational response of the sugar and phosphate backbone vibrations of hydrated DNA. Building on these previous results we extended our effort with femtosecond infrared spectroscopic studies of the interactions between DNA and its hydration shell at two different hydration levels [LGS17].

In previous years we have introduced vibrational excitations of the sugar-phosphate backbone as sensitive probes of structural fluctuations,electric fields exerted by the water shell and/or counterion atmosphere, and local hydrogen bond structure. Another important aspect is the energy exchange between DNA and its water shell. In a series of pump-probe experiments performed with native salmon testes DNA at different hydration levels, the response of the backbone to excitation of the water shell was mapped in a temporally and spectrally resolved way [LGS17]. The backbone vibrations in a frequency range from 900 to 1300 cm^{-1} (Fig. 1(a)) display pronounced absorption changes (Fig. 1(b)), following a biphasic response with a fast 1 ps component occurring in parallel to the formation of a hot ground state in the water shell and a subsequent slower contribution devel-oping with time constants between 10 and 20 ps (Fig. 2(a), (b)). This behavior is distinctly different from that of neat water (Figs. 1(c)). The symmetric PO_2 stretch vibration at 1090 cm^{-1} displays a marked blue-shift.

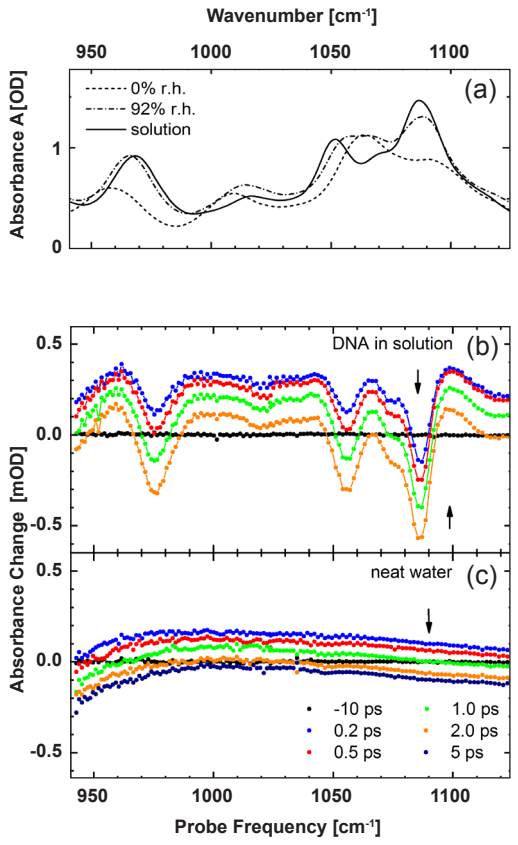

Fig. 1:
(a) Linear infrared absorption spectra of salmon testes DNA at different hydration levels. (b) Infrared absorption of DNA backbone modes. The spectra at 0% (less than 2 water molecules per base pair) and 92% r.h. (20 - 30 water molecules per base pair) were measured with DNA films in which the Na^+ counterions were replaced by ionic CTMA. The solution-phase sample contains DNA with Na^+ counterions. Transient pump-probe spectra of (b) DNA in solution, and (c) neat water after excitation of the water OH stretching vibration by pulses centered at 3450 cm^{-1}. The change of absorbance $\Delta A = -\log(T/T_0)$ in mOD is plotted as a function of probe frequency for different delay times (T, T_0: transmission of the sample with and without excitation).

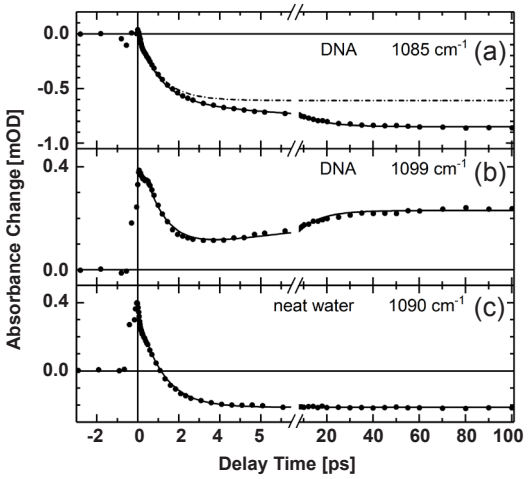

Fig. 2:
(a) Pump-probe transients measured at fixed probe frequencies (arrows in Fig. 1(b), (c) with (a, b) DNA in water, and (c) neat water. The DNA transients display a biphasic time evolution.

For an analysis of the relevant interactions, in-depth simulations of electric fields the water shell exerts on the phosphate group of the model compound dimethylphosphate (DMP) were performed for different temperatures. The time averaged radial distribution functions g(r) (Fig. 3(a)) display a decrease of water occupancy in the first layer with increasing temperature and a concomitant increase and broadening in the second layer. While spatial rearrangements are moderate, the electric field acting on the DMP phosphate group is decreased (Fig. 3(b) - (c)).

Coupling between the water shell and the backbone is predominantly mediated by the electric field the water shell exerts on the backbone. The electric field distribution changes upon formation of the hot water ground state which is connected with a limited relocation of water molecules in the first and second layers around the double helix. The fast component of the DNA response is due to this Coulomb-mediated coupling and the observed blue-shift of the symmetric PO_2 stretching band is in agreement with estimates based on MD simulations of the change in electric field distribution and the relevant force field (Fig. 3). Energy transfer into the DNA double helix occurs on a slower time scale of tens of picoseconds and establishes a common heated ground state of water shell and DNA. The redistribution of excess energy within the DNA structure requires energy delocalization throughout the double helix, a process occurring on a similar time scale of tens of picoseconds.

Our results demonstrate the pronounced sensitivity of biomolecular vibrations and their absorption spectra to electric fields exerted by an aqueous environment. The underlying Coulomb couplings are comparably strong and – in the present case – seem to prevail over anharmonic couplings and their impact on the vibrational spectra.

T2: Transient structure determination of hydrogen bonded acid-base pairs
(DFG NI 492/11.1; SAW-2016)

This activity aims at an analysis of the hydrogen bonded structure of acid-base pairs. By determining structure, the elementary chemical processes of proton release, transfer, and acceptance by the base will be elucidated most directly. Femtosecond infrared techniques are applied to unravel the dynamics of particular hydrogen bonded groups. This information will be complemented by steady-state and time-resolved methods ranging from NMR [KPA17], FT-IR to X-ray absorption [EQS17] and emission spectroscopies. The experimental results are analyzed in close collaboration with theory groups.

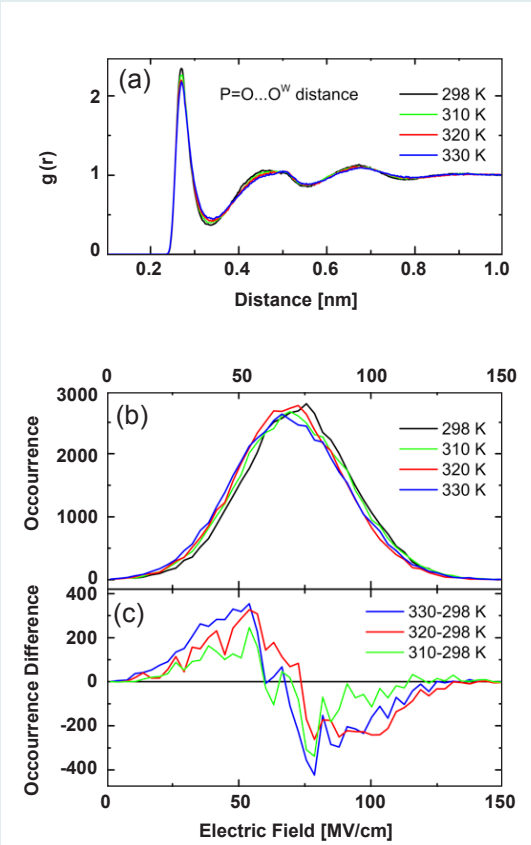

Fig. 3:
(a) Radial distribution functions g(r) of water molecules as a function of distance between the PO_2 oxygens of dimethyl phosphate and the water oxygens for four different sample temperatures. (b) Time averaged distribution of water shell imposed electric fields projected on the C_2 symmetry axis of the PO_2 unit at the midpoint of the oxygen-oxygen axis of DMP for the four different sample temperatures. (c) Occurrence difference of electric fields.

For both quasi-stationary and time-resolved X-ray spectroscopy, we have successfully applied the novel flatjet, which utilizes the phenomenon of formation of stable liquid sheets upon collision of two identical laminar jets. The liquid flatjet operates fully functional under vacuum conditions (<10^{-3} mbar), allowing soft-X-ray absorption spectroscopy (XAS) of the N K-edge of solutes in aqueous or alcohol solutions in transmission mode. Moreover, the L-edge absorption has been measured of particular metal-ligand complexes, which are model systems for light harvesting in antenna complexes.

In a multi-facetted investigation combining local soft-X-ray and vibrational spectroscopic probes with ab initio molecular dynamics simulations, hydrogen-bond interactions of two key principal amine compounds in aqueous solution are quantitatively assessed in terms of electronic structure, solvation structure, and dynamics [EQS17]. Ammonia (NH_3) and ammonium ion (NH_4^+), model compounds chosen, are crucial constituents in the nitrogen cycle and function as test cases for acid-base chemistry of amino acid compounds (which are themselves one important class of the building blocks of life). From the X-ray measurements (Fig. 3(a)), using novel liquid flatjet technology and from the complementary determination of the IR-active hydrogen stretching and bending modes of NH_3 and NH_4^+ in aqueous solution, the picture emerges of a comparatively strongly hydrogen-bonded NH_4^+ ion via N-H donating interactions, whereas NH_3 has a strong accepting hydrogen bond with one water molecule at the nitrogen lone pair but only weak N-H donating hydrogen bonds. In contrast to the case of hydrogen bonding amongst solvent water molecules, we find that energy mismatch between occupied orbitals of both the solutes NH_3 and NH_4^+ and the surrounding water prevents strong mixing between orbitals upon hydrogen bonding, and – thus – inhibits substantial charge transfer between solute and solvent. This is markedly different from hydrogen bonding interaction of liquid water, where a major charge transfer component has been found upon hydrogen bonding between water molecules, with large overlap and associated hybridization of the occupied $H_2O(3a_1)$ orbitals on neighboring water molecules. Our results provide a benchmark for hydrogen bonding of other nitrogen containing acids and bases, including (protonated) amine groups in protein structures.

Figure 4 compares the N K-edge spectra measured at the UE52-SGM beamline at the synchrotron radiation source BESSY II at the Helmholtz Zentrum Berlin with those calculated using ab initio molecular dynamics using density functional theory (DFT) with the quickstep program in the CP2K software suite. From each of the simulations, XA spectra were generated using the full-core-excitation (XFH) potential method. The good correspondence in pre-edge, main-edge and post-edge regions of the N K-edge spectra of both the solutes NH_3 and NH_4^+ is further substantiated by inspection of the unoccupied orbitals reached with N 1s excitations. Figure 5 shows a rather negligible orbital hybridization of the solute with hydration shell water for the LUMO states reached by pre-edge excitations, whereas a major delocalization occurs for post-edge transitions. This orbital delocalization with water molecules hydrogen bonded to the NH_3 lone pair, or to the N-H groups of NH_4^+ is reflected by the substantial increase of the post-edge transition cross section for both solutes in aqueous solution compared to the isolated gas phase case.

T3: Charge transport in biomimetic and biological systems
(DFG NI 492/13-1)

In this topical area, elementary charge transport dynamics in solution are investigated from the viewpoint of their functional role in biochemical processes. The objective is to elucidate the underlying mechanisms for electron transfer, proton transfer as well as proton-coupled electron transfer. This line of research builds on previous ultrafast studies of aqueous proton transfer using photoacids, as well as of photoinduced electron transfer in donor-acceptor complexes. Experimental techniques include transient UV/IR spectroscopy and photoelectron spectroscopy.

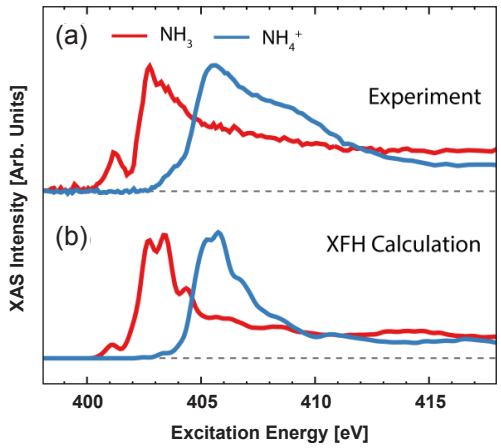

Fig. 4:
Simulated N K-edge X-ray absorption (XA) spectra of NH_3(aq) (red lines) and of NH_4^+(aq) (blue lines) sampled from the present AIMD simulations are compared to experimental spectra. Spectra have been calculated with the full-core-excitation (XFH) transition potential approximations.

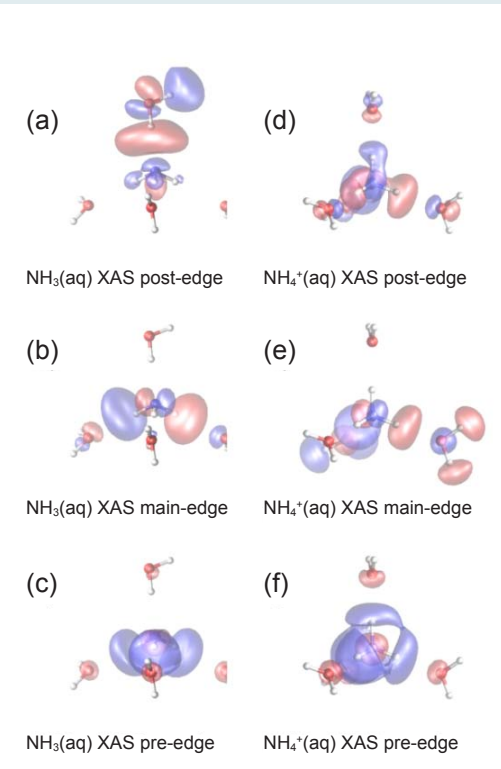

Fig. 5:
Unoccupied orbitals reached with the pre-edge, main edge and post-edge N 1s excitations. The orbitals are taken from XFH calculations of $NH_3(H_2O)_4$ and $NH_4^+(H_2O)_4$ clusters. The solutes are oriented with the C_3 symmetry axis vertical in the plane of the pictures.

Photoacids have been used to much effect as a means to phototrigger ultrafast proton transfer events in aqueous acid-base neutralization reactions using femtosecond UV-pump/IR-probe spectroscopy. Photoacids are typically aromatic molecular systems with a protic hydroxyl- or ammonium-group. Less well explored are the electron donor properties of photoacid aromatic alcohols. We have studied electron donor-acceptor interactions of 1-naphthol (1N) and 2-naphthol (2N) in halocarbon solvents (Fig. 6), by measurement of the fluorescence quenching of these prototype photoacids by using time-correlated single-photon-counting, femtosecond UV-pump/IR-probe spectroscopy (Fig. 7) and quantum chemistry computations [CRP17]. We find that halocarbon solvents facilitate a de-excitation mechanism via solute-solvent electron transfer. Decay rates are modulated by close contact interactions between the π-electronic structure of the naphthol chromophores and halocarbon molecules in their first solvation shell. 1N exhibits faster decay rates than 2N due to closer interactions with the solvent.

T4: Electronic excited state dynamics in molecular model systems
(DFG KO 4920/1-1; DFG FI 2043/1-1)

Determination of the ultrafast electronic excited state dynamics of organic molecules in solution is the main objective of this topical area. Photophysical events such as internal conversion, and photochemical transformations, trans/cis isomerization, ring opening or closure are examples of elementary processes to be studied in detail. The experiments address investigation of dynamics in electronically excited states with time-resolved pump-probe methods.

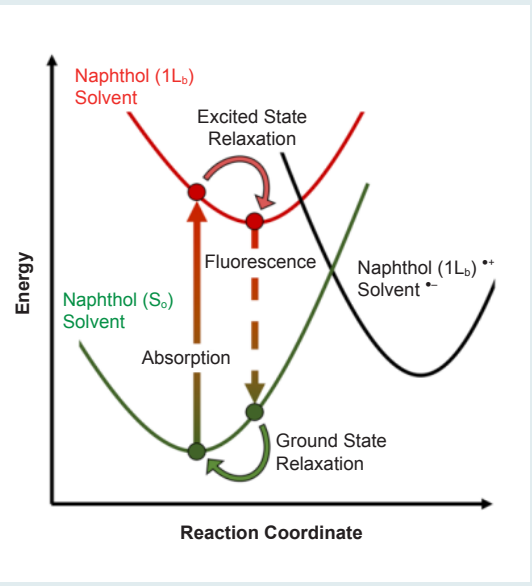

Fig. 6:
Schematic diagram showing the S_0—^1L_b (S_1) electronic transition of 1N and 2N with structural relaxations as the origin of the red shift in fluorescence as well as level crossing to a charge transfer state with the solvent.

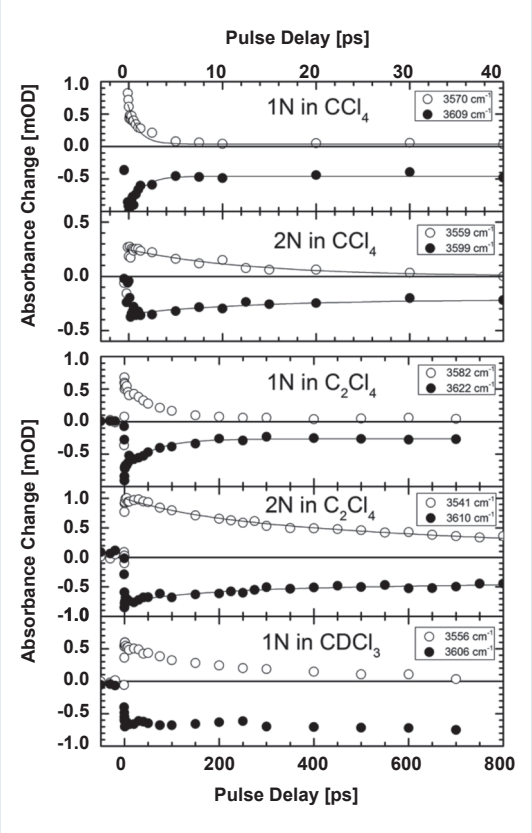

Fig. 7:
Transient kinetics of the O-H stretching marker mode, as recorded at frequency positions of the S_0- and S_1-states, for 1N and 2N. Note the distinct difference in time scales when comparing CCl_4 with C_2Cl_4 or $CDCl_3$ solvents. Multi-exponential fits are shown as solid lines.

We performed a comprehensive study of the ultrafast light induced C-Cl bond cleavage in diarylmethyl chlorides combining femtosecond transient absorption measurements with ab-intio simulations [RRT17]. The observed delayed appearance of radicals (80 fs) and cations (125 fs) (Fig. 8) is assigned to the movement of the excited state wavepacket, initially approaching two conical intersections, i.e., the ultrafast photochemistry with two product channels. The two spatially separated conical intersections lead to bond cleavage into the radical pair and into the ion pair, respectively (Fig. 9). The passing through these intersections determines the partitioning into the differing product channels. The different location of the conical intersections in configuration space explains the observed delay times. Molecular relaxation via subsequent planarization of the diarylmethyl fragment on the 200 – 300 fs timescale further affects the observed signal intensity imposing a delay of the signal in comparison to the wavepacket population.

The cooperative picture of highest temporal resolution, sensitivity measurements, and high-level quantum chemical and dynamical calculations establishes a novel picture where ultrafast photochemistry with two product channels arises due to wavepacket motion through two distinct conical intersections.

Employing the novel time delay compensated XUV monochromator beamline with the liquid jet endstation, we have continued the investigation of electronic structure and relaxation of large yellow dye molecules in solution. Results obtained for quinoline yellow have carefully been assessed with help of DFT calculations, support-

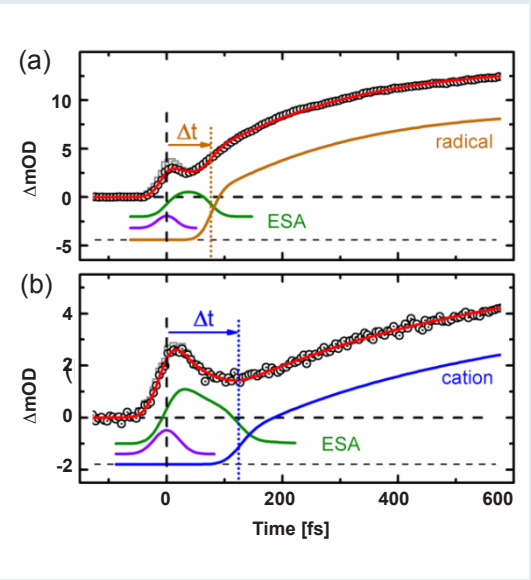

Fig. 8:
Transient absorption (black circles) after UV excitation of dimethylchloride (DPMC) in acetonitrile at a) 32 nm (diphenylmethyl radical) and b) 436 nm (diphenylmethyl cation). The coherent signal from the solvent is subtracted from the raw data (open grey squares) to yield the pure molecular signal. The fit is shown with a solid line (red). The excited state absorption (ESA) (green) and the product absorption from the cation (blue) and radical (orange) are labeled in the plot. Below the ESA is the coherent signal from the molecule (purple).

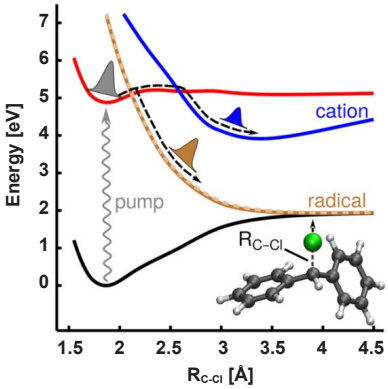

Fig. 9:
Diabatic potential energy curves vs. C-Cl distance R_{C-Cl} calculated on the ONIOM(CAS(12,10)/B3LYP) level of theory. Shown are the ground state S_0 (black), the excited states S_1 (red), S_2 (orange) and S_2' (orange-dashed) leading to the radical and S_3 (blue) leading to the cation.

ing the hypothesis that for the water soluble derivative the enol form is the most stable under aqueous solution conditions. Comparing our data obtained in aqueous solution with literature results reported on these type of compounds dissolved in alcohols, we tentatively assign the fastest observed dynamics (on a time scale of a few hundred femtoseconds) to solvent rearrangements, while slower dynamics correlate to excited state intramolecular proton transfer. Further experiments are underway to determine whether intermolecular hydrogen bonds to the solvent water play a decisive role. Careful calibration of the absolute molecular signal strengths of four different molecules has allowed to identify a negative correlation between molecule solubility and photoelectron signals that can be rationalized by surface densities and depth of the surface layer for these particular solutes.

Own Publications 2017 ff

(for full titles and list of authors see appendix 1)

CRP17: S. Chaudhuri *et al.*; Chem. Phys. Lett. **683** (2017) 49-56

DFN17: F. Dahms *et al.*; Science **357** (2017) 491-495

EQS17: M. Ekimova *et al.*; J. Am. Chem. Soc. **139** (2017) 12773-12783

KPA17: B. Koeppe *et al.*; Phys. Chem. Chem. Phys. **19** (2017) 1010-1028

LEH17a: D. Laage *et al.*; Chem. Rev. **117** (2017) 10694-10725

LEH17b: D. Laage *et al.*; Struct. Dyn. **4** (2017) 044018/1-14

LGS17: Y. Liu *et al.*; Struct. Dyn. **4** (2017) 044015/1-15

RRT17: E. Riedle *et al.*; Chem. Phys. Lett. **683** (2017) 128-134

in press

BSS: E. M. Bruening *et al.*; J. Phys. Chem. Lett.

Invited Talks at International Conferences

(for full titles see appendix 2)

T. Elsaesser; Conference on Time-Resolved Vibrational Spectroscopy, TRVS 2017 (Cambridge, UK, 2017-07)

B. P. Fingerhut; 5th Molcas Developers' Workshop (Jerusalem, Israel, 2017-02)

B. P. Fingerhut; FEMTO'13 (Cancun, Mexico, 2017-08)

B. P. Fingerhut; TRSC Vibrational Dynamics 2017 (Telluride, CO, USA, 2017-08)

E. T. J. Nibbering; 9th Int. Conference on Advanced Vibrational Spectroscopy, ICAVS9 (Victoria, BC, Canada, 2017-06)

3.2: Solids and Nanostructures: Electrons, Spins, and Phonons

C. v. Korff Schmising, M. Woerner (project coordinators)
and K. Busch, G. Folpini, A. Ghalgaoui, R. Grunwald, M. Hennecke, F. Intravaia, P. Jürgens, R. Kernke, F. Mahler, A. Mermillod-Blondin, T. Noll, M. Oelschläger, A. Perez-Leija, B. Pfau, I. Radu, D. Reiche, K. Reimann, D. Schick, V. Shokeen, T. Siebert, C. Somma, C. Strüber, J. Tomm, P. Varytis, D. Weder, R. Wehner, F. Willems

1. Overview

This project addresses ultrafast and nonlinear phenomena in solids and nanostructures. In correlated condensed-matter systems, interaction of electrons, phonons and spins lead to a broad range of novel and unusual phenomena, which are interesting from the point of view of both fundamental research and practical applications. To gain new insight into fundamental phenomena in this thriving field of research, experiments are performed with ultrafast time resolution and in a very wide spectral range extending from terahertz (THz) to X-ray frequencies. The work includes studies in the regime of nonperturbative light-matter interactions.

Our basic research is complemented by studies of light-matter interactions in materials processing with ultrashort optical pulses and by work on optoelectronic devices. The project includes five topics.

2. Topics and collaborations

T1: Nonlinear THz and mid-infrared spectroscopy

Cooperation partners: K. Biermann (Paul-Drude-Institut, Berlin, Germany), C. Flytzanis and D. Laage (École Normale Supérieure, Paris, France), I. Brener (Sandia National Laboratory, Albuquerque, New Mexico, USA), J. Hoja and A. Tkatchenko (University of Luxembourg).

T2: Material modification with femtosecond laser pulses

Project: DFG GR 1782/12-2.

Cooperation partners: J. Bonse and J. Krüger (Bundesanstalt für Materialprüfung – BAM, Germany), A. Pfuch and T. Toelke (INNOVENT, Jena), W. Seeber (Otto Schott Institute, FSU Jena, Germany), E. McGlynn (School of Physics, Dublin City University, Dublin, Ireland), F. Güell (University Barcelona, Spain), P. Kazansky (University Southampton, UK).

T3: Optoelectronic devices

The BMBF project “Spectroscopic analysis of GaN-based single emitters and bars, direct-blue kilowatt diode lasers” (BlauLas), 13N13901, is the main subject of the work of the group. With Trumpf Inc. (Cranbury, USA) we have a research contract on high-power diode lasers. Joint work on quantum dot emitters and GaN-based structures is carried out in cooperation with F. Yue from the University of Shanghai. Analytical work on GaN-based diode lasers is carried out in cooperation with M. Vanzi from the University of Cagliari. There is also a cooperation on the Adlershof campus with Jenoptik Diode Lab, the Ferdinand-Braun-Institut (FBH), and the Institut für Kristallzüchtung (IKZ).

T4: Magnetism and transient electronic structure

Projects: BMBF „DynaMaX: Messplatz für ultraschnelle Dynamik bei BESSY II“ in cooperation with TU Berlin and FU Berlin, Germany. BMBF „Femto-THz-X („THz Instrumentierung und weitere Entwicklungen am FemtoMAX Strahlrohr an MAX IV“) in cooperation with University Potsdam, Germany, and Lund University, Sweden. The DFG-funded Collaborative Research Center/Transregio 227 “Ultrafast Spin Dynamics” of Freie Universität Berlin and Martin-Luther-Universität Halle-Wittenberg together with the non-university institutions Fritz-Haber-Institut, Helmholtz Zentrum Berlin, and the Max-Planck-Institut für Mikrostrukturphysik, Germany, has been established at the end of the year for a start in January 2018.

Further cooperation partners: J. Lüning at Sorbonne Université, Paris, France, and S. Bonetti at Stockholm University, Sweden.

T5: Joint HU-MBI Group on Theoretical Optics

Projects: within the DFG-SPP-1839 “Tailored Disorder”, project Bu 1107/10-1 “Light-path engineering in disordered waveguiding systems”.

Cooperation partner: W. Pernice (Universität Münster, Germany).

Results in 2017

T1: Nonlinear THz and mid-infrared spectroscopy

Strong local-field enhancement of the nonlinear soft-mode response in a molecular crystal

Using two-dimensional THz spectroscopy we studied the nonlinear response of soft-mode excitations in polycrystalline acetylsalicylic acid (aspirin) [FRW17]. We demonstrated for the first time that the correlation of CH_3 rotational modes with collective oscillations of π electrons drives the system into the nonperturbative regime of light-matter interaction, even for a moderate electric field strength of the THz pulses on the order of 50 kV/cm. Nonlinear absorption around 1.1 THz leads to a blue shifted coherent emission at 1.7 THz, revealing the dynamic breakup of the strong electron-phonon

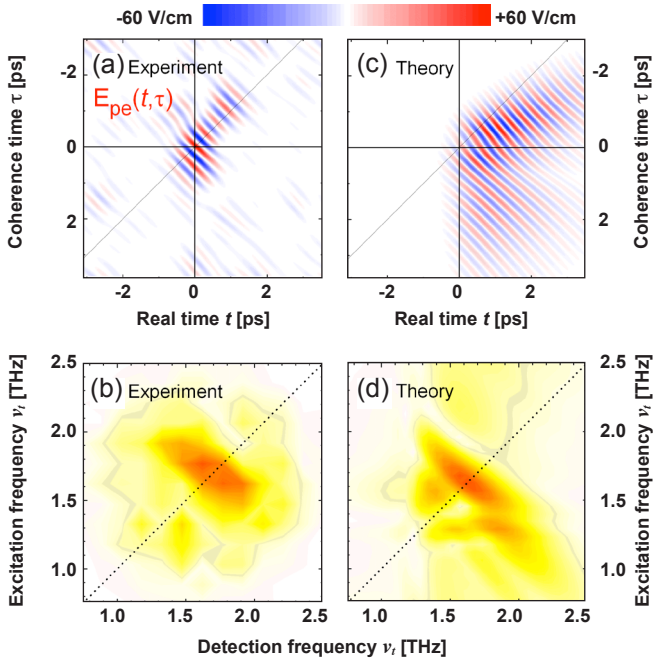

Fig. 1:
(a) Terahertz photon echo signal measured on a polycrystalline thin film of aspirin at a lattice temperature of T_L = 80 K. In contrast to conventional photon echo experiments typically performed on weakly interacting media in the $\chi^{(3)}$-limit the THz photon echo experiments on the soft mode of aspirin shows predominantly a signal at negative coherence times [panel (a)] and an elliptic shape in the 2D frequency domain [panel (b)] with its long axis perpendicular to the diagonal (dashed line). (c), (d) Theoretically calculated photon echo signals next to their experimental counterparts in (a) and (b).

correlations. The observed behavior is reproduced by theoretical calculations including dynamic local-field correlations. Because of the strong coupling between vibrations and electronic excitations, the frequency of this coupled excitation differs strongly between isolated molecules and molecules in a crystal. Furthermore, the frequency of this vibration increases upon increasing its amplitude, resulting in a new type of optical nonlinearity. Further details are presented in the Scientific Highlights, page 24.

In Fig. 1 we show the THz photon echo signal measured on a polycrystalline thin film of aspirin at a lattice temperature of T_L = 80 K. In two aspects, the signals observed here are different from conventional photon echo experiments typically performed on weakly interacting media in the $\chi^{(3)}$-limit. (a) The THz photon echo signal observed for the soft mode of aspirin shows predominantly a signal at negative coherence times, i.e. in the acausal range concerning an A-B-B pulse sequence generating the photon echo. The strong dipole-dipole interaction of the soft mode in aspirin crystallites leads to local driving fields which are dominated by the coherent soft-mode polarizations decaying on the picosecond time scale. The slow decay of the local field allows for photon echo signals at negative coherence times. (b) The elliptic shape in the 2D frequency domain of the photon echo signal has its long axis perpendicular to the diagonal (dashed line). This points to a destructive interference of photon echo signals in real time stemming from crystallites with different orientations relative to the THz driving field. Each individual crystallite shows a slowly decaying photon echo polarization leading to a small homogeneous width in the nonlinear 2D spectrum (panel (b)). In panels (c) and (d) we show theoretically calculated photon echo signals next to their experimental counterparts in panels (a) and (b).

Water librations in the hydration shell of phospholipids

Most biological and biochemical processes occur in a water-rich environment. In particular, most biomolecules are surrounded by several layers of water molecules. To get insight into the properties of interfacial water, we studied the librations of water molecules bound to phospholipid micelles by time-domain THz spectroscopy and compared the results to neat water. The observed differences allow to identify the contributions of hydrogen bonds between water molecules and the phospholipid head groups [FSW17]. The experiments focus on the L2 libration band, extending between 300 and 900 cm^{-1} in bulk water, a particularly sensitive probe for the local hydrogen bond geometry and strength at the interface between water and a biomolecule.

The hydrogen bond patterns formed by water molecules confined in DOPC reverse micelles (Fig. 2(a)) are explored by time domain THz spectroscopy. A picosecond broadband THz pulse is generated by pumping an OH1 organic nonlinear crystal with an amplified short pulse at 800 nm, and detected in amplitude and phase by time-resolved free-space electrooptic sampling. Figure 2(b) shows the transient THz field and its spectrum: the ultrabroadband pulse spans between 50 and 1000 cm^{-1}, allowing for direct observation of the L2 band at a high dynamic range. Figure 2(c) shows absorption spectra for hydration levels between w_0 = 2 and w_0 = 16 water molecules per phosphate heads, on top of the bulk water L2 band (shown as a blue line for comparison). At low hydration levels a feature emerges at 830 cm^{-1} which is assigned to water molecules forming hydrogen bonds with the phosphate units of the DOPC head groups. The frequency upshift corresponds to a higher force constant of the librational motion and thus to a hydrogen bond strength exceeding that of bulk water.

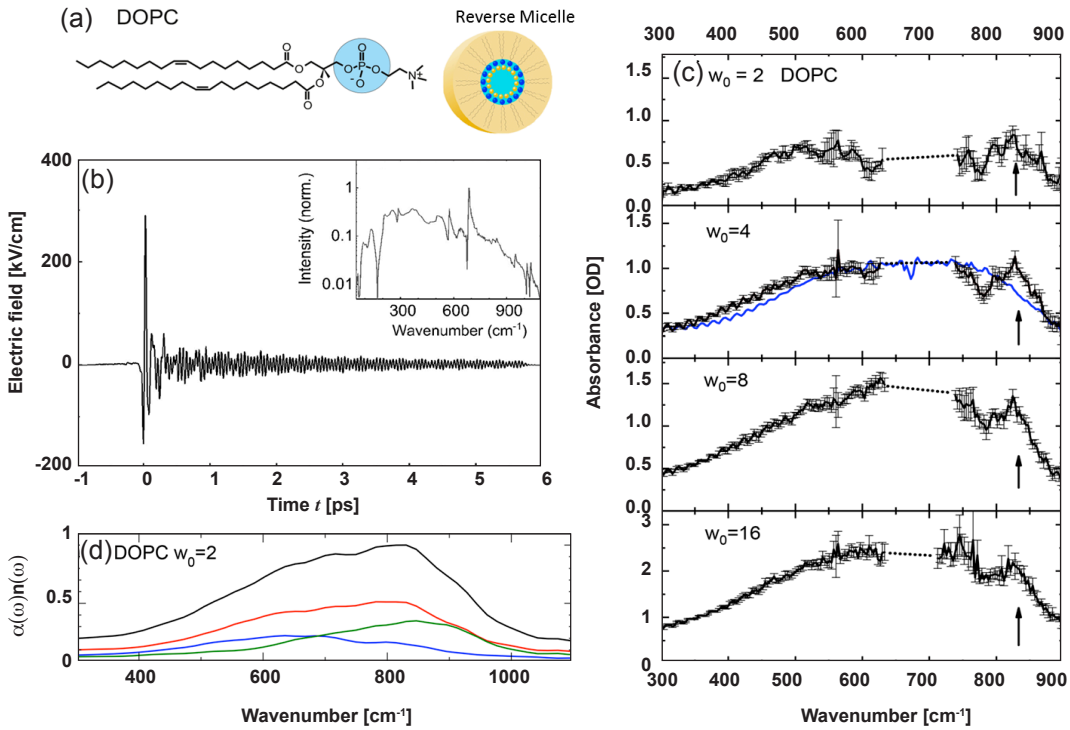

Fig. 2:
(a) Molecular structure of DOPC, the molecules building the micelles, and schematic view of a reverse micelle with a water nanopool in the center. (b) Multi-octave spanning THz pulse, generated using the organic crystal OH1 pumped with a broadband 800 nm pulse. (c) Absorption spectrum for four different hydration levels, from w_0 = 2 to w_0 = 16. The absorption spectrum of neat water is shown in the second panel as a solid blue line. (d) Calculated water vibrational spectra in DOPC reverse micelles at w_0 = 2 (solid black line). The contributions of individual water dipoles are separated according to the hydrogen-bonding environment: one hydrogen bond to a phosphate group (red), two hydrogen bonds to phosphate (green), and no hydrogen-bond to phosphate (blue).

This assignment is supported by molecular dynamics simulations. The total librational absorption of the water droplet (black line in Fig. 2(d) for w_0 = 2) is decomposed into the contributions arising from water molecules in different hydrogen-bond environments: molecules forming one (red) or two (green) hydrogen bonds to the phosphate group show a librational peak shifted to higher frequencies compared to those bonded to the water hydrogen bond network (blue line). For lower hydration levels the absorption peak is hence shifted to 830 cm^{-1}, while at w_0 = 16, where most of the water molecules are in a bulk-like state, the libration band peaks at 600 cm^{-1}.

T2: Material modification with femtosecond laser pulses

Dynamics of excitation and structure formation at semiconductor surfaces

In the focus of continued studies were the generation and the spatio-temporal management of plasmons at solid surfaces. Particular emphasis was laid on pump-probe diffraction and scattering experiments at silicon surfaces with high temporal resolution [LSE17, LSE]. A combined plasmonic and thermal mechanism of laser-induced nanostructure formation in silicon was established by the experiments. The pump source was a Ti:sapphire laser amplifier (Spitfire, Spectra Physics, λ = 800 nm, τ = 120 fs). The generated second harmonic at λ = 400 nm served as a probe with a variable time delay (minimum step width: 30 fs). The diffraction was detected by a sensitive high-resolution Electron Multiplying CCD camera (Andor). A combined nonthermal-thermal mechanism has to be assumed with subsequent steps including surface plasmon polariton generation in the initial phase and thermal structure formation and surface re-arrangement long after the end of the excitation pulses. This conclusion is strongly supported by recent results of other groups.

Laser-induced plasma formation in solid dielectrics

When strong-field ionization (SFI) occurs in a dielectric solid, the plasma density increases in a nearly stepwise fashion with two steps per optical cycle of the driving field (Fig. 3(a)). The Fourier series of the plasma density evolution $\rho_{SFI}(t)$ contains even harmonics of the incident laser field (Fig. 3(b)), the so-called Brunel harmonics. Since only the rapid variations of $\rho_{SFI}(t)$ contribute to the harmonic emission, time-resolved detection of Brunel harmonics allows to analyze sub-cycle ionization dy-

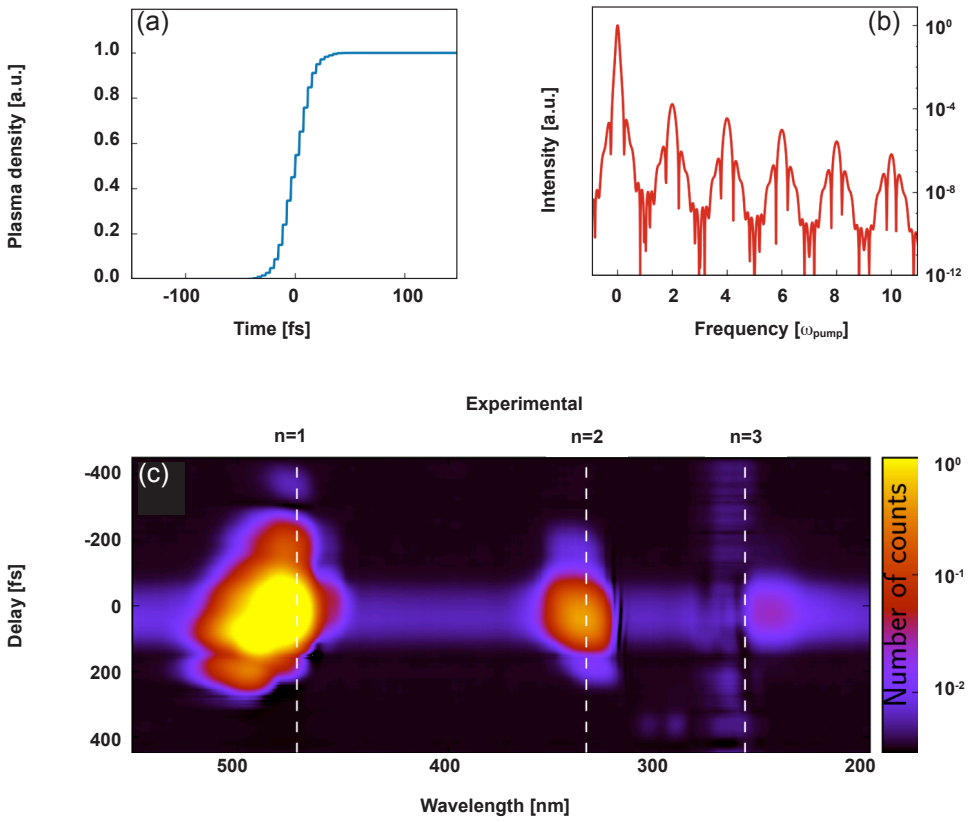

Fig. 3:
(a) Temporal evolution of the plasma density in fused silica irradiated by an ultrashort laser pulse.
(b) Fourier series expansion of (a) containing even harmonics of the driving laser field.
(c) Time-resolved experimental spectrogram resulting from two-colour irradiation of a 0.5 mm fused silica sample.

namics in the frequency domain. In a two-color pump-probe scheme Brunel harmonics occur at frequencies $\omega_n = \omega_{probe} + 2n \times \omega_{pump}$ where $n \in \mathbb{N}$. An experimental spectrogram displaying the first three orders of Brunel harmonics obtained from a two-color pump-probe experiment (λ_{pump} = 2300 nm, τ_{pump} = 150 fs, λ_{probe} = 790 nm, τ_{probe} = 40 fs) in the bulk of fused silica is shown in Fig. 3(c). By performing an iterative phase-retrieval on the experimental spectrogram, it is possible to reconstruct the plasma formation dynamics due to SFI. A simultaneous measurement of the total plasma density generated in the material reveals the relative importance of the two competing ionization mechanisms (SFI and electron impact ionization), thus allowing unprecedented insights into ultrafast plasma formation dynamics in solid dielectrics.

T3: Optoelectronic devices

Transient photoluminescence and micro-Raman spectroscopy is applied to optoelectronic devices and semiconductor structures. GaN-based high-power diode lasers are analyzed to identify their limitations in terms of emission power and thermal properties. The devices are provided by external partners within the frame of cooperative projects such as BlauLas together with Osram Opto Semiconductors, Coherent-Dilas, and Laserline, funded by the BMBF or within the frame of bilateral research contracts, e.g., with Jenoptik Diode Lab or Trumpf Inc.

Analysis of the Catastrophic Optical Damage (COD) in diode lasers, a prominent sudden degradation mechanism, is an important part of the work in cooperation with industry. COD is a generic mechanism, which originates from the interplay of localized light absorption and local temperature rise. The energy for this process is exclusively provided by device emission. The process can start at any absorbing site, including both facets of edge-emitting diode lasers, internal defects within the waveguide, as well as absorbing sites in passive waveguides. We provoked COD in 450 nm emitting GaN-based diode lasers in single high-power pulses. Afterwards, the devices were opened by focused ion beam (FIB) and inspected by scanning electron microscopy [MVH17, TKM]. Figure 4 shows results of an analysis of one COD-related defect. After having systematically analyzed a number of devices, we find that COD results in material loss including the formation of an empty channel that shows high uniformity along the laser axis. The damage patterns, shown in Fig. 4, result from a COD process, which lasted for ~700 ns. The process terminated because energy supply ended. As a re-

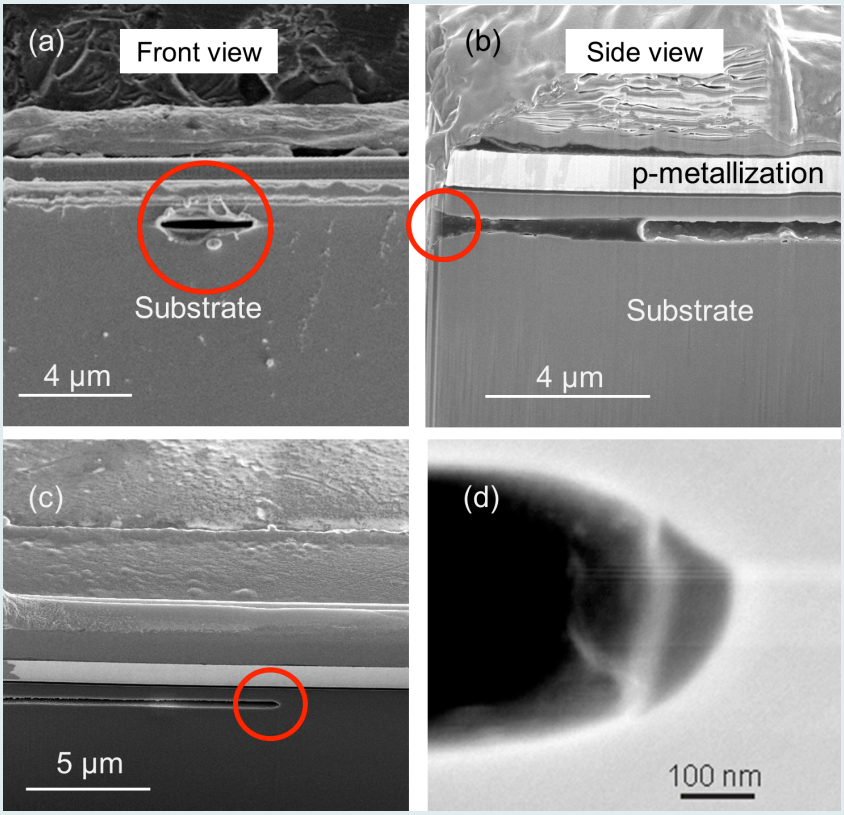

Fig. 4:
Front view to the emitting aperture at a laser facet. The red circle points to the hole created by the COD. (a) Side view to a FIB lamella taken across the center of the damage pattern shown in (a). Obviously, an empty channel is created starting at the front facet; see red circle. (b) End of the same channel revealed ~80 µm underneath the front facet. (c) The very end of the channel, which is marked in (c) by a red circle. In this image the quantum wells, see periodic structure in the upper part, represent the center of the active region of the device. With respect to them, the channel is further extended towards the n-side (bottom) than to the p-side (top).

sult, a channel length of 80 µm has been observed; see Fig. 4(b) und (d). The extension of the channel in growth direction was ~400 nm. From these results, a defect front propagation velocity along the laser axis of ~110 m/s is estimated. The laser structure in the immediate vicinity of the empty channel appears to be completely undamaged. (Fig. 4(d)). No recrystallized material is observed. The observed damage pattern resembles the shape of the optical mode. This suggests that defect growth during COD in GaN-based devices is fed by the optical mode, i.e., by laser energy. COD in GaN-based devices is a hot process that involves material decomposition and even vaporization of quantum-well and waveguide materials. As an upper limit for the temperature, we find 3500°C, as a lower limit ~1000°C. The decomposition behavior of GaN-based compounds and the actual device architecture point to a maximum temperature during COD close to the lower limit, ~1000°C [MVH17, TKM].

Another topic that has been addressed in cooperation with FBH is the thermal lens of broad area high-power diode lasers, playing a key role for their beam-parameter product M^2 [RWT17, RWK]. Thermal distributions in broad area lasers were investigated with micro thermography infrared (IR) measurements and simulations. Detailed measurements show an anomalous temperature step in the vertical direction at the transition between chip and submount. The simulation shows a lower active zone temperature increase which leads to a lower thermal resistance. A thermal barrier is responsible for an increase of the thermal resistance around 1 K/W and an up to 40% stronger curvature of the lateral thermal profile which leads to an increase of the M^2 of 1 mm×mrad. Thermal boundary conduction appears to influence the thermal barrier but the technological background has to be investigated further [RWT17, RWK].

T4: Magnetism and transient electronic structure

Ultrafast XUV spectroscopy of magnetic systems

Functional magnetic systems can be controlled by ultrashort laser pulses: magnetization can be quenched or even deterministically reversed; spin currents can be launched and injected into a non-magnetic material. In recent years femto-magnetism has developed into a versatile field of solid state physics, where an increasing number of different experimental approaches as well as theoretical efforts have started to provide a better understanding of the very complex microscopic physics. This research is also driven by opportunities for future efficient and high-density data storage as well as for novel spintronic devices. Here, technological progress is driven by a rapid development of increasingly complex, multicomponent ferromagnetic or antiferromagnetic heterostructures and their miniaturization for perpendicular recording in nanostructured media. To provide a comprehensive understanding of such magnetic systems, new experimental approaches need to be developed which cannot only disentangle the femtosecond, element-specific response but also allow access to magnetization on the nanoscale.

To this end we have set-up a new high harmonic laboratory for time resolved transient reflection and absorption spectroscopy as well as resonant small angle scattering and coherent imaging experiments (Fig. 5(a)). The

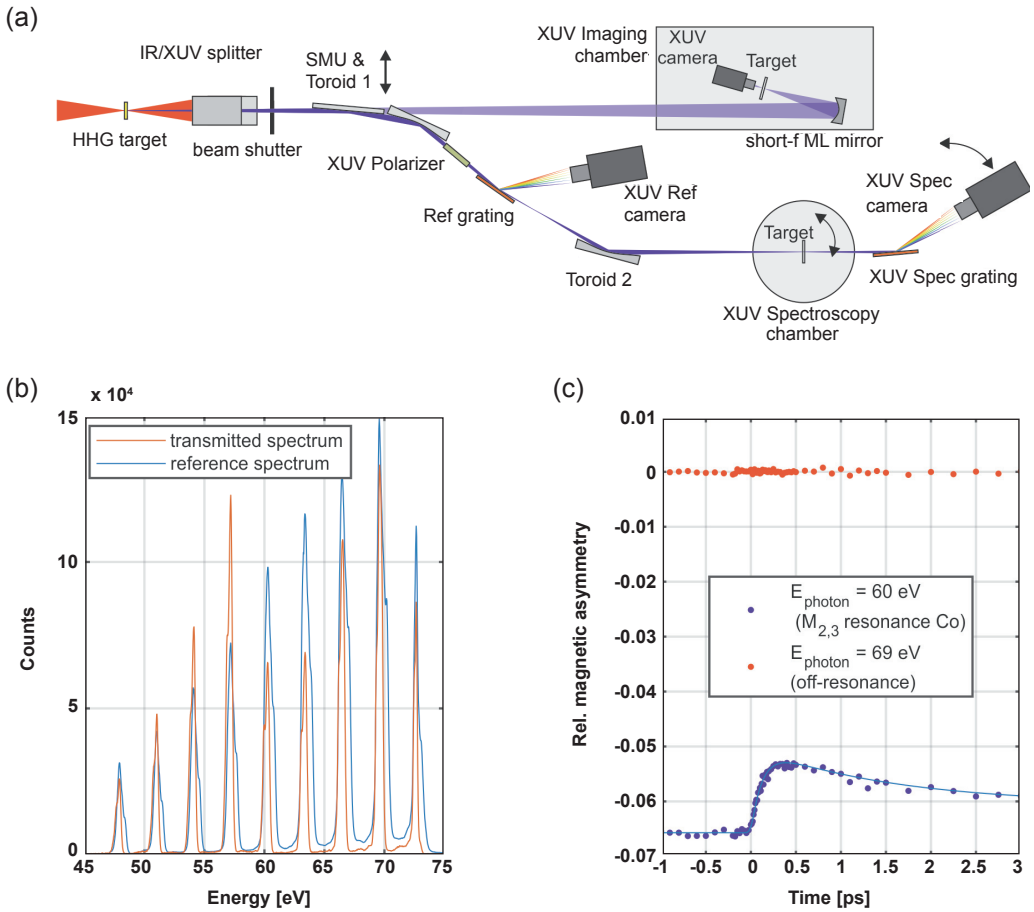

Fig. 5:
(a) Sketch of the new high harmonic beamline for transient absorption/reflection as well as small angle scattering and coherent imaging experiments. We generate circularly polarized radiation in the extreme ultraviolet (XUV) spectral range via a 4-mirror phase shifter [KWN17] to access the element-specific magnetization via magnetic circular dichroism. To improve the signal-to-noise ratio we normalize the transmitted spectrum to the incoming reference spectrum. In (b) we show the reference XUV spectrum (blue line) and the transmitted spectrum (red line) through a thin cobalt film exhibiting a pronounced absorption edge around the Co $M_{2,3}$ resonance at 60 eV. (c) The time resolved relative magnetic asymmetry at 60 eV shows a drop of the magnetization of almost 20% after femtosecond optical excitation; off-resonant radiation, e.g. at 69 eV, displays neither a magnetic signal nor any transient change. Its standard deviation is below 3×10^{-4}, demonstrating the excellent correlation between our two spectrometers.

spectroscopy beamline uses broadband radiation in the extreme ultraviolet (XUV) spectral range to simultaneously access the optically excited non-equilibrium magnetization in multicomponent systems via magnetic circular dichroism. The XUV radiation is circularly polarized by a 4-mirror phase shifter [KWN17]. Before interaction with the sample, a small fraction of the XUV radiation is diffracted towards a reference CCD camera and used for normalization. This significantly improves the signal-to-noise ratio in time resolved experiments. In Fig. 5(b), we show both, the reference spectrum and the transmitted spectrum through a thin cobalt film; here the $M_{2,3}$ absorption edge of Co at 60 eV is clearly visible. Figure 5(c) shows a time resolved transient of the relative magnetic asymmetry after optical excitation. At the $M_{2,3}$ resonance we observe a drop of the magnetic signal from 6.5% to 5.3% with a time constant of (120 ± 3) fs, corresponding to a reduction of the magnetization of almost 20%. At off-resonant energies, e.g. at 69 eV, we measure neither any magnetic signal nor any transient response. It is worth mentioning that this curve exhibits a mean value of only 3×10^{-6} with a standard deviation below 3×10^{-4}, demonstrating the excellent correlation between our two spectrometers, allowing for sensitive measurements of small effects. Currently, we are investigating Co/Pt heterostructures to study ultrafast spin transport and the influence of enhanced spin-orbit coupling at interfaces.

Complementary all-optical setups for ultrafast Kerr measurements as well as a Kerr microscope for studies of all optical magnetization switching are operational and have been used to explore ultrafast all-optical switching in ferrimagnetic alloy samples.

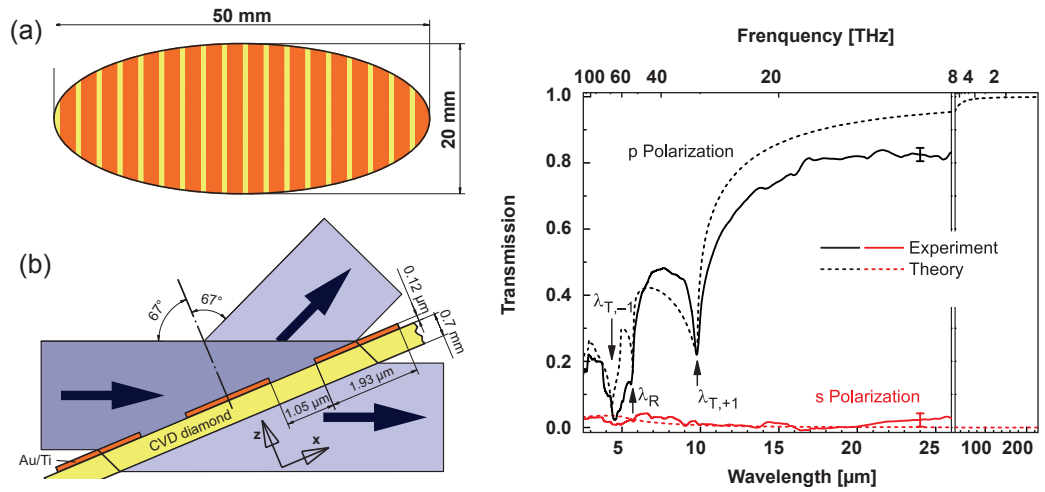

Fig. 6:
Left: (a) Top view of the beam splitter (Au stripes (dark) not to scale), (b) Principle of the beam splitter (CVD diamond substrate not to scale). Right: Experimental and numerical results for the spectral transmission (Brewster angle incidence). Adapted from [SRW17].

T5: Joint HU-MBI Group on Theoretical Optics

Mid-infrared beam splitter for ultrashort pulses

For typical time-resolved measurements it is necessary to split an incident pulse into two replicas. Such a beam splitter should have no losses and should preserve the pulse lengths of the two pulses generated. While this is standard in the visible and near-infrared, it becomes difficult in the mid-infrared and THz spectral ranges. In a joint project of the experimental team of T1 and the theoretical group T5 we designed a reflective beam splitter using polycrystalline diamond as the substrate [SRW17].

Specifically, in the mid-infrared spectral range, simple optical elements such as beam splitters become sensitive to dispersion occurring in the materials commonly used for their fabrication. In an experiment-theory collaboration, the joint HU-MBI Group designed a grating-based broad-band THz beam splitter with desired splitting ratios and analyzed the distortion of THz pulses upon propagation through such structures. Since the splitting ratio must be essentially constant over the bandwidth of the pulse, in order to reduce the absorption in the relevant spectral range, CVD diamond was chosen as the main material for the device. The split ratio was tuned by depositing Au/Ti stripes on it (see Fig. 6, left). To determine the optimal design (width and period of the stripes for a desired splitting ratio), we have performed computations using the so-called Fourier modal method, also known as rigorous coupled-wave analysis. This frequency-domain method allows the computation of the scattered electromagnetic field through periodically structured multi-layer systems.

The experimental measured values for the transmission coefficient and the corresponding computed results showed a very good agreement (see Fig. 6, right), validating our approach and the correct functioning of the beam splitter in in the mid-infrared and terahertz spectral range. In this region, the beam splitter featured a nearly perfect constant phase shift and a reasonably constant splitting ratio. The flexibility provided by our numerical simulation allows the adaptation the design for other wavelengths and other splitting ratios.

In a related context, the Joint HU-MBI Group on Theoretical Optics was also involved in the DFG priority program 1839 “Tailored Disorder – A science- and engineering based approach to materials design for advanced photonic application” with the aim to utilize disorder in photonic structures in order to enhance existing and/or realize novel functionalities. The group is part of a theory-experiment collaboration aiming to design of an ultra-compact wavelength selective spectrometer which utilizes disorder as main resource. Recently substantial progress has been achieved in this direction and numerical optimized devices have been handed for experimental validation.

Own Publications 2017 ff

(for full titles and list of authors see appendix 1)

BHK17: J. Bonse *et al.*; IEEE J. Sel. Top. Quant. Electron. **23** (2017) 9000615/1-15

BKH17: J. Bonse *et al.*; SPIE Proc. **10092** (2017)

BSM17: M. K. Bhuyan *et al.*; Optica **4** (2017) 951-958

CBR17: K. Carva *et al.*; in *Handbook of Magnetic Materials*, E. Brück ed. (Elsevier B.V, Delft, The Netherlands, 2017) 291-463

DKD17: A. Donges *et al.*; Phys. Rev. B **96** (2017) 024412/1-7

FRW17: G. Folpini *et al.*; Phys. Rev. Lett. **119** (2017) 097404/1-6

FSW17: G. Folpini *et al.*; J. Phys. Chem. Lett. **8** (2017) 4492-4497

FTK17: S. Friede *et al.*; SPIE Proc. **10123** (2017) 1012308/1-7

GOW17: A. Ghalgaoui *et al.*; J. Phys. Chem. Lett. **8** (2017) 2666-2671

HRK17: S. Höhm *et al.*; Phys. Scripta **92** (2017) 034003/1-7

IKT17: M. F. Ibad *et al.*; Microporous Mesoporous Mat. **254** (2017) 136-145

KWB17: H. Kissel *et al.*; SPIE Proc. **10086** (2017) 100860B/1-12

KWN17: C. v. Korff Schmising *et al.*; Rev. Sci. Instrum. **88** (2017) 053903/1-8

LSE17: A. Lübcke *et al.*; in *Reference Module in Chemistry, Molecular Sciences and Chemical Engineering* online (Elsevier, 2017), http://dx.doi.org/10.1016/B978-0-12-409547-2.14042-9

MVH17: G. Mura *et al.*; Phys. Status Solidi-R **11** (2017) 1700132/1-6

RCH17: A. Rudenko *et al.*; Sci. Rep. **7** (2017) 12306/1-14

RHK17: A. Rosenfeld *et al.*; in *Reference Module in Chemistry, Molecular Sciences and Chemical Engineering* online (Elsevier, 2017), https://doi.org/10.1016/B978-0-12-409547-2.14127-7

RWT17: J. Rieprich *et al.*; SPIE Proc. **10085** (2017) 1008502/1-10

SMG17a: T. Seuthe *et al.*; Sci. Rep. **7** (2017) 43815/1-10

SMG17b: T. Seifert *et al.*; SPIN **7** (2017) 1740010/1-11

SPB17: J. Sperling *et al.*; Phys. Rev. A **96** (2017) 032334/1-11

SRW17: C. Somma *et al.*; Opt. Lett. **52** (2017) 2918-2921

WKI17: T. Weber *et al.*; Opt. Express **25** (2017) 16947-16956

WRE17: M. Woerner *et al.*; in *Reference Module in Materials Science and Materials Engineering* online (Elsevier, 2017), https://www.sciencedirect.com/science/article/pii/B9780128035818095291

in press

BSG: J. Bonse *et al.*; Appl. Phys. A

LSE: A. Lübcke *et al.*; in *Encyclopedia of Interfacial Chemistry: Surface Science and Electrochemistry* (Elsevier)

WRE: M. Woerner *et al.*; in *Encyclopedia of Modern Optics II*

submitted

RWK: J. Rieprich *et al.*; J. Appl. Phys.

TKM: J. W. Tomm *et al.*; J. Electron. Mater.

Invited Talks at International Conferences

(for full titles see appendix 2)

K. Busch; 2nd Int. SFB/TRR 142 Workshop on Tailored Nonlinear Photonics (Paderborn, Germany, 2017-02)

K. Busch; CLEO Europe-EQEC (Munich, Germany, 2017-06)

S. Eisebitt; 633. WE-Heraeus-Seminar: Spin-Orbit Dynamics – Connecting Timescales from Nanoseconds to Femtoseconds (Bad Honnef, Germany, 2017-01)

S. Eisebitt; Photonics Spring Workshop (Brugg-Windisch, Switzerland, 2017-03)

S. Eisebitt; Moscow Int. Symposium on Magnetism, MISM-2017 (Moscow, Russia, 2017-07)

T. Elsaesser; APS March Meeting 2017 (New Orleans, LA, USA, 2017-03)

T. Elsaesser; Terametanano II (Venice, Italy 2017-05)

T. Elsaesser; XXXII Int. Union of Radio Science General Assembly & Scientific Symposium (Montreal, Canada, 2017-08)

I. Radu; 8th Int. Conference on Metamaterials, Photonic Crystals and Plasmonics, META'17 (Seoul, South Korea, 2017-07)

I. Radu; Spins, Waves and Interactions 2017 (Greifswald, Germany, 2017-07)

I. Radu; Physical Society of Japan Meeting (Morioka, Japan, 2017-09)

J. W. Tomm *together with* R. Kernke, G. Mura, M. Vanzi, M. Hempel, and B. Acklin; 2017 IEEE High Power Diode Lasers & Systems Conference (Coventry, UK, 2017-10)

M. Woerner; Int. Workshop on Finite Systems in Non-equilibrium: From Quantum Quench to the Formation of Strong Correlations (Natal, Brazil, 2017-09)

3.3: Transient Structures and Imaging with X-rays

M. Woerner, B. Pfau (project coordinators)
and C. Hauf, P. Hessing, A. Hernandez, M. Holtz, A. Jonas, C. v. Korff Schmising, J. Lebendig-Kuhla, M. Schneider, H. Stiel, J. Tümmler, D. Weder, J. Weißhaupt, K. Witte

1. Overview

The aim of project is the development and application of XUV, soft and hard X-ray sources for structure analysis and imaging with high spatial and temporal resolution down to atomic length scales. The current applications focus on ultrafast optically induced structural dynamics as, e.g., lattice motions in solids, transient charge density maps, and the interplay of soft mode excitations and charge dynamics investigated with time-resolved X-ray diffraction and absorption spectroscopy. A second focus is on imaging the nanometer scale spin structure in magnetic materials in equilibrium and after excitation. The evaluation of new imaging techniques utilizing the light from coherent, highly brilliant soft X-ray sources as well as the user operation of a laboratory based X-ray microscope for the water window region are subjects of collaboration with partners from academia and industry.

2. Topics and collaborations

T1: Nanoscale imaging and spectroscopy with soft X-rays

The topic is centered on imaging and spectroscopy of nanometer scale objects with XUV and soft X-ray radiation produced at synchrotron radiation sources and free-electron lasers as well as by laser-driven laboratory sources. Part of the research in this topic is performed in the framework of the Berlin Laboratory for Innovative X-ray Technologies (BLiX) which is jointly operated by the TU Berlin and MBI (cf. Project 4.2). The Project 3.3 also hosts the activities within the BMBF project Split-X-MID where a split-and-delay line for ultra-short X-ray pulses is developed and constructed for the Materials Imaging and Dynamics (MID) instrument at the XFEL facility in Hamburg.

Collaboration partners: F. Büttner (MIT, USA), J. Lüning and B. Vodungbo (Sorbonne Universités, UPMC, Paris, France), A. Madsen and L. Wei (XFEL, Germany), R. Harrison (University of Cambridge, UK), S. Wall (ICFO, Spain), HZB (Berlin, Germany), Fraunhofer ILT (Aachen, Germany), optiX fab GmbH (Jena, Germany), GIST (Gwangju, South Korea), KTH (Stockholm, Sweden), FSU Jena (Germany), greateyes GmbH (Berlin, Germany).

T2: Femtosecond X-ray diffraction and absorption

Investigation of transient electron density maps and structural dynamics in solids, in close collaboration with Project 3.2.

Collaboration partners: A. Borgschulte (Swiss Federal Laboratories for Materials Science and Technology, Dübendorf, Switzerland), and E. L. Shirley (National Institute of Standards and Technology, Gaithersburg, USA).

3. Results in 2017

T1: Nanoscale imaging and spectroscopy with soft X-rays

Multi-color imaging of magnetic Co/Pt multilayers

Magnetic systems based on multilayers with Co/Pt interfaces exhibit intriguing phenomena originating from the strong spin-orbit interaction at the interfaces. As a very recent example, it has been shown that the interplay between perpendicular magnetic anisotropy and the Dzyaloshinskii-Moriya exchange interaction can lead to the formation of room-temperature skyrmions – spin textures with a topology equivalent to a sphere – in multilayers with broken inversion symmetry. The skyrmions can be very effectively created and shifted by spin-orbit torques generated via spin Hall currents (see Scientific Highlights, page 13). Other phenomena observed in such multilayer systems are efficient ultra-broadband emission of terahertz radiation and optically induced helicity-dependent switching of the magnetization.

The investigation of these phenomena in such heterostructures calls for experimental techniques giving direct and simultaneous access to the element-specific magnetization with nanometer spatial and femtosecond temporal resolution. In our work, we demonstrate that the magnetic circular dichroism at the $M_{2,3}$ absorption edges of Co and the $O_{2,3}$ and $N_{6,7}$ edges of Pt gives rise to almost background-free magnetic scattering signals from magnetic labyrinth domains in Co/Pt multilayers [WKW17a]. Spatial resolution is achieved either in reciprocal space by detecting the small-angle scattering signal or in real space via Fourier-transform holography [WKW17b]. As the absorption edges of both elements are located in the XUV spectral range, high harmonic generation as well as XUV free-electron lasers (FEL) can be used as sources delivering ultra-short pulses of coherent radiation. In our study, we present the first realization of a two-color imaging experiment at the FEL facility FERMI encoding the real-space magnetic domain patterns of Co and Pt in a single hologram (Fig. 1) and, thus, a valuable tool to unravel ultrafast processes within the electronic and spin structure of complex multicomponent and multiphase materials.

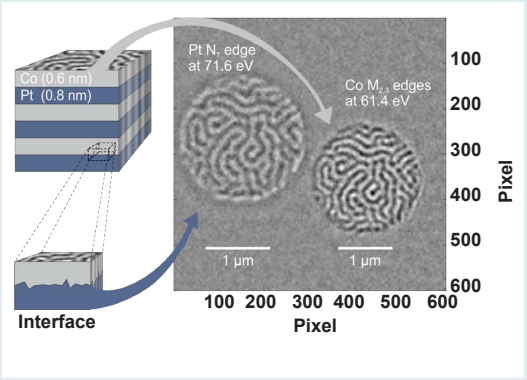

Fig. 1:
Reconstruction of a two-color hologram simultaneously recorded with two different photon energies tuned to the Co and Pt absorption edges as indicated. The image shows the ferromagnetic domain network formed in the Co/Pt multilayer sample with a circular field of view of 2 µm. Note that the circular magnetic dichroism exploited exhibits inverse contrast for Co and Pt and that the magnification is different due to the different photon energies used.

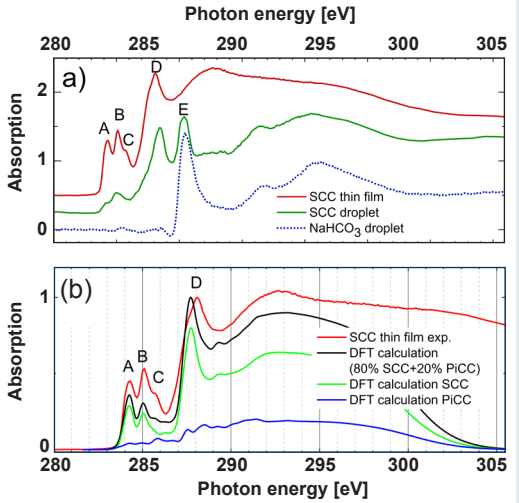

Fig. 2:
NEXAFS spectra of sodium copper chlorophyllin (SCC) and its breakdown products. (a) Droplet and thin film spectra in comparison with the spectrum of a $NaHCO_3$-droplet. The feature E can be assigned to a carbonate contamination of the SCC droplet. Features A-D belong to 1s-π transitions of the molecule. The shoulder (feature C) visible in the thin film spectrum probably belongs to the pink chlorophyll catabolite (PiCC). (b) DFT calculations for the SCC molecule and its breakdown product PiCC.*

Nanoscale imaging and X-ray spectroscopy using high-repetition rate laboratory-based soft-X-ray sources

Laboratory-based laser-driven short-pulse X-ray sources such as laser-produced plasmas (LPP) and high harmonic generation (HHG) exhibit a great potential for imaging and spectroscopy in the XUV and soft X-ray range complementary to large-scale facilities like synchrotron radiation sources or free-electron lasers.

We use a chirped-pulse amplification (CPA) laser system (1.5 ps, 150 mJ, 100 Hz) based on thin-disk technology developed at MBI (cf. Project 1.2) as a pump source for a laser-produced plasma. The LPP source operates in the wavelength region between 0.6 and 20 nm (photon energy 60-2000 eV) and will be applied for time-resolved NEXAFS investigations on carbon, nitrogen and oxygen K-edges of tetrapyrroles and L-edges of 3d elements in magnetic compounds. A pump-probe setup using the LPP source and a NEXAFS spectrometer based on reflection zone plates [MJW17] is currently under commissioning.

In 2017, our investigations were focused on thin films of sodium copper chlorophyllin (SCC) [WMS]. SCC is a water soluble chlorophyll derivative widely used as a food additive or as an absorber in photovoltaics. We investigate the electronic structure of SCC and its catabolites using NEXAFS spectroscopy in comparison with electronic structure calculations based on density functional theory (DFT). We found that the NEXAFS spectrum contains components from the SCC molecule as well as from its breakdown products (Fig. 2). Using various sample preparation methods and complementary spectroscopic methods (including UV/Vis and X-ray photoelectron spectroscopy), a comprehensive insight into the SCC breakdown process was gained. Via the DFT calculations, a detailed assignment of characteristic NEXAFS features to specific carbon bonds is possible [WMS].

Time-resolved Faraday microscopy to investigate all-optical magnetic switching

A new time-resolved Faraday microscope allows measuring the single-shot response of magnetic systems with 250 fs temporal and <1 µm spatial resolution. In a first experiment, a GdFe thin-film sample is placed in a transmission imaging geometry, where the response of the magnetization after pumping with 1030 nm light pulses is imaged with 515 nm radiation using a Faraday microscope.

GdFe has antiferromagnetically coupled magnetic sublattices which possess a different magnitude and temperature dependence of their respective magnetic moments. The experiment is carried out in the vicinity of the compensation point, where a small net magnetization is present, i.e., the system is ferrimagnetic, with a perpendicular magnetic anisotropy. Starting from a saturated state, switching of the magnetization direction is triggered by a single laser pulse (3 mJ/cm²) and can be followed with spatial and temporal resolution; three images are shown as examples in Fig. 3. Full demagnetization of the GdFe alloy film is obtained after 1.5 ps. After approximately 60 ps, a reversed magnetization state with about 50% of the (reversed) saturation magnetization is reached. A time trace of the magnetization evolution within a circular region of interest marked in the images is shown in the lower panel of Fig. 3. After the initial setup and characterization of the system, it is now used to study the mechanisms of all-optical magnetization switching in different sample systems.

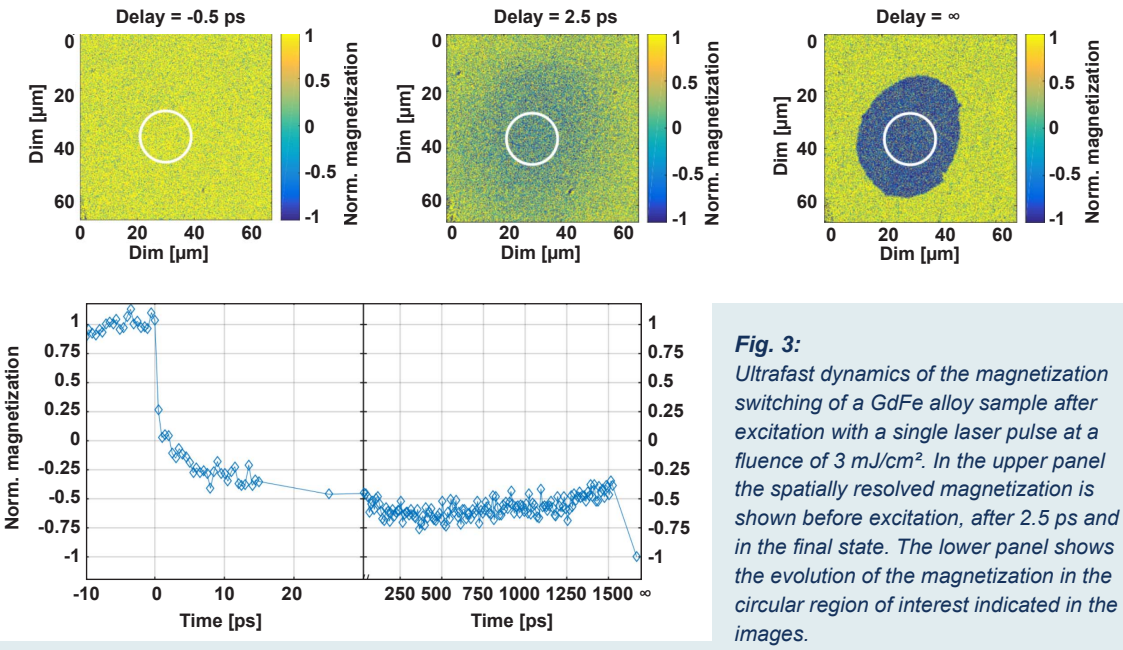

Fig. 3:
Ultrafast dynamics of the magnetization switching of a GdFe alloy sample after excitation with a single laser pulse at a fluence of 3 mJ/cm². In the upper panel the spatially resolved magnetization is shown before excitation, after 2.5 ps and in the final state. The lower panel shows the evolution of the magnetization in the circular region of interest indicated in the images.

T2: Femtosecond X-ray diffraction and absorption

Ultrasmall atom motions recorded with ultrashort X-ray pulses

Using a laser-driven high harmonic source we performed femtosecond X-ray absorption spectroscopy to map ultrafast changes of X-ray absorption by femtometer-scale coherent phonon displacements [WRW17a, WRW17b]. In the ionic crystal $LiBH_4$, displacements along an A_g phonon mode at 10 THz are induced by impulsive Raman excitation. The coherent phonon motion gives rise to oscillatory changes of X-ray absorption at the Li K edge. A direct comparison with transient electron density maps from femtosecond X-ray diffraction data show that the electric field of the pump pulse induces a charge transfer from the $(BH_4)^-$ to neighboring Li^+ ions, resulting in a differential Coulomb force that drives lattice vibrations in this virtual transition state. The experiments are presented in the Scientific Highlights, page 11.

Shot-noise-limited diffraction with table-top femtosecond hard X-ray sources

The analysis of the transient electron density $\rho(\mathbf{r},t)$ allows for resolving atomic motion or relocation of electronic charge on atomic length and time scales. $\rho(\mathbf{r},t)$ is typically gained from femtosecond X-ray diffraction employing an optical-pump/X-ray-probe setup. The necessary femtosecond hard X-ray pulses can be generated by accelerator-based sources or by laser-driven table-top sources. The advantages of the latter type include negligible timing jitter between pump and probe pulses, long-term access for lab-based experiments, and comparably low cost for implementation. However, the X-ray flux generated by this type of source displays fluctuations on various time scales. To reliably determine small changes in the diffracted intensity, efficient normalization and averaging methods are required.

In 2017, we have therefore investigated the photon statistics of X-ray pulses from a lab-based femtosecond laser-driven hard X-ray source to fully characterize the source and to elucidate the mechanisms behind intensity fluctuations [HHW17]. In a first step, the frequency spectrum of the fluctuations was determined, as shown for two cases in Fig. 4(a) and (b) in comparison to the spectrum of a source with a Poisson photon statistics and the same average flux. Both experimental spectra exhibit deviations from an ideal photon source with Poisson photon statistics, most notably narrow features between 1 and 30 Hz. These can mostly be traced to small residual mechanical instabilities of the setup in particular the spooling mechanism of the Cu-target tape used for the X-ray generation.

To remove the influence of these fluctuations most efficiently, we introduced an experimental concept in which the pump pulses of the pump-probe setup working at a 1 kHz repetition rate are mechanically chopped and the X-ray flux diffracted in subsequent events with and without pump is detected with a single detector. This allows for measuring small transient intensity changes with a time resolution of ~100 fs and a sufficient signal to noise ratio (SNR) in a comparably short data acquisition period. As an example, we present in Fig. 4(c) the time evolution of the change in diffracted intensity $\Delta I/I$ on the (111) Bragg reflection of a single crystalline 40 nm thick bismuth film upon excitation. After a measurement time of 90 minutes, a very good SNR of ~12 is obtained. As a second example $\Delta I/I$ of the (110) Bragg reflection of a $LiNbO_3$ single crystal upon excitation is shown in Fig. 4(d). This signal (black symbols) is related to a shift-current-induced strain wave traveling through the piezoelectric material. The significant improvement of the SNR that is achieved by introducing a mechanical chopper as a normalization scheme is evident from a comparison with a transient, in which the effect of the chopper has been artificially removed (orange symbols). Also included are two transients calculated for an X-ray source

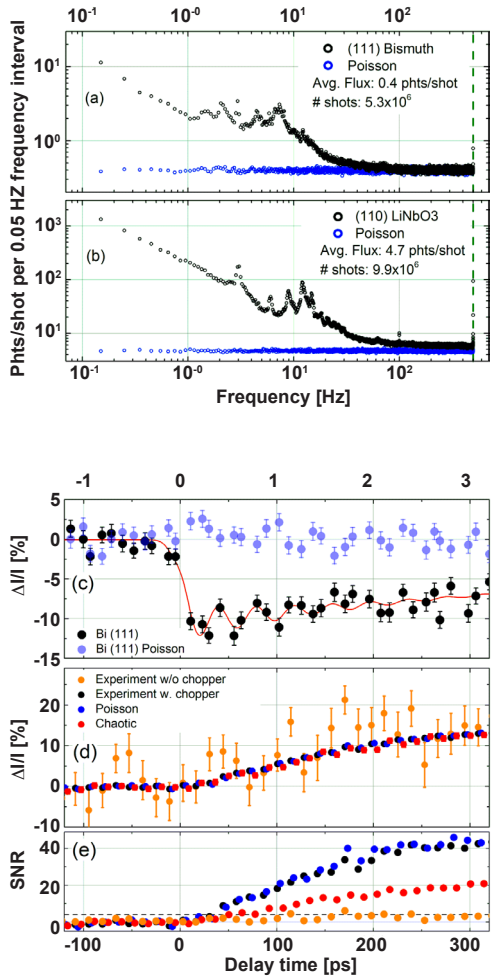

Fig. 4:
Power spectrum of the X-ray photon flux generated by our laser driven femtosecond hard X-ray source diffracted from (a) a Bi and (b) a $LiNbO_3$ crystal (black), in comparison to the spectrum of a source with a Poisson photon statistics and the same average flux (blue). Each point is averaged over a frequency interval of 0.05 Hz. Transient change in diffracted intensity $\Delta I/I$ as a function of the pump-probe delay for (c) the (111) Bragg reflection of a 40 nm thin Bismuth film and (d) the (110) Bragg reflection of a $LiNbO_3$ single crystal. The black symbols represent the actual experimental results in both cases, while the corresponding SNR for $LiNbO_3$ for different curves is shown in (e).

with purely Poissonian (blue symbols) or chaotic characteristics (red symbols) of the same average X-ray flux as the experimental source per delay point. These clearly point to a predominant Poissonian character of the X-ray source. The improved setup therefore allows for experiments with a high sensitivity close to the shot-noise limit.

Own Publications 2017 ff

(for full titles and list of authors see appendix 1)

BLS17: F. Büttner *et al.*; Nat.. Nanotechnol. **12** (2017) 1040-1044

FFS17: M. Fohler *et al.*; Rev. Sci. Instrum. **88** (2017) 103701/1-7

FMM17: S. Flewett *et al.*; Phys. Rev. B **95** (2017) 094430/1-11

GGS17: C. M. Günther *et al.*; J. Opt. **19** (2017) 064002/1-11

GSG17a: E. Guehrs *et al.*; J. Nanobiotechnol. **15:21** (2017) 1-11

HHW17: M. Holtz *et al.*; Struct. Dyn. **4** (2017) 054304/1-11

IIN17: M. Iqbal *et al.*; J. Korean. Phys. Soc., **70** (2017) 905-911

MJW17: I. Mantouvalou *et al.*; SPIE Proc. **10243** (2017) 1024308/1-8

PGH17: B. Pfau *et al.*; J Appl. Phys. **122** (2017) 043907/1-6

SBD17: H. Stiel *et al.*; SPIE Proc. **10243** (2017) 1024309/1-10

SBS17: S. Sharif *et al.*; Rev. Sci. Instrum. **88** (2017) 083303/1-7

WKW17a: F. Willems *et al.*; Struct. Dyn. **4** (2017) 014301/1-13

WKW17b: D. Weder *et al.*; IEEE Trans. Magn. **53** (2017) 6500905/1-5

WRW17a: J. Weisshaupt *et al.*; Physik in unserer Zeit **48** (2017) 113-114

WRW17b: J. Weisshaupt *et al.*; Phys. Rev. B (R) **95** (2017) 081101/1-5

ZJS17: M. Zürch *et al.*; Sci. Rep. **7** (2017) 5314/1-10

in press

SGP: M. Schneider *et al.*; Nat. Commun.

WMS: K. Witte *et al.*; J. Chem. Phys. B

WZJ: J. Weisshaupt *et al.*; in *Tabletop Intense Femtosecond Pulse Sources and Their Applications*, A. Baltuška and G. Cerullo eds. (Springer, Heidelberg)

submitted

HHH: C. Hauf *et al.*; Struct. Dyn.

WWo: J. Weisshaupt and M. Woerner; Struct. Dyn.

Invited Talks at International Conferences

(for full titles see appendix 2)

S. Eisebitt; Workshop on Timing Experiments at PETRA IV (Hamburg, Germany, 2017-03)

S. Eisebitt; The European Conference PHYSICS OF MAGNETISM 2017, PM'17 (Poznań, Poland, 2017-06)

S. Eisebitt; 2nd Int. Workshop on Novel Trends in Physics of Ferroics, NTPF 2017 (St. Petersburg, Russia, 2017-07)

T. Elsaesser; Kick-off and Laser Materials Meeting (Berlin, Germany, 2017-04)

T. Elsaesser; Fachtagung Prozessnahe Röntgenanalytik, PRORA (Berlin, Germany, 2017-12)

B. Pfau; 9th Int. Workshop on Nanoscale Spectroscopy and Nanotechnology (Gyeongju, South Korea, 2017-09)

C. v. Korff Schmising; 8th Ringberg Workshop on Science with FELs – From first results to future perspectives (Ringberg, Germany, 2017-02)

C. v. Korff Schmising; Int. Union of Crystallography 2017, IUCR 2017 (Hyderabad, India, 2017-08)

H. Stiel; SPIE Optics + Optoelectronics (Prague, Czech Republic, 2017-04)

H. Stiel; 52th Zakopane School of Physics (Zakopane, Poland, 2017-05)

M. Woerner; Int. Workshop on Finite Systems in Non-equilibrium: From Quantum Quench to the Formation of Strong Correlations (Natal, Brazil, 2017-09)

4.1: Implementation of Laser Systems and Measuring Techniques

I. Will, N. Zhavoronkov (project coordinators)
and U. Bengs, F. Furch, A. Giree, C. Kleine, G. Klemz, M. Kretschmar, L. Lochner, T. Nagy, J. Tümmler, T. Witting

1. Overview

The general goal of this project is the development of lasers and optical measurement systems tailored to applications specific to the MBI or laboratories of collaboration partners.

The generation of sub-10 fs pulses by means of Optical Parametric Chirped Pulse Amplification (OPCPA) technology has further increased in significance during the last years. The appropriate OPCPA systems are contained in topic 3 of this project

2. Topics and collaborations

The project is organized in the following topics:

T1: Lasers for particle accelerators

This topic contributes to the development of Free Electron Lasers (FELs) by providing highly specialized photo injector drive lasers. This work is carried out in cooperation with DESY, the Helmholtz-Zentrum Dresden-Rossendorf (HZDR), and the Helmholtz-Zentrum Berlin für Materialien und Energie (HZB).

T2: Femtosecond laser system with shaped pulses

The main task of this topic is the implementation of new concepts for the generation of few-cycle and/or shaped laser pulses for relevant experiments at MBI.

T3: Development of a Terawatt OPCPA system

A high-power OPCPA system that is pumped by a high-power thin-disk laser is being developed in the framework of this topic. This project aims to reach a pulse energy in excess of 30 mJ from the OPCPA with a pulse duration of less than 10 fs. The system runs at a repetition rate of 100 Hz.

T4: High repetition rate NOPA

The development of high repetition-rate Non-collinear OPA (NOPA) systems (repetition rate ≥100 kHz) is the goal of this topic. The NOPAs are pumped by fiber lasers and by a high-power thin-disk amplifier.

3. Results in 2017

T1: Lasers for particle accelerators

This topic deals with the development and systematic improvement of photocathode lasers for linear accelerators (linacs) of FELs. These lasers are needed to drive the photo injectors, where the electron bunches are generated which are then subsequently accelerated in the accelerator modules. Thus the parameters of the photocathode laser, in particular its wavelength, synchronization accuracy, pulse shape, and stability, have a substantial influence on proper operations of the linacs and FELs.

At present, several photocathode lasers developed at the MBI are in operation at DESY, both for the XFEL as well as for FLASH and PITZ, at HZB and at the superconducting RF gun at HZDR.

There is a continuous demand of these laboratories towards MBI for support to ensure suitable operation of the lasers and adapt them to new experiments. In 2017 we have repaired and improved the laser at HZDR (Rossendorf), at PITZ (DESY Zeuthen) and at HZB (Berlin).

The main work in 2017 was focused on the development of the photocathode laser for the bERLinPro energy recovery linac (ERL). This Linac is being developed at the Helmholtz Zentrum during the next years, and MBI is responsible for developing the appropriate photocathode laser. For detail see the MBI Annual Report 2016.

In 2017, we have set up the first version of the photoinjector drive laser for the bBERLinPro energy recovery linac. This first version runs with 50 MHz repetition rate and has to deliver only moderate power, i.e., 10 to 20 W in the IR, and 4 to 8 W of green light with 515 nm wavelength. Our present laser setup can generate pulses and pulse trains (bursts) of variable duration with 3 times larger power than required. However, further development of high-power amplifiers is required for the second version of the laser, which will operate at 1.3 GHz repetition rate, generating an average power of $P_{1030\ nm}$ >100 W in the IR and $P_{515\ nm}$ >40 W of green light. The power amplifiers use fiber rods as the amplifying element, which we operate at present with an IR output power up to 80 W.

We use a similar laser technology in a cooperation project with the Max Planck Institute for Intelligent Systems, department “Modern Magnetic Systems“ (Prof. G. Schütz). For joint experiments on the manipulation of magnetization with light pulses, a laser system which can be integrated with the soft X-ray scanning microscope MAXYMUS, operated at the synchrotron radiation

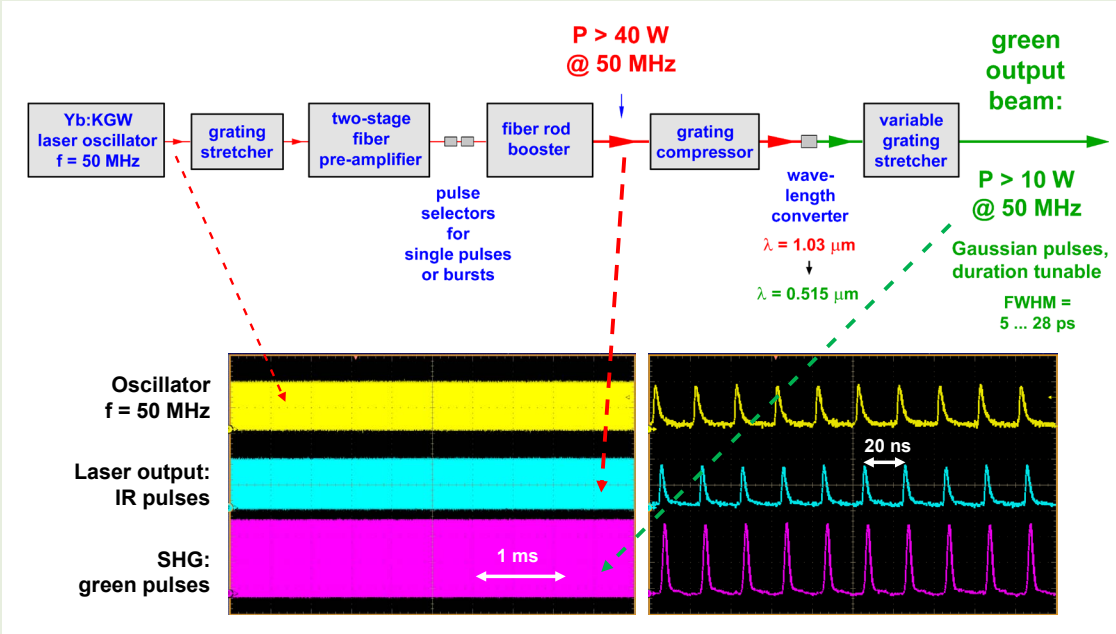

Fig. 1:
Top: Simplified scheme of the bERLinPro photocathode laser (stage I) under development at MBI. Bottom: 50 MHz pulse trains at 40 W power in the IR, and ~12 W power after conversion to green light.

facility BESSY II, is developed. It has to be compatible with the asynchronous pump-probe sampling scheme used in multibunch mode at MAXYMUS and requires fiber-delivery of the pulses in the very constraint space between sample and X-ray optics. The system will be applied in time-resolved pump-probe imaging experiments with optical excitation on a timescale of several picoseconds. This development will open the instrument for new research topics such as optically induced magnetization dynamics which is a research focus within the MBI Projects 3.2 and 3.3.

T2: Femtosecond laser system with shaped pulses

Intense few-cycle pulses are essential for studying light-matter interactions at ultrafast timescales, where availability of few to single cycle laser pulses within a broad spectral range is an essential prerequisite. The main purpose for the femtosecond laser system presented here is to deliver laser pulses with duration down to single cycle and to convert their frequency in a broad spectral range up to XUV-frequencies.

In 2017, the main efforts were directed towards the development and implementation of experimental hardware to produce few cycle pulses around 400 nm. First, the original radiation from a Ti:sapphire-based regenerative amplifier system (Spectra Physics: Spitre ACE), delivering pulses of 35 fs duration at a repetition rate of 1 kHz and 1.0 W output power, was converted to the second harmonic in a 100 μm thick BBO (β-barium-borate) nonlinear crystal. The resulting pulses with a wavelength centered around 395 nm and an energy up to 0.4 mJ were as short as 30 fs. To produce intense laser pulses routinely, a technique based on the nonlinear effects occurring in a gas-filled hollow core fiber (HCF) is used. We are applying the gradient HCF technique, which relies on delaying self-focusing of the beam prior to the entrance to the HCF, and maintaining the occurrence of self-phase modulation while the pulses travel inside the hollow fiber. The experimental setup is shown in Fig. 2(a).

The laser beam at 395 nm wavelength was focussed into an Ar-filled, 1 m long HCF with 0.25 mm diameter. We obtained a throughput energy as high as 0.1 mJ for the input pulses of 0.4 mJ energy.

Figure 2(b) depicts the spectra taken at the output of the HCF for different Ar pressure. Compression of the pulses was performed by a set of mirrors with negative dispersion. For fine tuning of dispersion, a pair of thin fused silica wedges with 2 degree of apex angle was inserted into the beam. The pulse duration was measured with an SD-FROG (self-diffraction frequency resolved optical gating). The FROG used is capable of measuring laser pulses with a duration down to 3 fs. The spectrum at the HCF output has a typical symmetrical shape around 400 nm. The pulse duration strongly depends on the gradient pressure insight the HCF. Whereas the Ar pressure at the low pressure side of the HCF does not exceed 10 mbar, the Ar pressure at the high pressure side can be increased up to 1.5 bar. As the Ar gradient pressure grows reaching the minimal detected duration of 5.12 fs at 1.2 bar, the duration of the compressed pulse decreases continuously. Figure 3 shows the measured FROG data of the few-cycle pulses.

In conclusion, the generated few cycle pulses in different spectral range will allow for new time resolved experiments, including high harmonic spectroscopy. The extremely short pulses produced around 400 nm are suitable for generation of powerful isolated attosecond pulses with adjustable polarization using the two-color

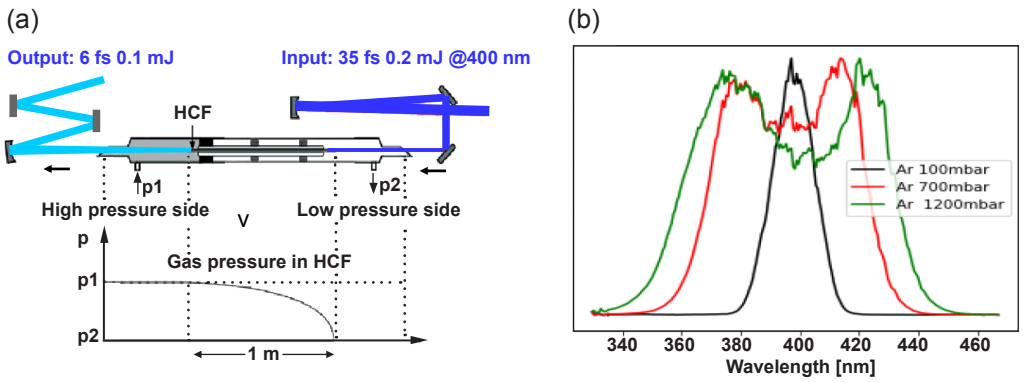

Fig. 2:
(a) Experimental setup.
(b) Spectra of the output radiation from 0.25 mm HCF filled with Ar at different pressure.

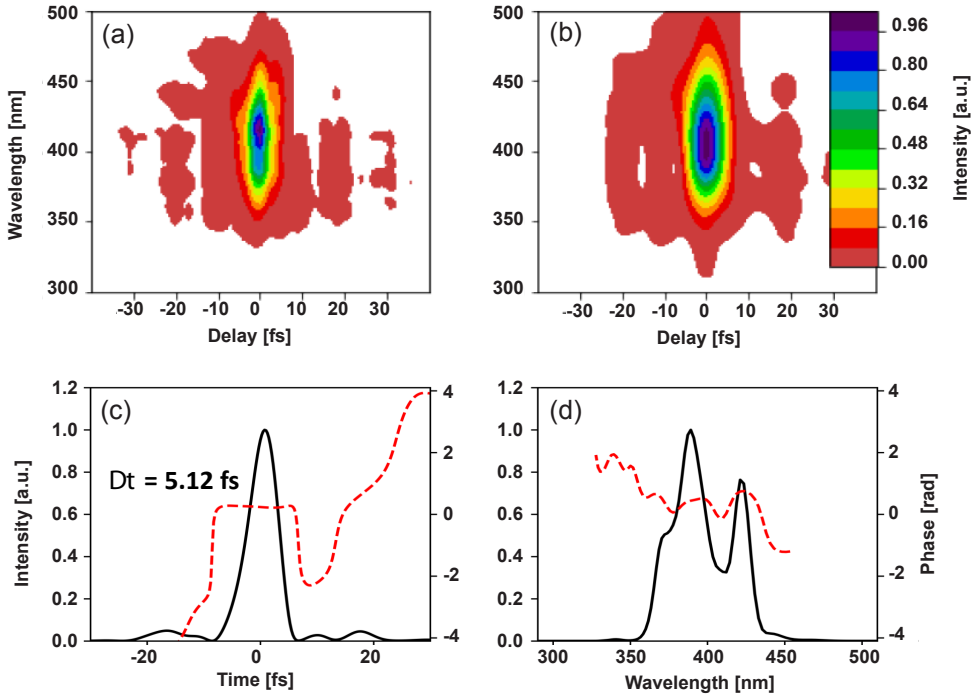

Fig. 3:
FROG traces measured (a) and retrieved (b) of the compressed few-cycle pulses at 400 nm (c) together with its phase and spectrum (d).

bi-circular approach described in the reports on the Projects 2.2 and 2.3.

T3: Terawatt OPCPA system

The goal of this topic is to set up an OPCPA system that produces high-energy (E >30 mJ) pulses with sub-10 fs duration. When applying these pulses to HHG, we aim to generate high harmonics at sufficient pulse energies for attosecond XUV-pump XUV-probe experiments as well as for time-resolved coherent diffractive imaging studies.

Our OPCPA design utilizes powerful thin-disk lasers as pump source that have been developed during the previous years in the framework of Project 1.2.

In 2017, the work was focused on three main topics:

- Installation of the new frontend
- Setup of a feedback system stabilizing the timing between pump and seed pulses in the OPA stages
- Reconstruction of the former High-Field Laser Application Laboratory (HFL), installation of suitable clean room equipment and transfer of the TW OPCPA system to this new lab.

Installation of the new frontend

The seed for the OPCPA stages is supplied by a commercial front-end from Light Conversion, Lithuania. In this system, the pulses from the Yb:KGW oscillator are amplified in a regenerative amplifier, frequency doubled afterwards and used to generate passively CEP-stabilized pulses utilizing Difference-Frequency-Generation (DFG). The frequency doubled radiation from regenerative amplifier is split, where one arm is used to generate a broadband white-light seed for the DFG process, being pumped by the other SH beam. Pump and seed of the DFG process are therefore synchronous. The mixing process itself enables the generation of passively CEP-stable pulses centered in the infrared spectral region (approx. 1400 nm). A second white-light generation stage delivers the desired seed pulses centered in the near-infrared spectral region (approx. 800 nm) with pulse energy of 1.5 µJ. Further amplification in fs-NOPA stages, which are also pumped by the front-end's regenerative amplifier, delivers pulses with approximately 70 µJ of pulse energy and a spectrum supporting sub-6 fs pulses centered at 810 nm. The seed pulses are stretched to approximately 5 ps in order to achieve the desired pump intensity in the OPCPA amplification stages.

Feedback system stabilizing the timing between pump and seed pulses in the OPA stages

In order to achieve a stable amplification in the chain of three OPA amplifiers, the high-energy pump beams (515 nm, ~5 ps duration) from the two regenerative thin-disk amplifiers have to be optically synchronized to the broadband seed pulse of the OPA.

A suitable synchronization system has to compensate for variations in the optical paths length mainly induced by either thermal drifts in the amplifier setups or by beam pointing fluctuations in the stretcher and compressor setup of the thin-disk amplifiers. We have chosen to

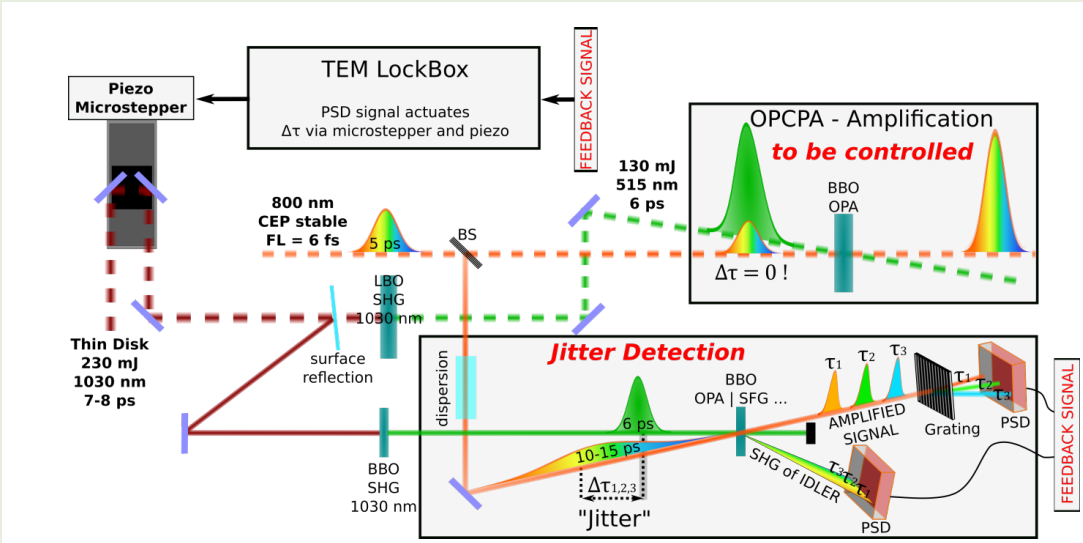

Fig. 4:
Scheme of the feedback system that stabilizes the mutual delay between the strong pump pulse and the broadband seed pulse of the OPA stages.

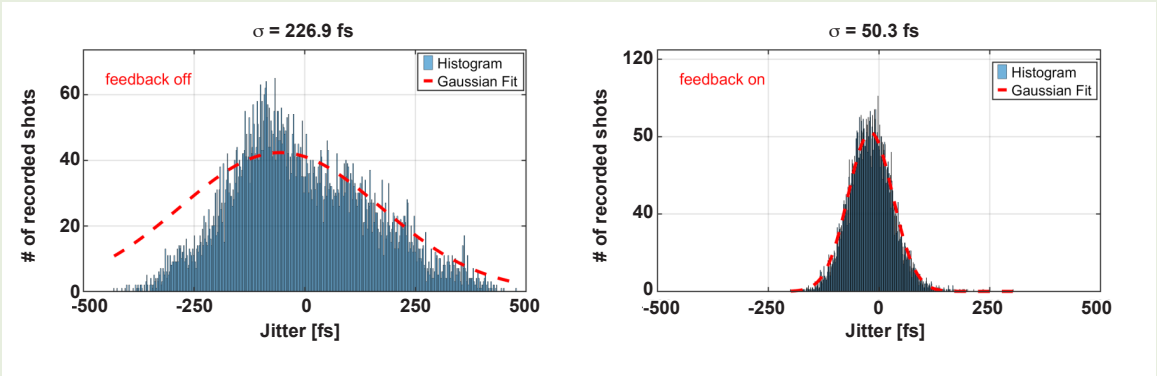

Fig. 5:
Obtained mutual delay between pump and seed pules at the OPCPA stages (top) and reduced jitter due to feedback stabilization (bottom).

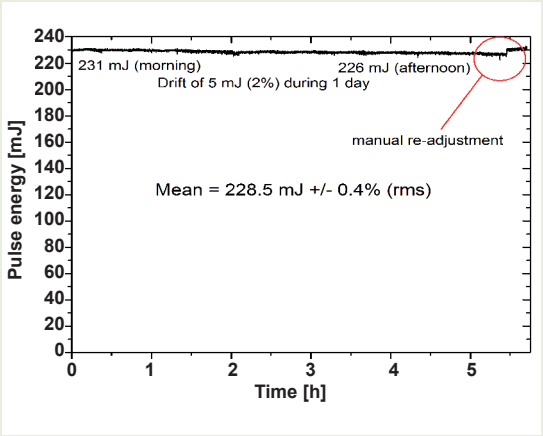

Fig. 6:
Stability of the output energy of one regenerative thin-disk pump laser recorded during 6 h of operation. A slow drift of the pulse energy from 231 mJ to 226 mJ (~2%) can be seen. This drift was compensated by manual re-adjustment of the amplifier.

detect the temporal drift between pump and seed pulses using separate low-power OPA stages that provide high sensitivity to temporal shifts (Fig. 4). In this setup, a small fraction of the broadband seed beam is split off and further stretched (approx. 8 - 20 ps) to well exceed the pulse duration of the pump beam. Mixing this beam with a small fraction of the pump radiation in a separate small OPA results in the amplification of the particular spectral components of the seed beam that temporally overlaps with the pump pulse. For feedback stabilization of the mutual delay between pump and seed pulses, the resulting spectral shift is recorded by a grating spectrometer equipped with a position-sensitive detector (PSD). The resulting feedback signal is used to re-adjust the motorized translation stages located in front of the high-power thin-disk regenerative amplifiers. Figure 5 shows the achieved temporal stability between the pump and seed-pulses for the unregulated and regulated case. It can be seen that the feedback improves the temporal synchronization by a factor of 4.4 to an accuracy of approximately 50 fs. This corresponds to a jitter of 1% of the duration of the stretched pulse, which amounts to 5 ps in the OPA stages.

Reconstruction of the former HFL and transfer of the TW OPCPA system to this new lab

A significant part of the work in 2017 was dedicated to the reconstruction of the former HFL and the installation of appropriate cleanroom equipment. Subsequently, the front end and pump laser of the OPCPA system were moved to the new lab. In the course of the re-installation of the pump laser a number of technical improvements were done on the system, which made the operation of the pump laser more stable. In Fig. 6 we show the pulse energy from one thin-disk amplifier during a one-day operation. We achieve a fluctuation of 0.4% rms and a pulse energy of 0.23 J in both arms of the pump laser. The laser pulses of the two amplifier arms with 1 ns pulse duration are compressed to 6.5 ps pulse duration (FWHM) and converted to the second harmonics. At 515 nm wavelength, we obtain pulse energy of 120 mJ in both arms in routine operation.

Figure 7 shows a view in the present laboratory with the thin-disk pump laser and the front end installed in right part of the picture. The laboratory is prepared to host both the TW OPCPA operating at 800 nm wavelength (right side), as well as the 2 µm OPCPA system (left side) covered in Project 4.2.

T4: High repetition rate NOPA

Coherent light sources producing Carrier-envelope Phase (CEP)-stable, few-cycle pulses at high average power and high repetition rate are extremely attractive for a multitude of applications in strong-field physics, attosecond science, and novel approaches in material processing, among others. In this activity we aim to develop such sources based on non-collinear parametric amplifiers (NOPAs) seeded by a Ti:sapphire oscillator.

Two systems are currently in operation: a 400 kHz NOPA delivering CEP-stable few-cycle (<7 fs) 10 µJ pulses and a 100 kHz NOPA with CEP-stable few-cycle pulses with energy approaching 200 µJ. The two systems share the front end and the architectures of the NOPAs are very similar. The basic architecture of each system is illustrated in Fig. 8, where the oscillator (OSC) and pulse shaper (PS) represent the shared front end.

Fig. 7:
Reconstructed laboratory of the former HFL with its clean-room technique.

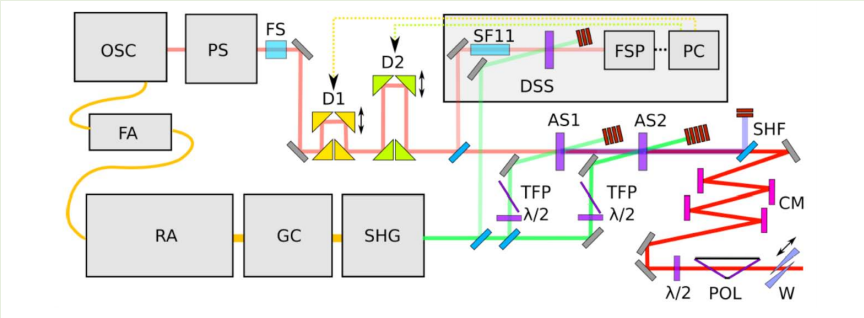

Fig. 8:
Block diagram of the complete system showing the common front end and the two pump lasers and corresponding NOPAs. Adapted from [WFV].

The CEP-stable, octave-spanning Ti:sapphire oscillator at 800 nm (Pulse:ONE, VENTEON Femtosecond Laser Technologies GmbH) seeds the NOPA. A fraction of the oscillator radiation with approximately 10 nm of bandwidth centered around 1030 nm is filtered out with a dichroic mirror, coupled into a polarization-maintaining optical fiber and used to seed a chirped pulse amplification (CPA) system whose output, after frequency doubling (SHG in the figure) will serve as pump for the NOPA. In both NOPAs the CPA consists of a fiber Bragg grating stretcher, several Yb-doped fiber pre-amplifiers (FA in the figure), a power Yb-based amplifier (RA) and a grating compressor (GC). In the case of the 400 kHz system the main amplifier is an Yb-doped rod-type amplifier (High Power Tangerine, Amplitude Systèmes) delivering, after frequency doubling, 300 fs pulses with 24 W of average power at 515 nm. For the 100 kHz system the main amplifier is a regenerative thin-disk Yb:YAG amplifier (Trumpf Scientific). After second harmonic generation this system delivers 120 W at 515 nm, in 900 fs pulses at a repetition rate of 100 kHz. The seed pulses are stretched by material dispersion in fused silica (FS) and go through a piezoelectric-controlled translation stage (D1) and a stepper-motor controlled stage (D2) to actively control the delay between seed and pump pulses in the NOPA. In order to characterize and control the delay an auxiliary NOPA is built (DSS) in which the seed is stretched to a pulse duration longer than the pump pulse duration by material dispersion in 5 cm of SF11. The amplified signal is measured by a spectrometer (FSP) and processed in a computer (PC) to generate the correction signals feeding back to stages D1 and D2. In this way the pump-seed delay is stabilized with a remaining jitter lower than 5 fs during hours of operation. This long term stability is of fundamental importance for the success of applications. The NOPA architecture (Fig. 8) reproduces the 100 kHz system. The pump pulses are split between two amplification stages (AS1 and AS2) based on type I phase matching in BBO crystals. The pump power into the stages is controlled by λ/2 wave plates and thin-film polarizers (λ/2, TFP). An optional second harmonic filter (SHF) rejects parasitic second harmonic. The pulses are compressed with a combination of chirped mirrors (CM) and thin fused silica wedges (W). The output power into the experiments is controlled by a broadband λ/2 waveplate and polarizer (POL).

Activities concerning the 400 kHz NOPA

During 2017 the system has been utilized for IR-IR pump-probe experiments with ion-ion coincidence detection utilizing a novel Timepix detector and for novel approaches in material processing (Projects 2.2 and 3.2 respectively).

Activities concerning the 100 kHz NOPA

The main application for the 100 kHz NOPA is to feed an attosecond pump-probe beamline with ion-electron coincidence detection (Project 2.3). In this context, the repetition rate is extremely important for fast data accumulation with the coincidence detection apparatus, while the energy, pulse duration and CEP stability are essential to generate high-order harmonics in the XUV, and moreover, to confine the harmonic emission to a single half cycle of the laser pulse in order to produce isolated attosecond pulses (IAP).

First results on high harmonics generation (HHG) were obtained during 2017 and reported in the context of Project 2.3. This is, to the best of our knowledge, the first time that HHG driven by few-cycle pulses with high repetition rate (≥100 kHz) is generated in a loose focus geometry (f# ~100).

Isolation of the harmonic emission to a single half cycle of our 7 fs driving pulses is possible utilizing a gating technique such as polarization gating. However, the efficiency of the process is dramatically reduced. A more attractive and efficient way of generating IAP is by driving the HHG process with close to single-cycle pulses. With that aim, we have collaborated with the group of Prof. A. Kung (National Tsing Hua University and Academia Sinica of Taiwan) to post-compress the pulses amplified in the NOPA. By broadening the spectrum through nonlinear propagation in two 50 µm thick quartz plates and recompressing with chirped mirrors, we were able to demonstrate pulse durations as short as 3.6 fs (1.5 cycle), the shortest pulse duration ever demonstrated for high average power, high repetition rate systems. Fig. 9 shows the spatio-temporal characterization of the compressed pulses utilizing the SEA-F-SPIDER technique.

Another crucial aspect for the generation of IAP is the CEP stability of the laser pulses. So far, high repetition rate NOPAs have been characterized utilizing f-to-2f interferometry. This technique has two main limitations: intensity fluctuations couple to phase noise during the white-light generation stage and it is not possible to detect in a single-shot base and detecting all the pulses in the pulse train for systems exceeding 10 kHz. During 2017 we have collaborated with the group of Prof.

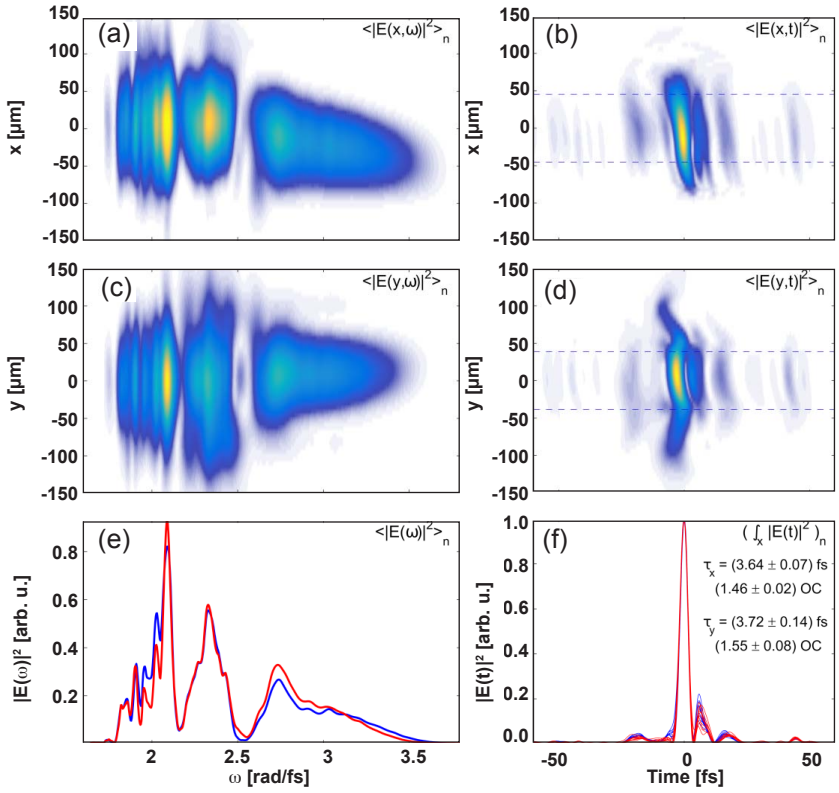

Fig. 9:
Spatio-temporal characterization of 1.5 cycle pulses. (a) and (c) show the spectrum as a function of position (along one direction across the beam), while (b) and (d) show the temporal reconstruction of the pulses as a function of position. (e) and (f) show the integration over the spatial coordinate for the spectra and temporal shapes respectively. Adapted from [LWH].

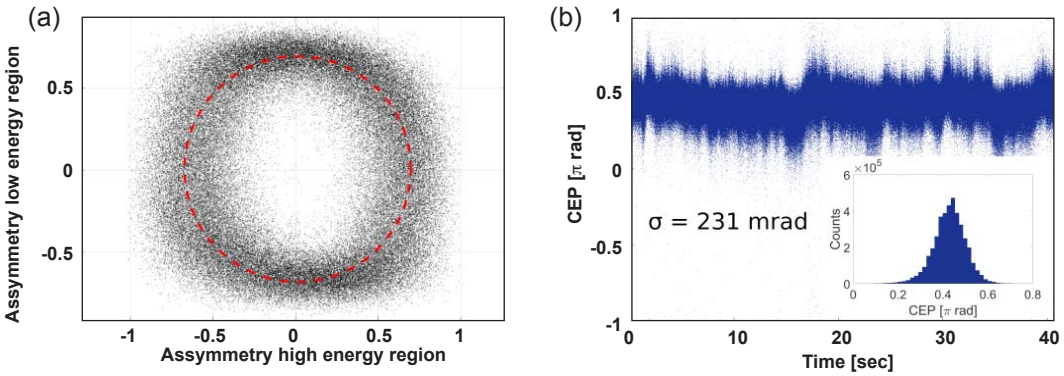

Fig. 10:
Characterization of the CEP of amplified pulses at 100 kHz with a stereo-ATI. (a) Parametric asymmetry plot when the oscillator is not CEP-stable. Each angle along the circle represents a value of CEP (red dashed line guides the eye). (b) CEP stability measured when the oscillator is CEP-stabilized. Inset: Histogram of measured CEP values.

G. Paulus (Helmholtz-Institut Jena, Institut für Optik und Quantenelektronik) in order to characterize the CEP stability of the pulses amplified in the NOPA utilizing the stereo Above-Threshold-Ionization technique. We have measured the CEP stability of amplified pulses in the high repetition rate NOPA on a single-shot base and measuring each and every pulse in the train. This is, to the best of our knowledge, the first time that the CEP stability of a high repetition rate NOPA is analyzed measuring every pulse in the train in a single-shot base. Figure 10 shows a parametric asymmetry plot with a typical circular shape for non-stabilized pulses, and the measured CEP values when the oscillator is running CEP-stable.

Publications

Publications which have emerged from work in this infrastructure project are listed under the relevant projects (1.2, 2.2, 2.3 and 3.2).

4.2: Application Laboratories and Technology Transfer

Femtosecond Application Laboratories (FAL)

V. Petrov (project coordinator)

1. Overview

Research at MBI requires interdisciplinary scientific staff, flexibility in the definition and organization of scientific projects, and a long term scientific infrastructure. MBI has chosen to concentrate some of its main experimental resources in the application laboratories, providing flexible, versatile and cost-effective access to expensive, state-of-the-art equipment for internal researchers. In addition, the application laboratories, started more than 20 years ago, are particularly suited for MBI's various access activities and collaboration programs extended to external partners from science and industry. At present the MBI offers access to the following femtosecond laboratories:

- MultiColor fs-system-I
- MultiColor fs-system-II
- UV/MIR fs-system
- High-power shaped pulse fs-system
- 80 MHz fs-system.

Since 2013 the further development of the existing application laboratories is confined to improvement of some application experiment related special parameters.

New upgrades in the high power shaped pulse fs lab in 2017 offer now the possibility for users to employ few-cycle (~5 fs) pulses generated around 400 nm by the in-house developed technology of a hollow core fiber (HCF) with gradient pressure.

In 2017, the MultiColor-II lab has been rearranged and the experimental area has been extended by an additional optical table, see Fig. 1. A new 3-meter-long HCF has been installed along with a new beam distribution system which provides free combination of the few-cycle pulses generated in the HCF with the tunable pulses of the two optical parametric amplification (OPA) modules.

For power scaling and thermal management in the 2 µm spectral range, unique epitaxial thin disks have been employed in the 80 MHz fs lab based on Tm- and Ho-doped monoclinic double tungstate crystals, Fig. 2. The high absorption cross sections and minimized fluorescence quenching enables in this case double-bounce pumping with a simple retro-reflection without the use of sophisticated multi-pass laser heads.

In 2017, an 8-bounce (16 active element pump passes) customized laser head module has been acquired which will enable the use of more conventional but thermomechanically more robust materials (crystals and ceramics) for further power scaling. The focus will be on Ho-doped materials pumped by polarized Tm-fiber sources.

2. User statistics 2017

In 2017 the internal use of the FAL by 7 project groups was 70% of the available access time (from KLR statistics). In estimated ~20% of the time external guests were involved in the experiments. We had 9 visiting scientists in 2017 from China, Russia and Spain, supported by the EC (LaserLab) or foreign funding programs.

Publications

All publications which have emerged from work in this facility are listed under the relevant research projects.

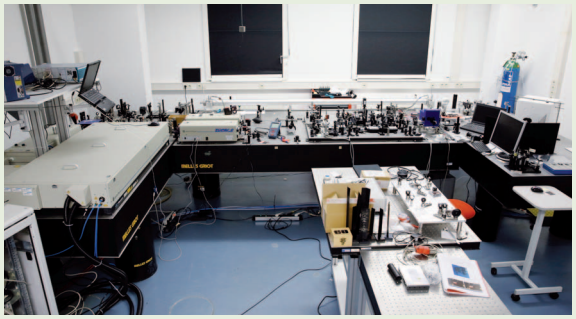

Fig. 1:
The MultiColor-II lab has been rearranged in 2017 offering more space for users and upgrades of the existing commercial system based on in-house developed pulse compression technology.

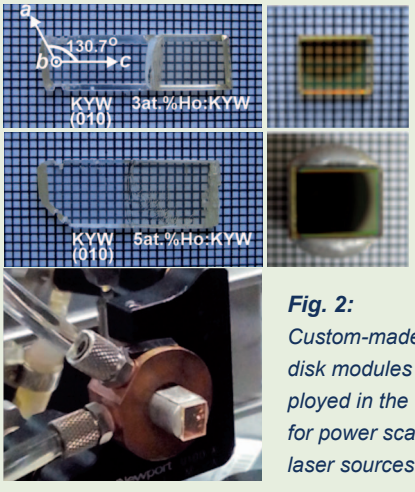

Fig. 2:
Custom-made epitaxial thin-disk modules have been employed in the 80 MHz fs lab for power scaling of the 2 µm laser sources.

NanoMovie – Application Laboratory for nanoscopic spectroscopy and imaging

M. Schnürer (project coordinator)
and L. Ehrentraut, T. Feng, L. v. Grafenstein, U. Griebner, A. Husakou, M. Merö, V. Petrov, G. Steinmeyer, Ch. Strüber, J. Tümmler, I. Will

1. Overview

The goal of the NanoMovie project is to establish an application laboratory where soft X-rays with photon energies up into the water window (i.e. about 300 to 500 eV) are reliably generated with high stability for use in application experiments. The project started in November 2016, when cofounding through the "European Regional Development Fund" (ERDF) could be secured, for a project duration of four years in total. When operational, the NanoMovie laboratory will enable fundamental and applied research with ultrashort soft X-rays pulses. Focus areas are:

- Nanospectroscopy and imaging with soft X-rays
- Study of dynamical processes at the nanometer scale
- Providing an experiment and testing platform for external users, including SMEs
- Development of laser-based soft X-ray technology.

The project comprises the development of a suitable, high average power laser system for the efficient generation of soft X-rays via high harmonic generation as well as the shaping and delivery of the radiation via suitable optics to experimental end stations for spectroscopy, scattering and imaging. The first phase of the project was devoted to the design of a 2.1 µm OPCPA laser system and the procurement of key components with long lead times, together with infrastructure preparations. The NanoMovie Application Laboratory will be established in the rooms of the former High-Field Laser Application Laboratory (HFL), which was completely reconstructed in 2017 for this purpose. The new laboratory will also host a powerful few cycle Ti:sapphire laser in the context of Project 4.1.

2. Results in 2017

So far, the generation of sub-picosecond coherent soft X-ray pulses for application experiments is mainly limited to free electron laser and synchrotron slicing facilities. Although femtosecond NIR-lasers (Ti:sapphire lasers at 800 nm) have opened up the area of attosecond science via high harmonic generation (HHG), the photon flux drops dramatically when going from the VUV spectral region towards the soft X-ray regime. While there has been substantial progress in reaching shorter wavelength in pioneering experiments, the limited photon numbers so far have precluded a widespread application. The limited photon flux at short wavelength is a consequence of the HHG – process itself. Accessing the soft X-ray region requires IR driver lasers with longer wavelength, balancing the photon energy and photon flux generated. For the initial system design phase a MBI-expert group was formed discussing various layout concepts. The subsequent detailed design was the focus of the work in 2017, together with procurement. The main hardware components will arrive in 2018. The system features a monolithic concept – this incorporates signal generation and amplification with the same pump laser. Only very recently suitable pump lasers became commercially available. The pump will be a 500 W Thin Disk Laser (TDL) DIRA500 by Trumpf Scientific GmbH. It delivers 1 ps pulses at a wavelength of 1030 nm and a pulse repetition rate of 5, 10 or 20 kHz.

Signal generation at a wavelength of 2100 nm will be realized with a frontend system which is developed by FASTLITE, France. The system uses 0.5 mJ pulses split from the DIRA500 output and produces IR pulses at about 30 µJ via white-light generation followed by frequency mixing and optical parametric amplification (OPA). Such a concept is possible because the DIRA output is sufficiently short (<1 ps) in pulse duration and sufficiently stable in intensity. Furthermore, the beam splitter unit allows tuning the pulse duration of the 500 W power beam separately.

The signal pulses from the frontend at around 400 fs pulse duration will be stretched further to about 1 ps and are subsequently amplified in two OPA stages pumped by the DIRA500. In the design of the OPA stages we realized a scheme with rather small (1 – 2 degree) non-collinear angles between pump and signal. Such geometry allows keeping the bandwidth of the signal pulse at a maximum, allows for a low spatial chirp and avoids pulse front tilt in the signal. Comprehensive simulations of the parametric amplification were carried out for the design of the detailed optical scheme. An example of such a calculation is depicted in Fig. 1.

In particular, it is important to obtain a broad bandwidth of nearly 600 nm around the central wavelength of 2100 nm, to make use of a few cycle, and therefore efficient, driver pulse for the HHG.

Due to residual absorption of 2100 nm radiation inside the crystals, we anticipate that thermal load will be a severe problem, given the high average power of the system. Different materials have been investigated via simulations and will be tested in experiment to find a tradeoff between absorption, signal amplification and damage threshold. Figure 2 provides a comparison of the absorption normalized to the same level of amplification.

The model calculations show that quite different pump intensities have to be realized for the different crystal materials, which has to be considered in the design for the pumping scheme.

Also, it has turned out that the phase matching in the crystals is a critical issue in order to maintain the amplification over a broad bandwidth. This situation is visualized in Fig. 3, where the degree of phase matching at the full required bandwidth is plotted as a function of the phase matching angle.

At the moment, considering all effects studied, we anticipate that we can arrive at a final pulse duration of about 25 fs for pulses with a central wavelength of 2100 nm and an average power of 50 W at 10 kHz repetition rate. This assumes a suitable pulse stretching and compression scheme which is currently studied intensively.

3. Users and publications

Infrastructure is under construction.

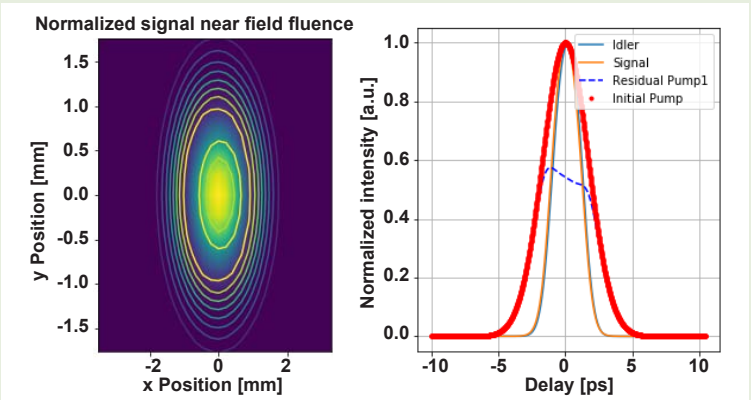

Fig. 1:
Simulation (by T. Feng) of OPA stage I with Sisyfos-software (collaboration with G. Arisholm, Forsvarets forskningsinstitutt, Norway). Parameter: BiBO-crystal 1.5 mm long, Type I phase matching, Fourier transformed seed pulse duration: 18 fs; seed pulse energy: 30 µJ, pump pulse duration: 2 ps, seed pulse duration: 1 ps, pump radius: 2 mm, seed radius: 2 mm, pump intensity: 60 GW/cm², absorption: 29 µJ, output signal energy: 1.7 mJ, output pulse duration: 19.3 fs.

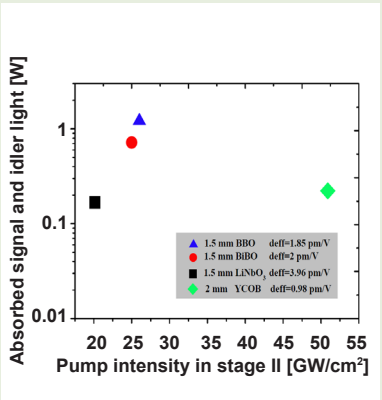

Fig. 2:
Simulation (by T. Feng) of optical parametric amplification in different nonlinear crystals: length and pump intensity are optimized for threefold power increase (14 W → 42 W) in OPA II.

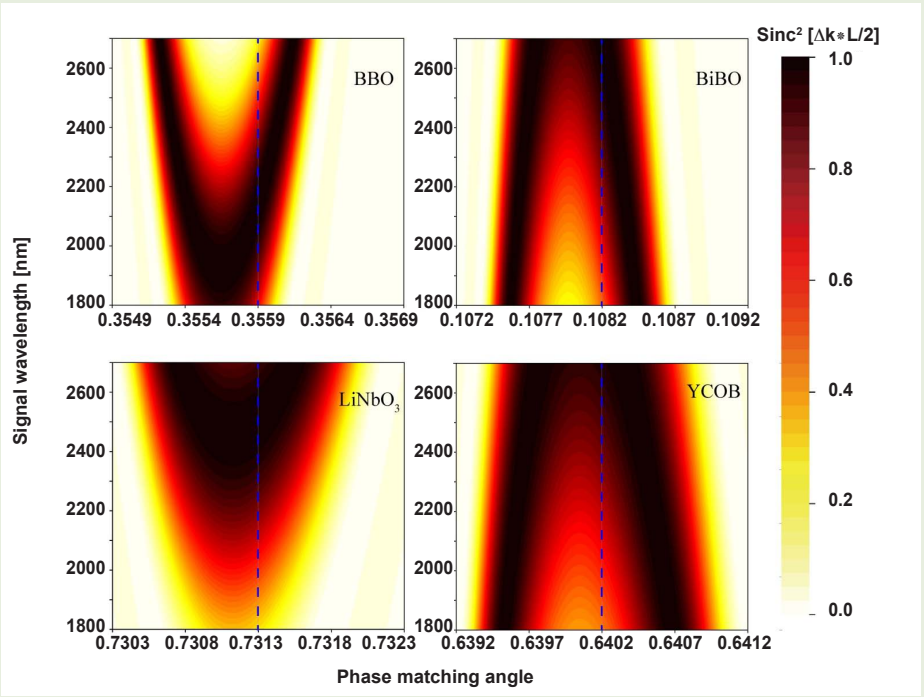

Fig. 3:
Simulation (by T. Feng): Phase mismatch condition for the different signal wavelength at an external non-collinear angle of 2°. The blue dashed line marks the phase matching angle in our case.

Berlin Laboratory for innovative X-ray Technologies (BLiX)

H. Stiel (project coordinator)

1. Overview

The Berlin Laboratory for innovative X-ray Technologies (BLiX, www.blix.tu-berlin.de) is jointly operated by the Institut für Optik und Atomare Physik (IOAP) of the Technische Universität Berlin and the Max-Born-Institut. BLiX is the „Leibniz-Applikationslabor" of MBI. It operates at the interface of scientific research and industrial application with the goal to transfer research results into instrument prototypes, with a focus on instruments and techniques that can be used in a laboratory environment without the need for large scale facilities. BLiX is supposed to be a place of collaborative technology development in the knowledge triangle of research – innovation – education.

The main fields of activity in BLiX are:

- Soft X-ray imaging using laboratory X-ray microscopy
- Confocal micro X-ray fluorescence analysis
- Detection of chemical speciation
- Soft X-ray absorption spectroscopy in the laboratory
- Customer inspired development of hard X-ray spectrometers based on highly annealed pyrolytic graphite optics.

MBI contributes to BLiX predominantly via:

- the support of development and operation of a soft-ray absorption spectroscopy beamline based on a laser produced plasma X-ray source and novel X-ray optics,
- the upgrade of a full field laboratory transmission X-ray microscope (LTXM) capable of tomographic nanoscale imaging and support of LTXM user operation,
- with transfer of know-how concerning the development and application of laser based sources, optics and detectors for the soft and hard X-ray region.

Near-edge X-ray absorption fine structure spectroscopy in the laboratory

A laser produced plasma (LPP) source based on long time experience of MBI in laser plasma dynamics has been implemented at BLiX in collaboration between IOAP/TU Berlin and BESTEC GmbH. The LPP source delivers soft X-ray pulses in the photon energy range between 100 and 1000 eV with 1 ns pulse duration, 100 Hz repetition rate and a maximum average brightness in selected emission lines of up to 10^{11} ph/s*mm^2*mrad^2.

For investigations of samples relevant for users from life and environmental sciences an X-ray absorption beamline has been implemented. The beamline is equipped with a novel two-channel reflection zone-plate (RZP) spectrometer combining a probe and a reference channel (collaboration with HZB and nob GmbH, Berlin) for near edge X-ray absorption fine structure (NEXAFS) spectroscopy investigations with a spectral resolution up to $E/\Delta E = 1000$ at carbon K-edge.

Laboratory X-ray microscopy

The full field laboratory transmission X-ray microscope (LTXM) operated at BLiX enables the detection of high quality nanoscopic images at 2.48 nm (500 eV) with a magnification up to 1000 in a field of view of about 30 µm and a typical data accumulation time of less than one minute. The spatial resolution amounts to 30 nm. This value is limited by the zone plate which is used as an objective. In order to meet user demands the work in 2017 was mainly focused on the improvement of the integrated light microscope and the stabilization of the liquid nitrogen target source.

2. Results in 2017

Results with direct participation of MBI personnel

NEXAFS spectroscopy of bio-organic molecules

Due to the relatively small penetration depth of soft X-rays the preparation of bio-organic samples for X-ray absorption experiments in transmission mode is a challenge. The main issue is the sample integrity after the preparation process. In the case of complex organic molecules (e.g. parts of the photosynthetic apparatus) the amount of material available for NEXAFS experiments is very limited. In order to investigate such samples in their native (aqueous) environment, the use of a liquid cell is the method of choice. We have developed and tested a liquid cell for NEXAFS measurements in fluorescence mode at BESSY (collaboration with PTB and HZB). Based on these results a liquid cell with a relative large aperture optimized for lab based NEAXFS investigations in transmission mode is currently under development (D. Grötzsch, TU Berlin, collaboration with Project 4.3).

NEXAFS investigations at carbon K-edges of bio-organic samples not soluble in water require other preparation techniques. Therefore, our work in 2017 has been concentrated on the development of an effusion cell technique for preparation of thin biomolecular films on silicon nitride windows capable for NEXAFS investigations. The technique was successfully applied for preparation of thin films of organic molecules. The sample integrity has been checked by additional

analytical methods such as UV/Vis and photoelectron spectroscopy. As an example, Fig. 1 shows a NEXAFS spectrum recorded with the BLiX RZP based spectrometer of a thin film of copper phthalocyanine. Phthalocyanine molecules are widely used in photovoltaics and optoelectronics.

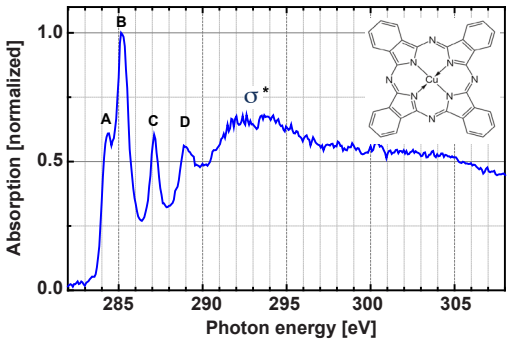

Fig. 1:
NEXAFS spectrum of a copper phthalocyanine thin film prepared by effusion cell technique. Thickness of the film: 250 nm. The NEXAFS spectrum was obtained with the RZP spectrometer at BLiX. Recording time: <1 s (20 shots at 100 Hz laser repetition rate). The characteristic fingerprints of 1s-π transitions (A, B, C, D) are clearly visible. (J. Lebendig-Kuhla, Master thesis, TU Berlin, 2017).*

The NEXAFS spectrometer has been used for investigations on electronic structure of copper chlorophyllin and its breakdown products. The results are reported in project 3.3.

Super resolution imaging in the optical and X-ray range

In the framework of a joint project (AIF ZIM KF 3412401AB4) with greateyes GmbH, Berlin-Adlershof, a new CCD detector has been developed. The so called super resolution (SR) camera employs a scientific CCD imaging sensor with 1054 x 1027 usable pixels and 13 µm pixel size. The sensor is a back-thinned silicon device with a broad spectral sensitivity ranging from approximately 1.1 eV to 10.000 eV. The sensor is mounted on a four stage Peltier element capable of cooling the sensor down to -80 °C in a high vacuum environment. Two dimensional partial translation of the sensor in the image sensor plane is realized by a piezo driven lever arm mechanism moving the stack of Peltier element and sensor. The image reconstruction algorithm has been developed at MBI. It is implemented in the camera software. The SR camera allows a sub-pixel spatial resolution in optical and X-ray imaging (cp. Fig. 2). Using an USAF resolution standard an improvement of the resolution by a factor of about 1.6 for each linear dimension has been demonstrated for radiation in the visible range.

In 2017 the performance of the SR camera could be evaluated for use with soft X-ray. Measurements were carried out at the BESSY II full field transmission X-ray microscope (U41-TXM, in collaboration with the group of G. Schneider, HZB) for photon energies ranging from 300 eV up to 1800 eV. Figure 2 shows as an example the image of a zone plate used as a test object recorded at 1400 eV with and without sub-pixel shifting, i.e. switching the super resolution mode on and off. The application of the built-in sub-pixel shift mechanism together with our SR algorithm improves the image quality making details visible not seen in images recorded in low resolution mode. We could show that the SR camera is capable for applications in soft X-ray imaging and spectroscopy for photon energies up to 1800 eV. An in-vacuum CCD camera based on this principle is now commercially available through greateyes GmbH.

Results by TU Berlin personnel, without direct participation of MBI scientists

In the following, results by non-MBI staff within BLiX are summarized to allow for a complete picture of the BLiX activities.

In the last years, the instrumentation for X-ray spectroscopy and microscopy developed in BLiX reached a state, where it can be used in applications. Prior to the commercialization of the instruments, however, demonstration applications in various fields of research are required by manufacturers. Therefore, interdisciplinary research cooperations were a focus of BLiX activities in 2017, in addition to the ongoing development of X-ray spectroscopy and microscopy methods.

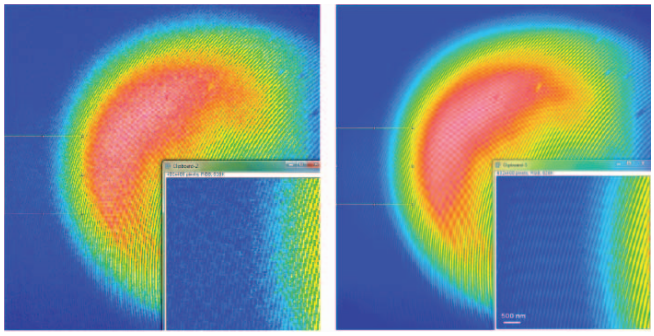

Fig. 2:
Images recorded with the super resolution CCD camera (patented) developed in a joint research project with greateyes GmbH. Left: nanoscopic image of a zone plate without sub-pixel shift. Right: nanoscopic image of a zone plate with sub-pixel shift. Photon energy: 1400 eV. The pixel size limited resolution without pixel shift amounts to 50 nm.
All data were collected with the super resolution CCD detector at the U41-TXM X-ray microscope. The support by G. Schneider and his group is highly appreciated.

With the Max-Planck-Institute for Chemical Energy Conversion, a long term contract to establish a laboratory with cutting edge X-ray spectroscopy instrumentation for the research in catalysis was signed.

Ongoing and newly initiated research cooperations are listed below.

X-ray absorption spectroscopy (XANES, EXAFS)

BLiX developed and operates a laboratory X-ray absorption spectrometer. This instrument is capable of producing XANES spectra with moderate energy resolution and excellent EXAFS spectra within reasonable acquistion times. The most important application projects are:

- Cu/mordenite catalysist for methane to methanol conversion (Prof. Dr. A. Thomas, TU Berlin, Center of Excellence UniCat)
- Structure and dynamics of (Mn,Fe)Ox-promoted Rh nanoparticles (Dr. Annette Trunschke, Fritz-Haber-Institut der Max-Planck-Gesellschaft)
- Quantitative analysis of species mixtures (Prof. Dr. C. Vogt, Technische Universtität Bergakademie Freiberg)
- EXAFS in industrial applications (Prof. Dr. I. Arcon, University of Nova Gorica).

Confocal micro-X-ray fluorescence spectroscopy (XRF)

A dedicated laboratory for micro-XRF and confocal micro-XRF is operated within BLiX for application projects. In 2017 the main focus was on biological samples, including the investigation of cryo-fixated samples.

With two laboratory spectrometers, investigations in the following projects were performed:

- Metal distribution in mussel tissue for the elucidation of the formation of byssus threads
- Uptake of heavy metals in corn and sunflower roots/shoots/leaves as a means to illuminate metal transport in plants
- Mineral exchange between host plant and cuscuta parasite
- Shape and distribution of Pt patches in self-activated catalysis particles
- Interface dynamics in teeth close to restauration.

Additionally, in cooperation with Excillum Ltd. and IfG/Helmut Fischer GmbH experiments were performed to assess the suitability of high brilliance metal jet sources for confocal micro-XRF.

3. Users and collaborations

Charité, Berlin, Germany; McGill University, Montreal, Canada; University of Ljubljana, Slovenia; The Arctic University of Norway, Tromsö, Norway; Institute for Chemistry, TU Berlin, Germany; Julius Wolff Institute, Charité, Berlin, Germany; FhG-ILT, Aachen, Germany; optixFab GmbH, Jena, Germany; greateyes GmbH, Berlin, Germany; HZB/BESSY, Berlin, Germany; PTB, Berlin, Germany; KTH, Stockholm, Sweden; BESTEC GmbH, Berlin, Germany; neutron optics berlin (nob) GmbH, Berlin, Germany; Excillum Ltd, Kista, Sweden; Helmut Fischer GmbH/IfG, Berlin/Sindelfingen, Germany; Optigraph GmbH, Berlin, Germany.

People

MBI: Andrea Lübcke, Julia Bränzel, Janina Lebendig-Kuhla, Robert Jung (now at TRUMPF Sci.).
TUB: Aurélie Dehlinger, Ioanna Mantouvalou, Adrian Jonas, Daniel Grötzsch, Christopher Schlesiger, Katharina Witte (now at PSI, Villigen), Wolfgang Malzer, Birgit Kanngießer.

Publications

All publications involving MBI scientists which have emerged from work in BLiX are listed under the relevant research projects (cp. Project 3.3).

Publications related exclusively to TU Berlin personnel, without contribution of MBI scientists

I. Mantouvalou, T. Lachmann, S. P. Singh, K. Vogel-Mikuš, and B. Kanngießer; Advanced absorption correction for 3D elemental images applied to the analysis of pearl millet seeds obtained with a laboratory confocal micro X-ray fluorescence spectrometer; Anal. Chem. **89** (2017) 5453

M. Dimitrakopoulou, X. Huang, J. Kröhnert, D. Teschner, S. Praetz, C. Schlesiger, W. Malzer, C. Janke, E. Schwab, F. Rosowkski, H. Kaiser, S. Schunk, R. Schlögl, and A. Trunschke; Insights into structure and dynamics of (Mn,Fe)Ox-promoted Rh nanoparticles, Faraday Discussions, 2017; DOI 10.1039/C7FD00215G

H. V. Le, S. Parishan, A. Sagaltchik, C. Göbel, C. Schliesiger, W. Malzer, A. Trunschke, R. Schomäcker, and A. Thomas; Solid-state ion-exchanged Cu/Mordenite catalysts for the direct conversion of methane to methanol; ACS Catal. **7** (2017) 1403

4.3: Nanoscaled Samples and Optics

D. Engel (project coordinator)
C. Günther (TU Berlin / guest)

1. Overview

The laboratory for Nanoscaled Samples and Optics supports several experiments of different scientific projects of the MBI. The thin-film samples, filters and membranes are produced by means of magnetron sputtering and thermal evaporation. The major deposition system enables the coating of up to 4" substrates using a maximum of 7 different materials without vacuum break. Lateral patterning of samples on the micrometer and/or nanometer scale is achieved via electron beam lithography or Focused-Ion-Beam (FIB) patterning, in close cooperation with the central facility for electron microscopy (ZELMI) at the TU Berlin. Topographic and magnetic characterization of thin film samples is carried out by atomic- and magnetic force microscopy (AFM/MFM), Kerr magnetometry (MOKE) and via Kerr microscopy.

Collaborations: Various scientists at the central facility for electron microscopy (ZELMI) of the Technische Universität Berlin, Germany, M. Albrecht (Augsburg University, Germany), M. Schmidbauer (Institut für Kristallzüchtung, Germany).

2. Objectives

A variety of research activities at MBI deal with dynamical processes which occur intrinsically on the nanometer length scale set by fundamental material properties such as inelastic mean free paths for transport of electrons or spins. Sensitivity to such processes can be obtained via several of experimental approaches using short pulses of light, XUV or X-rays. Nanoscale patterning of a sample in conjunction with the specific spectroscopy, scattering or imaging experiment are used to design unique experiments with specific information content or sensitivity, for example via integrated near field optics.

Furthermore, via the nanopatterning capabilities we are able to produce diffractive far field optics for experiments with XUV and soft X-rays, where structure sizes have to approach the wavelength of the radiation used. Examples are custom Fresnel zone plates, holographic masks or coded aperture arrays.

Finally, the study of ultrafast dynamic processes in magnetic materials requires the development of suitable sample materials in the form of thin multilayer films or alloys, coupled with the ability to characterize the static properties prior to time-resolved experiments.

3. Results in 2017

General thinning approach applicable for crystalline and amorphous bulk substrates

For many experiments with soft X-rays and XUV radiation it would be advantageous to be able to carry them out in a transmission geometry. Due to the short attenuation length in this spectral range in solids, which is typically below 1 µm, this requires suitably thin samples. Often, thin membranes of light elements materials such as polymers or Si_3N_4 are used as highly transparent growth substrate for thin films to be investigated. As these mem-

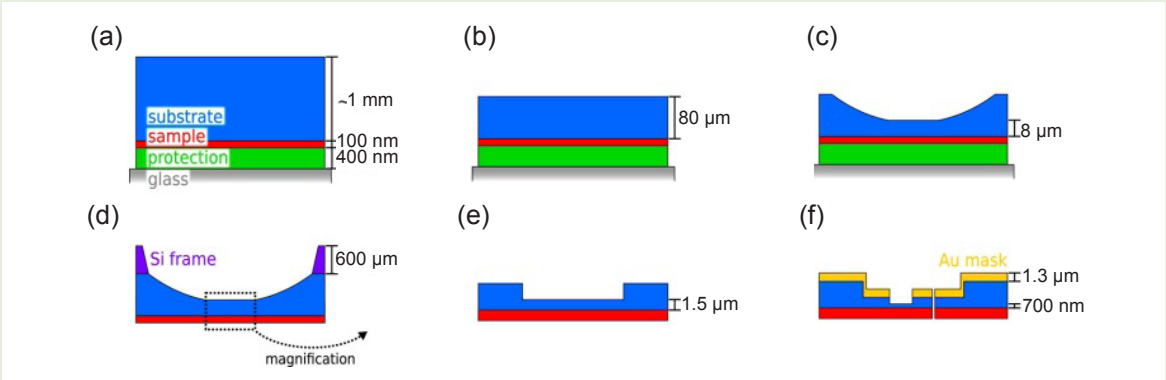

Fig. 1:
Sample preparation process: (a) Growth substrate (blue) with thin film layer of interest (red). A PMMA layer (green) protects the sample before the preparation holder (gray) is applied. (b) Substrate back-thinned by plane disk grinding and (c) dimple grinding. (d) A silicon frame (purple) surrounding the dimple area is applied to increase mechanical stability before the sample holder is removed. (e) Using FIB milling, the substrate is thinned down further to a membrane area. (f) A Cr/Au multilayer coating (yellow) is applied to be used for the FTH mask with an object hole and a reference through hole. The object area is thinned down further to the final substrate thickness.

branes are amorphous or polycrystalline, this approach does not allow for the study of epitaxial thin films. Typically, the lattice constants of a thin epitaxial film to be grown dictates the use of suitably matched growth crystals which are generally macroscopic in thickness and hence opaque to soft X-rays.

We have developed a thinning procedure which allows to locally thin down a growth substrate to sub-µm thickness, allowing to study thin films on such a substrate in transmission with soft X-rays or XUV radiation. The thinning procedure combines a two-step wet grinding technique with followed by FIB milling. Figure 1 illustrates the different processing steps of the preparation method, starting with a spin coated PMMA film of about 400 nm thickness to protect the thin film of interest during the thinning process. Disk grinding with a lubricant containing abrasive particles is used to reduce the substrate thickness to around 80 µm (Fig. 1(b)). Next, dimple grinding with a flat bronze wheel is employed to thin the sample down to a remaining 8 µm thickness at the lowest point of the dimple (Fig. 1(c)). After measures to avoid mechanical tension on the thin sample region, thinning to soft X-ray transparency is carried out with 30 kV focused Ga^+ ions under scanning electron microscopy (SEM) control [FFS17].

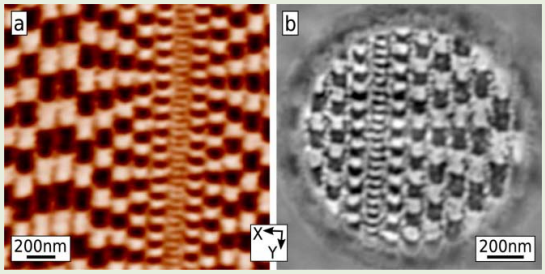

Fig. 2:
Comparative magnetization images of the test pattern written on a conventional HDD medium obtained via (a) SMRM, prior to back-thinning preparation and (b) reconstruction of the soft X-ray FTH measurement on the back-thinned sample.

A demonstration of this approach is carried out by spectro-holography with soft X-rays in order to image magnetic domains on a commercial magnetic hard drive disk via a transmission measurement using X-ray magnetic circular dichroism (XMCD) contrast at the Co L_3 absorption edge. The sample is a glass disk of 642 µm thickness coated with a CoCrPt-based thin film stack as a perpendicular magnetic recording medium. A magnetization test pattern was written using a read/write head in a scanning magnetoresistive microscope (SMRM). The pattern consisted of magnetization transitions with pitch sizes continuously varying from 30 nm to 210 nm in the y-direction (down-track), which were repeated over an area of about 100 × 100 $µm^2$.

In Fig. 2 the comparison of the magnetic domain test pattern obtained via SMRM imaging prior to the thinning procedure and as obtained via Fourier Transform X-ray Holography (FTH) in transmission after the thinning procedure is shown. The FTH reconstruction clearly reproduces the regular bit pattern in all detail down to the smallest pitch of 30 nm. In addition, the X-ray holography image allows us to recognize curved bit boundaries caused by the write head field shape as well as intra-bit magnetic structures such as small areas pinned in the opposite magnetization direction. The results show that the bit pattern was not altered during the thinning procedure and that high resolution transmission imaging with soft X-rays is possible, achieving sub-30 nm spatial resolution.

Publications

FFS17: M. Fohler *et al.;* Rev. Sci. Instrum. **88** (2017) 103701/1-7

Further publications are listed in the context of the Projects 3.2 and 3.3.

Appendices

Appendix 1

Publications

AAB17: R. M. Arkhipov, M. V. Arkhipov, I. Babushkin, A. V. Pakhomov, and N. N. Rosanov; Population difference gratings produced by unipolar subcycle pulses in a resonant medium; Quantum Electron. **47** (2017) 589-592

AAP17a: M. V. Arkhipov, R. M. Arkhipov, A. V. Pakhomov, I. V. Babushkin, A. Demircan, U. Morgner, and N. N. Rosanov; Generation of unipolar half-cycle pulses via unusual reflection of a single-cycle pulse from an optically thin metallic or dielectric layer; Opt. Lett. **42** (2017) 2189-2192

AAP17b: R. M. Arkhipov, M. V. Arkhipov, A. V. Pakhomov, I. Babushkin, and N. N. Rosanov; Nonlinear-photonics devices on the basis of the coherent interaction of optical radiation with resonant media (a review); Optics and Spectroscopy **122** (2017) 949-954

AAP17c: R. M. Arkhipov, M. V. Arkhipov, A. V. Pakhomov, I. Babushkin, and N. N. Rosanov; Light-induced spatial gratings created by unipolar attosecond pulses coherently interacting with a resonant medium; Laser Phys. Lett. **14** (2017) 095402/1-6

AAP17d: R. M. Arkhipov, M. V. Arkhipov, A. V. Pakhomov, I. Babushkin, and N. N. Rosanov; Collisions of unipolar subcycle pulses in a nonlinear resonantly absorbing medium; Optics and Spectroscopy **123** (2017) 610-614

ABL17: K. Amini, R. Boll, A. Lauer, M. Burt, J. W. L. Lee, L. Christensen, F. Brausse, T. Mullins, E. Savelyev, N. Berrah, C. Bomme, S. Düsterer, B. Erk, H. Höppner, P. Johnsson, T. Kierspel, F. Krecinic, J. Küpper, M. Müller, E. Müller, H. Redlin, A. Rouzée, N. Schirmel, J. Thøgersen, S. Techert, S. Toleikis, R.Treusch, S.Trippel, A. Ulmer, J. Wiese, A. Rudenko, H. Stapelfeldt, M. Brouard, and D. Rolles; Alignment, orientation, and coulomb explosion of difluoroiodobenzene studied with the Pixel Imaging Mass Spectrometry (PImMS) camera; J. Chem. Phys. **147** (2017) 013933/1-8

ABP17: M. V. Arkhipov, I. Babushkin, N. S. Pul'kin, R. M. Arkhipov, and N. N. Rosanov; On the emission of radiation by an isolated vibrating metallic mirror; Optics and Spectroscopy **122** (2017) 670-674

AJC17: L. Argenti, Á. Jiménez Galán, J. Caillat, R. Taïeb, A. Maquet, and F. Martín; Control of photoemission delay in resonant two-photon transitions; Phys. Rev. A **95** (2017) 043426/1-8

AJM17: D. Ayuso, Á. Jiménez Galán, F. Morales, M. Ivanov, and O. Smirnova; Attosecond control of spin polarization in electron-ion recollision driven by intense tailored fields; New J. Phys. **19** (2017) 073007/1-10

And17: A. A. Andreev; Relativistic Nano-Plasma Photonics; in *Progress in Photon Science, part of the Springer Series in Chemical Physics book series (CHEMICAL)*, K. Yamanouchi ed. (2017) Vol. 115, 3-13

APA17a: R. M. Arkhipov, A. V. Pakhomov, M. V. Arkhipov, I. Babushkin, A. Demircan, U. Morgner, and N. N. Rosanov; Population density gratings induced by few-cycle optical pulses in a resonant medium; Sci. Rep. **7** (2017) 12467/1-21

APA17b: R. M. Arkhipov, A. V. Pakhomov, M. V. Arkhipov, I. Babushkin, Y. A. Tolmachev, and N. N. Rosanov; Generation of unipolar pulses in nonlinear media; JETP Lett. **105** (2017) 408-418

APA17c: R. M. Arkhipov, A. V. Pakhomov, M. V. Arkhipov, I. V. Babushkin, Y. A. Tolmachev, and N. N. Rosanov; Radiation of a resonant medium excited by few-cycle optical pulses at superluminal velocity; Laser Phys. **27** (2017) 053001/1-10

APD17: D. Ayuso, A. Palacios, P. Decleva, and F. Martín; Ultrafast charge dynamics in glycine induced by attosecond pulses; Phys. Chem. Chem. Phys. **19** (2017) 19767-19776

APE17: U. Alvarez-Rodriguez, A. Perez-Leija, I.-L. Egusquiza, M. Gräfe, M. Sanz, L. Lamata, A. Szameit, and E. Solano; Advanced-retarded differential equations in quantum photonic systems; Sci. Rep. **7** (2017) 42933/1-13

BAA17: J. Braenzel, A. A. Andreev, F. Abicht, L. Ehrentraut, K. Platonov, and M. Schnürer; Amplification of relativistic electron bunches by acceleration in laser fields; Phys. Rev. Lett. **118** (2017) 014801/1-5

Bab17: I. Babushkin; Weak stochastic ratchets and dynamic localization in measurement-induced quantum trajectories; Phys. Rev. A **95** (2017) 042101/1-13

BAE17a: J. Braenzel, A. A. Andreev, L. Ehrentraut, and M. Schnürer; Direct acceleration in intense laser fields used for bunch amplification of relativistic electrons; SPIE Proc. **10240** (2017) 102400G

BAE17b: J. Braenzel, A. A. Andreev, L. Ehrentraut, D. Sommer, and M. Schnürer; Concerted manipulation of laser plasma dynamics with two laser pulses; SPIE Proc. **10240** (2017) 1024017

BAP17: J. Braenzel, A. A. Andreev, K. Y. Platonov, L. Ehrentraut, and M. Schnürer; Amplification of coherent synchrotron-like high harmonic emission from ultra-thin foils in relativistic light fields; Phys. Plasmas **24** (2017) 080704/1-6

BBD17: I. Babushkin, C. Brée, C. M. Dietrich, A. Demircan, U. Morgner, and A. Husakou; Terahertz and higher-order Brunel harmonics: from tunnel to multiphoton ionization regime in tailored fields; J. Mod. Opt. **64** (2017) 1078-1087

BBL17: M. Burt, R. Boll, J. W. L. Lee, K. Amini, H. Köckert, C. Vallance, A. S. Gentleman, S. R. Mackenzie, S. Bari, C. Bomme, S. Düsterer, B. Erk, B. Manschwetus, E. Müller, D. Rompotis, E. Savelyev, N. Schirmel, S. Techert, R. Treusch, J. Küpper, S. Trippel, J. Wiese, H. Stapelfeldt, B. C. de Miranda, R. Guillemin, I. Ismail, L. Journel, T. Marchenko, J. Palaudoux, F. Penent, M. N. Piancastelli, M. Simon, O. Travnikova, F. Brausse, G. Goldsztejn, A. Rouzée, M. Géléoc, R. Geneaux, T. Ruchon, J. Underwood, D. M. P. Holland, A. S. Mereshchenko, P. K. Olshin, P. Johnsson, S. Maclot, J. Lahl, A. Rudenko, F. Ziaee, M. Brouard, and D. Rolles; Coulomb-explosion imaging of concurrent CH2BrI photodissociation dynamics; Phys. Rev. A **96** (2017) 043415/1-8

BFe17: D. Bauer and T. Fennel; How to propagate a wavefunction?; in *Computational Strong-Field Quantum Dynamics*, Dieter Bauer ed. (De Gruyter Textbook, 2017) 1-44

BHD17: C. Brée, M. Hofmann, A. Demircan, U. Morgner, O. Kosareva, A. Savel'ev, A. Husakou, M. Ivanov, and I. Babushkin; Symmetry Breaking and Strong Persistent Plasma Currents via Resonant Destabilization of Atoms; Phys. Rev. Lett. **119** (2017) 243202/1-5

BHH17: D. S. Brambila, A. G. Harvey, K. Houfek, Z. Masin, and O. Smirnova; Role of electronic correlations in photoionization of NO_2 in the vicinity of the 2A1/2B2 conical intersection; Phys. Chem. Chem. Phys. **19** (2017) 19673-19682

BHI17: D. S. Brambila, A. Husakou, M. Ivanov, and N. Zhavoronkov; On-target diagnosing of few-cycle pulses by high-order-harmonic generation; Phys. Rev. A **96** (2017) 063825/1-5

BHK17: J. Bonse, S. Höhm, S. V. Kirner, A. Rosenfeld, and J. Krüger; Laser-induced periodic surface structures – A scientific evergreen; IEEE J. Sel. Top. Quant. Electron. **23** (2017) 9000615/1-15

BKB17: A. A. Boyko, N. Y. Kostyukova, V. Badikov, D. Badikov, V. Panyutin, G. Shevyrdyaeva, V. Pasiskevicius, A. Zukauskas, G. M. Marchev, D. B. Kolker, and V. Petrov; Intracavity difference-frequency mixing of optical parametric oscillator signal and idler pulses in $BaGa_4Se_7$; Appl. Opt. **56** (2017) 2783-2786

BKH17: J. Bonse, S. V. Kirner, S. Höhm, N. Epperlein, D. Spaltmann, A. Rosenfeld, and J. Krüger; Applications of laser-induced periodic surface structures (LIPSS); SPIE Proc. **10092** (2017) 100920N/1-9

BLS17: F. Büttner, I. Lemesh, M. Schneider, B. Pfau, C. M. Günther, P. Hessing, J. Geilhufe, L. Caretta, D. Engel, B. Krüger, J. Viefhaus, S. Eisebitt, and G. S. D. Beach; Field-free deterministic ultrafast creation of magnetic skyrmions by spin-orbit torques; Nat. Nanotechnol. **12** (2017) 1040-1044

BMC17: F. Bach, M. Mero, M.-H. Chou, and V. Petrov; Laser induced damage studies of $LiNbO_3$ using 1030-nm, ultrashort pulses at 10-1000 kHz; Opt. Mater. Express **7** (2017) 240-252

BMi17: W. Becker and D. B. Milošević; Above-threshold ionization in a bicircular field: quantum orbits unfolding in a plane; J. Phys. Conf. Ser. **826** (2017) 012008/1-8

BMP17: F. Bach, M. Mero, V. Pasiskevicius, A. Zukauskas, and V. Petrov; High repetition rate, femtosecond and picosecond laser induced damage thresholds of Rb:$KTiOPO_4$ at 1.03 µm; Opt. Mater. Express **7** (2017) 744-750

BPB17: G. Bart, C. Peltz, N. Bigaouette, T. Fennel, T. Brabec, and C. Varin; Massively parallel microscopic particle-in-cell; Comput. Phys. Commun. **219** (2017) 269-285

BPI17: T. Bredtmann, S. Patchkovskii, and M. Y. Ivanov; Strong-field assisted extreme-ultraviolet lasing in atoms and molecules; New J. Phys. **19** (2017) 073011/1-11

BSM17: M. K. Bhuyan, M. Somayaji, A. Mermillod-Blondin, F. Bourquard, J. P. Colombier, and R. Stoian; Ultrafast laser nanostructuring in bulk silica, a "slow" microexplosion; Optica **4** (2017) 951-958

BTG17: M. Bock, A. Treffer, and R. Grunwald; Nondiffracting self-imaging of ultrashort wavepackets; Opt. Lett. **42** (2017) 2374-2377

BTS17: I. Babushkin, A. Tajalli, H. Sayinc, U. Morgner, G. Steinmeyer, and A. Demircan; Simple route toward efficient frequency conversion for generation of fully coherent supercontinua in the mid-IR and UV range; Light: Sci. Appl. **6** (2017) e16218/1-8

CBR17: K. Carva, P. Baláž, and I. Radu; Laser-Induced Ultrafast Magnetic Phenomena; in *Handbook of Magnetic Materials*, E. Brück ed. (Elsevier B.V, Delft, The Netherlands, 2017) 291-463

CPL17: M. F. Ciappina, J. A. Pérez-Hernández, A. S. Landsman, W. A. Okell, S. Zherebtsov, B. Förg, J. Schötz, L. Seiffert, T. Fennel, T. Shaaran, T. Zimmermann, A. Chacón, R. Guichard, A. Zaïr, J. W. G. Tisch, J. P. Marangos, T. Witting, A. Braun, S. A. Maier, L. Roso, M. Krüger, P. Hommelhoff, M. F. Kling, F. Krausz, and M. Lewenstein; Attosecond physics at the nanoscale; Rep. Prog. Phys. **80** (2017) 054401/1-50

CRP17: S. Chaudhuri, B. Rudshteyn, M. Prémont-Schwarz, D. Pines, E. Pines, D. Huppert, E. T. J. Nibbering, and V. S. Batista; Ultrafast photo-induced charge transfer of 1-naphthol and 2-naphthol to halocarbon solvents; Chem. Phys. Lett. **683** (2017) 49-56

CTF17: C. Callegari, T. Takanashi, H. Fukuzawa, K. Motomura, D. Iablonskyi, Y. Kumagai, S. Mondal, T. Tachibana, K. Nagaya, T. Nishiyama, K. Matsunami, P. Johnsson, P. Piseri, G. Sansone, A. Dubrouil, M. Reduzzi, P. Carpeggiani, C. Vozzi, M. Devetta, D. Faccialà, F. Calegari, M. C. Castrovilli, M. Coreno, M. Alagia, B. Schütte, N. Berrah, O. Plekan, P. Finetti, E. Ferrari, K. C. Prince, and K. Ueda; Application of matched-filter concepts to unbiased selection of data in pump-probe experiments with free electron lasers; Appl. Sci. **7** (2017) 621/1-9

DFN17: F. Dahms, B. P. Fingerhut, E. T. J. Nibbering, E. Pines, and T. Elsaesser; Large-amplitude transfer motion of hydrated excess protons mapped by ultrafast 2D IR spectroscopy; Science **357** (2017) 491-495

DKD17: A. Donges, S. Khmelevskyi, A. Deak, R.-M. Abrudan, D. Schmitz, I. Radu, F. Radu, L. Szunyogh, and U. Nowak; Magnetization compensation and spin reorientation transition in ferrimagnetic $DyCo_5$: Multiscale modeling and element-specific measurements; Phys. Rev. B **96** (2017) 024412/1-7

DMT17: D. Darby-Lewis, Z. Mašín, and J. Tennyson; R-matrix calculations of electron impact electronic excitation of BeH; J. Phys. B **50** (2017) 175201/1-12

Els17a: T. Elsaesser; Introduction: Ultrafast processes in chemistry; Chem. Rev. **117** (2017) 10621-10622

Els17b: T. Elsaesser; Im Atomkino; Physik in unserer Zeit **48** (2017) 263

EQS17: M. Ekimova, W. Quevedo, Ł. Szyc, M. Iannuzzi, P. Wernet, M. Odelius, and E. T. J. Nibbering; Aqueous solvation of ammonia and ammonium: probing hydrogen bond motifs with FT-IR and soft x-ray spectroscopy; J. Am. Chem. Soc. **139** (2017) 12773-12783

FAP17: A. Y. Faenov, M. A. Alkhimova, T. A. Pikuz, I. Y. Skobelev, M. Nishiuchi, H. Sakaki, A. S. Pirozhkov, A. Sagisaka, N. P. Dover, K. Kondo, K. Ogura, Y. Fukuda, H. Kiriyama, A. Andreev, K. Nishitani, T. Miyahara, Y. Watanabe, S. A. P. Jr., M. Kando, R. Kodama, and K. Kondo; The effect of laser contrast on generation of highly charged Fe ions by ultra-intense femtosecond laser pulses; Appl. Phys. B **123** (2017) 197/1-7

FDS17: M. Floegel, J. Durá Diez, B. Schütte, M. Ivanov, A. Rouzée, and M. J. J. Vrakking; Rabi oscillations in extreme ultraviolet ionization of atomic argon; Phys. Rev. A **95** (2017) 021401R/1-5

FEC17: R. Feifel, J. H. D. Eland, S. Carniato, P. Selles, R. Püttner, D. Koulentianos, T.Marchenko, L. Journel, R. Guillemin, G. Goldsztejn, O. Travnikova, I. Ismail, B. C. de Miranda, A. F. Lago, D. Céolin, P. Lablanquie, F. Penent, M. N. Piancastelli, and M. Simon; Cationic double K-hole pre-edge states of CS_2 and SF_6; Sci. Rep. **7** (2017) 13317/1-11

FFP17: L. Fregnani, P. Farinello, F. Pirzio, X.-Y. Zhang, V. Petrov, and A. Agnesi; Threshold reduction and mode selection with uncoated Raman crystal acting as a low-finesse cavity; Appl. Opt. **56** (2017) 662-665

FFS17: M. Fohler, S. Frömmel, M. Schneider, B. Pfau, C. Günther, M. Hennecke, E. Guehrs, L. Shemilt, D. Mishra, D. Berger, S. Selve, D. Mitin, M. Albrecht, and S. Eisebitt; A general approach to obtain soft x-ray transparency for thin films grown on bulk substrates; Rev. Sci. Instrum. **88** (2017) 103701/1-7

FMM17: S. Flewett, D. Mishra, T. J. A. Mori, C. M. Günther, J. C. Denardin, S. Oyarzún, S. Michea, D. Engel, M. Fohler, T. C. R. Rocha, A. Ovalle F., L. T. Núñez. A., B. Pfau, J. Escrig, and S. Eisebitt; Three-dimensional characterization of Co/Pd multilayer thin films using resonant soft x-ray scattering; Phys. Rev. B **95** (2017) 094430/1-11

FPV17: A. Y. Faenov, T. A. Pikuz, G. A. Vergunova, S. A. Pikuz Jr., I. Y. Skobelev, A. Andreev, A. Zhidkov, and R. Kodama; Ultra-bright keV x-ray source generated by relativistic femtosecond laser pulse interaction with thin foils and its possible application for HEDS investigations; Laser Part. Beams **35** (2017) 450-457

FRW17: G. Folpini, K. Reimann, M. Woerner, T. Elsaesser, J. Hoja, and A. Tkatchenko; Strong local-field enhancement of the nonlinear soft-mode response in a molecular crystal; Phys. Rev. Lett. **119** (2017) 097404/1-6

FSW17: G. Folpini, T. Siebert, M. Woerner, S. Abel, D. Laage, and T. Elsaesser; Water librations in the hydration shell of phospholipids; J. Phys. Chem. Lett. **8** (2017) 4492-4497

FTK17: S. Friede, J. W. Tomm, S. Kuehn, V. Hoffmann, and H. Wenzel; Analysis of waveguide architectures of InGaN/GaN diode lasers by nearfield optical microscopy; SPIE Proc. **10123** (2017) 1012308/1-7

FWG17: F. J. Furch, T. Witting, A. Giree, C. Luan, F. Schell, G. Arisholm, C. P. Schulz, and M. J. J. Vrakking; CEP-stable few-cycle pulses with more than 190 µJ of energy at 100 kHz from a noncollinear optical parametric amplifier; Opt. Lett. **42** (2017) 2495-2498

GBU17: L. v. Grafenstein, M. Bock, D. Ueberschaer, K. Zawilski, P. Schunemann, U. Griebner, and T. Elsaesser; 5 µm few-cycle pulses with multi-GW peak power at a 1 kHz repetition rate; Opt. Lett. **42** (2017) 3796-3799

GGS17: C. M. Günther, E. Guehrs, M. Schneider, B. Pfau, C. v. Korff Schmising, J. Geilhufe, S. Schaffert, and S. Eisebitt; Experimental evaluations of signal-to-noise in spectro-holography via modified uniformly redundant arrays in the soft x-ray and extreme ultraviolet spectral regime; J. Opt. **19** (2017) 064002/1-11

GKY17: K. Gorbachenya, V. Kisel, A. Yasukevich, P. Loiko, X. Mateos, V. Maltsev, N. Leonyuk, M. Aguiló, F. Diaz, U. Griebner, V. Petrov, and N. Kuleshov; Graphene Q-switched Er,Yb:$GdAl_3(BO_3)_4$ laser at 1550 nm; Appl. Opt. **56** (2017) 4745-4749

GMA17: A. Giree, M. Mero, G. Arisholm, M. J. J. Vrakking, and F. J. Furch; Numerical study of spatiotemporal distortions in noncollinear optical parametric chirped-pulse amplifiers; Opt. Express **25** (2017) 3104-3121

GOW17: A. Ghalgaoui, A. Ouvrard, J. Wang, S. Carrez, W. Zheng, and B. Bourguignon; Electron to adsorbate energy transfer in nanoparticles: adsorption site, size, and support matter; J. Phys. Chem. Lett. **8** (2017) 2666-2671

GPJ17: G. Goldsztejn, R. Püttner, L. Journel, R. Guillemin, O. Travnikova, B. C. de Miranda, I. Ismail, S. Carniato, P. Selles, D. Céolin, A. F. Lago, R. Feifel, P. Lablanquie, F. Penent, M. N. Piancastelli, M. Simon, and T. Marchenko; Experimental and theoretical study of the double-core-hole hypersatellite Auger spectrum of Ne; Phys. Rev. A **96** (2017) 012513/1-9

GSG17a: E. Guehrs, M. Schneider, C. M. Günther, P. Hessing, K. Heitz, D. Wittke, A. L. S. Oliver, N. Jakubowski, J. Plendl, S. Eisebitt, and A. Haase; Quantification of silver nanoparticle uptake and distribution within individual human macrophages by FIB/SEM slice and view; J. Nanobiotechnol. **15:21** (2017) 1-11

GSG17b: M. C. E. Galbraith, S. Scheit, N. V. Golubev, G. Reitsma, N. Zhavoronkov, V. Despré, F. Lépine, A. I. Kuleff, M. J. J. Vrakking, O. Kornilov, H. Köppel, and J. Mikosch; Few-femtosecond passage of conical intersections in the benzene cation; Nat. Commun. **8** (2017) 1018/1-7

GSR17: M. C. E. Galbraith, C. T. L. Smeenk, G. Reitsma, A. Marciniak, V. Despré, J. Mikosch, N. Zhavoronkov, M. J. J. Vrakking, O. Kornilov, and F. Lépine; XUV-induced reactions in benzene on sub-10 fs timescale: nonadiabatic relaxation and proton migration; Phys. Chem. Chem. Phys. **19** (2017) 19822-19828

HAC17: A. Husakou, M. Alharbi, M. Chafer, B. Debord, F. Gerome, and F. Benabid; Theory of line narrowing by deep nano-trap lattice in raman gas; Nonlin. Phenomena Complex Syst. **20** (2017) 1-11

HBM17: E. Hasović, W. Becker, and D. B. Milošević; Electron rescattering in a bicircular laser field; J. Phys. Conf. Ser. **826** (2017) 012009/1-7

HES17a: J. Hyyti, E. Escoto, and G. Steinmeyer; Pulse retrieval algorithm for interferometric frequency-resolved optical gating based on differential evolution; Rev. Sci. Instrum. **88** (2017) 103102/1-14

HES17b: J. Hyyti, E. Escoto, and G. Steinmeyer; Third-harmonic interferometric frequency-resolved optical gating; J. Opt. Soc. Am. B **34** (2017) 2367-2375

HES17c: J. Hyyti, E. Escoto, G. Steinmeyer, and T. Witting; Interferometric time-domain ptychography for ultrafast pulse characterization; Opt. Lett. **42** (2017) 2185-2188

HHW17: M. Holtz, C. Hauf, J. Weisshaupt, A. Hernandez, M. Woerner, and T. Elsaesser; Towards shot-noise limited diffraction experiments with table-top femtosecond hard x-ray sources; Struct. Dyn. **4** (2017) 054304/1-11

HOB17: E. Hasović, S. Odžak, W. Becker, and D. B. Milošević; High-order harmonic generation in non-planar molecules driven by a bicircular field; Mol. Phys. **115** (2017) 1750-1757

HPM17: Z. Heiner, V. Petrov, and M. Mero; Compact, high-repetition-rate source for broadband sum-frequency generation spectroscopy; APL Photonics **2** (2017) 066102/1-7

HRK17: S. Höhm, A. Rosenfeld, J. Krüger, and J. Bonse; Laser-induced periodic surface structures on zinc oxide crystals upon two-colour femtosecond double-pulse irradiation; Phys. Scripta **92** (2017) 034003/1-7

Hus17: A. Husakou; Quasi-phase-matched high harmonic generation in corrugated micrometer-scale waveguide; J. Opt. Soc. Am. B **34** (2017) 137-141

IIN17: M. Iqbal, M. Ijaz, D. Y. Noh, K. A. Janulewicz, H. Stiel, and P. V. Nickles; Optimization of a laser plasma x-ray source for ultrafast x-ray absorption spectroscopy; J. Korean Phys. Soc. **70** (2017) 905-911

IKT17: M. F. Ibad, H. Kosslick, J. W. Tomm, M. Frank, and A. Schulz; Impact of the crystallinity of mesoporous polymeric graphitic carbon nitride on the photocatalytic performance under UV and visible light; Microporous Mesoporous Mat. **254** (2017) 136-145

IRH17: S.-J. Im, C.-S. Ri, K.-S. Ho, and J. Herrmann; Third-order nonlinearity by the inverse Faraday effect in planar magnetoplasmonic structures; Phys. Rev. B **96** (2017) 165437/1-6

IRP17: S.-J. Im, C.-S. Ri, J.-S. Pae, Y.-H. Han, and J. Herrmann; Magnetically-tunable cutoff in asymmetric thin metal film plasmonic waveguide; Appl. Phys. Lett. **111** (2017) 071102/1-4

JPS17: W. Jing, P. Loiko, J. M. Serres, Y. Wang, E. Vilejshikova, M. Aguiló, F. Diaz, U. Griebner, H. Huang, C. Kränkel, V. Petrov, and X. Mateos; Synthesis, spectroscopy, and efficient laser operation of “mixed” sesquioxide Tm:$(Lu,Sc)_2O_3$ transparent ceramics; Opt. Mater. Express **7** (2017) 4192-4202

JZS17: Á. Jiménez Galán, N. Zhavoronkov, M. Schloz, F. Morales, and M. Ivanov; Time-resolved high harmonic spectroscopy of dynamical symmetry breaking in bicircular laser fields: the role of Rydberg states; Opt. Express **25** (2017) 22880-22896

KBG17: S. Kelvich, W. Becker, and S. P. Goreslavski; Caustics and catastrophes in above-threshold ionization; Phys. Rev. A **96** (2017) 023427/1-5

KFD17: M. Kowalewski, B. P. Fingerhut, K. E. Dorfman, K. Bennett, and S. Mukamel; Simulating coherent multidimensional spectroscopy of nonadiabatic molecular processes: from the infrared to the X-ray regime; Chem. Rev. **117** (2017) 12165-12226

KHH17: K.-H. Kim, A. Husakou, and J. Herrmann; Ultrafast nonlinear optical effects of metal nanoparticles composites; in *Nanoplasmonics: Fundamentals and Applications*, G. Barbillon ed. (IntechOpen, 2017) 95-115

KLM17: E. Kifle, P. Loiko, X. Mateos, J. R. Vázquez de Aldana, A. Ródenas, U. Griebner, V. Petrov, M. Aguiló, and F. Diaz; Femtosecond-laser-written hexagonal cladding waveguide in Tm:$KLu(WO_4)_2$: μ-Raman study and laser operation; Opt. Mater. Express **7** (2017) 4258-4268

KMI17: K. Kato, K. Miyata, L. Isaenko, S. Lobanov, V. Vedenyapin, and V. Petrov; Phase-matching properties of $LiGaS_2$ in the 1.025-10.5910 μm range; Opt. Lett. **42** (2017) 4363-4366

KML17: E. Kifle, X. Mateos, P. Loiko, K. Yumashev, A. Yasukevich, V. Petrov, U. Griebner, M. Aguiló, and F. Díaz; Graphene Q-switched Tm:$KY(WO_4)_2$ waveguide laser; Laser Phys. **27** (2017) 045801/1-6

KMP17: K. Kato, K. Miyata, and V. Petrov; Phase-matching properties of $BaGa_4Se_7$ for SHG and SFG in the 0.901-10.5910 μm range; Appl. Opt. **56** (2017) 2978-2981

KMV17: E. Kifle, X. Mateos, J. R. Vázquez de Aldana, A. Ródenas, P. Loiko, S. Y. Choi, F. Rotermund, U. Griebner, V. Petrov, M. Aguiló, and F. Díaz; Femtosecond laser-written Tm:$KLu(WO_4)_2$ waveguide lasers; Opt. Lett. **42** (2017) 1169-1172

KPA17: B. Koeppe, S. A. Pylaeva, C. Allolio, D. Sebastiani, E. T. J. Nibbering, G. S. Denisov, H.-H. Limbach, and P. M. Tolstoy; Polar solvent fluctuations drive proton transfer in hydrogen bonded complexes of carboxylic acid with pyridines: NMR, IR and ab initio MD study; Phys. Chem. Chem. Phys. **19** (2017) 1010-1028

KRH17: G. Kewes, K. Herrmann, R. Rodríguez-Oliveros, A. Kuhlicke, O. Benson, and K. Busch; Limitations of particle-based spasers; Phys. Rev. Lett. **118** (2017) 237402/1-6

KTU17: E. Kukk, T. D. Thomas, K. Ueda, D. Céolin, S. Granroth, K. Kooser, O. Travnikova, D. Iablonsky, P. Decleva, D. Ayuso, R. Püttner, H. Levola, G. Goldsztejn, T. Marchenko, M. N. Piancastelli, and M. Simon; Photoelectron recoil in CO in the x-ray region up to 7 keV; Phys. Rev. A **95** (2017) 042509/1-12

KUP17: K. Kato, N. Umemura, and V. Petrov; Sellmeier and thermo-optic dispersion formulas for $CdGa_2S_4$ and their application to the nonlinear optics of $Hg_{1-x}Cd_xGa_2S_4$; Opt. Commun. **386** (2017) 49-52

KWB17: H. Kissel, P. Wolf, A. Bachmann, C. Lauer, H. Koenig, J. W. Tomm, B. Koehler, U. Strauß, and J. Biesenbach; Tailored bars at 976 nm for high-brightness fiber-coupled modules; SPIE Proc. **10086** (2017) 100860B/1-12

KWN17: C. v. Korff Schmising, D. Weder, T. Noll, B. Pfau, M. Hennecke, C. Strüber, I. Radu, M. Schneider, S. Staeck, C. M. Günther, J. Lüning, A. el dine Merhe, J. Buck, G. Hartmann, J. Viefhaus, R. Treusch, and S. Eisebitt; Generating circularly polarized radiation in the extreme ultraviolet spectral range at the free-electron laser FLASH; Rev. Sci. Instrum. **88** (2017) 053903 /1-8

LAH17: A. Lübcke, A. A. Andreev, S. Höhm, R. Grunwald, L. Ehrentraut, and M. Schnürer; Prospects of target nanostructuring for laser proton acceleration; Sci. Rep. **7** (2017) 44030/1-8

LAn17: Z. Lecz and A. A. Andreev; Bright synchrotron radiation from nano-forest targets Phys. Plasmas **24** (2017) 033113/1-7

LBB17: P. Loiko, P. Becker, L. Bohaty, C. Liebald, M. Peltz, S. Vernay, D. Rytz, J. M. Serres, X. Mateos, Y. Wang, X. Xu, J. Xu, A. Major, A. Baranov, U. Griebner, and V. Petrov; Sellmeier equations, group velocity dispersion, and thermo-optic dispersion formulas for $CaLnAlO_4$ (Ln=Y, Gd) laser host crystals; Opt. Lett. **42** (2017) 2275-2278

LEH17a: D. Laage, T. Elsaesser, and J. T. Hynes; Water dynamics in the hydration shells of biomolecules; Chem. Rev. **117** (2017) 10694-10725

LEH17b: D. Laage, T. Elsaesser, and J. T. Hynes; Perspective: Structure and ultrafast dynamics of biomolecular hydration shells; Struct. Dyn. **4** (2017) 044018/1-14

LFD17: J. Long, F. Furch, J. Durá Diez, A. S. Tremsin, J. Vallerga, C. P. Schulz, A. Rouzée, and M. J. J. Vrakking; Ion-ion coincidence imaging at high event rate using an in-vacuum pixel detector; J. Chem. Phys. **147** (2017) 013919/1-10

LGS17: Y. Liu, B. Guchhait, T. Siebert, B. P. Fingerhut, and T. Elsaesser; Molecular couplings and energy exchange between DNA and water mapped by femtosecond infrared spectroscopy of backbone vibrations; Struct. Dyn. **4** (2017) 044015/1-15

LHL17: C. Laulhé, T. Huber, G. Lantz, A. Ferrer, S. O. Mariager, S. Grübel, J. Rittmann, J. A. Johnson, V. Esposito, A. Lübcke, L. Huber, M. Kubli, M. Savoini, V. L. R. Jacques, L. Cario, B. Corraze, E. Janod, G. Ingold, P. Beaud, S. L. Johnson, and S. Ravy; Ultrafast formation of a charge density wave state in 1T−TaS_2: observation at nanometer scales using time-resolved x-ray diffraction; Phys. Rev. Lett. **118** (2017) 247401/1-6

LLZ17: J. Lu, H. Lin, G. Zhang, B. Li, L. Zhang, Z. Lin, Y.-F. Chen, V. Petrov, and W. Chen; Direct generation of an optical vortex beam from a diode-pumped Yb:$MgWO_4$ laser; Laser Phys. Lett. **14** (2017) 085807/1-6

LMC17: P. Loiko, X. Mateos, S. Y. Choi, F. Rotermund, C. Liebald, M. Peltz, S. Vernay, D. Rytz, Y. Wang, M. Kemnitzer, A. Agnesi, E. Vilejshikova, K. Yumashev, U. Griebner, and V. Petrov; Tm:$CaGdAlO_4$: Spectroscopy, microchip laser and passive Q-switching by carbon nanostructures; SPIE Proc. **10082** (2017) 1008228/1-6

LMW17: R. Lan, X. Mateos, Y. Wang, J. M. Serres, P. Loiko, J. Li, Y. Pan, U. Griebner, and V. Petrov; Semiconductor saturable absorber Q-switching of a holmium micro-laser; Opt. Express **25** (2017) 4579-4584

LSE17: A. Lübcke, M. Schnürer, L. Ehrentraut, R. Wehner, R. Grunwald, E. McGlynn, D. Byrne, and S. Lowry; Interaction of ultrafast laser pulses with nanostructure surfaces; in *Reference Module in Chemistry, Molecular Sciences and Chemical Engineering* online (Elsevier, 2017), http://dx.doi.org/10.1016/B978-0-12-409547-2.14042-9

LSM17a: P. Loiko, J. M. Serres, X. Mateos, M. Aguiló, F. Díaz, L. Zhang, Z. Lin, H. Lin, G. Zhang, K. Yumashev, V. Petrov, U. Griebner, Y. Wang, S. Y. Choi, F. Rotermund, and W. Chen; Monoclinic Tm^{3+}:$MgWO_4$: a promising crystal for continuous-wave and passively Q-switched lasers at ~2 μm; Opt. Lett. **42** (2017) 1177-1180

LSM17b: P. Loiko, J. M. Serres, X. Mateos, S. Tacchini, M. Tonelli, S. Veronesi, D. Parisi, A. D. Lieto, K. Yumashev, U. Griebner, and V. Petrov; Comparative spectroscopic and thermo-optic study of Tm:$LiLnF_4$ (Ln = Y, Gd, and Lu) crystals for highly-efficient microchip lasers at ~2 μm; Opt. Mater. Express **7** (2017) 844-854

LSM17c: P. Loiko, J. M. Serres, X. Mateos, X. Xu, J. Xu, V. Jambunathan, P. Navratil, A. Lucianetti, T. Mocek, X. Zhang, U. Griebner, V. Petrov, M. Aguiló, F. Diaz, and A. Major; Microchip Yb:$CaLnAlO_4$ lasers with up to 91% slope efficiency; Opt. Lett. **42** (2017) 2431-2434

LSM17d: P. Loiko, J. M. Serres, X. Mateos, X. Xu, J. Xu, K. Yumashev, U. Griebner, V. Petrov, M. Aguiló, F. Díaz, and A. Major; Highly-efficient multi-watt Yb:$CaLnAlO_4$ microchip lasers; SPIE Proc. **10082** (2017) 1008215/1-7

LSM17e: P. Loiko, J. M. Serres, X. Mateos, H. Yu, H. Zhang, J. Liu, K. Yumashev, U. Griebner, V. Petrov, M. Aguiló, and F. Diaz; Q-switching of ytterbium lasers by a graphene saturable absorber; in *Nano-Optics: Principles Enabling Basic Research and Applications*, B. D. Bartolo, J. Collins, and L. Silvestri eds. (Springer Science+Business Media Dordrecht, 2017) 533-535

LTB17: M. Liebmann, A. Treffer, M. Bock, T. Elsaesser, and R. Grunwald; Spectral anomalies and Gouy rotation around the singularity of ultrashort vortex pulses; Opt. Express **25** (2017) 26076-26088

LZW17: R. Lan, F. Zhang, Z. Wang, W. Xiong, H. Yuan, and T. Feng; Efficient near-infrared, multiwavelengths $PbWO_4$ Raman laser; Opt. Eng. **56** (2017) 096112/1-5

LZZ17a: H. Lin, G. Zhang, L. Zhang, Z. Lin, F. Pirzio, A. Agnesi, V. Petrov, and W. Chen; Continuous-wave and SESAM mode-locked femtosecond operation of a Yb:$MgWO_4$ laser; Opt. Express **25** (2017) 11827-11832

LZZ17b: H. Lin, G. Zhang, L. Zhang, Z. Lin, F. Pirzio, A. Agnesi, V. Petrov, and W. Chen; SESAM mode-locked Yb:GdYCOB femtosecond laser; Opt. Mater. Express **7** (2017) 3791-3795

MAK17: S. K. Mishra, A. Andreev, and M. P. Kalashnikov; Reflection of few cycle laser pulses from an inhomogeneous overdense plasma; Opt. Express **25** (2017) 11637-11651

MBC17: R. Morales, M. D. Barriga-Carrasco, and D. Casas; Instantaneous charge state of uranium projectiles in fully ionized plasmas from energy loss experiments; Phys. Plasmas **24** (2017) 042703/1-11

MBP17: L. Medišauskas, R. Bello, A. Palacios, A. González-Castrillo, F. Morales, L. Plimak, O. Smirnova, F. Martin, and M. Ivanov; A molecular clock for autoionization decay; J. Phys. B **50** (2017) 144001/1-8

MGJ17: T. Marchenko, G. Goldsztejn, K. Jänkälä, O. Travnikova, L. Journel, R. Guillemin, N. Sisourat, D. Céolin, M. Žitnik, M. Kavčič, K. Bučar, A. Mihelič, B. Cunha de Miranda, I. Ismail, A. F. Lago, F. Gel'mukhanov, R. Püttner, M. N. Piancastelli, and M. Simon; Potential energy surface reconstruction and lifetime determination of molecular double-core-hole states in the hard x-ray regime; Phys. Rev. Lett. **119** (2017) 133001/1-6

Mil17a: D. B. Milošević; Spin-dependent effects in high-order above-threshold ionization: spin-orbit interaction and exchange effects; J. Phys. B **50** (2017) 164003/1-10

Mil17b: D. B. Milošević; Semiclassical approximation for strong-laser-field processes; Phys. Rev. A **96** (2017) 023413/1-17

MJW17: I. Mantouvalou, A. Jonas, K. Witte, R. Jung, H. Stiel, and B. Kanngießer; Optimizing soft x-ray NEXAFS spectroscopy in the laboratory; SPIE Proc. **10243** (2017) 1024308/1-8

MLC17: X. Mateos, P. Loiko, S. Y. Choi, F. Rotermund, M. Aguiló, F. Díaz, U. Griebner, and V. Petrov; Single-walled carbon nanotubes oust graphene and semiconductor saturable absorbers in Q-switched solid-state lasers at 2 µm; Laser Phys. Lett. **14** (2017) 095801/1-7

MLS17a: X. Mateos, S. Lamrini, K. Scholle, P. Fuhrberg, S. Vatnik, P. Loiko, I. Vedin, M. Aguiló, F. Díaz, U. Griebner, and V. Petrov; Holmium thin-disk laser based on Ho:$KY(WO_4)_2$/$KY(WO_4)_2$ epitaxy with 60% slope efficiency and simplified pump geometry; Opt. Lett. **42** (2017) 3490-3493

MLS17b: X. Mateos, P. Loiko, J. M. Serres, K. Yumashev, U. Griebner, V. Petrov, M. Aguiló, and F. Díaz; Efficient micro-lasers based on highly doped monoclinic double tungstates; IEEE J. Quantum Electron. **53** (2017) 1700110/1-10

MPe17: M. Mero and V. Petrov; High-power, few-cycle, angular dispersion compensated mid-infrared pulses from a noncollinear optical parametric amplifier; IEEE Photonics J. **9** (2017) 3200408/1-8

MPK17: K. Miyata, V. Petrov, and K. Kato; Phase-matching properties of $LiGaSe_2$ for SHG and SFG in the 1.026-10.5910 µm range; Appl. Opt. **56** (2017) 6126-6129

MSL17: X. Mateos, J. M. Serres, P. Loiko, K. Yumashev, U. Griebner, V. Petrov, M. Aguiló, and F. Díaz; Spectroscopy and laser operation of Indium-modified Yb:KLuW: A promising crystal for femtosecond lasers; SPIE Proc. **10082** (2017) 1008214/1-6

MVH17: G. Mura, M. Vanzi, M. Hempel, and J. W. Tomm; Analysis of GaN based high-power diode lasers after singular degradation events; Phys. Status Solidi-R **11** (2017) 1700132/1-6

NCP17: R. S. Nagymihaly, H. Cao, D. Papp, G. Hajas, M. P. Kalashnikov, K. Osvay, and V. Chvykov; Liquid-cooled Ti:Sapphire thin disk amplifiers for high average power 100-TW systems; Opt. Express **25** (2017) 6664-6677

NJD17: P. Navratil, V. Jambunathan, S. P. David, F. Yue, J. M. Serres, X. Mateos, M. Aguiló, F. Diaz, U. Griebner, V. Petrov, A. Lucianetti, and T. Mocek; Continuous-wave and passively Q-switched cryogenic Yb:$KLu(WO_4)_2$ laser; Opt. Express **25** (2017) 25886-25893

ODF17: E. Oks, E. Dalimier, A. Y. Faenov, P. Angelo, S. A. Pikuz Jr., E. Tubman, N. M. H. Butler, R. J. Dance, T. A. Pikuz, I. Y. Skobelev, M. A. Alkhimova, N. Booth, J. Green, C. Gregory, A. A. Andreev, A. Zhidkov, R. Kodama, P. McKenna, and N. Woolsey; Using x-ray spectroscopy of relativistic laser plasma interaction to reveal parametric decay instabilities: a modeling tool for astrophysics; Opt. Express **25** (2017) 1958-1972

OHB17: S. Odžak, E. Hasović, W. Becker, and D. B. Milošević; Atomic processes in bicircular fields; J. Mod. Opt. **64** (2017) 971-980

OSM17a: A. F. Ordóñez-Lasso, J. L. Sanz-Vicario, and F. Martín; Effect of potential screening on the H_2 autoionizing states; Phys. Rev. A **96** (2017) 052503/1-13

OSM17b: T. Oelze, B. Schütte, M. Müller, J. P. Müller, M. Wieland, U. Frühling, M. Drescher, A. Al-Shemmary, T. Golz, N. Stojanovic, and M. Krikunova; Correlated electronic decay in expanding clusters triggered by intense XUV pulses from a free-electron laser; Sci. Rep. **7** (2017) 40736/1-8

PAB17: A. V. Pakhomov, R. M. Arkhipov, I. V. Babushkin, M. V. Arkhipov, Y. A. Tolmachev, and N. N. Rosanov; All-optical control of unipolar pulse generation in a resonant medium with nonlinear field coupling; Phys. Rev. A **95** (2017) 013804/1-8

PBK17: V. Petrov, A. A. Boyko, N. Y. Kostyukova, G. M. Marchev, V. Pasiskevicius, D. B. Kolker, V. Badikov, D. Badikov, G. Shevyrdyaeva, A. Zukauskas, and V. Panyutin; Frequency down-conversion of 1 µm laser radiation to the mid-IR using non-oxide nonlinear crystals in a cascaded intracavity configuration; SPIE Proc. **10088** (2017) 1008810/1-11

Pet17: V. Petrov; New applications of chalcopyrite crystals in nonlinear optics; phys. status solidi c **14** (2017) 1600161/1-9

PGH17: B. Pfau, C. M. Günther, T. Hauet, S. Eisebitt, and O. Hellwig; Thermally induced magnetic switching in bit-patterned media; J. Appl. Phys. **122** (2017) 043907/1-6

PJi17: E. Pisanty and Á. Jiménez Galán; Strong-field approximation in a rotating frame: High-order harmonic emission from p states in bicircular fields; Phys. Rev. A **96** (2017) 063401/1-18

PJK17: R. Puettner, K. Jankala, R. K. Kushawaha, T. Marchenko, G. Goldsztejn, O. Travnikova, R. Guillemin, L. Journel, I. Ismail, B. C. de Miranda, A. F. Lago, D. Ceolin, M. N. Piancastelli, and M. Simon; Detailed assignment of normal and resonant Auger spectra of Xe near the L edges; Phys. Rev. A **96** (2017) 022501/1-13

PSc17: S. Patchkovskii and M. S. Schuurman; Full-dimensional treatment of short-time vibronic dynamics in a molecular high-order-harmonic-generation process in methane; Phys. Rev. A **96** (2017) 053405/1-18

PVB17: C. Peltz, C. Varin, T. Brabec, and T. Fennel; Microscopic particle-in-cell approach; in *Computational Strong-Field Quantum Dynamics*, Dieter Bauer ed. (De Gruyter Textbook, 2017) 227-270

PZI17: J. Passig, S. Zherebtsov, R. Irsig, M. Arbeiter, C. Peltz, S. Göde, S. Skruszewicz, K.-H. Meiwes-Broer, J. Tiggesbäumker, M. F. Kling, and T. Fennel; Nanoplasmonic electron acceleration by attosecond-controlled forward rescattering in silver clusters; Nat. Commun. **8** (2017) 1181/1-7

QHH17: W. Quan, X. L. Hao, X. Q. Hu, Y. L. Wang, R. P. Sun, Y. J. Chen, S. G. Yu, S. P. Xu, Z. L. Xiao, X. Y. Lai, X. Y. Li, W. Becker, Y. Wu, J. G. Wang, X. J. Liu, and J. Chen; Laser-induced inelastic diffraction from strong-field double ionization; Phys. Rev. Lett. **119** (2017) 243203/1-6

QHW17: W. Quan, X. L. Hao, Y. L. Wang, Y. J. Chen, S. G. Yu, S. P. Xu, Z. L. Xiao, H. P. Sun, X. Y. Lai, S. L. Hu, M. Q. Liu, Z. Shu, W. D. Li, W. Becker, X. J. Liu, and J. Chen; Quantum interference in laser-induced nonsequential double ionization; Phys. Rev. A **96** (2017) 032511/1-9

RAA17: N. N. Rosanov, M. V. Arkhipov, R. M. Arkhipov, A. V. Pakhomov, and I. V. Babushkin; On diagnostics of media using extremely short terahertz radiation pulses; Opt. Spectrosc. **123** (2017) 100-104

RCH17: A. Rudenko, J.-P. Colombier, S. Höhm, A. Rosenfeld, J. Krüger, J. Bonse, and T. E. Itina; Spontaneous periodic ordering on the surface and in the bulk of dielectrics irradiated by ultrafast laser: a shared electromagnetic origin; Sci. Rep. **7** (2017) 12306/1-14

RDB17: D. Reiche, D. A. R. Dalvit, K. Busch, and F. Intravaia; Spatial dispersion in atom-surface quantum friction; Phys. Rev. B **95** (2017) 155448/1-10

Rei17: H. R. Reiss; Physical restrictions on the choice of electromagnetic gauge and their practical consequences; J. Phys. B **50** (2017) 075003/1-8

RFi17: M. Richter and B. P. Fingerhut; Coarse-grained representation of the quasi adiabatic propagator path integral for the treatment of non-Markovian long-time bath memory; J. Chem. Phys. **146** (2017) 214101/1-13

RFM17a: N. Raabe, T. Feng, M. Merö, H. Tian, Y. Song, W. Hänsel, R. Holzwarth, A. Sell, A. Zach, and G. Steinmeyer; Hidden amplitude-phase correlations in the carrier-envelope noise of mode-locked lasers; SPIE Proc. **10089** (2017) 1008907/1-7

RFM17b: N. Raabe, T. Feng, M. Mero, H. Tian, Y. Song, W. Hänsel, R. Holzwarth, A. Sell, A. Zach, and G. Steinmeyer; Excess carrier-envelope phase noise generation in saturable absorbers; Opt. Lett. **42** (2017) 1068-1071

RFM17c: D. Rupp, T. Fennel, and T. Möller; Atomare Cluster im Fokus - Intensive Röntgenpulse enthüllen die Struktur und ultraschnelle Entwicklung einzelner Nanoteilchen; Physik Journal **11** (2017) 33-39

RFW17: N. Raabe, T. Feng, T. Witting, A. Demircan, C. Brée, and G. Steinmeyer; Role of intrapulse coherence in carrier-envelope phase stabilization; Phys. Rev. Lett. **119** (2017) 123901/1-5

RHK17: A. Rosenfeld, S. Höhm, J. Krüger, and J. Bonse; Dynamics of ultrashort double-pulse laser ablation of solid surfaces; in *Reference Module in Chemistry, Molecular Sciences and Chemical Engineering* online (Elsevier, 2017), https://doi.org/10.1016/B978-0-12-409547-2.14127-7

RML17: D. Rupp, N. Monserud, B. Langbehn, M. Sauppe, J. Zimmermann, Y. Ovcharenko, T. Möller, F. Frassetto, L. Poletto, A. Trabattoni, F. Calegari, M. Nisoli, K. Sander, C. Peltz, M. J. J. Vrakking, T. Fennel, and A. Rouzée; Coherent diffractive imaging of single helium nanodroplets with a high harmonic generation source; Nat. Commun. **8** (2017) 493/1-6

RRP17: R. Román-Ancheyta, I. Ramos-Prieto, A. Perez-Leija, K. Busch, and R. de J. León-Montiel; Dynamical Casimir effect in stochastic systems: Photon-harvesting through noise; Phys. Rev. A **96** (2017) 032501/1-6

RRT17: E. Riedle, M. K. Roos, S. Thallmair, C. F. Sailer, N. Krebs, B. P. Fingerhut, and R. de Vivie-Riedle; Ultrafast photochemistry with two product channels: Wavepacket motion through two distinct conical intersections; Chem. Phys. Lett. **683** (2017) 128-134

RSL17: P. Rupp, L. Seiffert, Q. Liu, F. Süßmann, B. Ahn, B. För, C. G. Schäfer, M. Gallei, V. Mondes, A. Kessel, S. A. Trushin, C. Graf, E. Rühl, J. Lee, M. S. Kim, D. Kim, T. Fennel, M. F. Kling, and S. Zherebtsov; Quenching of material dependence in few-cycle driven electron acceleration from nanoparticles under many-particle charge interaction; J. Mod. Opt. **64** (2017) 995-1003

RWT17: J. Rieprich, M. Winterfeldt, J. W. Tomm, R. Kernke, and P. Crump; Assessment of factors regulating the thermal lens profile and lateral brightness in high power diode lasers; SPIE Proc. **10085** (2017) 1008502/1-10

SBB17: E. Savelyev, R. Boll, C. Bomme, N. Schirmel, H. Redlin, B. Erk, S. Düsterer, E. Müller, H. Höppner, S. Toleikis, J. Müller, M. K. Czwalinna, R. Treusch, T. Kierspel, T. Mullins, S. Trippel, J. Wiese, J. Küpper, F. Brauße, F. Krecinic, A. Rouzée, P. Rudawski, P. Johnsson, K. Amini, A. Lauer, M. Burt, M. Brouard, L. Christensen, J. Thøgersen, H. Stapelfeldt, N. Berrah, M. Müller, A. Ulmer, S. Techert, A. Rudenko, and D. Rolles; Jitter-correction for IR/UV-XUV pump-probe experiments at the FLASH free-electron laser; New J. Phys. **19** (2017) 043009/1-13

SBD17: H. Stiel, J. Braenzel, A. Dehlinger, R. Jung, A. Lübcke, M. Regehly, S. Ritter, J. Tümmler, M. Schnürer, and C. Seim; Soft x-ray nanoscale imaging using highly brilliant laboratory sources and new detector concepts; SPIE Proc. **10243** (2017) 1024309/1-10

SBG17: J. Sánchez-Barriga, M. Battiato, E. Golias, A. Varykhalov, L. V. Yashina, O. Kornilov, and O. Rader; Laser-induced persistent photovoltage on the surface of a ternary topological insulator at room temperature; Appl. Phys. Lett. **110** (2017) 141605/1-5

SBK17: J. Sánchez-Barriga, M. Battiato, M. Krivenkov, E. Golias, A. Varykhalov, A. Romualdi, L. V. Yashina, J. Minár, O. Kornilov, H. Ebert, K. Held, and J. Braun; Subpicosecond spin dynamics of excited states in the topological insulator Bi_2Te_3; Phys. Rev. B **95** (2017) 125405/1-10

SBS17: S. Sharif, J. Braenzel, M. Schnürer, R. Prasad, M. Borghesi, V. Tikhonchuk, and S. Ter-Avetisyan; Gated ion spectrometer for spectroscopy of neutral particles; Rev. Sci. Instrum. **88** (2017) 083303/1-7

Sch17: B. Schütte; Tracing Nonlinear Cluster Dynamics Induced by Intense XUV, NIR and MIR Laser Pulses; in *Progress in Ultrafast Intense Laser Science XIII* (Springer, Cham, 2017) 85-110

SDe17: G. Steinmeyer and A. Demircan; Are rogue waves really rogue?; in *Nonlinear Guided Wave Optics*, S. Wabnitz ed. (IOP Publishing, Bristol, UK, 2017) 11/1-18

SFC17: L. Seiffert, T. Fennel, F. Calegari, and M. F. Kling; Attosekunden-Stoppuhr für inelastische Elektronenstöße; Physik in unserer Zeit **48** (2017) 217-218

SGK17: D. Sofikitis, P. Glodic, G. Koumarianou, H. Jiang, L. Bougas, P. C. Samartzis, A. A. Andreev, and T. P. Rakitzis; Highly nuclear-spin-polarized deuterium atoms from the UV photodissociation of deuterium iodide; Phys. Rev. Lett. **118** (2017) 233401/1-5

SHR17: L. Seiffert, P. Henning, P. Rupp, S. Zherebtsov, P. Hommelhoff, M. F. Kling, and T. Fennel; Trapping field assisted backscattering in strong-field photoemission from dielectric nanospheres; J. Mod. Opt. **64** (2017) 1096-1103

SIN17: L. Shi, B. Iwan, R. Nicolas, Q. Ripault, J. R. C. Andrade, S. Han, H. Kim, W. Boutu, D. Franz, T. Heidenblut, C. Reinhardt, B. Bastiaens, T. Nagy, I. Babushkin, U. Morgner, S.-W. Kim, G. Steinmeyer, H. Merdji, and M. Kovacev; Self-optimization of plasmonic nanoantennas in strong femtosecond fields; Optica **4** (2017) 1038-1043

SKP17: L. Seiffert, J. Köhn, C. Peltz, M. F. Kling, and T. Fennel; Signatures and mechanisms of plasmon-enhanced electron emission from clusters in few-cycle laser fields; J. Phys. B **50** (2017) 224001/1-8

SLM17: J. M. Serres, P. Loiko, X. Mateos, J. Liu, H. Zhang, K. Yumashev, U. Griebner, V. Petrov, M. Aguiló, and F. Díaz; Multi-watt passively Q-switched Yb:YAB/Cr:YAG microchip lasers; SPIE Proc. **10082** (2017) 100820T/1-6

SLR17: A. S. Stodolna, F. Lépine, A. Rouzée, S. Cohen, A. Gijsbertsen, J. H. Jungmann-Smith, C. Bordas, and M. J. J. Vrakking; Interference-encoded photoionization time delays in the hydrogen atom; J. Phys. B **50** (2017) 164001/1-7

SLZ17: L. Seiffert, Q. Liu, S. Zherebtsov, A. Trabattoni, P. Rupp, M. C. Castrovilli, M. Galli, F. Süßmann, K. Wintersperger, J. Stierle, G. Sansone, L. Poletto, F. Frassetto, I. Halfpap, V. Mondes, C. Graf, E. Rühl, F. Krausz, M. Nisoli, T. Fennel, F. Calegari, and M. F. Kling; Attosecond chronoscopy of electron scattering in dielectric nanoparticles; Nat. Phys. **13** (2017) 766-770

SMG17a: T. Seuthe, A. Mermillod-Blondin, M. Grehn, J. Bonse, L. Wondraczek, and M. Eberstein; Structural relaxation phenomena in silicate glasses modified by irradiation with femtosecond laser pulses; Sci. Rep. **7** (2017) 43815/1-10

SMG17b: T. Seifert, U. Martens, S. Günther, M. A. W. Schoen, F. Radu, X. Z. Chen, I. Lucas, R. Ramos, M. H. Aguirre, P. A. Algarabel, A. Anadón, H. S. Körner, J. Walowski, C. Back, M. R. Ibarra, L. Morellón, E. Saitoh, M. Wolf, C. Song, K. Uchida, M. Münzenberg, I. Radu, and T. Kampfrath; Terahertz spin currents and inverse spin Hall effect in thin-film heterostructures containing complex magnetic compounds; SPIN **7** (2017) 1740010/1-11

SML17: J. M. Serres, X. Mateos, P. Loiko, U. Griebner, V. Petrov, K. Yumashev, M. Aguiló, and F. Díaz; Indium-modified Yb:KLu$(WO_4)_2$ crystal: Growth, spectroscopy and laser operation; J. Lumines. **183** (2017) 391-400

SPB17: J. Sperling, A. Perez-Leija, K. Busch, and I. A. Walmsley; Quantum coherences of indistinguishable particles; Phys. Rev. A **96** (2017) 032334/1-11

SPP17: D. E. Shipilo, D. V. Pushkarev, N. A. Panov, D. S. Uryupina, V. A. Andreeva, R. V. Volkov, A. V. Balakin, A. P. Shkurinov, I. Babushkin, U. Morgner, O. G. Kosareva, and A. B. Savel'ev; Near-infrared conical emission from 800 nm filament in air; Laser Phys. Lett. **14** (2017) 035401/1-6

SRW17: C. Somma, K. Reimann, M. Woerner, T. Kiel, K. Busch, A. Braun, M. Matalla, K. Ickert, and O. Krueger; Mid-infrared beam splitter for ultrashort pulses; Opt. Lett. **52** (2017) 2918-2921

SVR17: B. Schütte, M. J. J. Vrakking, and A. Rouzée; Tracing transient charges in expanding clusters; Phys. Rev. A **95** (2017) 063417/1-5

SWV17: K. J. Schafer, Z. Wie, and M. J. J. Vrakking; Editorial: Special issue celebrating 25 years of re-collision physics; J. Phys. B **50** (2017) 170201/1-2

TBW17: A. Treffer, M. Bock, U. Wallrabe, and R. Grunwald; Array-specific propagation effects of flexibly structured ultrashort pulses; SPIE Proc. **10120** (2017) 01200S/1-8

TCG17: T. Takanashi, N. V. Golubev, C. Callegari, H. Fukuzawa, K. Motomura, D. Iablonskyi, Y. Kumagai, S. Mondal, T. Tachibana, K. Nagaya, T. Nishiyama, K. Matsunami, P. Johnsson, P. Piseri, G. Sansone, A. Dubrouil, M. Reduzzi, P. Carpeggiani, C. Vozzi, M. Devetta, M. Negro, D. Faccialà, F. Calegari, A. Trabattoni, M. C. Castrovilli, Y. Ovcharenko, M. Mudrich, F. Stienkemeier, M. Coreno, M. Alagia, B. Schütte, N. Berrah, O. Plekan, P. Finetti, C. Spezzani, E. Ferrari, E. Allaria, G. Penco, C. Serpico, G. D. Ninno, B. Diviacco, S. D. Mitri, L. Giannessi, G. Jabbari, K. C. Prince, L. S. Cederbaum, P. V. Demekhin, A. I. Kuleff, and K. Ueda; Time-resolved measurement of interatomic Coulombic decay induced by two-photon double excitation of Ne_2; Phys. Rev. Lett. **118** (2017) 033202/1-6

TSm17: L. Torlina and O. Smirnova; Coulomb time delays in high harmonic generation; New J. Phys. **19** (2017) 023012/1-13

VHV17: D. M. Villeneuve, P. Hockett, M. J. J. Vrakking, and H. Niikura; Coherent imaging of an attosecond electron wave packet; Science **365** (2017) 1150-1153

WCM17: Y. Wang, W. Chen, M. Mero, L. Zhang, H. Lin, Z. Lin, G. Zhang, F. Rotermund, Y. J. Cho, P. Loiko, X. Mateos, U. Griebner, and V. Petrov; Sub-100 fs Tm:$MgWO_4$ laser at 2017 nm mode locked by a graphene saturable absorber; Opt. Lett. **42** (2017) 3076-3079

WKI17: T. Weber, T. Kiel, S. Irsen, K. Busch, and S. Linden; Near-field study on the transition from localized to propagating plasmons on 2D nano-triangles; Opt. Express **25** (2017) 16947-16956

WKW17a: F. Willems, C. v. Korff Schmising, D. Weder, C. M. Günther, M. Schneider, B. Pfau, S. Meise, E. Guehrs, J. Geilhufe, A. el dine Merhe, E. Jal, B. Vodungbo, J. Lüning, B. Mahieu, F. Capotondi, E. Pedersoli, D. Gauthier, M. Manfredda, and S. Eisebitt; Multi-color imaging of magnetic Co/Pt heterostructures; Struct. Dyn. **4** (2017) 014301/1-13

WKW17b: D. Weder, C. v. Korff Schmising, F. Willems, C. M. Günther, M. Schneider, B. Pfau, A. Merhe, E. Jal, B. Vodungbo, J. Lüning, B. Mahieu, F. Capotondi, E. Pedersoli, and S. Eisebitt; Multi-color imaging of magnetic Co/Pt multilayers; IEEE Trans. Magn. **53** (2017) 6500905/1-5

WLM17: Y. Wang, R. Lan, X. Mateos, J. Li, C. Li, S. Suomalainen, A. Härkönen, M. Guina, V. Petrov, and U. Griebner; Thulium doped LuAG ceramics for passively mode locked lasers; Opt. Express **25** (2017) 7084-7091

WRE17: M. Woerner, K. Reimann, and T. Elsaesser; in *Reference Module in Materials Science and Materials Engineering*: Multidimensional Terahertz Spectroscopy online (Elsevier, 2017), https://www.sciencedirect.com/science/article/pii/B9780128035818095291

WRW17a: J. Weisshaupt, A. Rouzée, and M. Woerner; Atomschwingungen in Superzeitlupe; Physik in unserer Zeit **48** (2017) 113-114

WRW17b: J. Weisshaupt, A. Rouzée, M. Woerner, M. J. J. Vrakking, T. Elsaesser, E. L. Shirley, and A. Borgschulte; Ultrafast modulation of electronic structure by coherent phonon excitations; Phys. Rev. B (R) **95** (2017) 081101/1-5

WXC17: Y. L. Wang, S. P. Xu, Y. J. Chen, H. P. Kang, X. Y. Lai, W. Quan, X. J. Liu, X. L. Hao, W. D. Li, S. L. Hu, J. Chen, W. Becker, W. Chu, J. Yao, B. Zeng, Y. Cheng, and Z. Z. Xu; Wavelength scaling of atomic nonsequential double ionization in intense laser fields; Phys. Rev. A **95** (2017) 063415/1-7

YLG17: A. S. Yasukevich, P. Loiko, N. V. Gusakova, J. M. Serres, X. Mateos, K. V. Yumashev, N. V. Kuleshov, V. Petrov, U. Griebner, M. Aguiló, and F. Díaz; Modelling of graphene Q-switched Tm lasers; Opt. Commun. **389** (2017) 15-22

Zlv17: N. Zhavoronkov and M. Ivanov; Extended ellipticity control for attosecond pulses by high harmonic generation; Opt. Lett. **42** (2017) 4720-4723

ZJS17: M. Zürch, R. Jung, C. Späth, J. Tümmler, A. Guggenmos, D. Attwood, U. Kleineberg, H. Stiel, and C. Spielmann; Transverse coherence limited coherent diffraction imaging using a molybdenum soft x-ray laser pumped at moderate pump energies; Sci. Rep. **7** (2017) 5314/1-10

ZLM17: X. Zhang, P. Loiko, J. M. Serres, X. Mateos, J. Ren, Z. Wang, S. Guo, X. Xu, E. Vilejshikova, U. Griebner, V. Petrov, M. Aguiló, and F. Díaz; Highly-efficient laser operation of a novel trigonal silicate crystal Yb^{3+}:$Ca_3NbGa_3Si_2O_{14}$; Opt. Mater. Express **7** (2017) 3626-3633

ZLW17: Z. Zhang, P. Loiko, H. Wu, X. Mateos, J. M. Serres, H. F. Lin, W. D. Chen, G. Zhang, L. Z. Zhang, F. Diaz, M. Aguiló, V. Petrov, U. Griebner, Y. C. Wang, Z. Lin, E. Vilejshikova, K. Yumashev, and Z. B. Lin; Disordered Tm:$Ca_9La(VO_4)_7$: A novel crystal with potential for broadband tunable lasing; Opt. Mater. Express **7** (2017) 484-493

ZLZ17: L. Zhang, H. Lin, G. Zhang, X. Mateos, J. M. Serres, M. Aguiló, F. Díaz, U. Griebner, V. Petrov, Y. Wang, P. Loiko, E. Vilejshikova, K. Yumashev, Z. Lin, and W. Chen; Crystal growth, optical spectroscopy and laser action of Tm^{3+}-doped monoclinic magnesium tungstate; Opt. Express **25** (2017) 3682-3693

ZPI17: H. Zimmermann, S. Patchkovskii, M. Ivanov, and U. Eichmann; Unified time and frequency picture of ultrafast atomic excitation in strong laser fields; Phys. Rev. Lett. **118** (2017) 013003/1-5

ZSM17: D. Zille, D. Seipt, M. Möller, S. Fritzsche, G. G. Paulus, and D. B. Milošević; Spin-dependent quantum theory of high-order above-threshold ionization; Phys. Rev. A **95** (2017) 063408/1-6

in press

ADP: D. Ayuso, P. Decleva, S. Patchkovskii, and O. Smirnova; Chiral dichroism in bi-elliptical high-order harmonic generation; J. Phys. B online

BCD: S. Beaulieu, A. Comby, D. Descamps, B. Fabre, G. A. Garcia, R. Géneaux, A. G. Harvey, F. Légaré, Z. Mašín, L. Nahon, A. F. Ordonez, S. Petit, B. Pons, Y. Mairesse, O. Smirnova, and V. Blanchet; Photoexcitation circular dichroism in chiral molecules; Nat. Phys.

BSG: J. Bonse, T. Seuthe, M. Grehn, M. Eberstein, A. Rosenfeld, and A. Mermillod-Blondin; Time-resolved microscopy of fs-laser-induced heat flows in glasses; Appl. Phys. A

BSS: E. M. Bruening, J. Schauss, T. Siebert, B. Fingerhut, and T. Elsaesser; Vibrational dynamics and couplings of the hydrated RNA backbone – A 2D-IR study; J. Phys. Chem. Lett.

CKE: B.-H. Chen, M. Kretschmar, D. Ehberger, A. Blumenstein, P. Simon, P. Baum, and T. Nagy; Compression of picosecond pulses from a thin-disk laser to 30fs at 4W average power; Opt. Express

ETN: E. Escoto, A. Tajalli, T. Nagy, and G. Steinmeyer; Advanced phase retrieval for dispersion scan: a comparative study; J. Opt. Soc. Am. B

HPM: J. Hyyti, M. Perestjuk, F. Mahler, R. Grunwald, F. Güell, C. Gray, E. McGlynn, and G. Steinmeyer; Field enhancement of multiphoton induced luminescence processes in ZnO nanorods; J. Phys. D

JDP: Á. Jiménez Galán, G. Dixit, S. Patchkovskii, O. Smirnova, F. Morales, and M. Ivanov; Attosecond recorder of the polarization state of light; Nat. Commun.

JZA: Á. Jiménez Galán, N. Zhavoronkov, D. Ayuso, F. Morales, S. Patchkovskii, M. Schloz, E. Pisanty, O. Smirnova, and M. Ivanov; Control of attosecond light polarization in two-color bicircular fields; Phys. Rev. A

LGG: G. Loisch, J. Goo, M. Gross, H. Huck, I. Isaev, M. Krasilnikov, O. Lishilin, A. Oppelt, Y. Renier, F. Stephan, R. Brinkmann, F. Gruner, and I. Will; Photocathode laser based bunch shaping for high transformer ratio plasma wakefield acceleration; Nucl. Instrum. Meth. A

LSE: A. Lübcke, M. Schnürer, L. Ehrentraut, E. McGlynn, D. Byrne, S. Lowry, R. Wehner, and R. Grunwald; Interaction of ultrafast laser pulses with nanostructure surfaces; in *Encyclopedia of Interfacial Chemistry: Surface Science and Electrochemistry* (Elsevier)

MBe: D. B. Milošević and W. Becker; Channel-closing effects in strong-field ionization by a bicircular field; J. Phys. B

NSG: M. Närhi, G. Steinmeyer, and G. Genty; Effect of coherence on all-optical signal amplification by supercontinuum generation; J. Opt. Soc. Am. B

OGH: T. M. Ostermayr, J. Gebhard, D. Haffa, D. Kiefer, C. Kreuzer, K. Allinger, C. Bömer, J. Braenzel, M. Schnürer, I. Cermak, J. Schreiber, and P. Hilz; A transportable Paul-trap for levitation and accurate positioning of micron-scale particles in vacuum for laser-plasma experiments; Rev. Sci. Instrum.

PLS: A. Perez-Leija, R. de J. León-Montiel, J. Sperling, H. Moya-Cessa, A. Szameit, and K. Busch; Two-particle four-point correlations in dynamically disordered tight-binding networks; J. Phys. B

SBSa: F. Schell, T. Bredtmann, C. P. Schulz, M. J. J. Vrakking, S. Patchkovskii, and J. Mikosch; Separation of strong-field ionization continua in laser-driven electron rescattering in the molecular frame; Proceedings of the ATTO06 Conference, Springer Proceedings in Physics Series

SBSb: F. Schell, T. Bredtmann, C. P. Schulz, S. Patchkovskii, M. J. J. Vrakking, and J. Mikosch; Molecular orbital imprint in laser-driven electron recollision; Sci. Adv.

Sch: B. Schütte; Tracing nonlinear cluster dynamics induced by intense XUV, NIR and MIR laser pulses; in *Progress in Ultrafast Intense Laser Science XIII*, K. Yamanouchi, W. Hill, and G. Paulus eds. (Springer International Publishing)

SGP: M. Schneider, C. M. Günther, B. Pfau, F. Capotondi, M. Manfredda, M. Zangrando, N. Mahne, L. Raimondi, E. Pedersoli, D. Naumenko, and S. Eisebitt; In situ single-shot diffractive fluence mapping for x-ray free-electron laser pulses; Nat. Commun.

SIR: L. Shi, B. Iwan, Q. Ripault, J. R. C. Andrade, S. Han, H. Kim, W. Boutu, D. Franz, R. Nicolas, T. Heidenblut, C. Reinhardt, B. Bastiaens, T. Nagy, I. Babuskin, U. Morgner, S.-W. Kim, G. Steinmeyer, H. Merdji, and M. Kovačev; Resonant-plasmon-assisted subwavelength ablation by a femtosecond oscillator; Phys. Rev. Appl.

WFV: T. Witting, J. Furch, and M. J. J. Vrakking; Spatio-temporal characterisation of a 100 kHz 24 W sub-3-cycle NOPCPA laser system; J. Opt.

WMS: K. Witte, I. Mantouvalou, R. Sánchez-de-Armas, H. Lokstein, J. Lebendig-Kuhla, A. Jonas, F. Roth, B. Kanngießer, and H. Stiel; On the electronic structure of Cu chlorophyllin and its breakdown products: A carbon K-edge x-ray absorption spectroscopy study; J. Phys. Chem. B

WRE: M. Woerner, K. Reimann, and T. Elsaesser; Multidimensional Terahertz Spectroscopy; in *Encyclopedia of Modern Optics II* (Elsevier)

WZJ: J. Weisshaupt, F. Zamponi, V. Juvé, M. Holtz, M. Woerner, and T. Elsaesser; Femtosecond x-ray diffraction: Laser-driven hard x-ray plasma sources and methods for analyzing spatio-temporal charge dynamics in crystals; in *Tabletop Intense Femtosecond Pulse Sources and Their Applications*, A. Baltuška and G. Cerullo eds. (Springer, Heidelberg)

ZFR: C. Zhang, T. Feng, N. Raabe, and H. Rottke; Strong-field ionization of xenon dimers: The effect of two-equivalent-center-center interference and of driving ionic transitions; Phys. Rev. A

ZMK: H. Zimmermann, S. Meise, A. Khujakulov, A. Magaña, A. Saenz, and U. Eichmann; Limit on excitation and stabilization of atoms in intense optical laser fields; Phys. Rev. Lett.

submitted

BGA: F. Braußе, G. Goldsztejn, K. Amini, R. Boll, S. Bari, C. Bomme, M. Brouard, M. Burt, B. C. de Miranda, S. Düsterer, B. Erk, M. Géléoc, R. Geneaus, A. Gentleman, R. Guillemenin, I. Ismail, P. Johnsson, L. Journel, T. Kierspel, H. Köckert, J. Küpper, P. Lablamquie, J. Lahl, J. W. L. Lee, S. R. Mackenzie, S. Maclot, B. Manschwetus, A. S. Mereshchenko, T. Mullins, P. K. Olshin, J. Palaudoux, S. Patchkovskii, F. Penent, M. N. Paincastelli, D. Rompotis, T. Ruchon, A. Rudenko, E. Savelyev, N. Schirmel, S. Techert, O. Travnikosa, S. Trippel, J. G. Underwood, C. Vallence, J. Wiese, M. Simon, D. Holland, T. Marchenko, A. Rouzée, and D. Rolles; Time-resolved inner-shell photoelectron spectroscopy: from a bound molecule to an isolated atom; Phys. Rev. Lett.

BMK: E. Balogh, B. Major, K. Kovacs, S. Han, B. Schütte, P. Weber, M. J. J. Vrakking, V. Tosa, A. Rouzée, and K. Varju; Spectral shifts and asymmetries in mid-infrared assisted high-order harmonic generation, J. Opt. Soc. Am. B

EWo: T. Elsaesser and M. Woerner; Femtosecond X-ray diffraction: Nuclear motions and charge dynamics; in *Dynamic Structural Science: Monitoring Chemical and Biological Processes Across Time Domains* (Wiley Publishing)

GBG: L. v. Grafenstein, M. Bock, and U. Griebner; Bifurcation analysis in high repetition rate regenerative amplifiers; IEEE J. Sel. Top. Quant. Electron.

GBM: A. Gazibegović-Busuladžić, W. Becker, and D. B. Milošević; Helicity asymmetry in strong-field ionization of atoms by a bicircular field; New J. Phys.

HHH: C. Hauf, A. Hernandez, M. Holtz, M. Woerner, and T. Elsaesser; Soft-mode driven polarity switching in ferroelectrics mapped by ultrafast x-ray diffraction; Struct. Dyn.

HHL: S. L. Hu, X. L. Hao, H. Lu, T. X. Yang, H. F. Xu, M. X. Jin, D. J. Ding, Q. G. Li, W. D. Li, M. Q. Liu, W. Becker, and J. Chen; Quantum dynamics of atomic Rydberg excitation in an intense laser field; Phys. Rev. Lett.

KML: E. Kifle, X. Mateos, P. Loiko, S. Y. Choi, J. E. Bae, F. Rotermund, M. Aguiló, F. Díaz, U. Griebner, and V. Petrov; Tm:$KY_{1-x-y}Gd_xLu_y(WO_4)_2$ planar waveguide laser passively Q-switched by single-walled carbon nanotubes; Opt. Express

KWF: F. Krecinic, P. Wopperer, B. Frusteri, F. Braußе, J.-G. Brisset, U. D. Giovannini, A. Rubio, A. Rouzée, and M. J. J. Vrakking; Multiple orbital effects in laser-induced electron diffraction of aligned molecules; Phys. Rev. Lett.

LKM: P. Loiko, P. Koopmann, X. Mateos, J. M. Serres, V. Jambunathan, A. Lucianetti, T. Mocek, M. Aguiló, F. Diaz, U. Griebner, V. Petrov, and C. Kränkel; Highly-efficient, compact Tm^{3+}:RE_2O_3 (RE: Y, Lu, Sc) sesquioxide lasers based on thermal guiding; IEEE J. Quantum Electron.

LTB: M. Liebmann, A. Treffer, M. Bock, T. Seiler, T. Elsaesser, and R. Grunwald; Spectral anomaly of ultrashort vortex pulses with axially oscillating twist; SPIE Proc.

LWH: C.-H. Lu, T. Witting, A. Husakou, M. J. J. Vrakking, A. H. Kung, and F. J. Furch; Sub-4 fs laser pulses at high average power and high repetition rate from an all-solid-state setup; Opt. Express

MKS: M. Moeferdt, T. Kiel, T. Sproll, F. Intravaia, and K. Busch; Plasmonic modes in nanowire dimers: A study based on the hydrodynamic Drude model including nonlocal and nonlinear effects; Phys. Rev. B

MLLa: X. Mateos, P. Loiko, S. Lamrini, K. Scholle, P. Fuhrberg, S. Suomalainen, A. Härkönen, M. Guina, S. Vatnik, I. Vedin, M. Aguiló, F. Diaz, Y. Wang, U. Griebner, and V. Petrov; Ho:$KY(WO_4)_2$ thin-disk laser passively Q-switched by a GaSb-based SESAM; Opt. Express

MLLb: X. Mateos, P. Loiko, S. Lamrini, K. Scholle, P. Fuhrberg, S. Vatnik, I. Vedin, M. Aguiló, F. Díaz, U. Griebner, and V. Petrov; Thermo-optic effects in Ho:$KY(WO_4)_2$ thin-disk lasers; Opt. Mater. Express

MRM: S. F. Mährlein, I. Radu, P. Maldonado, A. Paarmann, M. Gensch, A. M. Kalashnikova, R. V. Pisarev, M. Wolf, P. M. Oppeneer, and T. Kampfrath; Ultrafast spin dynamics driven by strong phonon magnetic fields; Nature

NKS: C. Neidel, A. Kuehn, C. P. Schulz, I.V. Hertel, M.W. Linscheid, and T. Schultz; Femtosecond laser-induced dissociation (fs-LID) as an activation method in mass spectrometry; Chem. Phys.

PGL: A. Perez-Leija, D. Guzman-Silva, R. de J. León-Montiel, M. Gräfe, M. Heinrich, H. Moya-Cessa, K. Busch, and A. Szameit; Endurance of quantum coherence in Born-Markov open quantum systems; Phys. Rev. X

RWK: J. Rieprich, M. Winterfeldt, R. Kernke, J. W. Tomm, and P. Crump; Chip-carrier thermal barrier and its impact on lateral thermal lens profile and beam parameter product in high power broad area lasers; J. Appl. Phys.

SBSc: F. Schell, A. E. Boguslavskiy, C. P. Schulz, S. Patchkovskii, M. J. J. Vrakking, A. Stolow, and J. Mikosch; Sequential and direct ionic excitation in the strong-field ionization of 1-butene molecules; Phys. Chem. Chem. Phys.

SLJ: J. M. Serres, P. Loiko, V. Jambunathan, X. Mateos, V. Vitkin, A. Lucianetti, T. Mocek, M. Aguiló, F. Diaz, U. Griebner, and V. Petrov; Efficient diode-pumped Er:$KLu(WO_4)_2$ laser at ~1.61 µm; Opt. Lett.

SMS: M. P. Schneider, C. Martens, T. Sproll, and K. Busch; Decay properties of an atom coupled to a disordered waveguide; J. Opt. Soc. Am. B

TKL: J. W. Tomm, R. Kernke, A. Löffler, B. Stojetz, A. Lell, and H. König; Defect evolution during catastrophic optical damage in 450-nm emitting InGaN/GaN diode lasers; SPIE Proc.

TKM: J. W. Tomm, R. Kernke, G. Mura, M. Vanzi, M. Hempel, and B. Acklin; Catastrophic optical damage of GaN-based diode lasers: Sequence of events, damage pattern, and comparison with GaAs-based devices; J. Electron. Mater.

VGM: L. Vidas, C. M. Günther, T. A. Miller, B. Pfau, M. Schneider, E. Guehrs, R. E. Marvel, K. A. Hallman, R. F. Haglund Jr, S. Eisebitt, and S. Wall; Resonant x-ray holographic imaging of the insulator-metal phase transformation in VO_2; Nano Lett.

WWo: J. Weisshaupt and M. Woerner; Quantum theory allowing for a continuous transition from a hot classical plasma to the condensed phase of matter with quantum correlations; Struct. Dyn.

General Publications

WWK17: D. Weder, F. Willems, C. v. Korff Schmising, C. M. Günther, M. Schneider, B. Pfau, E. Gührs, J. Geilhufe, A. Merhe, E. Jal, B. Vodungbo, J. Lüning, B. Mahieu, F. Capotondi, E. Pedersoli, D. Gauthier, M. Manfredda, and S. Eisebitt; Multi-color imaging of magnetic domains in Co/Pt heterostructures; Elletra Highlights (2017) 54-55

Master and PhD theses

Master theses

Fre17: F. K. Freyse; *An electrostatic ion beam trap for structural imaging of transition state dynamics* (Supervisor: M. J. J. Vrakking and J. Mikosch), Freie Universität Berlin, 2017-06

Leb17: J. Lebendig; *Optimized sample preparation for near edge x-ray absorption fine structure spectroscopy in transmission mode* (Supervisor: B. Kanngießer and H. Stiel), Technische Universität Berlin, 2017-07

May17: N. Mayer; *Interference stabilization of complex molecular fano resonances* (Supervisor: M. Ivanov and O. Kornilov), Humboldt-Universität zu Berlin, 2017-10

Sch17: M. Schloz; *Polarization control of attosecond pulse trains by bicircular driving fields* (Supervisor: M. Ivanov and U. Eichmann), Humboldt-Universität zu Berlin, 2017-07

PhD theses

Fol17: G. Folpini; *Exploring nonresonant interactions in condensed matter by two-dimensional terahertz spectroscopy* (Supervisor: T. Elsaesser), Humboldt-Universität zu Berlin, 2017-12

Kos17: C. Koschitzki; *Injection mechanism in laser wakefield acceleration* (Supervisor: A. Jankowiak), Humboldt-Universität zu Berlin, 2017-03

Kre17: F. Krecinic; *Ultrafast electron diffraction and imaging using ionized electrons* (Supervisor: A. Rouzée and M. J. J. Vrakking), Freie Universität Berlin, 2017-06

Liu17: Y. Liu; *Structural dynamics of DNA hydration shell studied by 2D IR and pump-probe technique* (Supervisor: K. Rademann and T. Elsaesser), Humboldt-Universität zu Berlin Berlin, 2017-07

Nei17: C. Neidel; *Attosecond time-resolved experiments - towards biomolecules* (Supervisor: M. J. J. Vrakking and Th. Schultz), Freie Universität Berlin, 2017-06

Ser17: V. Serbinenko; *Multidimensional high harmonic spectroscopy* (Supervisor: O. Smirnova and A. Knorr), Technische Universität Berlin, 2017-07

Som17: C. Somma; *Coherent multidimensional off-resonant THz spectroscopy on semiconductors* (Supervisor: T. Elsaesser), Humboldt-Universität zu Berlin, 2017-06

Wan17: Y. Wang; *Passive mode-locking of 2 µm solid-state lasers: towards sub-10 optical cycle pulse generation* (Supervisor: M. J. J. Vrakking), Freie Universität Berlin, 2017-11

Wit17: K. Witte; *Einzelschuss Röntgenabsorptionsspektroskopie an organischen Molekülen* (Supervisor: B. Kanngießer and H. Stiel), Technische Universität Berlin, 2017-05

Appendix 2

External Talks, Teaching

Invited talks at conferences

A. A. Andreev; 2nd EMP Working Day (Warsaw, Poland, 2017-01): *Generation of extreme currents and quasi-static fields at an interaction of relativistic intense laser pulses with nanostructure targets*

A. A. Andreev; Global Summit on Laser Optics & Photonics (Valencia, Spain, 2017-06*): Relativistic laser nano-plasma photonics*

D. Ayuso; Annual Meeting Quantum Dynamics in Tailored Intense Fields, QUTIF (Dresden, Germany, 2017-02): *Attosecond control of spin polarization in electron-ion recollision driven by intense tailored fields*

W. Becker *together with* S. Kelvich, and S. P. Goreslavski; 26th Annual Int. Laser Physics Workshop, LPHYS'17 (Kazan, Russia, 2017-07): *The low-energy structure in above-threshold ionization as a catastrophe*

J. Braenzel; 3rd Targetry for High Repetition Rate Laser-Driven Sources, Targ3 (Salamanca, Spain, 2017-06): *Targetry for high repetition rate laser-driven sources*

K. Busch; 2nd Int. SFB/TRR 142 Workshop on Tailored Nonlinear Photonics (Paderborn, Germany, 2017-02): *Discontinuous Galerkin methods in nano-photonics*

K. Busch; SPIE Optics + Optoelectronics (Prague, Czech Republic, 2017-04): *Light-matter interaction in planar plasmonic and metamaterial systems: Equilibrium and non-equilibrium effects*

K. Busch; CLEO Europe-EQEC 2017 (Munich, Germany, 2017-06): *Discontinuous Galerkin methods in nano-photonics*

K. Busch; PIERS 2017, Keynote Talk in the Focus Session "Electromagnetic Waves in Complex Nanostructures" (Singapore, 2017-11): *Equilibrium and non-equilibrium atom-surface interactions: Material models and computations*

U. Eichmann; Intense Field, Short Wavelength Atomic and Molecular Processes, ISWAMP, ICPEAC Satellite Meeting (Brisbane, Australia, 2017-07*): Atomic strong-field excitation from low to high frequency fields*

S. Eisebitt; 633. WE-Heraeus-Seminar: Spin-Orbit Dynamics – Connecting Timescales from Nanoseconds to Femtoseconds (Physikzentrum Bad Honnef, Germany, 2017-01): *Manipulating magnetization with pulses of light*

S. Eisebitt; Workshop on Timing Experiments at PETRA IV (DESY Hamburg, Germany, 2017-03*): Pump-probe holographic imaging with X-rays*

S. Eisebitt; Workshop on Timing Experiments at PETRA IV (DESY Hamburg, Germany, 2017-03): *New science opportunities with coherent soft X-rays at PETRA IV*

S. Eisebitt; Photonics Spring Workshop (Paul Scherrer Institute, FHNW University of Applied Sciences and Arts Northwestern Switzerland, Brugg-Windisch, Switzerland, 2017-03): *Fast and ultrafast magnetic phenomena*

S. Eisebitt; The European Conference PHYSICS OF MAGNETISM 2017, PM'17 (Poznań, Poland, 2017-06): *Field-free deterministic creation and inertial properties of single skyrmions*

S. Eisebitt; 2nd Int. Workshop on Novel Trends in Physics of Ferroics, NTPF 2017 (St. Petersburg, Russia, 2017-07): *Field-free deterministic creation and inertial properties of single skyrmions*

S. Eisebitt; Moscow Int. Symposium on Magnetism (MISM-2017) (Moscow, Russia, 2017-07): *Manipulating magnetization with pulses of light*

S. Eisebitt; Workshop on Opportunities for Soft X-ray Science at PETRA IV (DESY, Hamburg, 2017-09): *New science opportunities with coherent soft X-rays at PETRA IV*

T. Elsaesser; APS March Meeting 2017 (New Orleans, LA, USA, 2017-03): *Phase-resolved two-dimensional terahertz spectroscopy – A probe of highly nonlinear light-matter interactions*

T. Elsaesser, Kick-off and Laser Materials Meeting (Berlin, Germany, 2017-04): *Solid-state laser drivers for generating ultrashort X-ray pulses*

T. Elsaesser; Terametanano II (Venice, Italy 2017-05): *Charge transport and soft-mode excitations in correlated materials mapped by nonlinear terahertz spectroscopy*

T. Elsaesser; Conference on Time-Resolved Vibrational Spectroscopy, TRVS 2017 (Cambridge, UK, 2017-07): *The hydrated excess proton in polar solvents studied by ultrafast infrared spectroscopy*

T. Elsaesser; XXXII Int. Union of Radio Science General Assembly & Scientific Symposium (Montreal, Canada, 2017-08): *Local field effects and coherent charge dynamics in dielectrics driven by ultrashort electric field transients*

T. Elsaesser; Fachtagung Prozessnahe Röntgenanalytik, PRORA (Berlin, Germany, 2017-12): *Neue Laborquellen für ultrakurze harte Röntgenimpulse und Anwendungen in der Festkörperphysik*

T. Fennel; Annual Meeting Quantum Dynamics in Tailored Intense Fields, QUTIF (Dresden, Germany, 2017-02): *Controlling photoemission with tailored near-fields*

T. Fennel; DPG Spring Meeting (Dresden, Germany, 2017-03): *Intense laser-cluster interactions: nanoscale plasmas in motion* (plenary talk)

B. P. Fingerhut; 5th Molcas Developers' Workshop (Jerusalem, Israel, 2017-02): *Scientific perspective talk: Nonadiabatic processes in molecules monitored with coherent ultrafast nonlinear spectroscopic techniques*

B. P. Fingerhut; 11th Triennial Congress of the World Association of Theoretical and Computational Chemists (Munich, Germany, 2017-08): *Numerical exact MACGIC-QUAPI simulations of electron transfer dynamics in Drosophila cryptochrome (dCRY)*

B. P. Fingerhut; FEMTO'13 (Cancun, Mexico, 2017-08): *The hydrated excess proton - ultrafast vibrational dynamics of the Zundel cation* $(H_5O_2)^+$

B. P. Fingerhut; TRSC Vibrational Dynamics 2017 (Telluride, CO, USA, 2017-08): *Large-amplitude transfer motion of hydrated excess protons mapped by ultrafast 2D-IR spectroscopy*

U. Griebner *together with* L. v. Grafenstein, M. Bock, and T. Elsaesser; OSA Laser Congress 2017 (Nagoya, Aichi, Japan, 2017-10): *High-energy femtosecond mid-IR OPCPA at kHz repetition rates*

F. Intravaia; META 2017 (Seoul, South Korea, 2017-07): *Tailoring fluctuation-induced interactions with nanostructures*

F. Intravaia, Workshop on Dispersion Forces and Dissipation (Leipzig, Germany, 2017-11): *Thermodynamics of overdamped electromagnetic modes*

M. Ivanov *together with* T. Bredtmann, F. Morales, and S. Patchkovskii; The Winter Colloquium on the Physics of Quantum Electronics, PQE-2017 (Snowbird, Utah, USA, 2017-01): *Strong-field pumped lasing in atoms and molecules: The bound states of the free electron* (plenary talk)

M. Ivanov; Workshop Advanced Material Sciences (Dresden, Germany, 2017-09): *High harmonic generation spectroscopy of ultrafast phase transitions in strongly correlated solids*

M. Ivanov; Int. Workshop on Computational and Theoretical Nanoscience (Madrid, Spain, 2017-11): *High harmonic spectroscopy of laser-induced phase transitions in strongly correlated systems*

M. P. Kalashnikov; High-Power, High-Energy, and High-Intensity Laser Technology (Prague, Czech Republic, 2017-04): *Picosecond temporal contrast of Ti:sapphire lasers*

J. W. Kim *together with* S. Y. Choi, J. Bae, X. Mateos, F. Díaz, U. Griebner, V. Petrov, G.-H. Kim, and F. Rotermund; 25th Int. Conference on Advanced Laser Technologies, ALT 2017 (Busan, Korea, 2017-09): *Comparative analysis of evanescent field interaction with carbon nanotubes in the Q-switched Yb:KYW planar waveguide laser*

O. Kornilov; Intense Field, Short Wavelength Atomic and Molecular Processes, ISWAMP, ICPEAC Satellite Meeting (Brisbane, Australia, 2017-07): *Interference stabilization of a complex Fano resonance*

X. Mateos *together with* P. Loiko, S. Lamrini, K. Scholle, P. Fuhrberg, S. Vatnik, I. Vedin, M. Aguiló, F. Díaz, U. Griebner, and V. Petrov; 25th Int. Conference on Advanced Laser Technologies, ALT 2017 (Busan, Korea, 2017-09): *Monoclinic double tungstate thin-disk lasers at 2 microns*

A. Mermillod-Blondin, Int. Conference on Laser Ablation, COLA 2017 (Marseille, France, 2017-09): *Direct imaging of fs-laser induced heat flows in glasses*

M. Mero; Photonic Net Workshop "Simulationen in der Photonik" (Hannover, Germany, 2017-04): *Nonlinear excitation and damage in dielectric optical coatings*

J. Mikosch; Int. Conference on Molecular Energy Transfer in Complex Systems, ICOMET 2017 (Innsbruck, Austria, 2017-01): *Molecular dynamics studied with attosecond XUV pulses*

F. Morales *together with* M. Spanner, M. Richter, O. Smirnova, and M. Ivanov; The Winter Colloquium on the Physics of Quantum Electronics, PQE-2017 (Snowbird, Utah, USA, 2017-01): *Optical lasing during laser filamentation in the Nitrogen molecule: Ro-vibrational inversion*

E. T. J. Nibbering; 9th Int. Conference on Advanced Vibrational Spectroscopy, ICAVS9 (Victoria, BC, Canada, 2017-06): *Ultrafast vibrational dynamics of the Zundel cation*

S. Patchkovskii, 30th Int. Conference on Photonic Electronic and Atomic Collisions, ICPEAC XXX (Cairns, Australia, 2017-07): *Probing molecules with photoelectron rescattering and harmonics generation:* CH_4 *and* C_4H_6

S. Patchkovskii, Intense Field, Short Wavelength Atomic and Molecular Processes, ISWAMP, ICPEAC Satellite Meeting (Brisbane, Australia, 2017-07): *SCID-TDSE: A tool for fully-converged strong-field TDSE calculations for atomic systems with a single active electron*

S. Patchkovskii, 6th Int. Conference on Attosecond Physics, ATTO'17 (Xi'an, China, 2017-07): *A complete treatment of non-adiabatic vibronic dynamics in molecular high-harmonics generation process in methane*

V. Petrov; SPIE Photonics West 2017 (San Francisco, CA, USA, 2017-01): *Frequency down-conversion of 1 µm laser radiation to the mid-IR using non-oxide nonlinear crystals in a cascaded intracavity configuration*

V. Petrov *together with* V. V. Badikov, D. V. Badikov, V. B. Laptev, K. V. Mitin, G. S. Shevyrdyaeva, A. Kwasniewski, E. Boursier, N. I. Shchebetova, A. Tyazhev, G. Marchev, V. Panyutin, P. Segonds, and B. Boulanger; The 6th Advanced Lasers and Photon Sources, ALPS'17 (Yokohama, Japan, 2017-04): *New Ba-based crystals for nonlinear frequency conversion in the Mid-IR*

V. Petrov *together with* V. V. Badikov, D. V. Badikov, V. B. Laptev, K. V. Mitin, G. S. Shevyrdyaeva, N. Kostyukova, A. Boyko, E. Boursier, V. Panyutin, N. I. Shchebetova, A. Tyazhev, G. Marchev, A. Kwasniewski, D. Kolker, P. Segonds, and B. Boulanger; 25th Int. Conference on Advanced Laser Technologies, ALT 2017 (Busan, Korea, 2017-09): *New Ba-based nonlinear crystals for frequency conversion of near-IR lasers into the Mid-IR*

V. Petrov *together with* V. Badikov, D. Badikov, V. Laptev, K. Mitin, G. Shevyrdyaeva, N. Kostyukova, A. Boyko, E. Boursier, V. Panyutin, N. Shchebetova, A. Tyazhev, G. Marchev, A. Kwasniewski, D. Kolker, P. Segonds, and B. Boulanger; The 7th Asian Conference on Crystal Growth and Crystal Technology, CGCT-7 (Changchun, China, 2017-10): *New Barium compounds for nonlinear frequency conversion in the Mid-IR: Characterization and first applications* (plenary talk)

V. Petrov; Sino-German Symposium, Ultrafast Optics and Photonics (Tianjin, China, 2017-11): *Sub-100 fs pulses near 2 micron by passive mode-locking of novel Tm-doped laser materials*

B. Pfau; 9th Int. Workshop on Nanoscale Spectroscopy and Nanotechnology (Gyeongju, South Korea, 2017-09): *Ultrafast deterministic creation and inertial properties of single skyrmions*

I. Radu; TELBE-Nutzertreffen (HZDR, Helmholtz-Zentrum Dresden-Rossendorf, Germany, 2017-02): *Controlling ultrafast magnetism by selective excitations of phonons and magnons*

I. Radu; 8th Int. Conference on Metamaterials, Photonic Crystals and Plasmonics, META'17 (Seoul, South Korea, 2017-07): *Ultrafast magnetization switching of Ferrimagnetic oxides*

I. Radu; Spins, Waves, and Interactions 2017 (Greifswald, Germany, 2017-07): *THz-driven ultrafast magnetization switching*

I. Radu; The Physical Society of Japan Meeting (Morioka, Japan, 2017-09): *Ultrafast magnetization dynamics studied by time-resolved XMCD*

H. Reiss; 26th Annual Int. Laser Physics Workshop, LPHYS'17 (Kazan, Russia, 2017-07): *Fields, not gauges*

H. Reiss; 26th Annual Int. Laser Physics Workshop, LPHYS'17 (Kazan, Russia, 2017-07): *Unique gauge for laser effects*

M. Richter *together with* M. Matthewes, T. Bredtmann, A. Patas, A. Lindinger, J. Gateau, S. Hermelin, J. Kasparian, O. Smirnova, F. Morales, J.-P. Wolf, and M. Ivanov; The Winter Colloquium on the Physics of Quantum Electronics, PQE-2017 (Snowbird, Utah, USA, 2017-01): *Light amplification by nearly free electrons in a laser filament*

A. Rouzée; DPG Spring Meeting 2017 (Mainz, Germany, 2017): *Single-shot coherent diffractive imaging of individual clusters using a high harmonic source*

D. Rupp; Int. DESY Photon Science Workshop: Future of science at FLASH (Hamburg, Germany, 2017-09): *The power of XUV - 3D diffractive imaging of transient nanostructures and ultrafast dynamics*

D. Rupp; Int. Conference on Extreme Light, ICEL 2017 (Szeged, Hungary, 2017-11*): Imaging nanoparticles and ultrafast nanoplasma dynamics*

C. v. Korff Schmising; 8th Ringberg Workshop on Science with FELs – From first results to future perspectives (Ringberg, Germany, 2017-02): *Imaging ultrafast magnetization dynamics*

C. v. Korff Schmising; Int. Union of Crystallography 2017, IUCR'17 (Hyderabad, India, 2017-08): *Two color imaging of ultrafast magnetization dynamics*

B. Schütte; Extreme Atomic Systems 2017 (Riezlern, Austria, 2017-01): *Real-time observation of cluster charging in strong fields*

R. E. F. Silva; MURI Mid-Infrared Meeting 2017, MURI MIR (Washington, USA, 2017-04*): High harmonic imaging of ultrafast many-body dynamics in strongly correlated systems*

O. Smirnova *together with* R. E. F. Silva, I. V. Blinov, A. N. Rubtsov, and M. Ivanov; The Winter Colloquium on the Physics of Quantum Electronics, PQE-2017 (Snowbird, Utah, USA, 2017-01): *High harmonic generation spectroscopy of laser induced phase transitions in strongly correlated systems* (presented by M. Ivanov)

O. Smirnova; WPC Theory Workshop (DESY, Hamburg, 2017-06*): New frontiers of chiral dynamics at electronic time scales*

O. Smirnova; 30th Int. Conference on Photonic, Electronic and Atomic Collisions, ICPEAC XXX (Cairns, Australia, 2017-07): *Looking inside chiral molecules on femtosecond time-scale*

O. Smirnova; 14th Int. Conference on Multiphoton Processes, ICOMP (Budapest, Hungary, 2017-09): *Controlled chiral dynamics in strong and weak fields*

O. Smirnova; Workshop on Chiral and Topological Matter (Vancouver, Canada, 2017-12): *Extending chiral measurements to topology*

G. Steinmeyer *together with* N. Raabe, T. Feng, M. Merö, H. Tian, Y. Song, W. Hänsel, R. Holzwarth, A. Sell, and A. Zach; SPIE Photonics West 2017 (San Francisco, CA, USA, 2017-01): *Hidden amplitude-phase correlations in the carrier-envelope noise of mode-locked lasers*

G. Steinmeyer; Workshop "Nonlinear phenomena in strong fields" (Hannover, Germany, 2017-01): *Channel mergers as the trigger of rogue events during multiple filamentation*

G. Steinmeyer; Nonlinear Waves and Turbulences in Optics and Hydrodynamics (Berlin, Germany, 2017-03): *Determinism and predictability of rogue waves*

G. Steinmeyer; PIERS 2017 (St. Petersburg, Russia, 2017-05): *Measuring the electro-optic Kerr effect in air via the carrier-envelope phase*

G. Steinmeyer; CLEO/Europe-EQEC 2017 (Munich, Germany, 2017-06): *Short course: Ultrashort pulse characterization*

G. Steinmeyer; SPIE Laser Damage (Boulder, CO, USA, 2017-09): *Interferometric frequency-resolved optical gating for probing optical nonlinearities as the verge of multiphoton-induced breakdown* (plenary talk)

G. Steinmeyer; Sino-German Ultrafast Optics and Photonics Symposium (Tianjin, China, 2017-11*): The role of the carrier-envelope phase in four-wave mixing processes: intrapulse coherence degradation vs. the electro-optical Kerr-effect*

H. Stiel; SPIE Optics + Optoelectronics (Prague, Czech Republic, 2017-04): *Soft X-ray nanoscale imaging using highly brilliant laboratory sources and new detector concepts*

H. Stiel; 52nd Zakopane School of Physics (Zakopane, Poland, 2017-05): *Nanoscale imaging and X-ray absorption spectroscopy using laser based laboratory sources*

G. Thomas; CLEO/Europe-EQEC 2017 (Munich, Germany, 2017-06): *High power and high energy diode-pumped Alexandrite lasers*

J. W. Tomm *together with* R. Kernke, G. Mura, M. Vanzi, M. Hempel, and B. Acklin; 2017 IEEE High Power Diode Lasers & Systems Conference (Coventry, UK, 2017-10): *Comparison of catastrophic optical damage events in GaAs- and GaN-based diode lasers*

M. J. J. Vrakking; European Conference on Nonlinear Optical Spectroscopy, ECONOS 2017 (Jena, Germany, 2017-04): *Applications of ultrashort XUV pulses*

M. J. J. Vrakking; Int. Symposium on Molecular Beams 2017, ISMB 2017 (Nijmegen, The Netherlands, 2017-06): *Applications of ultrashort XUV pulses*

M. J. J. Vrakking; ATTO 2017 (Xi'an, China, 2017-07): *Attosecond field-driven electron dynamics*

M. J. J. Vrakking; Artemis and Research Complex User Meeting 2017 (Oxford, UK, 2017-09): *The many benefits of high-harmonic radiation*

M. J. J. Vrakking; QUTIF Int. Conference 2017 (Bad Honnef, Germany, 2017-09): *The many benefits of high harmonic radiation*

I. Will; European Workshop on Photocathodes for Particle Accelerator Applications, EWPAA 2017 (Berlin, Germany, 2017-09): *Photocathode drive laser development*

M. Woerner; Int. Workshop on Finite Systems in Non-Equilibrium: From Quantum Quench to the Formation of Strong Correlations (Natal, Brazil 2017-09): *Nonlinear softmode dynamics studied by 2D terahertz spectroscopy and femtosecond X-ray diffraction*

Invited talks at seminars and colloquia

W. Becker; Seminar (Institute for Applied Physics and Computational Mathematics, Beijing, China, 2017-05): *Strong-field physics with tailored fields*

W. Becker; Seminar (Institute of Theoretical Physics and Department of Physics, Shanxi University, Taiyuan, China, 2017-05): *Atoms in intense laser fields: Light at the end of the tunnel*

K. Busch; Applied Nano-Photonics Colloquium (Twente, The Netherlands, 2017-12): *Equilibrium and non-equilibrium atom-surface Interactions: Material models and computations*

S. Eisebitt; Seminar (Paul-Drude-Institut für Festkörperelektronik, Berlin, Germany, 2017-02): *Watching spins move*

S. Eisebitt; Göttinger Physikalisches Kolloquium (Georg-August-Universität Göttingen, Germany, 2017-02): *Watching spins move*

S. Eisebitt; Greifswalder Physikalisches Kolloquium (Ernst-Moritz-Arndt-Universität, Greifswald, Germany, 2017-11): *A Holographic view on magnetic skyrmions*

T. Elsaesser; Chemistry Colloquium (École Normal Supérieure, Paris, France, 2017-03): *Electric interactions of hydrated biomolecules and protons studied by femtosecond infrared spectroscopy*

T. Elsaesser; Physics Colloquium (École Normal Supérieure, Paris, France, 2017-04): *Electron and lattice dynamics in solids mapped by ultrafast X-ray methods*

T. Elsaesser; Colloquium Klung-Wilhelmy-Wissenschaftspreis (Freie Universität Berlin, Germany, 2017-11): *Laudatio für Claus Ropers*

T. Elsaesser; Physics Colloquium (Universität Regensburg, Germany, 2017-11): *Charge dynamics in polar solids mapped by ultrafast X-ray methods*

T. Fennel; European XFEL Seminar (Hamburg, Germany, 2017-01): *Ultrafast nanoplasma dynamics meets X-ray imaging*

T. Fennel; Colloquium (ETH Zürich, Switzerland, 2017-09): *Probing the 3D shape and ultrafast dynamics of isolated nanostructures via single-shot XUV coherent diffractive imaging*

T. Fennel; Workshop Cluster Pysik im Europäischen Raum 2017 (Bachrach, Germany, 2017-09): *Attosecond control of electron dynamics in clusters*

T. Fennel, Colloquium (University of Oldenburg, Germany, 2017-12): *Attosecond control of electron dynamics in clusters*

T. Fennel; Int. Workshop "15 Years of Russian-German Laboratory at BESSY II" (Helmholtz-Zentrum, Berlin, Germany, 2017-12): *Control and ultrafast imaging of electron dynamics in clusters*

B. P. Fingerhut *together with* M. Richter; 53rd Symposium on Theoretical Chemistry, STC 2017 (Basel, Switzerland, 2017-08): *Towards the numerical exact treatment of charge transfer dynamics in drosophila cryptochrome (dCRY) via MACGIC-QUAPI*

R. Grunwald; Keynote Lecture (Brandenburgische Technische Universität Cottbus-Senftenberg, Germany, 2017-09): *Thermal-plasmonic mechanism of laser-induced nanograting formation in silicon*

F. Intravaia; Seminar (Graduiertenkolleg: Int. Research Training Group, Freiburg, Germany, 2017-12): *Fluctuation-induced interactions in meso- and microscopic systems*

F. Intravaia; Seminar (Department of Physics, University of Palermo, Italy, 2017-12): *An introduction to the theory of fluctuation-induced interactions*

F. Intravaia; Seminar (Department of Physics, University of Palermo, Italy, 2017-12): *Non-equilibrium and equilibrium atom-surface interactions: The failure of the Markov and of other common approximations*

F. Intravaia; Seminar (Huygens Laboratory, University of Leiden, Germany, 2017-12): *Non-equilibrium atom-surface interactions: the role of the Markov and of the local thermal equilibrium approximation*

E. T. J. Nibbering; Colloquium (Freie Universität Berlin, Germany, 2017-02): *Hydrogen bond and proton transfer dynamics using IR and soft-X-ray local spectroscopic probes*

E. T. J. Nibbering; Seminar (University of California, Berkeley, CA, USA, 2017-04): *Hydrogen bond and proton transfer dynamics using IR and soft-X-ray local spectroscopic probes*

E. T. J. Nibbering; Seminar (SLAC, Stanford, CA, USA, 2017-04): *Hydrogen bond and proton transfer dynamics using IR and soft-X-ray local spectroscopic probes*

V. Petrov; Seminar (Fujian Institute of Research on the Structure of Matter, Chinese Academy of Sciences, Fuzhou, China, 2017-10): *Nonlinear frequency conversion and mid-IR coherent sources based on novel ternary and quaternary Ba-compounds*

V. Petrov; Seminar (Technical Institute of Physics and Chemistry, Beijing, China, 2017-11): *Nonlinear frequency conversion and mid-IR coherent sources based on ternary and quaternary Ba-compounds*

V. Petrov; Seminar (Shandong University, Jinan, China, 2017-11): *Sub-10 optical-cycle mode-locked Tm ceramic laser at 2057 nm*

B. Pfau; Seminar (Bundesinstitut für Risikobewertung, BfR, Berlin, Germany, 2017-09): *Holografie mit Röntgenstrahlen*

I. Radu; Seminar (Institut de Physique et Chimie des Matériaux de Strasbourg, IPCMS, France, 2017-06): *When THz meets X-rays: An ultrafast view on magnetism*

I. Radu; Seminar (SPring-8 Synchrotron and Institute for Solid State Physics, University of Tokyo, Japan, 2017-09): *When THz meets X-rays: An ultrafast view on magnetism*

I. Radu; Seminar (College of Science and Technology, Nihon University, Japan, 2017-09): *Ultrafast Magnetization Switching: From X-rays to THz radiation*

D. Rupp; Seminar (PTB Summer School – Frontiers of the measurable, Braunschweig, Germany, 2017-08): *Diffractive imaging of nanoparticles and ultrafast nanoplasma dynamics*

D. Rupp; Seminar (Graduiertenkolleg: Int. Research Training Group, Freiburg, Germany, 2017-10): *Imaging excitation and plasma formation in a single nanoparticle*

D. Schick; Condensed Matter Seminar (Stockholm University, Sweden, 2017-10): *The interplay of spins and lattice studied by femtosecond soft X-rays*

C. v. Korff Schmising; Seminar (Indian Institute of Technology Hyderabad, India, 2017-08): *Ultrafast magnetization dynamics – an element specific view on the nanoscale*

C. v. Korff Schmising; Seminar (Universität Augsburg, 2017-12): *Domain texture of thin Co/Pt multilayers in single- and multi-shot helicity dependent all optical switching*

O. Smirnova; Kolloquium (Philipps-Universität Marburg, FB Physik, Marburg, Germany 2017-06): *Looking inside chiral molecules at ultrafast time scales*

G. Steinmeyer; 9th Int. Summer School New Frontiers in Optical Technologies (Tampere, Finland, 2017-08): *Ultrafast laser pulses and their characterization*

G. Steinmeyer; Seminar (Technische Universität Chemnitz, Germany, 2017-12): *Coherence of ultrashort optical pulses*

J. W. Tomm; Seminar (Fraunhofer-Institut für Zuverlässigkeit und Mikrointegration, IZM, Berlin, Germany, 2017-11): *Untersuchungen an optoelektronischen Bauelementen*

M. J. J. Vrakking; HZB Photon School (Berlin, Germany, 2017-03): *Applications of ultrashort X-ray pulses*

M. J. J. Vrakking; CFEL Seminar (Hamburg, Germany, 2017-WS 2017/18): *The many benefits of High-Harmonic Generation*

I. Will; Seminarreihe Photokathodes (Universität Mainz, Germany, 2017-10): *Photocathode drive laser development*

M. Woerner; Seminar of SFB 1242 (Duisburg, Germany, 2017-11): *Nonlinear softmode dynamics studied by 2D terahertz spectroscopy and femtosecond X-ray dif-fraction*

Academic teaching

A. A. Andreev; Vorlesung, 2 SWS (Universität Oldenburg, WS 2017/18): *Quantum Optics/Plasma Physics/ Specialization Laser & Optics on request as Module Advanced Physics II*

A. A. Andreev *together with* H. J. Brückner, S. Koch, M. Schellenberg, B. Struve, U. Teubner, W. Neu, W. Garen, T. Schüning, S. Wild *et al.*; Vorlesung, 2 SWS (Universität Oldenburg/Emden, Germany, WS 2017/18*): Laboratory Project I*

A. A. Andreev; Vorlesung, 2 SWS (Universität Oldenburg, Germany, WS 2017/18): *Laser Plasma Physics and Applications*

O. Benson *together with* K. Busch, T. Elsaesser, H.-W. Hübers, M. Ivanov, S. Kowarik, A. Peters, A. Saenz, and G. Schneider; Optik/Photonik: Projekt und Seminar, 2 SWS (Humboldt-Universität zu Berlin, SS 2017): *Laserphysik*

T. Bredtmann; Übungen, 2 SWS (Humboldt-Universität zu Berlin, SS 2017): *Nichtlineare Optik*

T. Bredtmann; Vorlesung, 2 SWS (Humboldt-Universität zu Berlin, SS 2017): *Nichtlineare Optik*

K. Busch; Vorlesung, 2 SWS (Humboldt-Universität zu Berlin, SS 2017): *Statistische Physik*

K. Busch; Übungen, 2 SWS (Humboldt-Universität zu Berlin, SS 2017): *Statistische Physik*

K. Busch; Vorlesung, 2 SWS (Humboldt-Universität zu Berlin, SS 2017): *Computerorientierte Photonik*

K. Busch *together with* D.-N. Huynh, and T. Kiel; Übungen, 2 SWS (Humboldt-Universität zu Berlin, SS 2017): *Computerorientierte Photonik*

K. Busch *together with* A. Perez-Leija; Vorlesung, 2 SWS (Humboldt-Universität zu Berlin, WS 2017/18): *Diskrete Quantenoptik*

K. Busch *together with* A. Perez-Leija, D.-N. Huynh, and P. Varytis; Übungen, 2 SWS (Humboldt-Universität zu Berlin, WS 2017/18*): Diskrete Quantenoptik*

U. Eichmann *together with* O. Dopfer; Vorlesung und Übungen, 4 SWS (Technische Universität Berlin, WS 2016/17): *Quantensysteme I*

U. Eichmann *together with* O. Dopfer; Vorlesung und Übungen, 4 SWS (Technische Universität Berlin, WS 2017/18): *Quantensysteme I*

S. Eisebitt *together with* T. Kampfrath, B. Kanngießer, M. Krikunova, M. Lehmann, and T. Niermann; Vorlesung und Übungen, 4 SWS (Technische Universität Berlin, SS 2017): *Optik und Photonik II*

S. Eisebitt *together with* B. Kanngießer, and T. Möller; Vorlesung und Übungen, 2 SWS (Technische Universität Berlin, SS 2017): *Röntgenphysik II*

S. Eisebitt *together with* B. Kanngießer, and T. Möller; Vorlesung und Übungen, 4 SWS (Technische Universität Berlin, WS 2017/18): *Röntgenphysik I*

S. Eisebitt; Vorlesung, 2 SWS (Technische Universität Berlin, WS 2017/18): *Optik und Photonik I*

S. Eisebitt; RACIRI 2017 Summer School – Grand Challenges and Opportunities with the Best X-ray and Neutron Sources (Ronneby, Sweden, 2017-08): *An X-ray view on ultrafast magnetic phenomena*

S. Eisebitt; 19th HERCULES Specialized Course “Quantitative Imaging using X-rays and Neutrons”, (Grenoble, France, 2017-05): *X-ray holography*

S. Eisebitt *together with* B. Pfau; Graduate Days of CUI 2017, (The Hamburg Centre for Ultrafast Imaging, 2017-03): *Ultrafast X-ray scattering and holography*

T. Elsaesser *together with* A. Saenz, Vorlesung, 4 SWS (Humboldt-Universität zu Berlin, WS 2016/17): *Laserphysik*

T. Elsaesser; Vorlesung und Übungen, 4 SWS (Humboldt-Universität zu Berlin, SS 2017): *Physik ultraschneller Prozesse*

I. V. Hertel; Seminar, 2 SWS (Humboldt-Universität zu Berlin, SS 2017): *Moderne Physik und Schule*

I. V. Hertel; Seminar, 2 SWS (Humboldt-Universität zu Berlin, WS 2017/18): *Forschungspraktikum mit Seminar*

F. Intravaia; Vorlesung, 2 *SWS (Humboldt-Universität zu Berlin, SS 2017): Fluktuations-induzierte Phänomene*

F. Intravaia *together with* M. Olschläger; Übungen, 2 SWS (Humboldt-Universität zu Berlin, SS 2017): Fluktuations-induzierte Phänomene

M. Ivanov; Vorlesung, 2 SWS (Humboldt-Universität zu Berlin, Germany, WS 2017/18): *Quantum dynamics in strong laser fields*

M. Ivanov; Übungen, 2 SWS (Humboldt-Universität zu Berlin, Germany, WS 2017/18): Quantum dynamics in strong laser fields

A. Perez-Leija; Vorlesung, 2 SWS (National Institute of Astrophysics, Optics, and Electronics in Puebla, Mexico, 2017-12): *Introduction to quantum computing with linear optics*

O. Smirnova *together with* U. Woggon; Vorlesung und Übungen, 4 SWS (Technische Universität Berlin, WS 2017/18): *Höhere Optik I*

M. J. J. Vrakking; Vorlesung, 2 SWS (Freie Universität Berlin, WS 2017/18): *Ultrafast Laserphysics*

M. J. J. Vrakking; Übungen, 2 SWS (Freie Universität Berlin, WS 2017/18): *Ultrafast Laserphysics*

M. Woerner; Übungen, 2 SWS (Humboldt-Universität zu Berlin, WS 2016/17): *Übungen zur Vorlesung Laserphysik*

Appendix 3

Ongoing Bachelor, Master, and PhD theses

Bachelor theses

T. Doerries; *Analyse von Röntgenstreubildern einzelner Xenoncluster mit Mie-Simulationen* (Supervisor: D. Rupp and T. Möller), Technische Universität Berlin

C. Klose; *Erzeugung und Manipulation von magnetischen Bubble-Domänen* (Supervisor: S. Eisebitt and Dähne), Technische Universität Berlin und FSU Jena

M. Liebmann; *Anfertigen spektraler maps von few-cycle-gepulsten Vortexstrahlen mit Hilfe eines Nanopositionierers* (Supervisor: R. Grunwald), Technische Universität Wildau

L. Loechner; *Erzeugung und Verkürzung von Lichtpulsen mit nichtlinearer Optik* (Supervisor: M. J. J. Vrakking), Freie Universität

F. Stolberg; *Aufbau einer durchstimmbaren Pump-Strecke für Labor-NEXAFS-Untersuchungen* (Supervisor: B. Kanngießer and S. Stiel), Technische Universität Berlin

Master theses

U. Bengs; *High-harmonic generation driven by bicircular few-cycle laser pulses* (Supervisor: M. Ivanov and N. Zhavaronkov), Humboldt-Universität zu Berlin, Germany

L. Glöggler; *First pump-probe NEXAFS experiments using a laser-based plasma source* (Supervisor: B. Kanngießer and S. Stiel), Technische Universität Berlin

L. Hecht; *Zweifarben-Streubildaufnahme von Helium-Nanotröpfchen – Planung, Durchführung und erste Ergebnisse* (Supervisor: D. Rupp and T. Möller), Technische Universität Berlin

A. Heilrath; *Ultrafast ionization dynamics of methane clusters in XUV double pulses* (Supervisor: D. Rupp and T. Möller), Technische Universität Berlin

J. Jordan; *Untersuchung von lichtinduzierter Dynamik in Metallclustern mittels Röntgenbeugung* (Supervisor: D. Rupp and T. Möller), Technische Universität Berlin

T. Kubail Kalousdian; *Generation and characterization of ultrashort UV pulses* (Supervisor: M. J. J. Vrakking and H.-J. Freund), Freie Universität Berlin

S. Kholaif; *Ultrafast time-resolved magneto-optical imaging with femtosecond time and Nm spatial resolution* (Supervisor: S. Eisebitt and C. Spielmann), Technische Universität Berlin und FSU Jena

S. Marschner; *Erzeugung, Kontrolle und Charakterisierung der Entstehung großflächiger periodischen Oberflächenstrukturen im Nanometerbereich für tribologische Anwendungen* (Supervisor: A. Rosenfeld), Technische Hochschule (FH) Wildau

A. Santagostino*; Investigation of Ti:sapphire laser pumped Tm:YAG laser ceramics with different doping level in the CW regime* (Supervisor: V. Petrov), University of Pavia, Italy

J. Schauss; *Ultrafast vibrational spectroscopy of dimethylphosphate in an aqueous environment* (Supervisor: T. Elsaesser), Humboldt-Universität zu Berlin

P. Stammer; *Laser induced electron diffraction on strongly aligned and oriented molecules* (Supervisor: A. Rouzée), Technische Universität Berlin

S. Tacchini; *Design and characterization of CW and passively Q-switched diode-pumped Tm-doped microchip lasers at 2 μm* (Supervisor: V. Petrov and X. Mateos), University of Pavia, Italy

F. Trigub; *The role of dissipative processes in nonequilibrium atom-surface interactions* (Supervisor: K. Busch and F. Intravaia), Humboldt-Universität zu Berlin

K. Tschernig; *Pseudo-energy representation of multiphoton processes in multiport systems* (Supervisor: K. Busch and A. Perez-Leija), Humboldt-Universität zu Berlin

P. Weber; *Generation of ultrashort soft X-ray pulses by two-color high harmonic generation* (Supervisor: A. Rouzée and M. J. J. Vrakking), Freie Universität Berlin

S. Wenzel; *Verstärkung Pikosekunden-Laserquelle bei 2050 nm mittels Tm- und Ho-dotierten Waveguide- und Faserverstärkern* (Supervisor: T. Elsaesser), Humboldt-Universität zu Berlin

PhD theses

F. Branchi; *Ultrafast structural dynamics in molecules by time-resolved photoelectron holography* (Supervisor: M. J. J. Vrakking), Freie Universität Berlin

F. Braußе; *Core-shell molecular frame photoelectron angular distribution of photoexcited molecules* (Supervisor: A. Rouzée, and M. J. J. Vrakking), Freie Universität Berlin

M.-A. Codescu; *Ultraschnelle Dynamik von photoinduzierten Prozessen* (Supervisor: T. Elsaesser), Humboldt-Universität zu Berlin

F. Dahms; *Nichtlineare Schwingungsspektroskopie an biomolekularen Systemen* (Supervisor: T. Elsaesser), Humboldt-Universität zu Berlin

L. Drescher; *Attosecond Transient Absorption Spectroscopy* (Supervisor: J. Mikosch and M. J. J. Vrakking), Freie Universität Berlin

M. Fohler; *Kohärente Röntgenstreuung und Holografie* (Supervisor: S. Eisebitt), Technische Universität Berlin

A. Giree; *High repetition rate optical parametric chirped-pulse amplification* (Supervisor: M. J. J. Vrakking and co-supervisor: Amplitude Technologies), Freie Universität Berlin

L. v. Grafenstein; *Generation of intense few-cycle pulses in the mid-wave infrared* (Supervisor: T. Elsaesser), Humboldt-Universität zu Berlin

M. Hennecke; *Ultraschnelle Spindynamik untersucht mit Femtosekunden-Röntgenpulsen* (Supervisor: S. Eisebitt), Technische Universität Berlin Dissertation

A. S. Hernández; *Femtosekunden-Röntgenbeugung an ionischen Materialien* (Supervisor: T. Elsaesser), Humboldt-Universität zu Berlin Berlin

P. Hessing; *Ptychographie mit weichen Röntgenstrahlen* (Supervisor: S. Eisebitt), Technische Universität Berlin

M. Holtz; *Ultrakurzzeit-Röntgenbeugung an ionischen Festkörpern* (Supervisor: T. Elsaesser), Humboldt-Universität zu Berlin

J. Hummert; *Femtosecond XUV photoelectron spectroscopy of organic molecules in aqueous solution* (Supervisor: M. J. J. Vrakking and K. Heyne), Freie Universität Berlin

J. Hyyti; *Investigation of pulse measurement schemes for coherence characterization and spectroscopic applications at the few-cycle scale* (Supervisor: T. Elsaesser), Humboldt-Universität zu Berlin

A. Jonas; *Zeitaufgelöste NEXAFS-Spektroskopie* (Supervisor: B. Kanngießer and S. Stiel), Technische Universität Berlin

P. Juergens; *Plasma formation during ultrashort pulse laser micromachining of solid dielectrics* (Supervisor: M. J. J. Vrakking and T. Baumert), Freie Universität Berlin

N. Khodakovskiy; *Methods of ultrafast laser contrast diagnostics and optimization* (Supervisor: M. J. J. Vrakking and M. Kalashnikov), Freie Universität Berlin

B. Langbehn; *X-ray imaging of ultrafast dynamics in single helium nanodroplets* (Supervisor: D. Rupp and T. Möller), Technische Universität Berlin

J. Lebendig-Kuhla; *Role of delocalized states for the excited state dynamics of nucleotide oligomers* (Supervisor: M. J. J. Vrakking), Freie Universität Berlin

F. Mahler; *Spektroskopische Untersuchungen an III-V-Halbleiterstrukturen* (Supervisor: T. Elsaesser), Humboldt-Universität zu Berlin

S. Meise; *Korrelationen und molekulare Fragmentationsdynamiken in starken IR- und FEL-Laserfeldern* (Supervisor: U. Eichmann), Technische Universität Berlin

N. Monserud; *Photo-induced dynamics in molecule photo-induced dynamics on the sub-femtosecond to few-femtosecond timescale* (Supervisor: A. Rouzée and M. J. J. Vrakking), Freie Universität Berlin

M. Oelschläger; *Theory of fluctuation-induced phenomena in nanophotonic systems* (Supervisor: K. Busch and F. Intravaia), Humboldt-Universität zu Berlin

M. Oßwald; *Theoretical description and simulation of non-linear spectroscopic signals of the light induced primary processes in (6-4) photolyase* (Supervisor: K. Busch), Humboldt-Universität zu Berlin

P. Varytis; *Light-path engineering in disordered waveguiding systems* (Supervisor: K. Busch), Humboldt-Universität zu Berlin

S. Raabe; *Time-resolved soft-X-ray photoelectron spectroscopy of molecular dynamics at conical intersection* (Supervisor: A. Rouzée and M. J. J. Vrakking), Freie Universität Berlin

N. Raabe; *CEP stabilization of kHz CPA lasers and their application* (Supervisor: M. J. J. Vrakking and G. Steinmeyer), Freie Universität Berlin

D. Reiche; *Role of material, geometrical and statistics properties in equilibrium and nonequilibrium fluctuation-induced interactions* (Supervisor: K. Busch and F. Intravaia), Humboldt-Universität zu Berlin

K. Reininger; *Structural imaging of transition state dynamics* (Supervisor: J. Mikosch and M. J. J. Vrakking), Freie Universität Berlin

M. Sauppe; *Zeitaufgelöste Experimente an Clustern mit intensiven XUV-Doppelpulsen* (Supervisor: D. Rupp and T. Möller), Technische Universität Berlin

F. Schell; *Coincident detection of correlated electron and nuclear dynamics induced by ultra short laser pulses* (Supervisor: C. P. Schulz and M. J. J. Vrakking), Freie Universität Berlin

M. Schneider; *Nonlinear resonant scattering of femtosecond XUV radiation* (Supervisor: S. Eisebitt), Technische Universität Berlin

D. Weder; *Time-resolved investigation of ultrafast magnetization dynamics* (Supervisor: S. Eisebitt), Technische Universität Berlin

J. Weißhaupt; *Ultrakurzzeit-Röntgenmethoden zur Untersuchung struktureller Dynamik in Festkörpern* (Supervisor: T. Elsaesser), Humboldt-Universität zu Berlin

F. Willems; *The role of transport processes in ultrafast demagnetization dynamics* (Supervisor: S. Eisebitt), Technische Universität Berlin

J. Zimmermann; *Analyzing large data sets of diffraction images from individual nanoparticles using neural network approaches for feature extraction* (Supervisor: D. Rupp and T. Möller), Technische Universität Berlin

H. Zimmermann; *Untersuchung angeregter neutraler Fragmente nach frustrierter Tunnelionisation* (Supervisor: U. Eichmann), Technische Universität Berlin

Appendix 4

Guest Lectures at the MBI

N. Epperlein, Bundesanstalt für Materialforschung und -prüfung, Nanomaterial Technologies, Berlin; Seminar A: Attosecond Physics, 2017-01-06: *Characterization of a digital holographic microscope and laser-induced nanostructures*

G. Paulus, Friedrich-Schiller-Universität Jena; Institutskolloquium, 2017-01-18: *Cross-sectional nanoscale imaging using high harmonics*

M. Chergui, École Polytechnique Fédérale de Lausanne, Faculty of Basic Sciences, ISIC, Switzerland; Institutskolloquium, 2017-02-01: *Charge carrier dynamics in solar materials*

C. Rödel, Friedrich-Schiller-Universität Jena and SLAC National Accelerator Lab., USA; Seminar B: Transient Electronic Structure and Nanoscience, 2017-02-09: *High harmonic generation using relativistically oscillating mirrors*

P. Rupprecht, Technische Universität München; Seminar A, 2017-02-10: *Optical development for VUV pump/X-ray probe and X-ray pump/probe experiments at LCLS*

B. Weaver, Imperial College, London, UK; Seminar A, 2017-02-13): *Simpler ultrashort characterization with a new kind of frequency resolved optical gating*

H. Qian, DESY Zeuthen; Seminar B, 2017-02-21: *High brightness electron source at PITZ for ultrafast electron diffraction applications*

J. McCord, Christian-Albrechts-Universität zu Kiel; Institutskolloquium, 2017-02-22: *Advanced magneto-optical microscopy of magnetic materials: Magnetoelectric sensors, spin-waves and beyond*

H. C. Allen, Department of Chemistry and Biochemistry, Ohio State University, USA; Seminar C: Ultrafast and Nonlinear Phenomena: Condensed Phase, 2017-02-23: *Organization, hydration, ion binding, and inherent electric fields at aqueous surfaces*

M. Savoini, Institute for Quantum Electronics, ETH Zürich, Switzerland, Seminar B, 2017-03-02: *Time resolved hard X-ray: A versatile tool to study changes in the ferroic order*

P. Polynkin, College of Optical Sciences, University of Arizona, USA; Seminar A, 2017-03-06: *Atmospheric applications of intense ultrashort-pulse lasers*

M. Garcia, Institute of Physics, University of Kassel; Seminar A, 2017-03-14: *Ab-initio and classical molecular dynamics simulations of ultrafast structural phenomena in laser excited solids*

M. H. M. Janssen, University of Twente, Enschede, The Netherlands; Seminar A, 2017-03-23: *Direct enantiomer selective Mass Spectrometry of chiral mixtures by MS-PECD*

S. Carlström, Lund University, Sweden; Seminar A, 2017-03-24: *Subcycle control of strong-field processes on the attosecond timescale*

G. Achazi, Institute of Applied Physics, University of Bern, Switzerland; Seminar B, 2017-03-30: *Tools and methodologies for UV and deep-UV coherent spectroscopy*

D. Schick, Institut für Methoden und Instrumentierung der Forschung mit Synchrotronstrahlung, Helmholtz-Zentrum Berlin für Materialien und Energie; Seminar B, 2017-04-05: *Disentangling spin and lattice dynamics in magnetic nanostructures*

O. Karnbach, Imperial College, London, UK; Seminar A, 2017-04-12: *Ultrafast streaking at biased nanotip*

C. Bacellar, University of California, Berkeley, CA, USA; Seminar A, 2017-04-13: *Ultrafast dynamics in pure and doped Helium nanodroplets*

D. R. Austin, Imperial College London, UK; Seminar A, 2017-04-25: *High-harmonic generation with intense 1.8 μm pulses – Spectroscopy and water-window attosecond bursts*

F. X. Kaertner, DESY – CFEL & MIT, Dep. of Electrical Engineering and Computer Science, Cambridge, USA; Institutskolloquium, 2017-04-26: *How to shrink an accelerator: From the European X-FEL to compact X-ray sources*

A. Kalashnikova, Ferroics Physics Laboratory, Ioffe Institute of RAS, St. Petersburg, Russia; Seminar B, 2017-05-09: *Ultrafast changes of magnetic anisotropy in low-symmetry magnetic films by femtosecond laser pulses*

B. Hillebrands, Leibniz-Institut für Festkörper- und Werkstoffforschung Dresden; Institutskolloquium, 2017-05-17: *Advanced magnonics*

C.-H. Lu, Institute of Atomic and Molecular Sciences, Academia Sinica, Taipei, Taiwan; Seminar A, 2017-05-22: *Intense, near single-cycle pulse generation in multiple thin plates*

L. Young, Argonne National Laboratory, The University of Chicago, USA; Institutskolloquium 2017-05-24: *Towards ultrafast imaging and spectroscopy in the water window*

T. Fennel, Institute of Physics, University of Rostock; Seminar A, 2017-06-08: *Strong-field physics with nanospheres*

J. Tian, Department of Physics and Astronomy, University of Rochester, New York, USA; Seminar A, 2017-06-19: *The numerical-detector method in atomic single ionizations*

M.-C. Chen, Institute of Photonics, National Tsing Hua University, Taiwan; Seminar A, 2017-06-20: *Control of the photon energy and polarization of tabletop high-order harmonic generation*

S. Johnson, ETH Zürich, Zwitzerland; Institutskolloquium, 2017-06-21: *Ultrashort light pulses as a tool for atomic-scale control of solids*

A. Beige, School of Physics and Astronomy, University of Leeds, UK; Seminar A, 2017-07-19: *Quantizing the electromagnetic field near semitransparent mirrors*

N. Holetzke, H. Westermann, and J. Schneider; 'Jugend forscht', Landeswettbewerb Baden-Württemberg 2017; Seminar A: Sonderseminar, 2017-07-20: *Farben ohne Farbe – Nanostrukturen bei Schmetterlingen auf der Spur*

A. Monmayrant, Laboratory of Analysis and Architecture of Systems, LAAS-CNRS, Toulouse, France; Seminar A, 2017-07-25: *Sub-wavelength grating for narrow-band spectral filters & adaptive hyperspectral imaging*

O. Graydon, Nature Photonics, London, UK; Seminar C, 2017-08-22: *Publishing in Nature Photonics*

C.-D. Lin, Kansas State University, USA; Seminar A, 2017-09-19: *Phase retrieval of broadband attosecond light pulses and electron wave packets*

H. Niikura, Department of Applied Physics, Waseda University, Tokyo, Japan, Seminar A, 2017-09-19: *Phase and momentum-resolved imaging of an attosecond electron wavepacket*

R. Huber, Universität Regensburg; Institutskolloquium, 2017-09-20: *Faster than a cycle of light*

U. Atxitia, Freie Universität Berlin; Seminar B, 2017-10-26: *Computational modeling of ultrafast magnetic switching and magnetic domain motion control in antiferromagnets*

K. Bergmann, OPTIMAS Research Center of the Technische Universität Kaiserslautern and TOPTICA-Project; Seminar A, 2017-11-09: *A new concept of high accuracy laser ranging*

A. Lichtenstein, Institut für Theoretische Physik, Universität Hamburg and European XFEL; Seminar A, 2017-11-21: *Electronic structure of correlated systems*

A. V. Popov, Department of Physics, Moscow State University, Russia; Seminar A, 2017-11-27: *Spontaneous emission of atoms dressed by high-intensity laser field*

V. Shokeen, Institut de Physique et Chimie des Matériaux de Strasbourg, CNRS, Université de Strasbourg, France; Seminar A, 2017-12-07: *Ultrafast magnetization dynamics in ferromagnetic transition metals: A study of non-thermal spin flip vs spin transport induced by femtosecond optical pulses and of coupled oscillators excited by picosecond acoustic pulses*

C. Lienau, Universität Oldenburg; Institutskolloquium, 2017-12-13: *Coherent ultrafast charge and energy transfer processes in nanostructures*

Appendix 5

Grants and Contracts

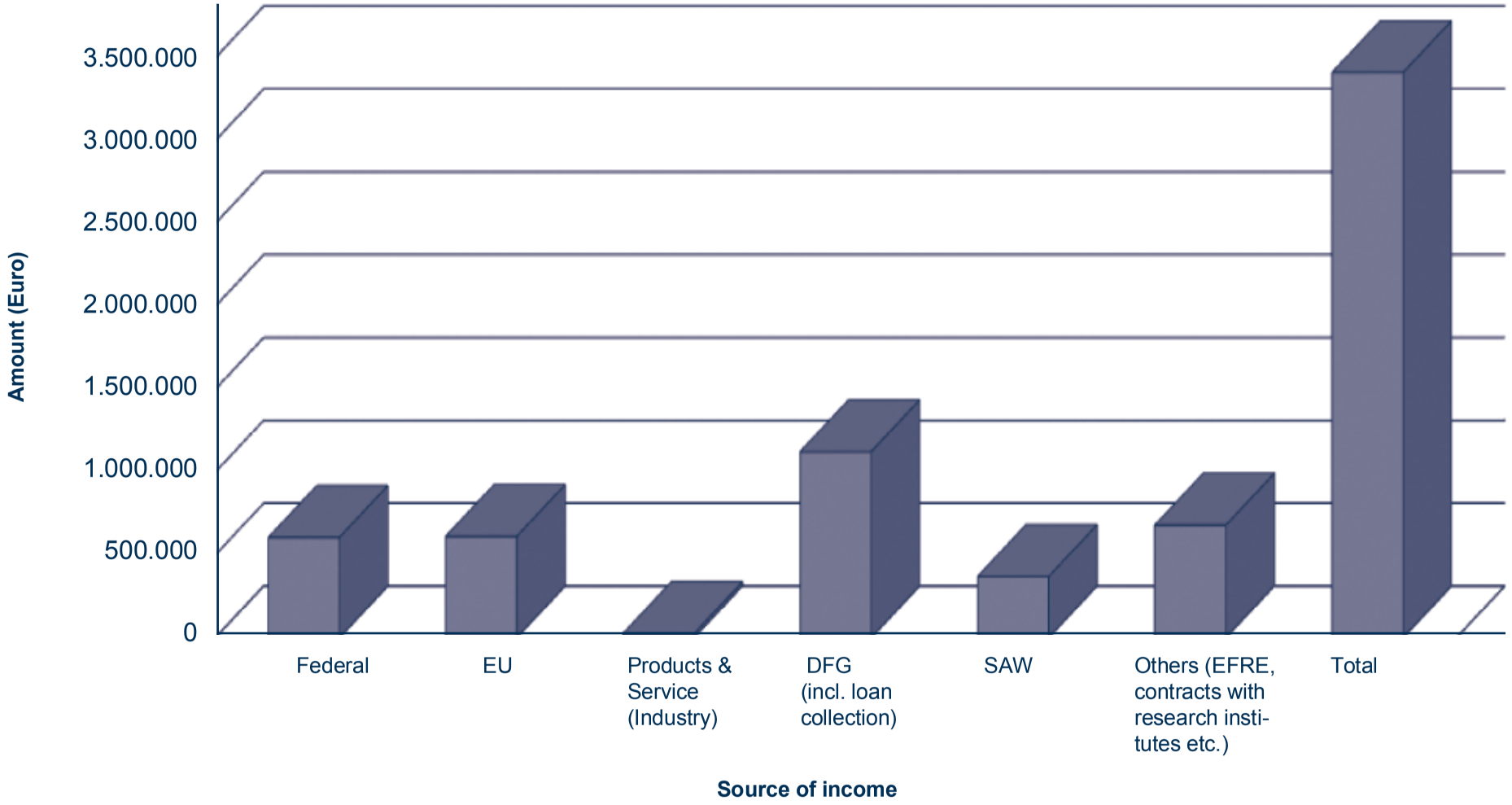

Total amounts spent in 2017: 3.411.024,67 Euro

Appendix 6

Activities in Scientific Organizations

A. A. Andreev

Member, Scientific Advisory Committee, ELI-ALPS, Extreme Light Infrastructure-Attosecond Light Pulse Source, Attosecond and Strong Field Science Division (Szeged, Hungary)

W. Becker

Co-Chair, Seminar 2, Strong Field & Attosecond Physics of the 26th Annual Int. Laser Physics Workshop, LPHYS'17 (Kazan, Russia)

Member, Advisory Board and Program Committee, 26th Annual Int. Laser Physics Workshop, LPHYS'17 (Kazan, Russia)

Member, Int. Program Committee, 14th Int. Conference on Multiphoton Processes (Budapest, Hungary)

Member, Editorial Board, Laser Phys. Lett.

Member, Editorial Board, ScienceOpen

Member, Editorial Board, Appl. Sci.

K. Busch

MC substitute member, EU-COSTMP1403, Nanoscale Quantum Optics

S. Eisebitt

Member, BMBF-Gutachterausschuss

Member, DESY Photon Science Committee

Chair, Scientific Advisory Committee, European XFEL

Chair, Komitee Forschung mit Synchrotronstrahlung

Member, Extended Governing Board, Ioffe-Röntgen-Institute

Member, Int. Advisory Committee, Int. Workshop on Nanoscale Spectroscopy and Nanotechnology

Member, RACIRI Summer School Scientific Committee

T. Elsaesser

Member, IRIS Adlershof, Humboldt-Universität zu Berlin

Member, Berlin Brandenburg Academy of Sciences

Member of the Board, Berlin Brandenburg Academy of Sciences

Member, Advisory Board, Int. Conference on Coherent Multidimensional Spectroscopy

Member, Advisory Board, Conference Series on Time Resolved Vibrational Spectroscopy

Member, Science Policy Committee, SLAC, Menlo Park

Chair, Prize Committee Ellis R. Lippincott Award, OSA

Chair, Physics Group, Gesellschaft Deutscher Naturforscher und Ärzte

Associate Editor, Struct. Dyn., AIP

Member, Editorial Board, J. Chem. Phys., AIP

Member, Editorial Board, Chem. Phys. Lett.

Member, Proposal Review Panel for the LCLS X-ray FEL facility

Member, Peer Review Panel FXE, European XFEL, Schenefeld

T. Fennel

Chair, Peer Review Panel for AMO Science at the LCLS (Stanford, USA)

Guest Editor, J. Phys. B

R. Grunwald

Member, Editorial Advisory Board, The Open Optics Journal, Bentham Open

Member, Editorial Board, Sci. Rep.

Member, Program Committee, Complex Light and Optical Forces, Photonics West, SPI

M. P. Kalashnikov

Co-Chair, Seminar 4, Physics of Lasers of the 26th Annual Int. Laser Physics Workshop, LPHYS'17 (Kazan, Russia)

Member, Advisory Board and Program Committee, 26th Annual Int. Laser Physics Workshop, LPHYS'17 (Kazan, Russia)

Member Scientific Advisory Committee ELI-ALPS, Extreme Light Infrastructure-Attosecond Light Pulse Source (Szeged, Hungary)

E. T. J. Nibbering

Member, Scientific Selection Panel, Helmholtz-Zentrum Berlin - BESSY II

Member, Proposal Review Panel for the LCLS X-ray FEL facility

Member, Central Laser Facility Access Panel (STFC Rutherford Application Laboratory, UK)

Member, Editorial Board, J. Photoch. Photobio. A

Member, Program Committee, TRVS Time Resolved Vibrational Spectroscopy

V. Petrov

Member, Technical Program Committee of CLEO/ EQEC 2017 (München, Germany)

I. Radu

Member, Peer Review Panel, Diamond Light Source (Didcot, Oxfordshire, UK)

Organizer and Chair, Session EA "When THZ meets X-rays: An ultrafast view on magnetism" at INTERMAG Europe 2017 (Dublin, Ireland)

D. Rupp

Discussion Leader, Gordon Research Conference: Clusters and Nanostructures (Mount Holyoke, MA, USA)

Elected Member, DESY Photon Science User Committee

G. Steinmeyer

Voting member, Quantum Electronics and Optics Division, European Physical Society

General Chair, Program Committee, High-Intensity Lasers and High-Field Phenomena, HILAS 2018

Chair, Commission D: Int. Union of Radio Science

Session Convener, Fibers and Waveguide Optics, International Union of Radio Science (URSI), General Assembly 2017

Chair, Program Committee, Ultrafast Optics 2017 (Jackson Hole, WY, USA)

Committee Member, Symposium on Ultrafast and Nonlinear Optics, CLEO Pacific Rim (Hongkong, China)

Committee Member, CLEO Focus Meeting (Rome, Italy)

Member, Editorial Board, Opt. Lett.

Member, Editorial Board, Phys. Rev. A

J. W. Tomm

Member, Scientific Committee of the "Semiconductor nanostructures towards electronic & opto-electronic device applications VI", Conference of the E-MRS

Permanent Member, Int. Steering Committee, Int. Conference on Defects - Recognition, Imaging and Physics of Semiconductors, DRIP (Berlin, Germany)

Member, Program Committee, 29th European Symposium on Reliability of Electron Devices, Failure Physics and Analysis (Aalborg, Denmark)

Member, Executive Committee, European Materials Research Society (Strasbourg, France)

Member, Editorial Board, J. Electron. Mater.

Member, Editorial Board, J. Commun. Phys.

M. J. J. Vrakking

Chair, SAC of the Advanced Research Centre for Nanolithography (Amsterdam, The Netherlands)

Member, CEA's Visiting Committee

Chair, SAC of the EUCALL Integrated Infrastructures network

Member, Access Panels of LCLS and FLASH

Chair, Access Panel of the ARTEMIS user facility at RAL

Chair, DPG-Fachverband Atomphysik (A), Sektion Atome, Moleküle, Quantenoptik und Plasmen

Deputy Editor, J. Phys. B

Editor, Advances in Physics: X

Max-Born-Institut (MBI)
für Nichtlineare Optik und Kurzzeitspektroskopie
im Forschungsverbund Berlin e. V.

Mail Address: Max-Born-Institut
Max-Born-Straße 2 A
12489 Berlin
Germany

Phone: (++49 30) 6392 1505
Fax: (++49 30) 6392 1519
mbi@mbi-berlin.de
www.mbi-berlin.de

The Divisions of the Max-Born-Institut

Division A: Attosecond Physics
Prof. Dr. M. J. J. Vrakking

Division B: Transient Electronic Structure and Nanoscience
Prof. Dr. S. Eisebitt

Division C: Nonlinear Processes in Condensed Matter
Prof. Dr. T. Elsaesser

City district: Berlin Treptow-Koepenick
Subdistrict: Berlin-Adlershof

Site: Berlin-Adlershof
Street: Max-Born-Straße 2 A

S-Bahn: S45, S46, S85, S8, and S9
Station: Berlin-Adlershof
from there:
Bus 162, 164 to Magnusstraße
Tram: 61, 63 to Karl-Ziegler-Straße

Subway: U7
Station: Rudow
from there:
Bus 162 to Magnusstraße

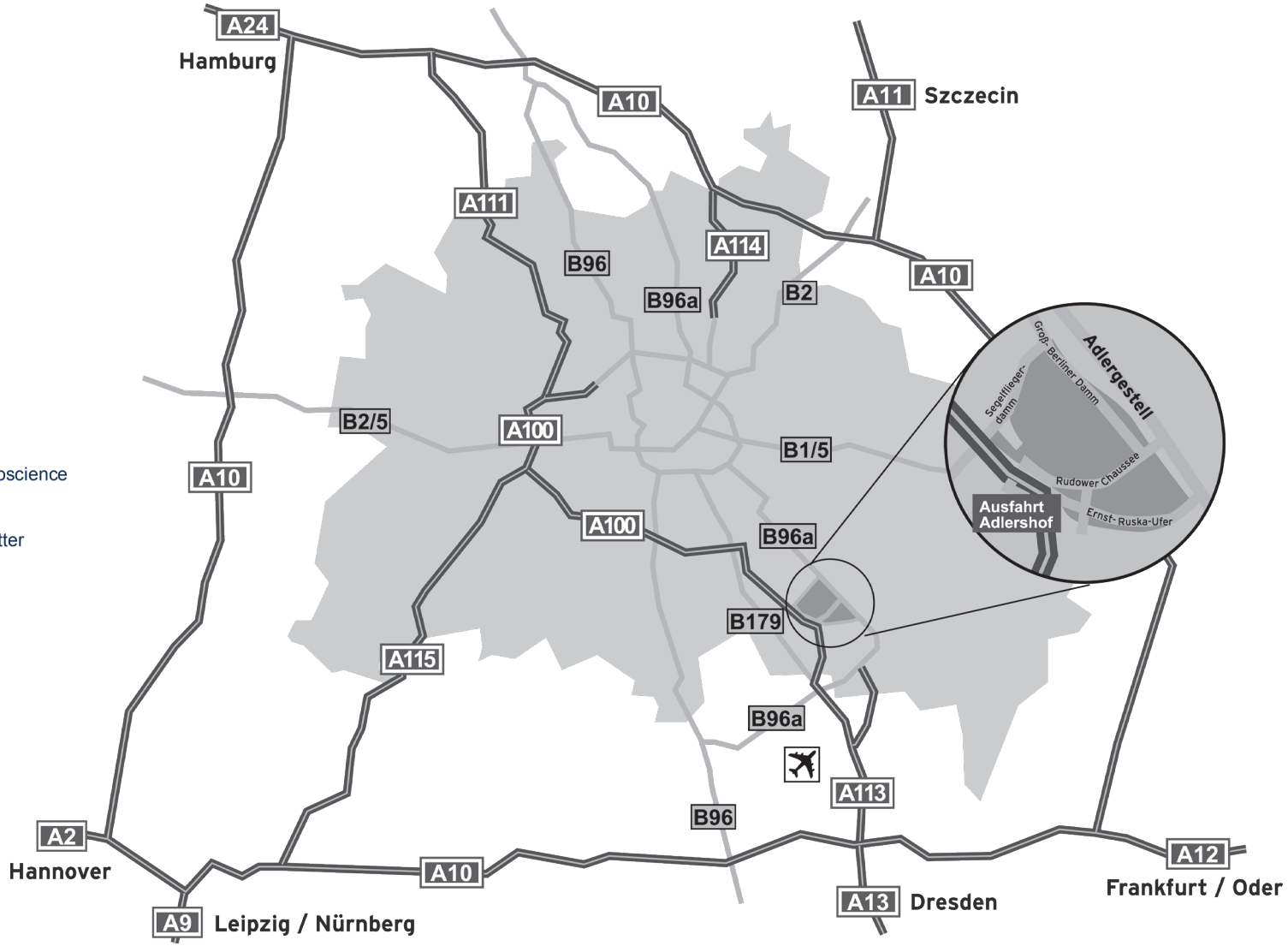

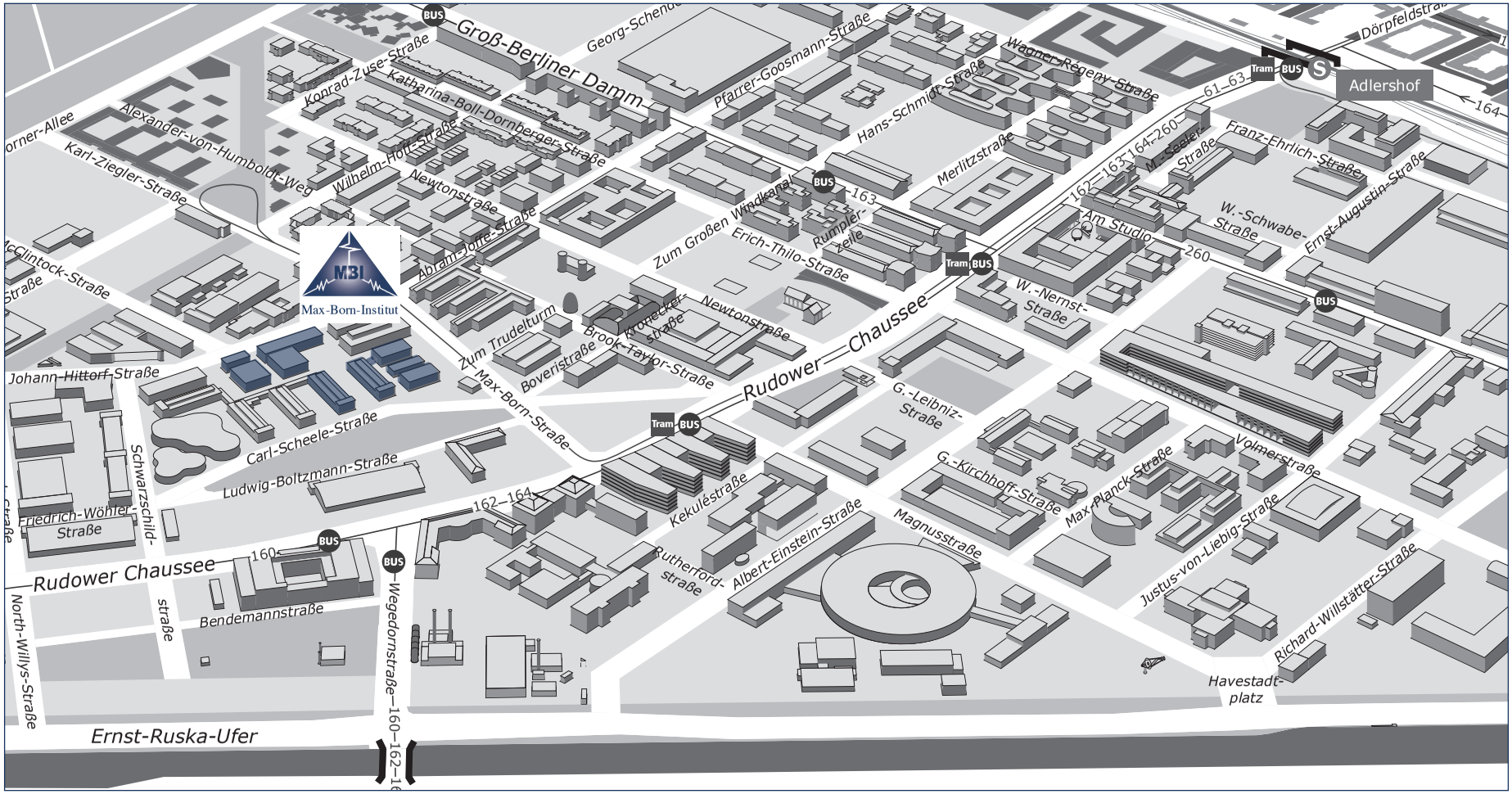
Groß-Berliner Damm
Georg-Schenu
Konrad-Zuse-Straße
Katharina-Boll-Dornberger-Straße
Pfarrer-Goosmann-Straße
Hans-Schmidt-Straße
Wagner-Régeny-Straße
Dörpfeldstra
Adlershof
Tram
BUS
S
61–63
164–
Alexander-von-Humboldt-Weg
Karl-Ziegler-Straße
Wilhelm-Hoff-Straße
Newtonstraße
Merlitzstraße
162–163–164–260–
W.-Seeler-Straße
Franz-Ehrlich-Straße
Ernst-Augustin-Straße
W.-Schwabe-Straße
Am Studio
260
Zum Großen Windkanal
Rumpler-zeile
163
Erich-Thilo-Straße
Abram-Joffe-Straße
MBI
Max-Born-Institut
Johann-Hittorf-Straße
Zum Trudelturm
Boveristraße
Brook-Taylor-Straße
Rotbrecker-straße
Newtonstraße
W.-Nernst-Straße
Rudower Chaussee
G.-Leibniz-Straße
Max-Born-Straße
Carl-Scheele-Straße
Ludwig-Boltzmann-Straße
Schwarzschild-straße
Friedrich-Wöhler-Straße
Kekuléstraße
162–164
G.-Kirchhoff-Straße
Max-Planck-Straße
Volmerstraße
Justus-von-Liebig-Straße
Albert-Einstein-Straße
Magnusstraße
Rutherford-straße
160
Bendemannstraße
Wegedornstraße
160–162–16
North-Willys-Straße
straße
Richard-Willstätter-Straße
Havestadt-platz
Ernst-Ruska-Ufer

Max-Born-Institut
für Nichtlineare Optik
und Kurzzeitspektroskopie
im Forschungsverbund Berlin e.V.

Max-Born-Straße 2 A
D-12489 Berlin

Phone: (++49 30) 63 92 - 15 05
Fax: (++49 30) 63 92 - 15 19
e-mail: mbi@mbi-berlin.de
http://www.mbi-berlin.de